NASA CR-134618
BCAC D6-41529

SCALE MODEL TESTING OF THE JET NOISE CHARACTERISTICS OF THE JT8D REFAN ENGINE NOZZLE SYSTEM

by D. H. Reed

BOEING COMMERCIAL AIRPLANE COMPANY
A DIVISION OF
THE BOEING COMPANY

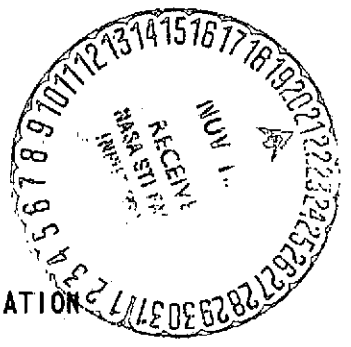

Prepared for
NATIONAL AERONAUTICS AND SPACE ADMINISTRATION
NASA Lewis Research Center
Contract NAS3-17842

1. Report No.	2. Government Accession No.	3. Recipient's Catalog No.
CR- 134618		

4. Title and Subtitle	5. Report Date
Scale Model Testing of the Jet Noise Characteristics of the JT8D Refan Engine Nozzle System	March 1974
	6. Performing Organization Code
7. Author(s)	8. Performing Organization Report No.
D. H. Reed	D6-41529
	10. Work Unit No.
9. Performing Organization Name and Address	
BOEING COMMERCIAL AIRPLANE COMPANY P.O. Box 3707 Seattle, Washington 98124	11. Contract or Grant No. NAS3-17842
	13. Type of Report and Period Covered
12. Sponsoring Agency Name and Address	Contractor Report
NATIONAL AERONAUTICS AND SPACE ADMINISTRATION WASHINGTON, D.C. 20546	14. Sponsoring Agency Code

15. Supplementary Notes

ASSOCIATE CHIEF V/STOL AND NOISE DIVISION, R. W. SCHROEDER
NASA LEWIS RESEARCH CENTER, CLEVELAND, OHIO 44135

16. Abstract

This report presents the results of static scale model acoustic tests of the nozzle system for the JT8D-9 baseline engine and candidate nozzle systems for JT8D-109, JT8D-115, and JT8D-117 refan engines. The tests were conducted by the Aircraft Noise Staff of the Boeing Commercial Airplane Company in support of the NASA JT8D Refan Program. The objective of these tests was to determine the jet noise benefit of the three refan engine cycles relative to the baseline JT8D-9, and to provide acoustic information toward selection of the optimum primary-secondary area match and centerbody contour for the refan engine cycles. One of the nozzle configurations was tested with and without simulated turbine exit swirl to determine what effect, if any, swirl has on jet noise. The JT8D-109 cycle was found to afford approximately 9 dB (OASPL) jet noise reduction relative to the JT8D-9 when compared on an equal static thrust basis. The JT8D-115 and JT8D-117 afford an 8 dB and 6 dB reduction, respectively, relative to the JT8D-9, at equal static thrust. Turbine exit swirl was found to have no significant effect on the jet noise of the JT8D-109 nozzle system.

17. Key Words (Suggested by Author(s))	18. Distribution Statement
JT8D Refan Jet Noise Swirl Bypass Ratio	Unclassified - Unlimited

19. Security Classif. (of this report)	20. Security Classif. (of this page)	21. No. of Pages	22. Price*
Unclassified	Unclassified	162	

* For sale by the National Technical Information Service, Springfield, Virginia 22151

FOREWORD

The scale model nozzle system jet noise tests described in this report were performed by the JT8D Refan Noise Technology Staff of the Boeing Commercial Airplane Company, a division of The Boeing Company, Seattle, Washington. The work, sponsored by NASA Lewis Research Center and reported herein, was performed between August and December, 1973.

This report has been reviewed and is approved by:

C G Hodge Date 1 Oct. 1974

C. G. Hodge, Group Engineer
JT8D Refan Noise Technology Staff

J A Ferrell Date 7 OCT 1974

J. A. Ferrell
Chief, Technology Staff
JT8D Refan Program

K P Rice Date 10/25/74

K. P. Rice
Program Manager
JT8D Refan Program

TABLE OF CONTENTS

1.0 SUMMARY

Scale model acoustics tests of the nozzle system for the JT8D-9 baseline engine and candidate nozzle systems for JT8D-109, JT8D-115, and JT8D-117 refan engines were conducted as part of the NASA Refan Program. The purpose of these tests was to evaluate the static jet noise characteristics of the three refan engine cycles relative to those of the baseline engine and to investigate the effect on jet noise of minor variations in primary-secondary area match and centerbody contour. The tests were conducted at the Wall Isolation Facility at North Boeing Field, which had been specially modified to include a high temperature muffler to minimize valve and burner noise.

The test results show that the JT8D-109 refan engine cycle affords a jet noise benefit of up to 9 dB (OASPL) relative to the JT8D-9 (compared at equal static thrust), 1 to 2 dB less than had been predicted. Test results also show that the benefit of the JT8D-115 cycle will approximately 1 dB less than that of the JT8D-109 (again compared at equal thrust), and the JT8D-117 cycle will afford about 3 dB less benefit than the JT8D-109 cycle.

The results of this test point out some deficiencies in the jet noise prediction procedure, which is a part of the Boeing engine component noise prediction procedure used to predict airplane community noise levels. The test data has been used to update this prediction procedure, and thereby improve the confidence level of predicted community noise levels for refanned JT8D powered 727 airplanes.

2.0 INTRODUCTION

The fundamental goal of the NASA-funded JT8D refan program is to produce airplanes which are significantly quieter than those powered by conventional JT8D engines, primarily by virtue of large reduction in jet noise. The baseline JT8D nozzle system is a 1:1 bypass-ratio, free mixing, retracted primary, dual flow nozzle. The refan JT8D engine employs a similar nozzle concept with a 2:1 bypass ratio. Jet noise being the dominant community noise component on both the baseline JT8D and treated JT8D refan, it is important to have an accurate assessment of the jet noise characteristics of all of the candidate nozzle systems.

As the refan program has progressed, interest has increased in the JT8D-115 and JT8D-117 versions of the refan engine. These growth engines have engine cycles somewhat different than the JT8D-109, and consequently have different jet noise characteristics. At the same time there was some question as to what should be the optimum primary/secondary area match for each of the three engine cycles. One further question was that of the optimum size and shape of the primary plug (centerbody). As a result of these variables -- i.e., engine cycle, area match, and centerbody contour -- a total of 14 different JT8D refan nozzle system models were fabricated for performance testing. Of these, seven were selected for acoustic tests.

This report is a description of the acoustic aspects of this test program. The propulsion aspects are discussed in a companion report, NASA-CR-134617, "727/JT8D-100 Series Engine Exhaust System Propulsion Performance Model Test".

3.0 NOMENCLATURE

dB	-	decibels re. .0002 microbar
F_n/δ	-	corrected net thrust - lbs. (full scale)
OASPL	-	overall sound pressure level, dB
PNL	-	perceived noise level, PNdB
P_{TP}	-	total pressure ratio, - primary
P_{TS}	-	total pressure ratio, - secondary
T_{TP}	-	total temperature - primary, °R
T_{TS}	-	total temperature - secondary, °R
v	-	jet velocity, ft/sec
W_{PRI}	-	mass flow primary - lbs/sec (model scale)
WIF	-	Wall Isolation Facility
W_{SEC}	-	mass flow secondary - lbs/sec (model scale)

4.0 MODEL AND TEST DESCRIPTION

4.1 MODEL DESCRIPTION

The test nozzles included 1/8th scale models of the following nozzle systems:

- JT8D-9 - Baseline
- JT8D-109 - Phase I
- JT8D-109 - P&WA
- JT8D-109 - P&WA (with swirl vanes)
- JT8D-109 - Boeing
- JT8D-115 - P&WA
- JT8D-115 - Boeing
- JT8D-117 - P&WA
- JT8D-117 - Boeing (2 variations)

Sketches of the components used to assemble the above models are shown in Figures 1 and 2. Table 1 shows the hardware combinations for each of the above configurations listed in the sequence of testing. Photographs of the nozzle hardware are shown on Figures 3 thru 5. In addition to the above models, a 2" conical single flow nozzle was used in facility checkout.

4.2 TEST FACILITY

The tests were conducted at the Wall Isolation Facility at North Boeing Field, which had been specially modified to include a high temperature muffler intended to minimize valve and burner noise. The facility includes a 50 ft. by 13 ft. by 16 ft. concrete chamber which houses air supply lines, air heating equipment, plenum chanbers, mufflers, flow measuring devices, and control valves (Figure 6). Test nozzles were attached to air supply lines which protrude through a 24" circular opening cut through the wall at one end of the chamber. Primary air was heated by means of a kerosene burner and was channeled through a fiberglas lined muffler section before exhausting through

the test nozzles. Secondary air was introduced from a 300 psi plant air supply into a 30" diameter plenum immediately upstream of the test nozzles.

Outside the chamber (Figure 7), where the acoustic data were recorded, the face of the test cell and the ground plane under the centerline of the jet were treated with panels of 4" thick fiberglas to minimize sound reflections. Microphones were located on a 25' vertical arc above the jet axis.

4.3 INSTRUMENTATION

Acoustic data were recorded on a 14 channel Ampex tape recorder from 8 B&K 1/4" condenser microphones mounted on a 25' radius vertical arc. Acoustic data were monitored on-line by means of a General Radio 1/3rd octave band analyzer. Performance data were recorded on punch paper tape from a number of pressure and temperature transducers, yielding primary and secondary total pressures, total temperatures, mass flows and ideal velocities.

4.4 TEST PROCEDURE

The test nozzles were affixed one at a time to the test fixture, and total temperatures and pressures in the supply lines were adjusted to the desired test conditions. These parameters were continuously monitored until stability was achieved. Acoustic data were then recorded for approximately 30 seconds, and nozzle conditions were recorded during a 3 second interval about midway through the 30 second interval.

4.5 TEST CONDITIONS

A total of 227 test conditions were run as shown in Table II. The test conditions for the refan and baseline nozzles represent ground static power lines for their respective engine cycles. In addition, each nozzle was run at flight power settings equivalent to the engine cycle conditions which exist at representative FAR 36 points for a 727-200 airplane. For the

purposes of this simulation, absolute (as opposed to relative) primary and secondary velocities were matched to those of the equivalent flight conditions.

One of the major difficulties in performing the model simulation resulted from the lack of capability to heat the secondary air. With this restriction, an exact match of engine cycle conditions was not possible. Secondary air total temperatures for the JT8D-9 engine range up to 240°F at takeoff power and those for the JT8D-109 refan engine range up to 180°F at takeoff power, whereas the test rig secondary air temperature was limited to ambient temperature of 40°F to 60°F. However, since jet velocity is the dominant parameter in determining jet noise level, it was decided to use a correct primary/secondary velocity match, and to allow other flow parameters to deviate from engine cycle conditions. This method of modeling resulted in a lower secondary temperature and higher total pressure and density than those of the actual engine cycle. The higher secondary pressure resulted in excessive encroachment of the secondary stream on the primary, and consequently, the secondary mass flow was too large and the primary mass flow too small. This problem is discussed further in Section 5.4.

4.6 DATA REDUCTION & ANALYSIS

The acoustic analog tapes were reduced at the Boeing Acoustics Laboratory to (27) as-measured 1/3rd octave band levels from 200 Hz to 80 KHz using a General Radio real time analyzer. The 1/3rd octave band digital data were recorded on magnetic tape and sent to the Boeing CDC 6600 computer tape library where it could be accessed for further analysis.

A dynamic editor program was used to shift the model scale digital data to full scale frequencies by simply changing the frequency designation of any particular model scale band level to its full scale equivalent (each frequency was reduced by a factor of 8, the geometric scale factor of the sub-scale model test). All frequencies shown on the graphs in this report are full

scale frequencies, except those on Figures 9 thru 38 which refer to the muffler evaluation (those spectra are shown at as-measured frequencies). A data bank program was used to sort and reformat the data. A third program was used to extrapolate the full scale acoustic data to a 150 ft. polar arc and to 200 ft. and 1500 ft. sidelines. These extrapolations were performed using only inverse square energy decay and atmospheric attenuation based on ARP 866 (Society of Automotive Engineers, Aerospace Recommended Practice 866).

5.0 DISCUSSION OF TEST RESULTS

5.1 MUFFLER EVALUATION

Prior to the test, a high temperature muffler was installed in the primary flow system downstream of the burner to prevent burner noise from influencing the jet noise data. To demonstrate that the muffler effectively reduced internal noise to a level satisfactorily lower than the jet noise level for a baseline and refan nozzle conditions, a two inch diameter single flow conical nozzle was run, both with and without the muffler in the system, at mass flows and velocities similar to those of the primary system for the baseline and refan nozzles. When the noise data from this test is plotted versus log of jet velocity, the jet noise can be identified by its linear fit (80 logV), while internal noise can be identified by its departure from a V^8 linear fit. Analyzing the data in this manner shows that internal noise does not influence the jet noise data for any nozzle conditions tested when the muffler is in the system, and that internal noise is a significant factor only for the lowest jet velocities when the muffler is removed from the system. A more detailed description of this test is given in the following paragraphs.

The nozzle was first run with unheated airflow, to check the muffler attenuation with very low jet velocities. The results of this test sequence are summarized on Figure 8, where it is seen that the muffler provides about 7 dB attenuation in OASPL at the lowest flow velocities tested (430 ft/sec). The OASPL attenuation decreases as the flow velocity is increased and the jet noise floor begins to dominate the spectra. A more detailed look at this transition is given by scanning the spectra of Figures 9 thru 18.

A result similar to that of the cold flow case was obtained when the burner was turned on. For a 1010°R jet temperature (Figure 19), the muffler provided some attenuation in OASPL at the lowest jet velocities tested, but at higher jet velocities (> 800 ft/sec) the OASPL attenuation was masked by jet noise

floor. At a jet temperature of 1420°R (Figure 20) the muffler shows no significant attenuation in OASPL for any jet velocity tested. These results can be seen more clearly by examining the spectra plots. Scanning from Figures 21 thru 30, the jet noise is seen to increase with increasing velocity at a more rapid rate than does the internal noise (those frequencies which are affected by the muffler), until at the highest velocity (Figures 29 and 30) the entire spectrum is jet noise dominated. Figures 31 thru 38 show that the spectra are jet noise dominated over the entire velocity range for the 1400°R jet temperature conditions (900 to 1600 ft/sec). This result seems reasonable, since at fixed jet velocity internal noise would be expected to be a strong function of internal Mach number, and therefore temperature; whereas jet noise is only a weak function of temperature (for fixed jet velocity).

A full evaluation of the internal noise characteristics of the primary flow system would require a complete parametric study (nozzle area, mass flow, velocity), which is beyond the scope of the present test. However, based on the present data, the following general statement can be made: With the muffler in the system, the internal noise floor of the primary flow system is acceptable for all baseline and refan nozzle conditions of interest from a jet noise standpoint.

5.2 EVALUATION OF SWIRL EFFECT

A set of swirl vanes was fabricated to simulate the turbine exhaust swirl of a JT8D-109 at takeoff power, in order to determine what effect, if any, primary swirl has on low frequency exhaust noise. Although the swirl vanes produced the correct swirl angle (approximately 18° at hub, 0° at tip) only at takeoff power, test conditions were run over the entire power range. While this certainly is not a valid simulation of the low power swirl for a JT8D-109, it does provide some information on the effect of swirl as a function of jet velocity. The results of this test are summarized on Figures 39 and 40, which show that at the 140° directivity angle, the swirl vanes produced a small effect on OASPL at high power settings and a lesser effect at lower power. At the 110° directivity angle, the effect of the swirl vanes is negligible.

The thrust values shown on these figures are based on total temperature and pressure measurements made upstream of the station where the swirl vanes were installed, and therefore do not include the effect of any losses caused by the vanes. However, measurements made in performance tests of this same nozzle indicate that thrust loss caused by the swirl vanes is less than 0.5%. This thrust loss has a jet noise equivalent of about .1 to .2 dB, and therefore cannot entirely explain the noise reduction afforded by the swirl vanes. One possible explanation for this noise reduction is that the swirl may have enhanced mixing of the primary and secondary streams, thus yielding a lower average primary jet velocity.

The spectra plots of Figures 41 thru 55 show more detail of the effect of the swirl vanes. These plots show that the swirl vanes caused an increase in mid frequency noise (500 Hz to 5000 Hz) at all power settings and a decrease in low frequency noise, which was most noticeable at the higher power settings. It is believed that the mid frequency noise increase is due to noise generated by the swirl vanes themselves, and this effect may or may not be present in a real engine nozzle. In either case, this small difference in mid frequency noise is not an important factor when viewed in light of overall jet noise.

5.3 ENGINE CYCLE COMPARISON

Noise data for ground static power line conditions for all JT8D refan and baseline nozzle configurations that were tested are compared on Figures 56 thru 71. The four basic engine cycles are comapred on Figures 56 and 57 (throttling curves) and Figures 58 and 59 (spectra). These figures show the distinct jet noise benefits afforded by refanning the JT8D engine. This benefit is seen to increase with thrust*, to maximum of approximately 8 dB (OASPL) for the JT8D-109 at 15,000 lbs. thrust and to 6 to 7 dB for JT8D-115

* Whenever the term "thrust" is used in this report with reference to a model nozzle, it is meant as the full scale engine static thrust corresponding to the primary jet velocity at which the model was run.

and -117 cycles. These deltas are compared with earlier results in Section 5.4, and with predictions in Section 5.5. The spectral comparisons of Figures 58 and 59 show an orderly progression in the noise levels of the three refan cycles, in the direction that would be expected from considerations of the engine cycle parameters.

Figures 60 thru 63 show comparisons of the three JT8D-109 nozzles that were tested. These figures show no experimentally significant differences between the three JT8D-109 nozzles. Figures 64 thru 67 show a similar comparison for the two JT8D-115 nozzles. Again, there appears to be no significant difference between the two.

A similar comparison for the three JT8D-117 nozzles is shown on Figures 68 thru 71. Here, one of the Boeing JT8D-117 nozzles (Configuration 10 from Table I) is distinctly noisier than the other two -117 nozzles. Performance data from the companion report on the propulsion characteristics of these nozzles (NASA CR-134617; "727/JT8D-100 Series Engine Exhaust System Propulsion Performance Test") show that this nozzle did not achieve the proper JT8D-117 primary-secondary area split resulting in a bypass ratio lower than that of the engine cycle. This nozzle also exhibited thrust losses approximately 0.5% greater than those of the two other JT8D-117 nozzle configurations. Based on both the acoustic and propulsion results, this configuration has been determined not to be a suitable candidate for the JT8D-117 nozzle system.

Additional test data are presented on Figures 83 thru 122. Figures 83 thru 92 include throttling curves for all baseline and refan configurations with log of primary jet velocity as abcissa. Also, included are OASPL directivity plots (Figures 93 thru 102) and spectra at approach, cutback and takeoff power settings for all configurations.

5.4 COMPARISONS WITH PHASE I RESULTS

Two of the nozzle configurations included in the present 1/8th scale model test were among the 1/20th scale model nozzles tested in Phase I of the NASA funded program. These configurations were the JT8D-9 baseline nozzle and a JT8D-109 configuration referred to as "Phase I refan". The airflow facilities for the two tests were substantially different, and each test had its own particular cycle match limitations. The Phase I test employed electrical air heaters for both the primary and secondary airflow. This equipment provided adequate heating for the secondary air over most of the power range, but the primary air was limited to a maximum temperature of approximately $1100^{o}R$. When the velocities were matched to those of the engine cycle, this resulted in primary air densities higher than those for the real engine cycle, and consequently, the bypass ratios for the test were slightly lower than those of the engine cycle. The Phase II test used a kerosene burner to heat the primary airflow, but there was no capability to heat the secondary air. This combination resulted in bypass ratios higher than those for the real engine cycle, as discussed in Section 4.5.

Noise data from the Phase I and Phase II tests are compared on Figures 72 and 73. These figures show throttling curves for the two nozzle configurations that were run in both tests. Only that Phase I data for which the primary and secondary velocity match was a correct simulation of real engine conditions is shown. This condition was met for all Phase II data. The difference in bypass ratio for the two tests is believed to be responsible for the difference in noise level, which is greatest at the highest power settings.

As will be explained later, one would expect the Phase II noise data to be somewhat lower than the noise levels for equivalent real engine cycle conditions, with this increment increasing with increasing thrust. The Phase I noise data would be expected to be somewhat higher than equivalent engine levels, with the JT8D-9 showing a larger departure from the engine cycle than does the JT8D-109 (the JT8D-109 has a lower temperature primary and it was, therefore, more closely simulated in the test than was the JT8D-9).

Following this line of reasoning, the curves on Figures 72 and 73 are believed to be representative of the jet noise characteristics of the real engine cycles of the JT8D-9 and the JT8D-109 engines. These curves show a refan benefit of 8 to 10 dB throughout the power range.

This contention is supported by the results of a brief experiment which was conducted during the Phase II testing of the JT8D-109 nozzle (Phase I refan). At three different power settings, the nozzle was run at the same primary velocity as that of the real engine cycle. First, at the proper primary temperature and then at a greatly reduced primary temperature. Secondary temperature and velocity remained unchanged. The primary temperature change resulted in a large change in bypass ratio, and yielded a direct measurement of the effect of bypass ratio on noise at fixed primary and secondary velocities. For the highest power setting (F_n/δ = 16,300), the bypass ratio decreased from 5.7 to 1.8 when the primary temperature was reduced, yielding a pair of test conditions which bracket the real engine cycle conditions. For the lower power settings, the change was from approximately 5 to approximately 3. The low bypass ratio points are shown as inverted triangles on Figures 72 and 73. At the highest power setting, the change in bypass ratio produced a noise change of approximately 4 dB, while at the lower settings, the change was less than 1 dB. This result indicates that the Phase II engine cycle test conditions are a reasonably good simulation of the jet noise features of a real engine cycle over most of the power range. At the highest thrust settings, however, the departure of nozzle test conditions from real engine cycle conditions (secondary temperature, secondary density, and bypass ratio) is so large that the effect of the bypass ratio error on noise level cannot be neglected. The low bypass ratio mode of operation, which gives an approximately correct simulation of JT8D-109 engine bypass ratio, should produce noise levels higher than those of the real engine cycle because of excessive mass flow in both the primary and secondary; the high bypass ratio mode should produce noise levels lower than real engine cycle conditions because the noise increase produced by the excessive secondary mass flow is more than compensated by the noise decrease produced by the effective reduction in primary area, since the jet noise is dominated by primary stream conditions. The noise levels of

the real engine cycle should lie between the noise levels of these two modes of operation, as shown on Figures 72 and 73.

5.5 IMPACT ON PREDICTION PROCEDURE

Acoustic data were predicted for the precise nozzle conditions that were run in the then test (as opposed to the "equivalent" real engine cycle conditions) using the current Boeing jet noise-prediction procedure (identified here as TEE215). This procedure does not give good agreement with the measured data. The predictions under-estimate the measured OASPL by 5 to 6 dB for the refan nozzles and by 3 to 4 dB for the baseline nozzle. This comparison is shown on Figures 74 thru 77 for JT8D-9, JT8D-109, JT8D-115, and JT8D-117 engines.

The Boeing TEE215 jet noise prediction procedure calculates the jet noise for a dual flow jet nozzle in the following manner: (1) noise is calculated for the primary "core" jet as if it were a single flow turbojet; (2) a "bypass" correction based on the primary-secondary shear layer interaction is subtracted from the "core" jet level. This correction increases with increasing bypass ratio; (3) noise is calculated for a coalesced single jet having the same total momentum and airflow as do the primary and secondary streams together; (4) this "momentum averaged" secondary jet noise is then added logarithmically to the corrected primary jet noise to yield the jet noise prediction. It is believed that an excessively large bypass correction in this prediction procedure is responsible for the error in the predictions of the present test data, based on the fact that the procedure underpredicts by a smaller amount at lower bypass ratios (this procedure did substantially better at predicting the low bypass ratio Phase I data). This error is particularly important because it causes the procedure to underpredict the higher bypass ratio refan engine jet noise by more than it underpredicts the baseline JT8D-9, resulting in an overly optimistic prediction of the refan jet noise benefit. A comparison of the predictions of refan and baseline

engine jet noise for sea level static engine cycle conditions is shown on Figures 78 and 79. Figure 79 shows a refan (JT8D-109) benefit of 12 dB OASPL at maximum thrust for the JT8D-9. This compares to an improvement of only 10 dB for a similar condition from the test data (Figure 73).

While the test data points out the shortcomings of the prediction procedure with regard to the bypass correction, at the same time it substantiates some other features of the procedure. Figures 74 thru 77 show that the procedure does a remarkably good job of predicting the shape of the throttling curves, and of predicting the increments among the three refan engine cycles.

Two other computerized jet noise prediction procedures are available at Boeing, and these have also been used to predict the present test data. One of the procedures was developed by the Boeing Acoustics Research Staff and is similar to the TEE215 procedure described above, except that it adds a third source, that of the secondary shear layer. This procedure is identified here as JEN1. The other prediction procedure was developed by Rolls Royce, and is similar to the proposed SAE jet noise prediction procedure. This procedure simply calculates the jet noise for the primary and then corrects for the presence of the fan flow depending on area ratio and velocity ratio. This procedure calculates the primary jet noise in a manner identical to that used in the JEN1 procedure, and the two differ only in the manner in which account is taken of the effect of the secondary jet (i.e., the bypass correction). Predictions from the three procedures are compared with test data on Figures 80 thru 82. These curves show that the RR/SAE procedures comes closer to predicting the test data than do the Boeing procedures. This adds credence to the supposition that the Boeing procedures use an excessively large bypass correction. More important than that, however, these curves show that all three procedures need further refinement.

The present data will be used to update the Boeing jet noise prediction procedure and this will result in substantially improved predictions of the community noise benefit of refan engines.

6.0 CONCLUSIONS

The JT8D-109 engine cycle affords a jet noise benefit of approximately 9 dB (OASPL) relative to the JT8D-9 baseline engine compared on an equal thrust basis at maximum JT8D-9 static thrust. The JT8D-115 and JT8D-117 afford approximately 1 dB and 3 dB less jet noise benefit, respectively, than does the JT8D-109, when compared on an equal thrust basis.

The turbine exhaust swirl of the JT8D-109 engine produces no significant effects on the jet noise characteristics of that engine.

The Boeing jet noise prediction procedure does not give good agreement with the test data on an absolute noise level basis. On an incremental noise level basis, the prediction procedure is substantially better, but it is still in need of some improvement. This procedure should be reviewed and updated to reflect the results of this test data.

The method used in this test to simulate engine cycle conditions (correct primary and secondary velocity match, excessive bypass ratio), creates problems which make analysis of the data very difficult. (However, when no secondary heating capability is available, the alternative method (matching primary and secondary total temperature ratio to engine conditions) is also difficult.) In both cases, the correction required to convert noise data to real engine cycle conditions is unknown, and must be obtained by indirect means. Data analysis would be simplified and reliability of results would be enhanced if exact engine cycle conditions could be matched. For future noise testing of retracted primary dual flow jet nozzles, this facility improvement is strongly recommended.

7.0 TABLES AND FIGURES

7.1 TABLES

TABLE 1

MODEL HARDWARE

TEST SEQUENCE

CONFIGURATION		HARDWARE NOTATION (FROM FIGURES 1 & 2)			
NO.	DESCRIPTION	OUTER NOZZLE WALL	SPLITTER	PLUG	NOZZLE EXIT
1	2" Conical Nozzle	N.A.			
2	3.25" Conical Nozzle	N.A.			
3	JT8D-9 Production	C2	S1	P1	C2
4	JT8D-109 P&WA Ref.	C3	S2	P2A	E2
5	JT8D-109 (Phase I Refan)	N.A.			
6	JT8D-109 P&WA Ref. (Swirl)	C3	S2	P2A	E2
7	JT8D-117 P&WA Ref.	C3	S4	P2A	E4
8	JT8D-109 Boeing	C4	S5	P5-1	E5
9	JT8D-117 Boeing	C4	S7	P5-1	E7
10	JT8D-117 Boeing	C4	S5	P5-3	E7
11	JT8D-115 Boeing	C4	S6	P5-1	E5
12	JT8D-115 P&WA Ref.	C3	S3	P2A	E3
13	2" Conical Nozzle	N.A.			

N.A. - Figures 1 and 2 not applicable

TABLE 2

SUMMARY OF TEST CONDITIONS

		PRIMARY					SECONDARY			
CONFIGURATION	RUN	P_{TP}	T_{TP}	$F_{N/\delta}$	W_{PRI}	V_{PRI}	P_{TS}	T_{TS}	V_{SEC}	W_{SEC}
1 (2" CONICAL)	2	1.03	531		.45	238				
	3	1.10	531		.81	427				
	4	1.20	531			553				
	5	1.37	528		1.51	742				
	6	1.62	528		1.94	904				
	7	1.82	526		2.27	999				
	8	1.11	1016		.55	594				
	9	1.21	1022		.77	805				
	10	1.42	1012		1.12	1077				
	11	1.62	1008		1.38	1249				
	12	1.83	1014		1.58	1391				
	14	1.19	1431		.64	909				
	15	1.41	1414		.73	1259				
	16	1.60	1429		1.11	1477				
	17	1.80	1420		1.33	1632				
5 (PHASE I REFAN)	41	1.10	1237	4000	.657	641	1.19	504	540	3.95
	42	1.16	1265	6000	.786	791	1.30	503	659	5.07
	43	1.19	1286	7000	.885	871	1.33	503	691	5.27
	44	1.22	1295	8000	.943	934	1.39	505	738	5.77
	45	1.27	1321	9000	1.04	1021	1.45	506	784	6.19
	46	1.31	1328	10000	1.12	1098	1.52	506	829	6.66
	47	1.36	1352	11000	1.25	1169	1.56	506	852	6.81
	48	1.40	1376	12000	1.27	1236	1.62	507	884	7.12
	49	1.43	1393	13000	1.26	1278	1.69	507	922	7.74
	50	1.48	1427	14000	1.27	1350	1.76	507	955	8.15
	51	1.53	1443	15000	1.34	1414	1.83	508	984	8.49
	52	1.62	1454	12380*	1.53	1504	1.91	508	1013	8.76
	53	1.43	1378	8640*	1.39	1275	1.64	507	897	7.19
	54	1.29	1343	6310*	1.17	1070	1.44	508	779	5.92
	55	1.36	1127	6310*	1.65	1068	1.44	509	779	5.59
	56	1.56	1119	8640*	2.18	1272	1.65	509	900	6.67
	57	2.06	1026	12380*	3.93	1519	1.91	508	1017	7.06
	58	2.28	1024		4.34	1610	2.14	508	1093	7.93

* Corrected Net Thrust for FAR 36 Flight Conditions, 727-200 Airplane -

TABLE 2 (continued)

SUMMARY OF TEST CONDITIONS

		PRIMARY					SECONDARY			
CONFIGURATION	RUN	P_{TP}	T_{TP}	$F_{N/\delta}$	W_{PRI}	V_{PRI}	P_{TS}	T_{TS}	V_{SEC}	W_{SEC}
3	61	1.20	1186	4000	.759	842	1.35	513	715	2.76
(JT8D-9)	62	1.33	1216	6000	1.06	1076	1.50	513	819	3.12
	63	1.40	1247	7000	1.12	1178	1.60	513	882	3.43
	64	1.46	1265	8000	1.18	1256	1.71	514	938	3.81
	65	1.55	1317	9000	1.29	1369	1.80	514	978	3.99
	66	1.61	1343	10000	1.32	1437	1.90	514	1019	4.30
	67	1.69	1376	11000	1.31	1521	2.05	514	1070	4.73
	68	1.78	1409	12000	1.40	1606	2.13	514	1094	4.85
	69	1.87	1440	13000	1.41	1688	2.30	515	1144	5.32
	70	1.93	1483	14000	1.38	1755	2.43	515	1177	5.74
	71	2.03	1528	15000	1.38	1845	2.59	515	1214	6.10
	72	2.05	1510	12380*	1.39	1846	2.62	515	1220	6.26
	73	1.74	1310	8640*	1.56	1520	1.99	518	1052	4.32
	74	1.51	1216	6310*	1.44	1278	1.65	518	911	3.37
4	77	1.11	1232	4000	.850	664	1.19	507	539	3.22
(P&WA-109)	78	1.15	1267	6000	.909	783	1.29	507	652	4.13
	79	1.20	1284	7000	1.07	886	1.34	507	700	4.46
	80	1.24	1304	8000	1.17	960	1.39	508	741	4.76
	83	1.27	1321	9000	1.20	1024	1.45	511	784	5.12
	84	1.32	1334	10000	1.35	1103	1.51	512	825	5.42
	85	1.36	1365	11000	1.42	1180	1.56	512	855	5.64
	86	1.38	1369	12000	1.43	1204	1.63	512	897	6.18
	87	1.44	1391	13000	1.55	1294	1.69	513	925	6.38
	88	1.50	1424	14000	1.63	1370	1.75	514	957	6.69
	89	1.53	1442	15000	1.60	1412	1.82	513	986	7.10
	90	1.62	1454	12380*	1.84	1509	1.88	515	1012	7.19

* Corrected Net Thrust for FAR 36 Flight Conditions, 727-200 Airplane -

TABLE 2 (continued)

SUMMARY OF TEST CONDITIONS

		PRIMARY					SECONDARY			
CONFIGURATION	RUN	P_{TP}	T_{TP}	$F_{N/\delta}$	W_{PRI}	V_{PRI}	P_{TS}	T_{TS}	V_{SEC}	W_{SEC}
6	93	1.11	1233	4000	.812	664	1.19	520	549	3.20
(P&WA -109	94	1.15	1265	6000	.938	783	1.28	519	648	3.98
SWIRL)	95	1.19	1282	7000	1.05	872	1.33	519	702	4.38
	96	1.23	1310	8000	1.11	955	1.39	519	748	4.73
	97	1.26	1323	9000	1.21	1018	1.44	518	834	5.05
	98	1.33	1319	10000	1.39	1113	1.51	518	834	5.44
	99	1.35	1352	11000	1.43	1164	1.56	518	860	5.64
	100	1.39	1369	12000	1.42	1223	1.62	518	898	6.06
	101	1.44	1374	13000	1.55	1286	1.68	518	927	6.33
	102	1.51	1429	14000	1.64	1389	1.75	519	960	6.61
	103	1.54	1440	15000	1.63	1423	1.81	518	988	6.95
	104	1.62	1442	12380*	1.83	1502	1.89	519	1018	7.24
7	107	1.09	1263	4000	.532	606	1.13	516	465	3.04
(-117 P&WA)	108	1.23	1343	6000	.947	963	1.27	515	644	4.21
	109	1.27	1354	7000	1.11	1032	1.30	516	666	4.31
	110	1.31	1383	8000	1.16	1121	1.35	516	715	4.69
	111	1.36	1394	9000	1.22	1188	1.41	516	760	5.08
	112	1.41	1420	10000	1.29	1263	1.45	516	790	5.31
	113	1.46	1431	11000	1.44	1335	1.49	517	818	5.49
	114	1.52	1469	12000	1.48	1415	1.55	517	852	5.78
	115	1.57	1490	13000	1.59	1474	1.60	517	884	6.10
	116	1.64	1515	14000	1.66	1551	1.67	517	920	6.43
	117	1.70	1547	15000	1.73	1621	1.73	517	948	6.72
	118	1.76	1563	16000	1.79	1681	1.79	517	978	7.07
	119	1.81	1606	16900	1.81	1744	1.85	517	1002	7.27

* Corrected Net Thrust for FAR 36 Flight Conditions, 727-200 Airplane -

TABLE 2 (continued)

SUMMARY OF TEST CONDITIONS

		PRIMARY								
CONFIGURATION	RUN	P_{TP}	T_{TP}	$F_{N/\delta}$	W_{PRI}	V_{PRI}	P_{TS}	T_{TS}	V_{SEC}	W_{SEC}
8	125	1.10	1233	4000	.816	646	1.18	521	540	3.21
(BOEING-109)	126	1.16	1258	6000	.961	796	1.28	519	652	4.06
	127	1.21	1282	7000	1.14	902	1.33	518	700	4.41
	128	1.23	1304	8000	1.12	949	1.39	518	752	4.85
	129	1.27	1323	9000	1.22	1027	1.45	518	792	5.17
	130	1.32	1338	10000	1.36	1108	1.50	518	826	5.44
	131	1.36	1358	11000	1.41	1168	1.56	518	859	5.71
	132	1.40	1369	12000	1.48	1225	1.62	517	895	6.14
	133	1.44	1391	13000	1.52	1291	1.68	518	928	6.42
	134	1.48	1422	14000	1.58	1345	1.74	517	954	6.73
	135	1.54	1436	15000	1.67	1416	1.81	517	987	7.06
	136	1.62	1447	12380*	1.80	1502	1.89	517	1016	7.34
	137	1.42	1382	8460*	1.53	1262	1.63	518	902	6.08
	138	1.29	1334	6310*	1.32	1069	1.43	519	782	4.94
9	141	1.08	1263	4000	.529	584	1.13	513	460	2.98
(BOEING-117)	142	1.21	1341	6000	.927	924	1.26	511	623	4.01
	143	1.26	1362	7000	1.08	1031	1.31	511	675	4.37
	144	1.31	1371	8000	1.18	1113	1.35	512	711	4.61
	145	1.36	1396	9000	1.26	1187	1.40	512	750	4.90
	146	1.42	1418	10000	1.35	1273	1.45	513	785	5.14
	147	1.46	1443	11000	1.46	1333	1.49	514	819	5.43
	148	1.52	1469	12000	1.52	1418	1.56	514	856	5.73
	149	1.58	1499	13000	1.60	1487	1.60	515	883	5.93
	150	1.64	1515	14000	1.70	1556	1.67	515	916	6.25
	151	1.70	1544	15000	1.78	1626	1.73	516	947	6.53
	152	1.76	1562	16000	1.84	1681	1.78	516	972	6.78
	153	1.82	1592	16900	1.87	1744	1.85	516	998	7.07

* Corrected Net Thrust for FAR 36 Flight Conditions, 727-200 Airplane -

TABLE 2 (continued)

SUMMARY OF TEST CONDITIONS

		PRIMARY					SECONDARY			
CONFIGURATION	RUN	P_{TP}	T_{TP}	$F_{N/\delta}$	W_{PRI}	V_{PRI}	P_{TS}	T_{TS}	V_{SEC}	W_{SEC}
10	159	1.09	1262	4000	.625	597	1.14	522	473	2.81
(BOEING-117)	160	1.23	1349	6000	1.09	962	1.27	521	641	3.81
	161	1.27	1352	7000	1.21	1033	1.30	521	673	4.01
	162	1.31	1378	8000	1.28	1113	1.36	521	722	4.36
	163	1.35	1391	9000	1.36	1179	1.40	521	757	4.64
	164	1.41	1413	10000	1.46	1260	1.45	520	792	4.90
	165	1.46	1442	11000	1.57	1340	1.49	521	822	5.09
	166	1.52	1469	12000	1.63	1415	1.56	521	862	5.46
	167	1.58	1490	13000	1.76	1484	1.60	521	888	5.63
	168	1.63	1512	14000	1.81	1547	1.67	521	922	5.94
	169	1.70	1542	15000	1.87	1621	1.73	522	953	6.21
	170	1.76	1567	10000	1.96	1685	1.79	521	978	6.42
	171	1.82	1590	16900	2.04	1744	1.85	522	1005	6.71
11	177	1.20	1321	6000	.946	890	1.26	510	626	4.04
(BOEING-115)	178	1.24	1338	7000	1.09	983	1.30	511	665	4.28
	179	1.28	1358	8000	1.15	1053	1.35	511	708	4.63
	180	1.32	1376	9000	1.19	1121	1.40	511	748	4.98
	181	1.36	1391	10000	1.32	1208	1.47	511	797	5.41
	182	1.42	1411	11000	1.39	1276	1.51	511	824	5.59
	183	1.47	1443	12000	1.41	1346	1.58	511	870	6.09
	184	1.51	1456	13000	1.48	1402	1.64	511	899	6.39
	185	1.56	1476	14000	1.61	1475	1.68	512	920	6.52
	187	1.62	1496	15000	1.60	1525	1.76	512	958	7.01
	188	1.67	1521	16000	1.66	1585	1.81	512	981	7.21
	189	1.72	1535	16718	1.75	1633	1.85	512	998	7.38
	190	1.73	1519	12885*	1.58	1634	1.96	512	1039	8.17
	191	1.46	1393	8445*	1.39	1317	1.59	514	873	6.14
	192	1.30	1350	6310*	1.12	1083	1.41	515	758	5.13

* Corrected Net Thrust for FAR 36 Flight Conditions, 727-200 Airplane -

TABLE 2 (continued)

SUMMARY OF TEST CONDITIONS

		PRIMARY					SECONDARY			
CONFIGURATION	RUN	P_{TP}	T_{TP}	$F_{N/\delta}$	W_{PRI}	V_{PRI}	P_{TS}	T_{TS}	V_{SEC}	W_{SEC}
12	195	1.21	1317	6000	1.00	911	1.26	516	631	3.94
(P&WA-115)	196	1.24	1336	7000	1.04	986	1.30	515	671	4.24
	197	1.28	1374	8000	1.11	1065	1.35	514	712	4.56
	198	1.33	1374	9000	1.22	1137	1.40	514	755	4.90
	199	1.37	1394	10000	1.27	1207	1.46	514	796	5.29
	200	1.42	1411	11000	1.38	1276	1.51	514	827	5.51
	201	1.46	1431	12000	1.39	1330	1.57	514	866	5.95
	202	1.51	1452	13000	1.46	1401	1.63	515	899	6.22
	203	1.58	1478	14000	1.58	1478	1.69	515	927	6.47
	204	1.61	1503	15000	1.57	1526	1.75	515	958	6.85
	205	1.68	1524	16000	1.64	1595	1.82	515	988	7.19
	206	1.70	1546	16718	1.64	1624	1.85	515	1000	7.33
	207	1.73	1517	12885*	1.53	1635	1.97	515	1044	8.16
	208	1.45	1393	8445*	1.38	1307	1.58	516	874	6.09
	209	1.30	1343	6310*	1.12	1084	1.40	516	752	4.98
13	212	1.03	1030		.270	321	2.506			
(2" CONICAL	213	1.10	1030		.500	590	2.770			
- NO	214	1.20	1050		.702	807	2.906			
MUFFLER)	215	1.40	1030		1.00	1068	3.028			
	216	1.60	1026		1.25	1253	3.097			
	217	1.80	1026		1.45	1383	3.140			
	218	1.20	1425		.583	945	2.975			
	219	1.40	1422		.831	1258	3.099			
	220	1.60	1421		1.02	1477	3.169			
	221	1.80	1427		1.16	1629	3.211			
	222	1.80	563		1.97	1026	3.011			
	223	1.60	561		1.70	924	2.965			
	225	1.40	557		1.40	784	2.895			
	226	1.20	561		.999	590	2.770			
	227	1.10	563		.713	440	2.64			

* Corrected Net Thrust for FAR 36 Flight Conditions, 727-200 Airplane -

TABLE 3 - P&WA SPLITTER COORDINATES

EXH STA	SPLITTER CONFIGURATION NO.					
	S2		S3		S4	
	R_I~IN.	R_o~IN.	R_I~IN.	R_o~IN.	R_I~IN.	R_o~IN.
-1.07	------	------	------	------	14.943	16.765
-1.00	------	------	------	16.765	------	------
-0.42	14.943	16.765	14.943	16.730	14.943	------
0.0	------	------	------	------	------	16.680
0.58	14.943	16.765	14.943	16.644	14.943	------
1.00	------	------	------	------	------	16.586
1.58	15.030	16.780	14.950	16.530	14.943	------
2.00	------	------	------	------	------	16.410
2.58	15.245	16.810	15.100	16.400	14.950	------
3.00	------	------	------	------	------	16.264
3.58	15.650	16.835	15.280	16.276	14.975	------
4.00	------	------	------	------	------	16.086
4.58	16.000	16.860	15.400	16.140	15.050	------
5.00	------	------	------	------	------	15.906
5.58	16.270	16.890	15.460	15.990	15.135	------
6.00	------	------	------	------	------	15.728
6.58	16.455	16.900	15.478	15.850	15.175	------
7.00	------	------	------	------	------	15.544
7.58	16.520	16.840	15.436	15.700	15.110	------
8.00	------	------	------	------	------	15.332
8.58	16.515	16.735	15.330	15.516	14.960	------
9.00	------	------	------	------	------	15.048
9.58	16.400	16.575	------	------	14.710	------
9.85	------	------	------	------	14.630	14.790
9.86	------	------	15.140	15.300	------	------
10.00	16.330	16.500	------	------	------	------

TABLE 4 - BOEING SPLITTER COORDINATES

EXH STA	SPLITTER CONFIGURATION NO.					
	S5		S6		S7	
	R_I ~ IN.	R_o ~ IN.	R_I ~IN.	R_o ~ IN.	R_I ~ IN.	R_o ~ IN.
0	14.943	16.765	14.943	16.765	14.943	16.765
2.0	14.923	16.623	14.810	16.491	14.760	16.430
4.0	14.902	16.481	14.677	16.216	14.579	16.093
6.0	14.882	16.339	14.544	15.942	14.396	15.774
8.0	14.862	16.197	14.410	15.668	14.214	15.405
10.0	14.842	16.055	14.277	15.394	14.632	15.054
12.0	14.821	15.913	14.144	15.120	13.850	14.699
14.0	14.801	15.771	14.011	14.815	13.668	14.338
16.0	14.781	15.574	13.878	14.458	13.485	13.972
18.0	14.760	15.240	13.745	14.098	13.303	13.601
20.0	14.740	14.827	13.612	13.730	13.121	13.222
21.0	14.730	14.730	13.545	13.545	13.030	13.030

TABLE 5 - BOEING PLUG COORDINATES

EXH STA	PLUG CONFIGURATION NO.				
	P5-1	P5-2	P5-3	P5-3A	P7
	R_{PL}~IN.	R_{PL}~IN.	R_{PL}~IN.	R_{PL}~IN.	R_{PL}~IN.
0	5.651	5.651	5.651	5.651	5.651
2.0	5.530	5.651	5.651	5.651	5.530
4.0	5.255	5.702	5.708	5.708	5.419
6.0	4.923	5.869	5.898	5.898	5.310
8.0	4.568	6.030	6.178	6.178	5.198
10.0	4.191	6.188	6.544	6.544	5.091
12.0	3.780	6.339	6.987	6.987	4.985
14.0	3.325	6.490	7.329	7.329	4.880
16.0	2.803	6.637	7.588	7.588	4.776
18.0	2.166	6.712	7.653	7.653	4.602
20.0	-----	6.683	7.618	7.609	4.226
21.0	-----	6.661	7.599	7.555	4.005
23.0	-----	6.351	-----	7.380	3.464
25.0	-----	6.026	7.049	7.116	2.826
27.0	-----	-----	-----	6.762	1.996
29.0	-----	5.322	6.457	6.316	-----
33.0	-----	4.517	5.841	5.134	-----
37.0	-----	3.549	5.095	3.538	-----
41.0	-----	2.192	4.263	1.477	-----
45.0	-----	-----	3.233	-----	-----

7.2 FIGURES

EXH STA	NOZZLE OUTER WALL C4 *RADIUS~IN.
0	24.50
21.0	22.10
57.3	20.44

* FULL SCALE DIMENSIONS

EXH STA	NOZZLE EXIT CONFIGURATION NO. E5 *RADIUS ~IN.	E6 *RADIUS~IN.	E7 *RADIUS~IN.
66.0	19.24(D) 19.23(A)		
66.75		19.01(D) 19.01(A)	
66.99			18.93(D) 18.92(A)

NOTE: D - DESIGN DIMENSIONS
A - ACTUAL HARDWARE DIMENSIONS

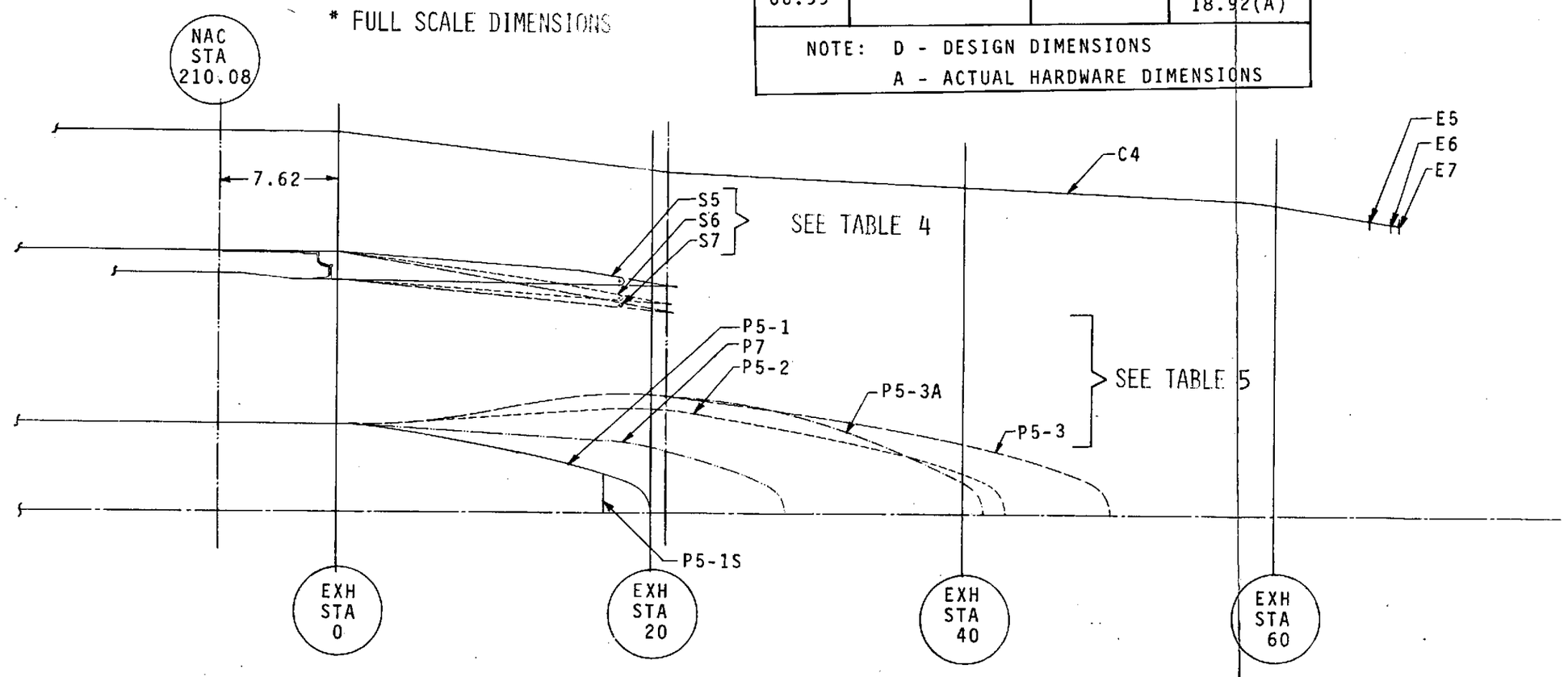

FIGURE 1 - BOEING CONFIGURATION NO. 2 EXHAUST NOZZLE TEST CONFIGURATIONS

FOLDOUT FRAME 1

FOLDOUT FRAME 2

EXH STA	NOZZLE OUTER WALL CONFIGURATION NO. C2 *RADIUS~IN.	C3 *RADIUS~IN.
0	20.5	24.5
6.0	18.0	----
21.0	----	22.1
27.08	17.18	22.1
46.76	17.18	22.1
52.03	-----	22.1

EXH STA	NOZZLE EXIT CONFIGURATION NO. E1 *RADIUS~IN.	E2 *RADIUS~IN.	E3 *RADIUS~IN.	E4 *RADIUS~IN.
60.64	14.92(D) 14.96(A)			
70.0		19.24(D) 19.22(A)	19.01(D) 18.99(A)	18.93(D) 18.92(A)

NOTE: D - DESIGN DIMENSIONS
A - ACTUAL HARDWARE DIMENSIONS

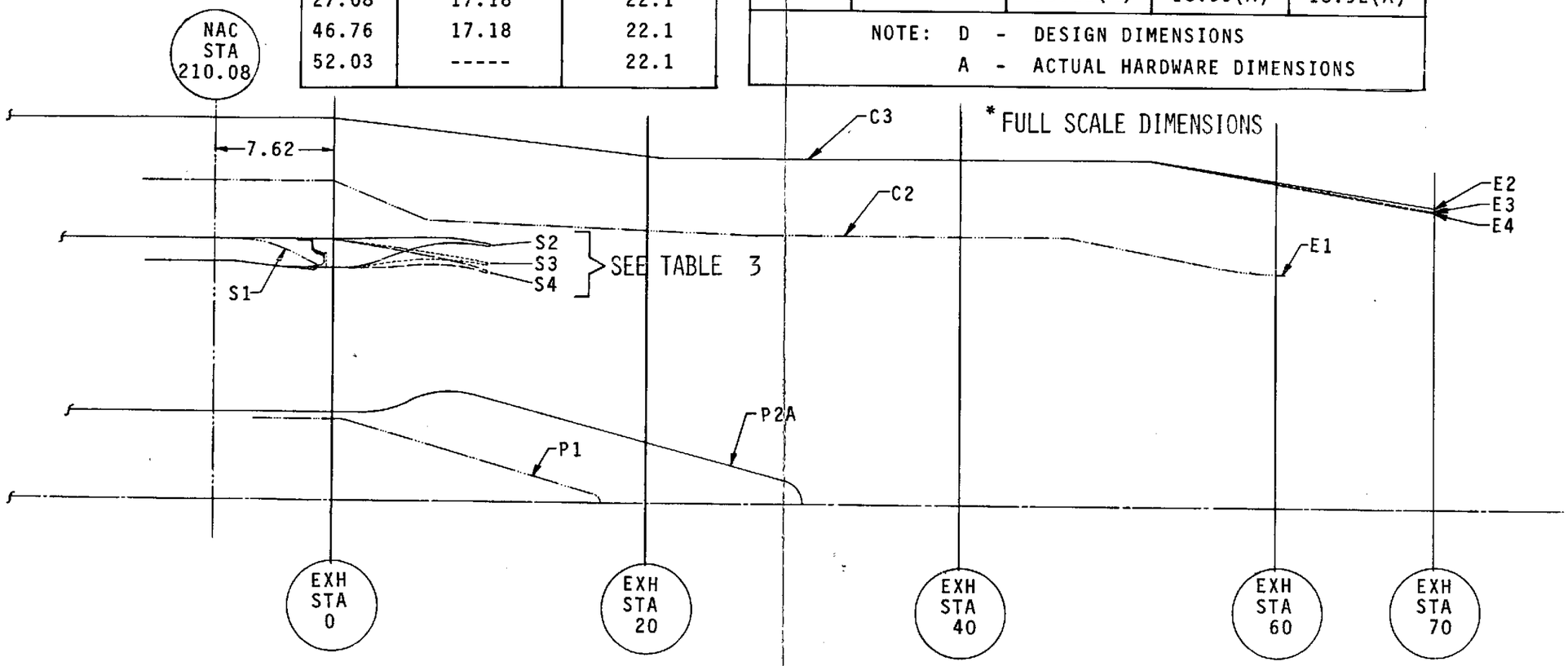

*FULL SCALE DIMENSIONS

FIGURE 2 - JT8D-9/727 & P&WA JT8D-100 REFERENCE NOZZLE TEST CONFIGURATIONS

FOLDOUT FRAME 1

FOLDOUT FRAME 2

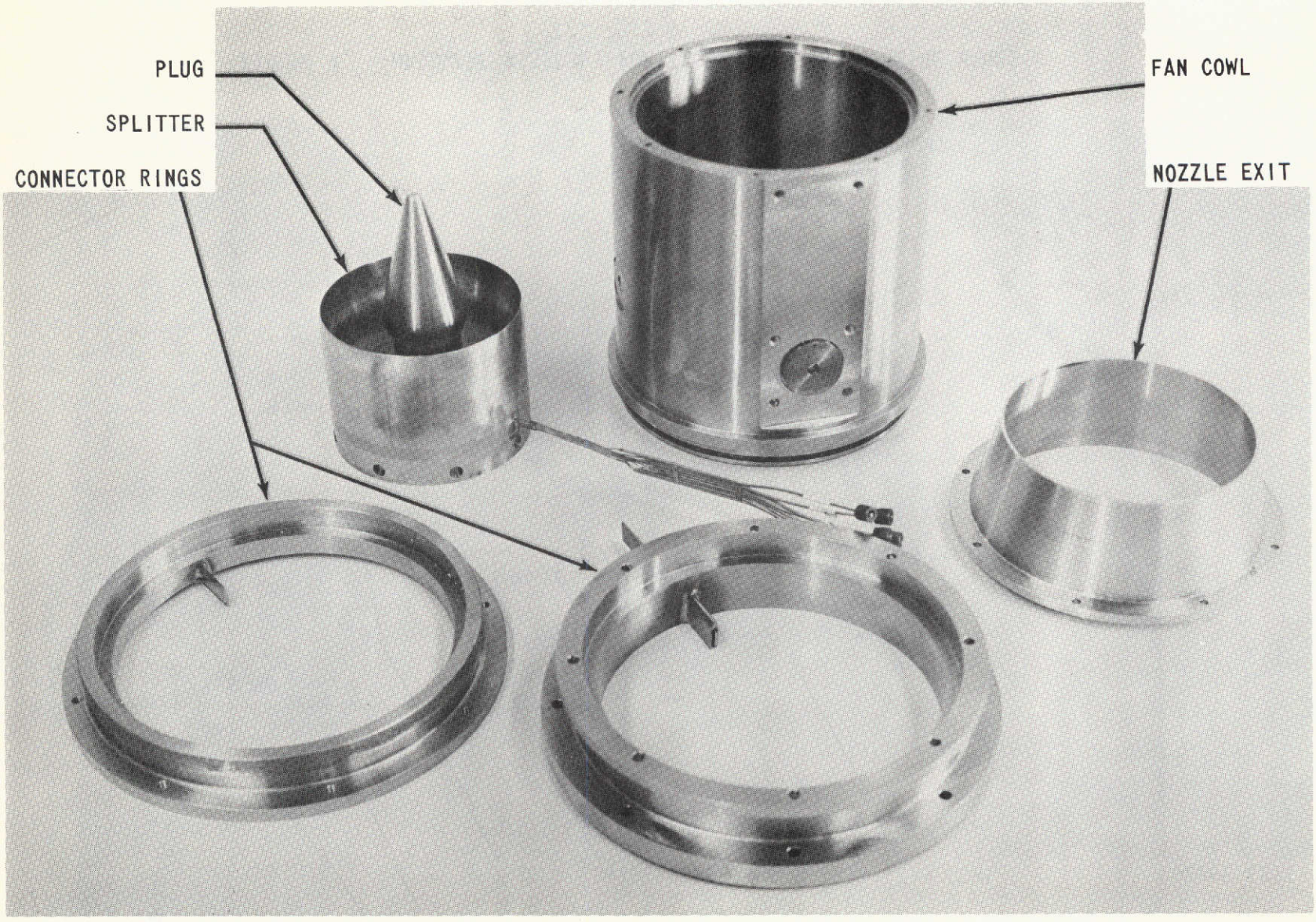

FIGURE 3. - HARDWARE COMPONENTS FOR TYPICAL TEST NOZZLE

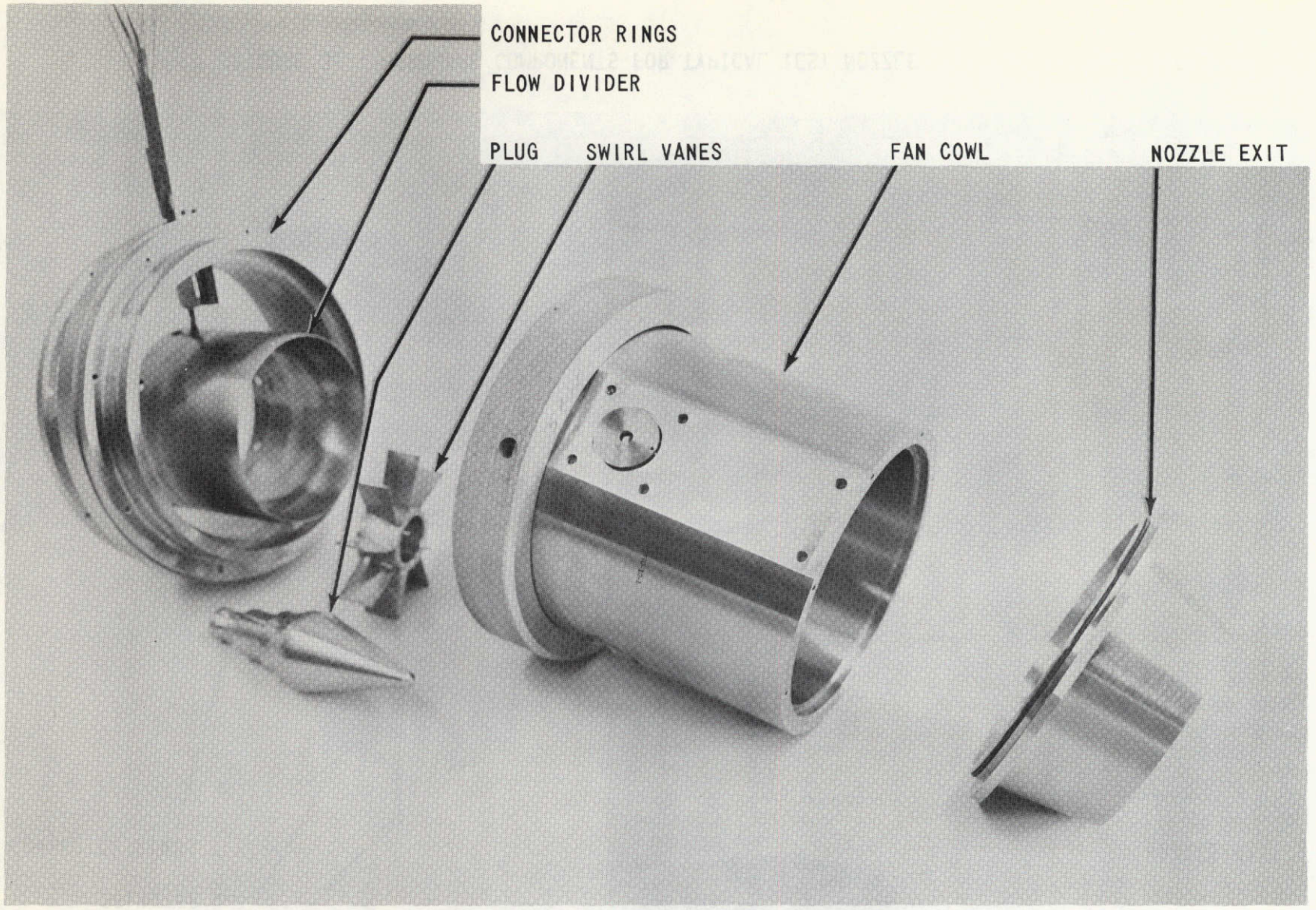

FIGURE 4. - HARDWARE ASSEMBLY FOR TEST NOZZLE WTIH SWIRL VANES

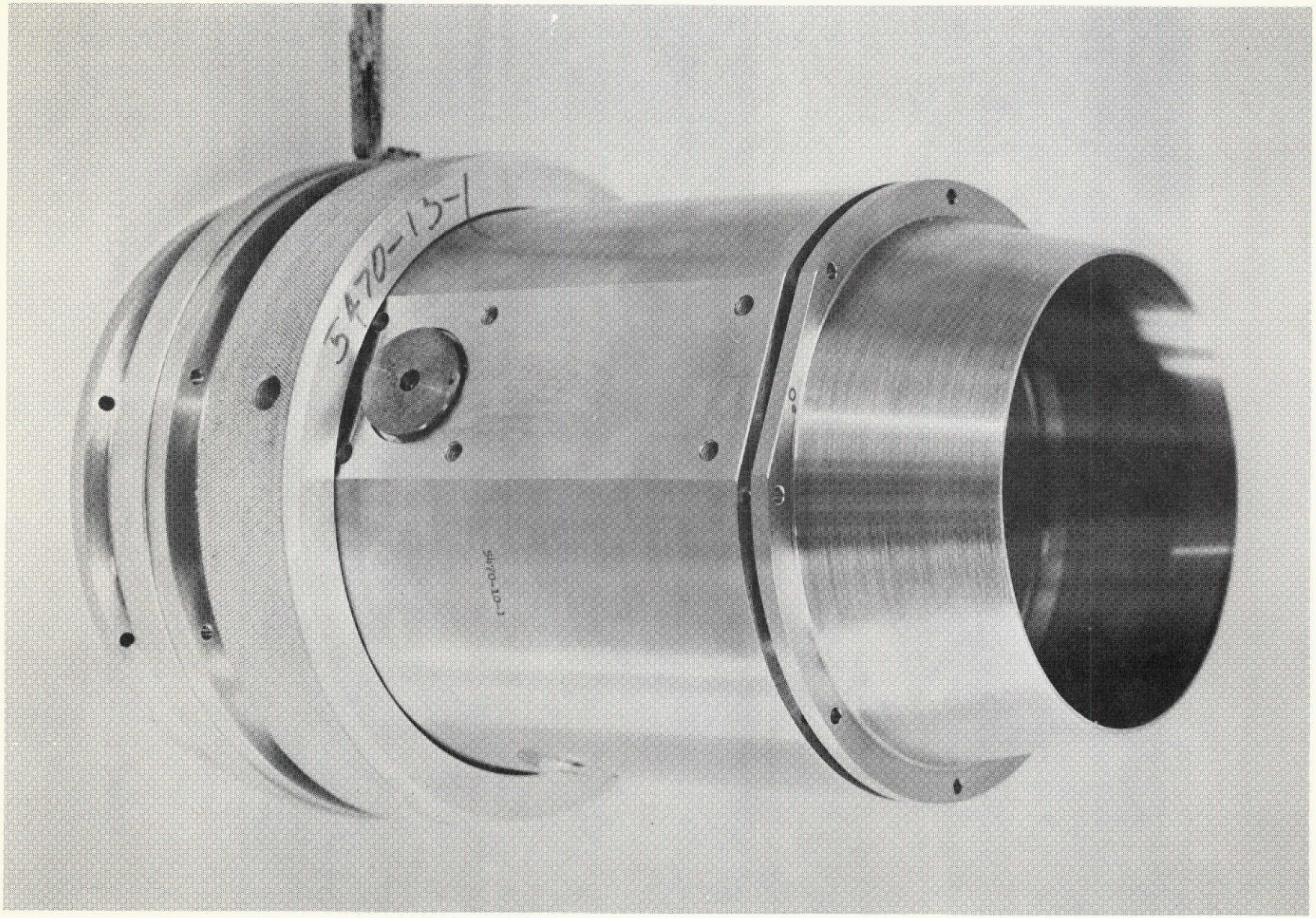

FIGURE 5. - TYPICAL TEST NOZZLE, ASSEMBLED

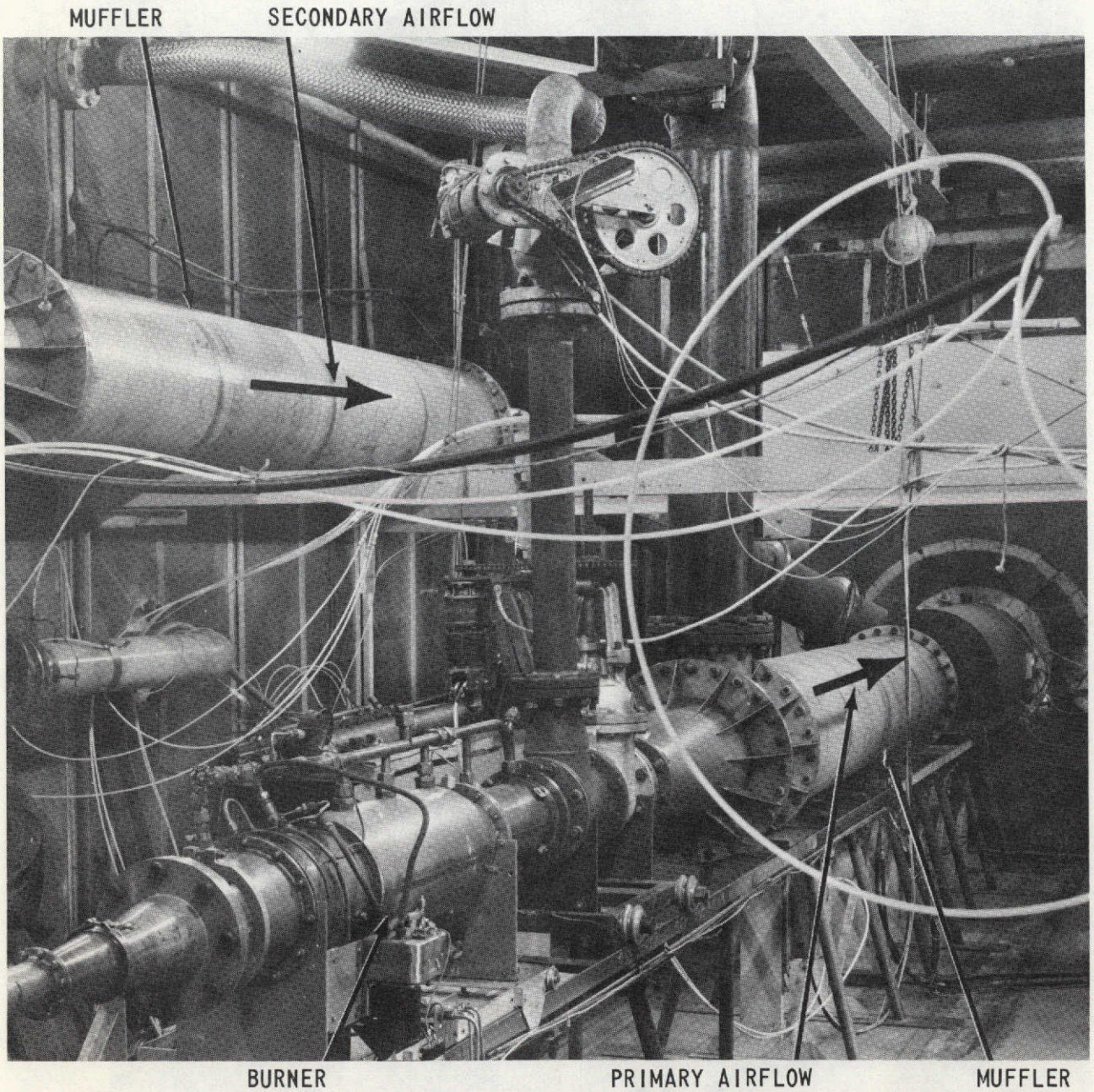

FIGURE 6. - INTERIOR VIEW OF WALL ISOLATION FACILITY

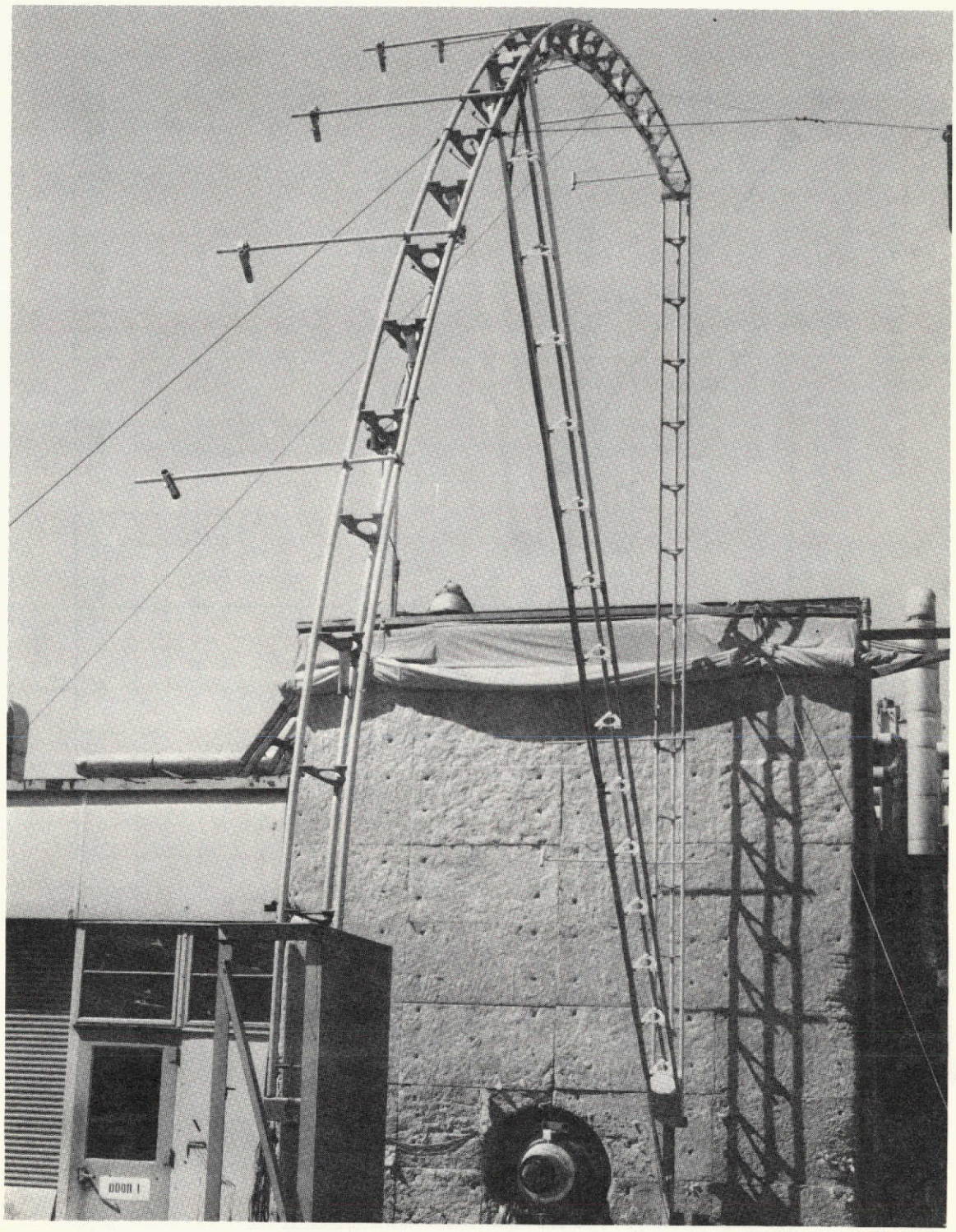

FIGURE 7. - ACOUSTIC TEST ARENA, WALL ISOLATION FACILITY

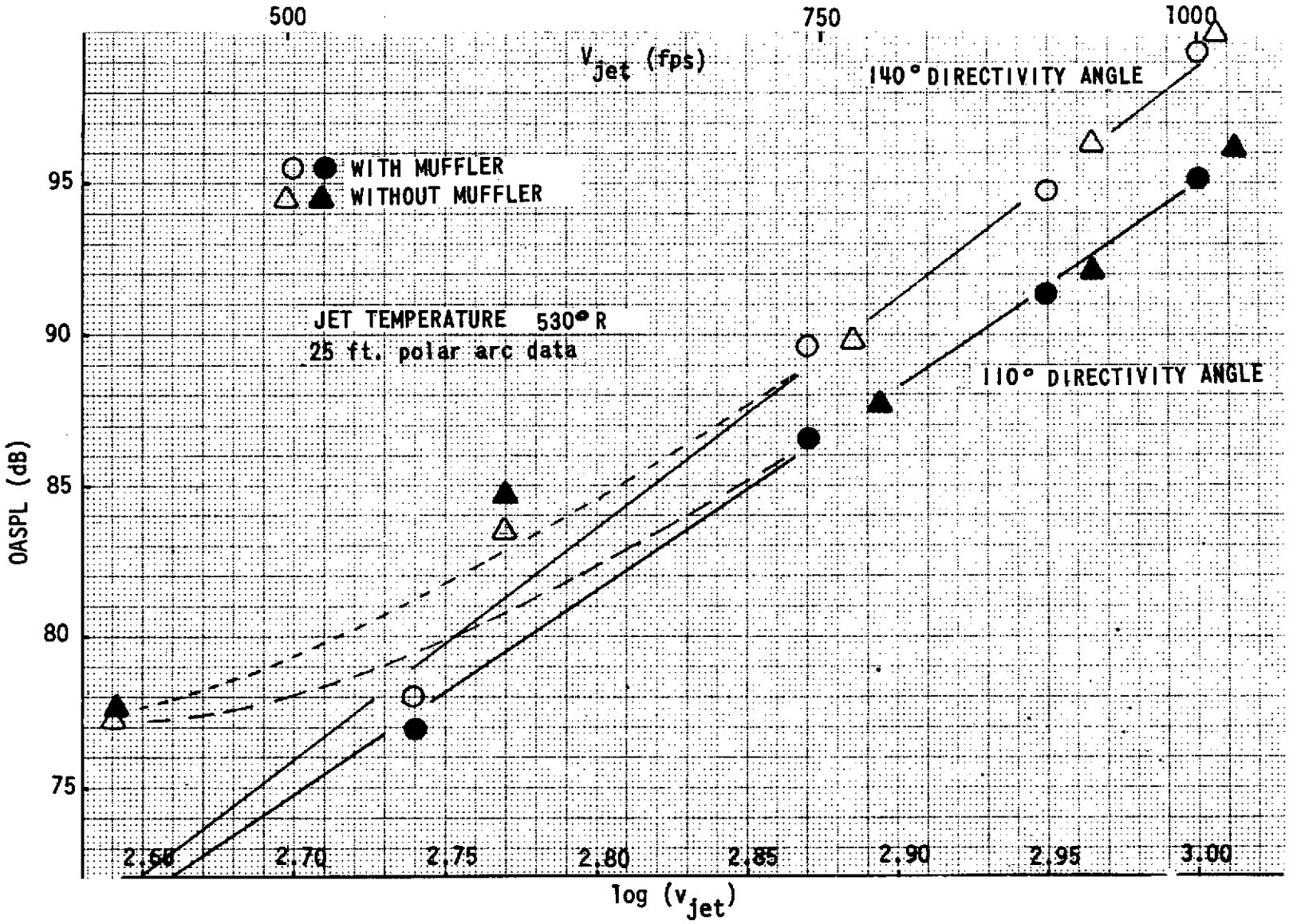

FIGURE 8. - COMPARISON OF 2" CONICAL NOZZLE THROTTLING CURVE WITH AND WITHOUT MUFFLER

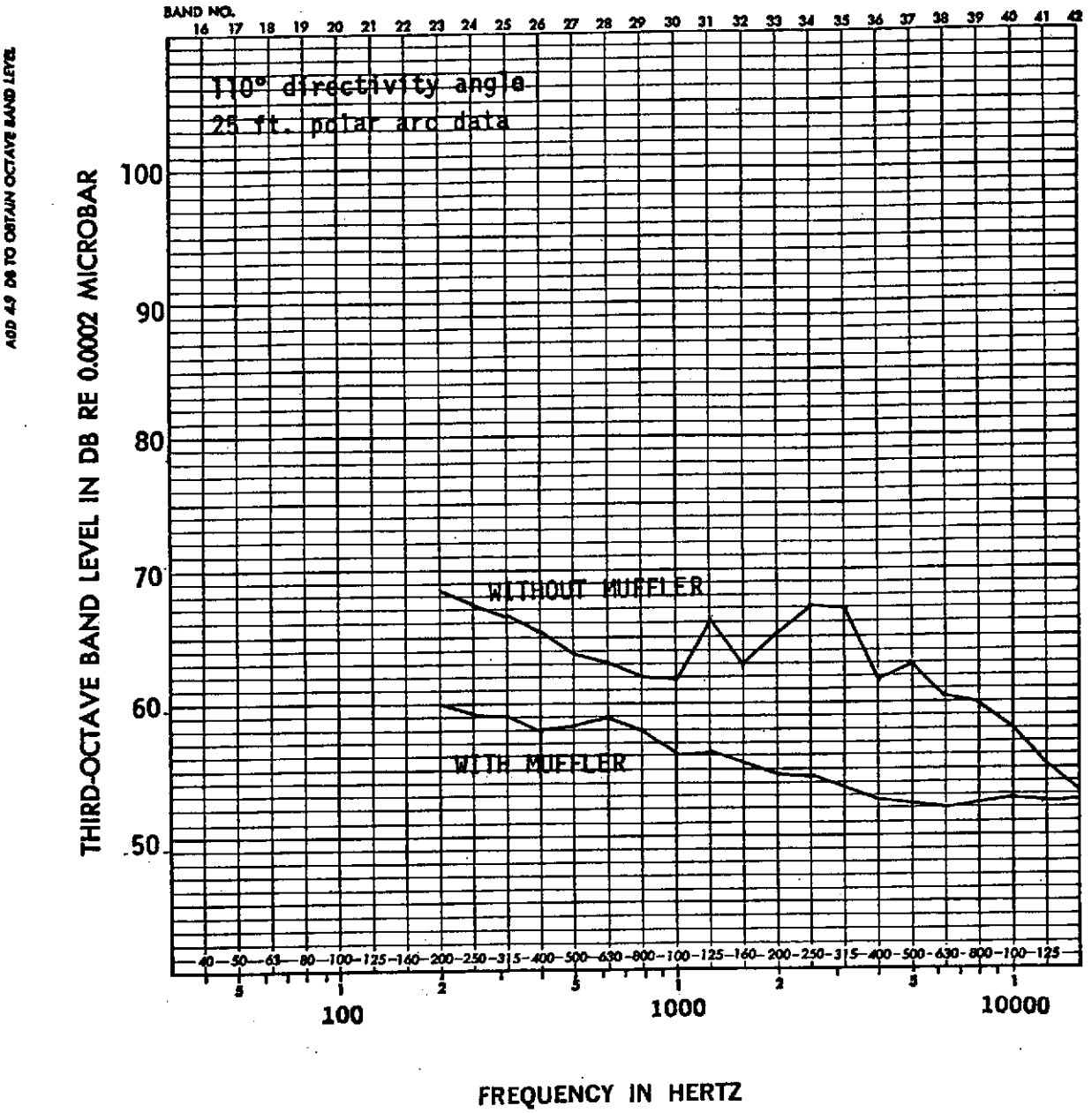

FIGURE 9. 2" CONICAL NOZZLE SPECTRA
v = 427 ft/sec
T = 530 °R

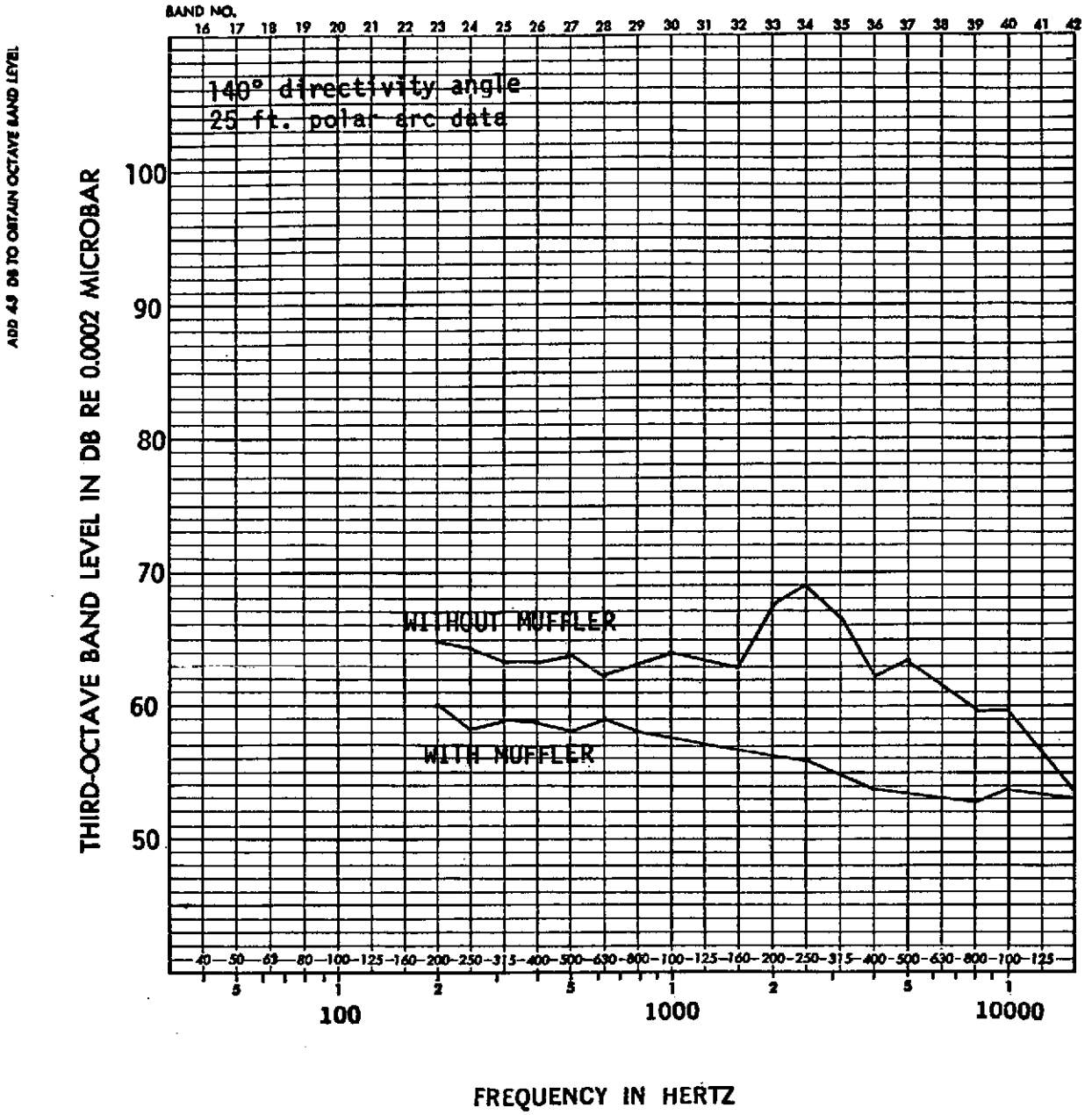

FIGURE 10. 2" CONICAL NOZZLE SPECTRA
v = 427 ft/sec
T = 530 ^{o}R

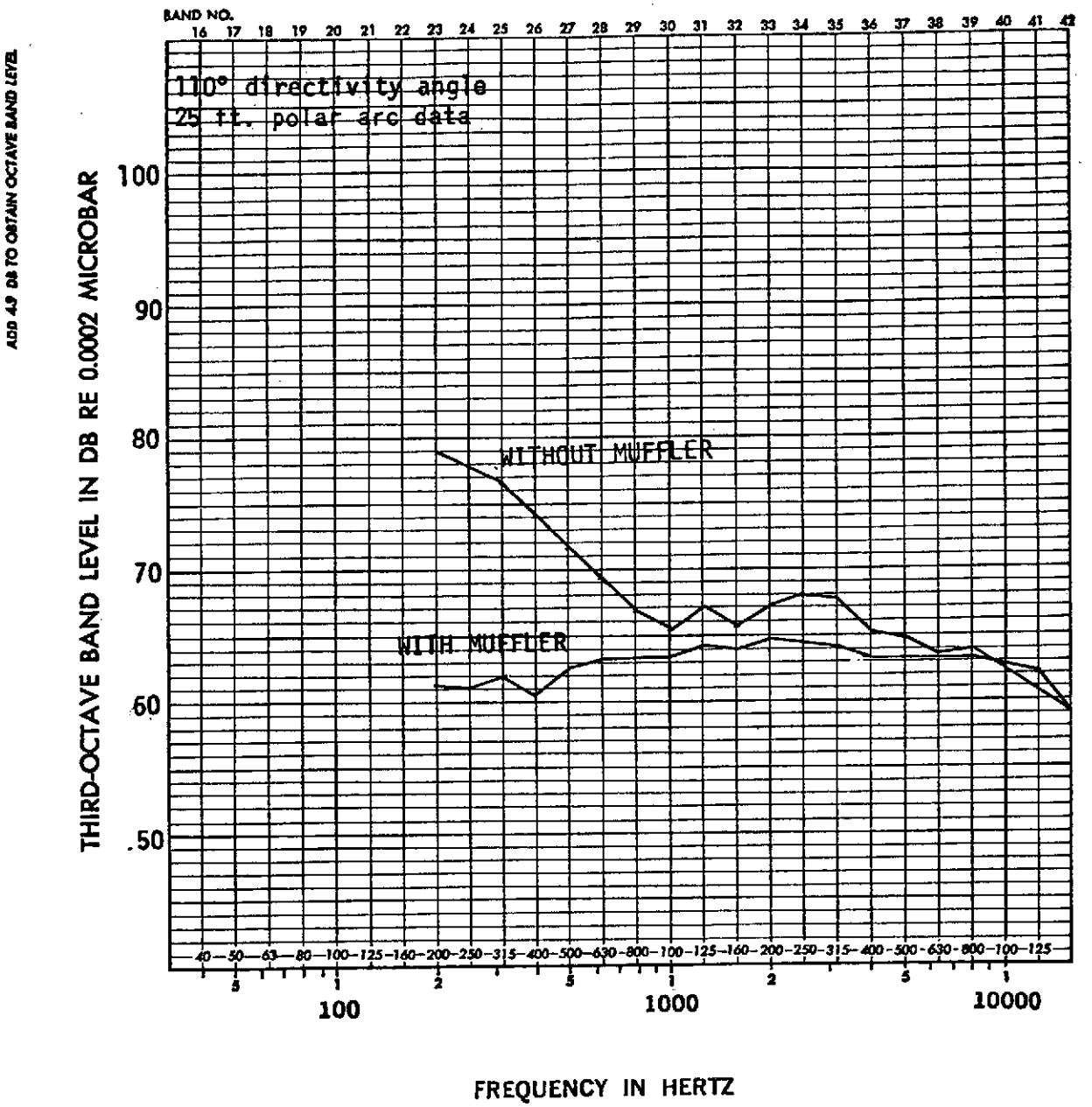

FIGURE 11. 2" CONICAL NOZZLE SPECTRA
v = 553 ft/sec
T = 530 ^{0}R

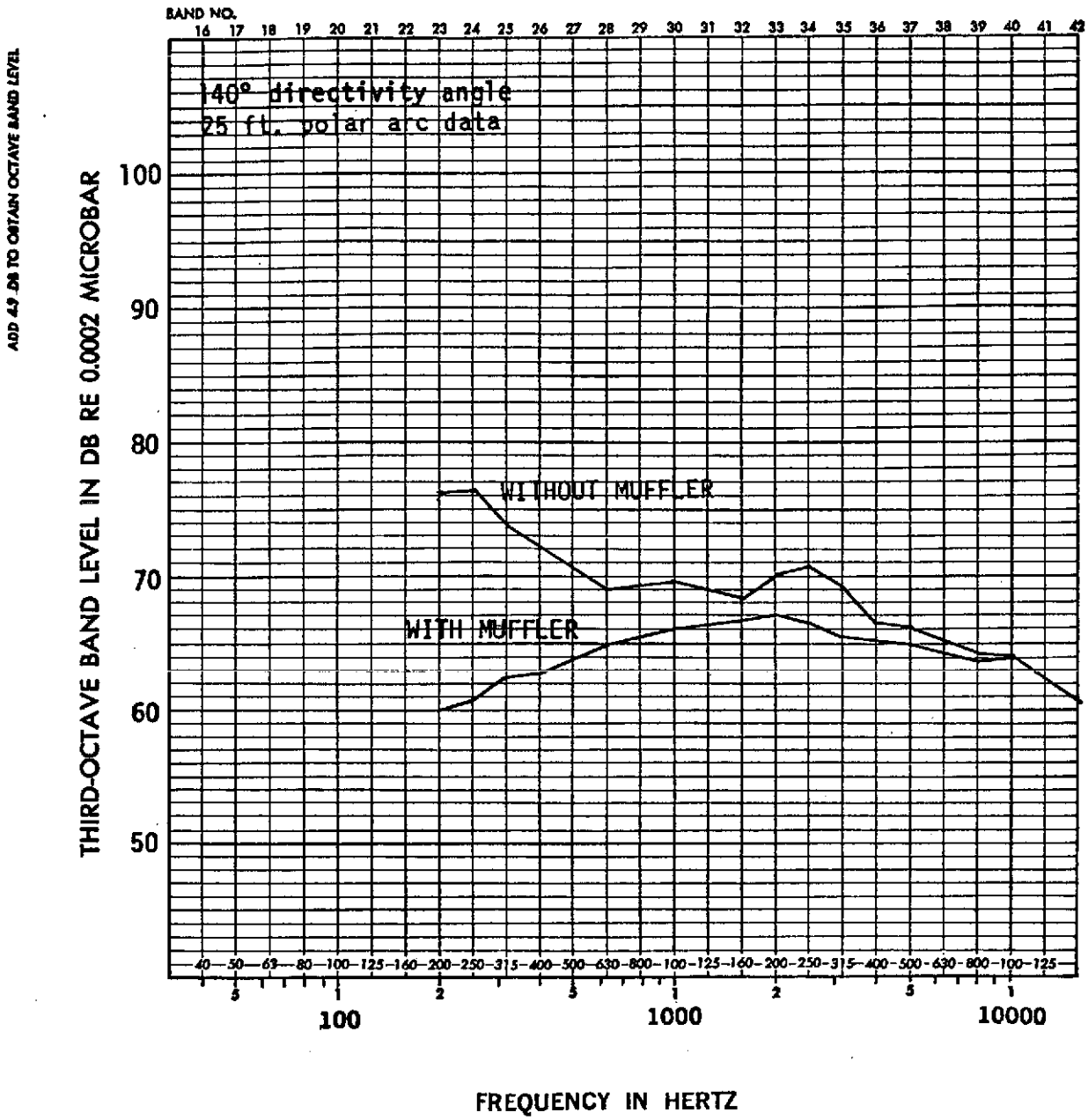

FIGURE 12. 2" CONICAL NOZZLE SPECTRA
v = 553 ft/sec
T = 530 ^{o}R

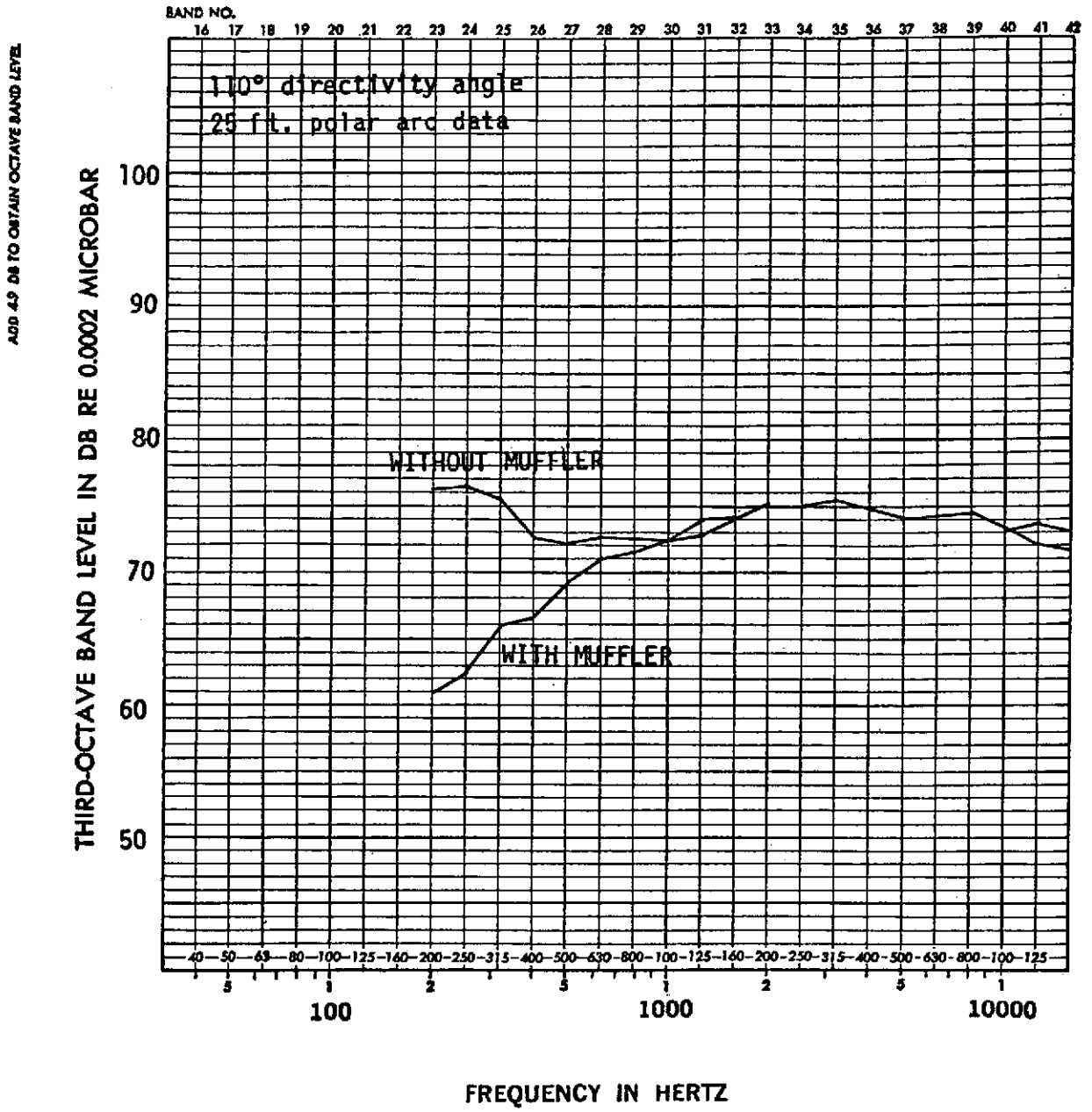

FIGURE 13. 2" CONICAL NOZZLE SPECTRA
v = 742 ft/sec
T = 530 ^{o}R

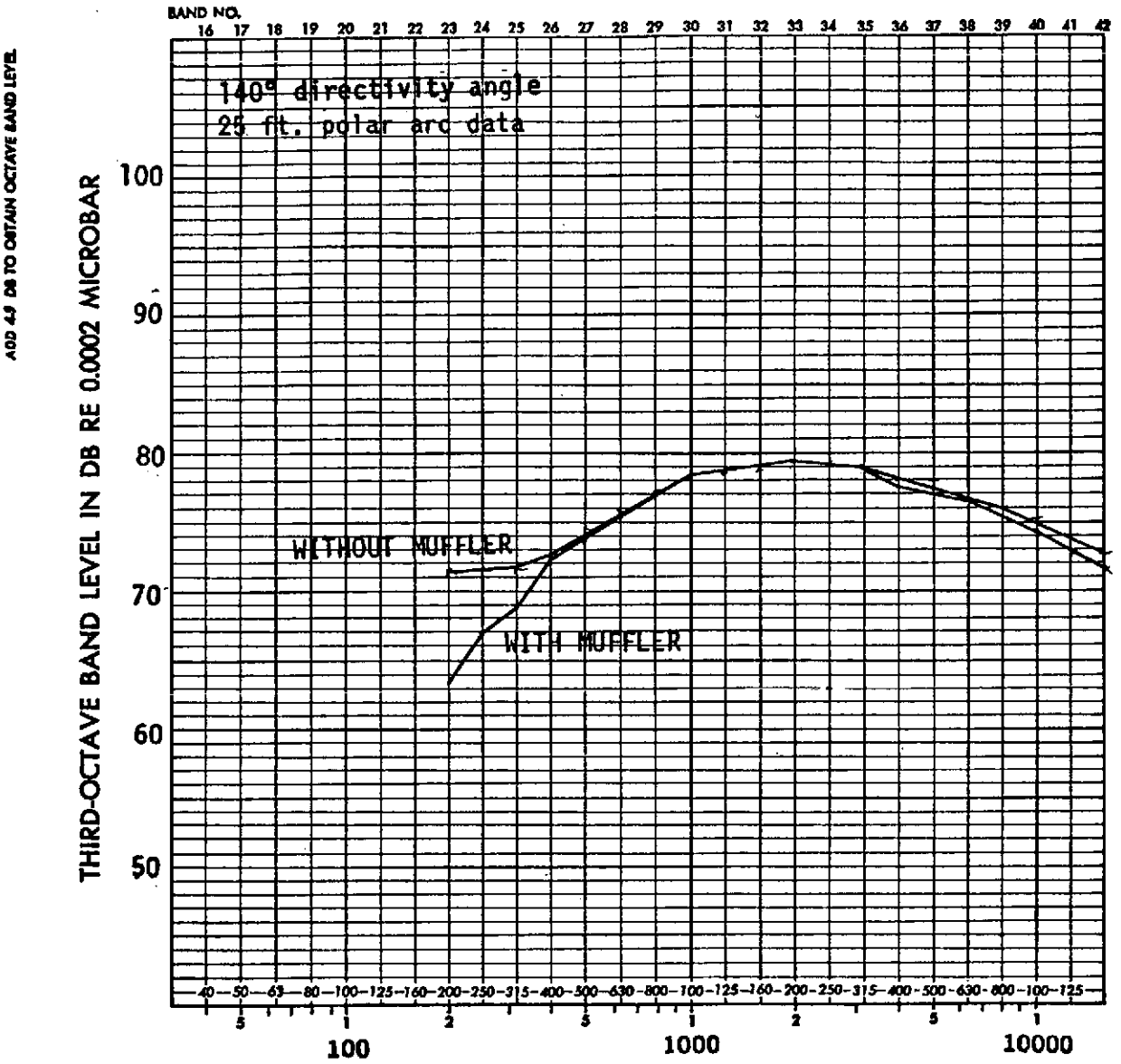

FIGURE 14. 2" CONICAL NOZZLE SPECTRA
v = 742 ft/sec
T = 530 °R

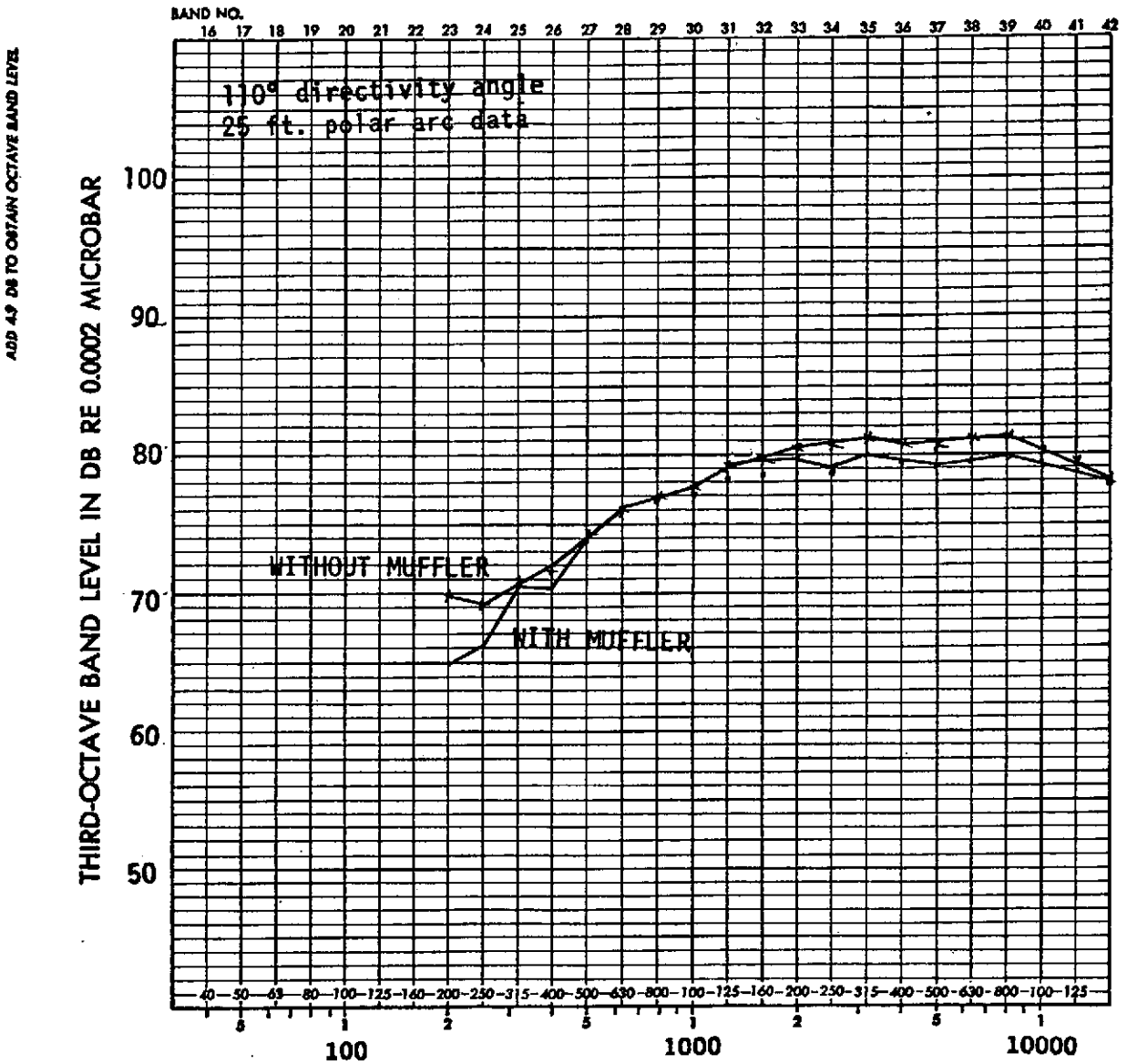

FIGURE 15. 2" CONICAL NOZZLE SPECTRA
V = 904 ft/sec
T = 530°R

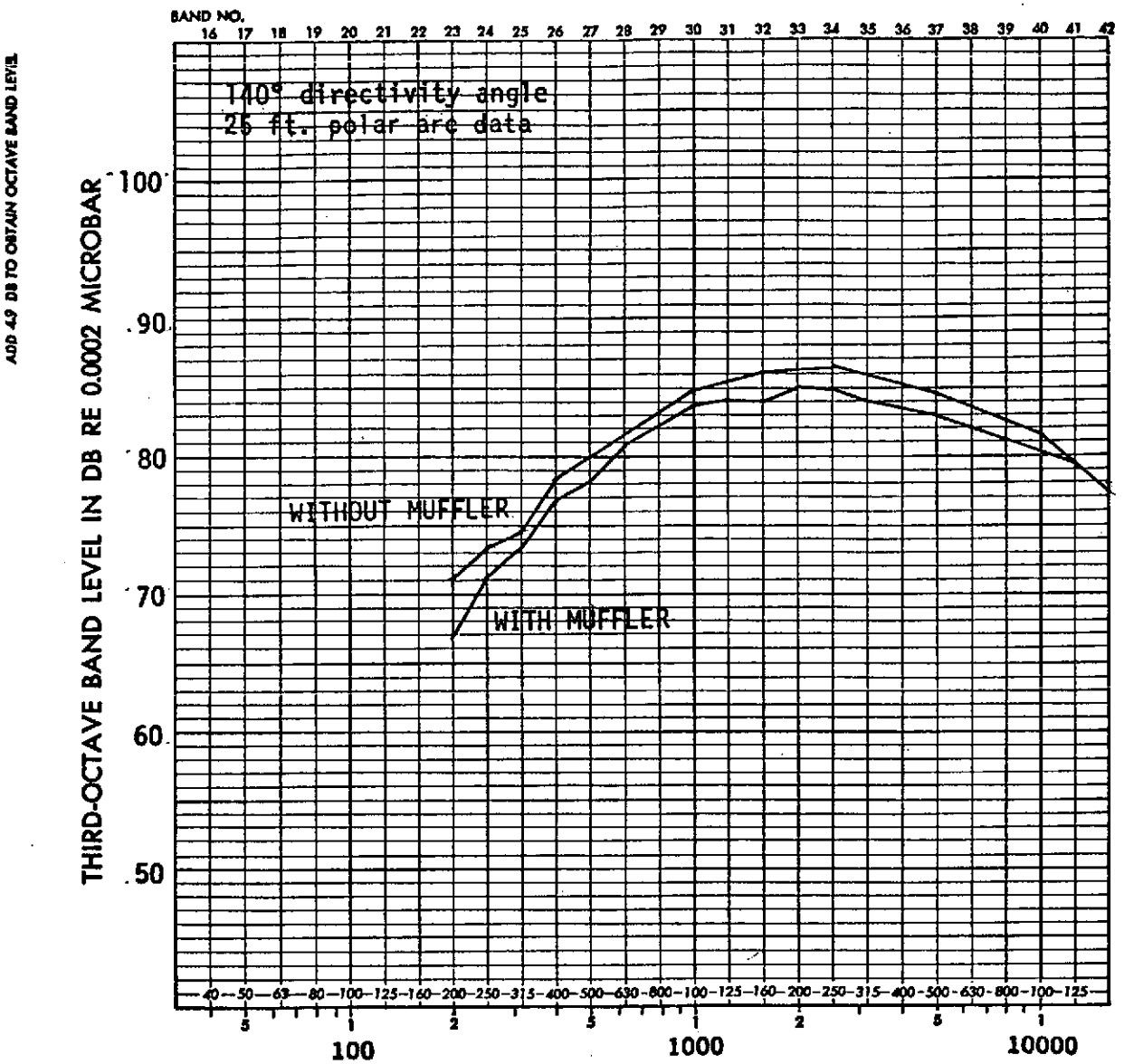

FIGURE 16. 2" CONICAL NOZZLE SPECTRA
v = 904 ft/sec
T = 530 ^{o}R

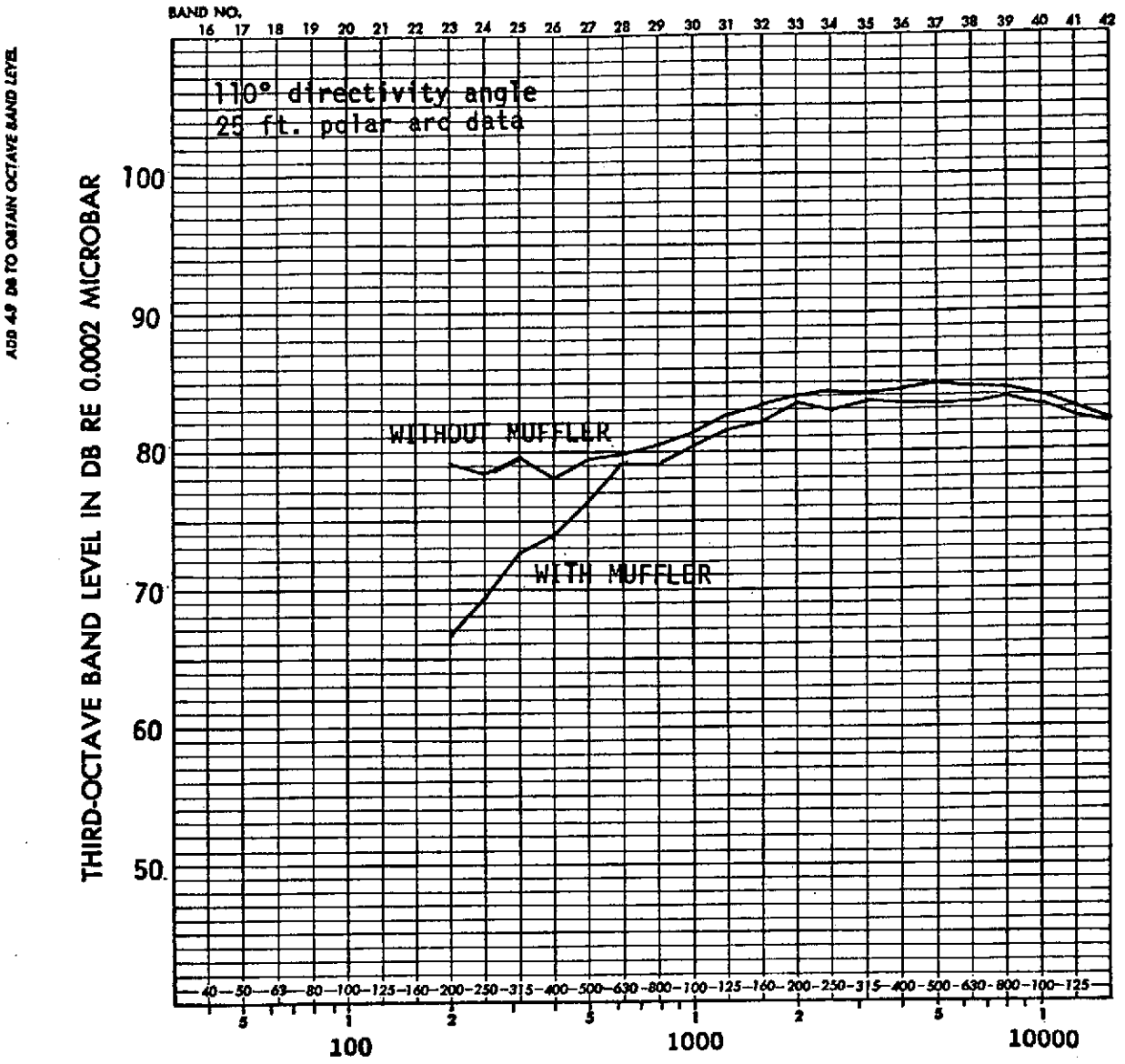

FIGURE 17. 2" CONICAL NOZZLE SPECTRA
v = 999 ft/sec
T = 530 °R

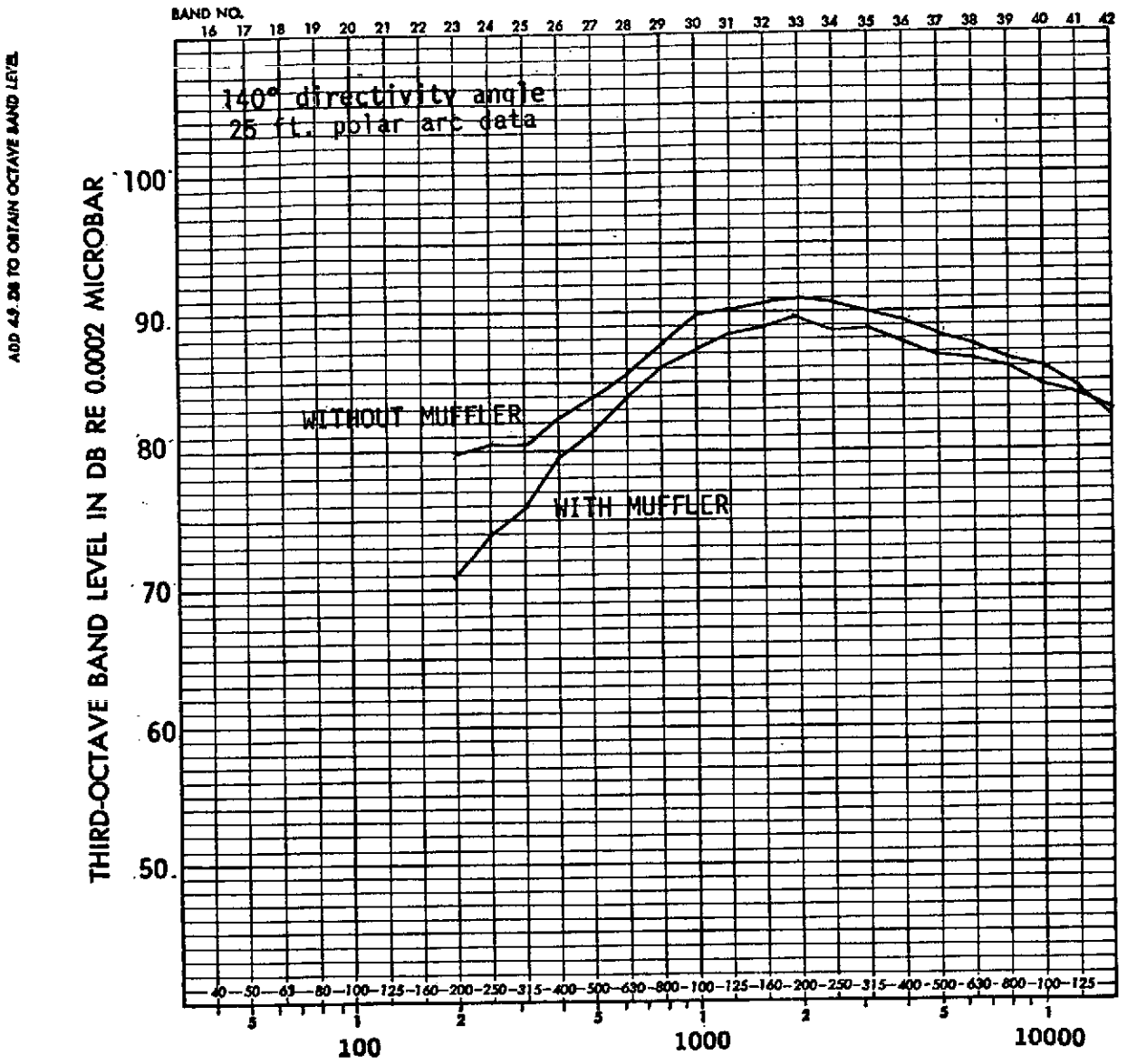

FIGURE 18. 2" CONICAL NOZZLE SPECTRA
v = 999 ft/sec
T = 530 °R

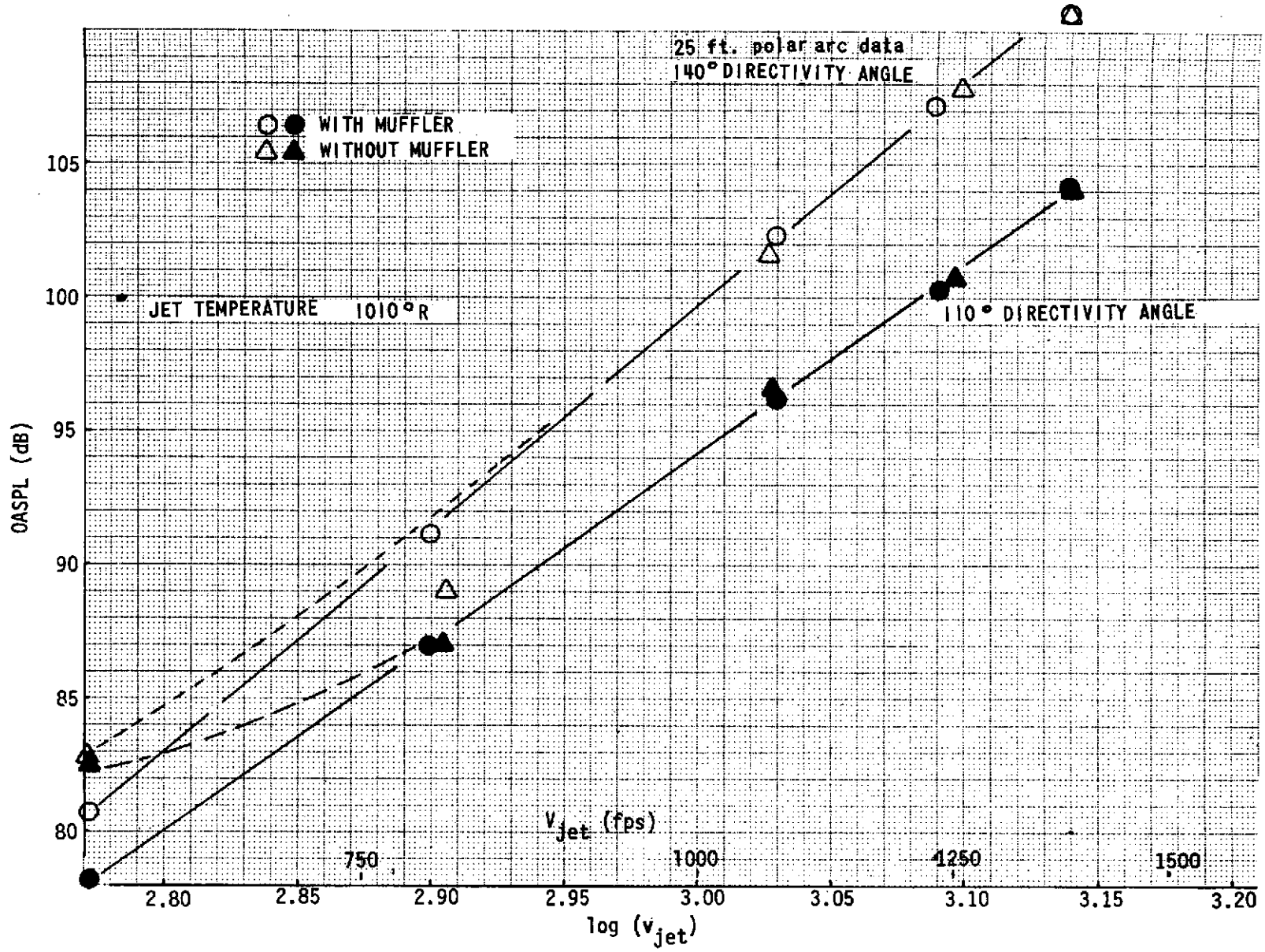

FIGURE 19. - COMPARISON OF 2" CONICAL NOZZLE THROTTLING CURVE WITH AND WITHOUT MUFFLER

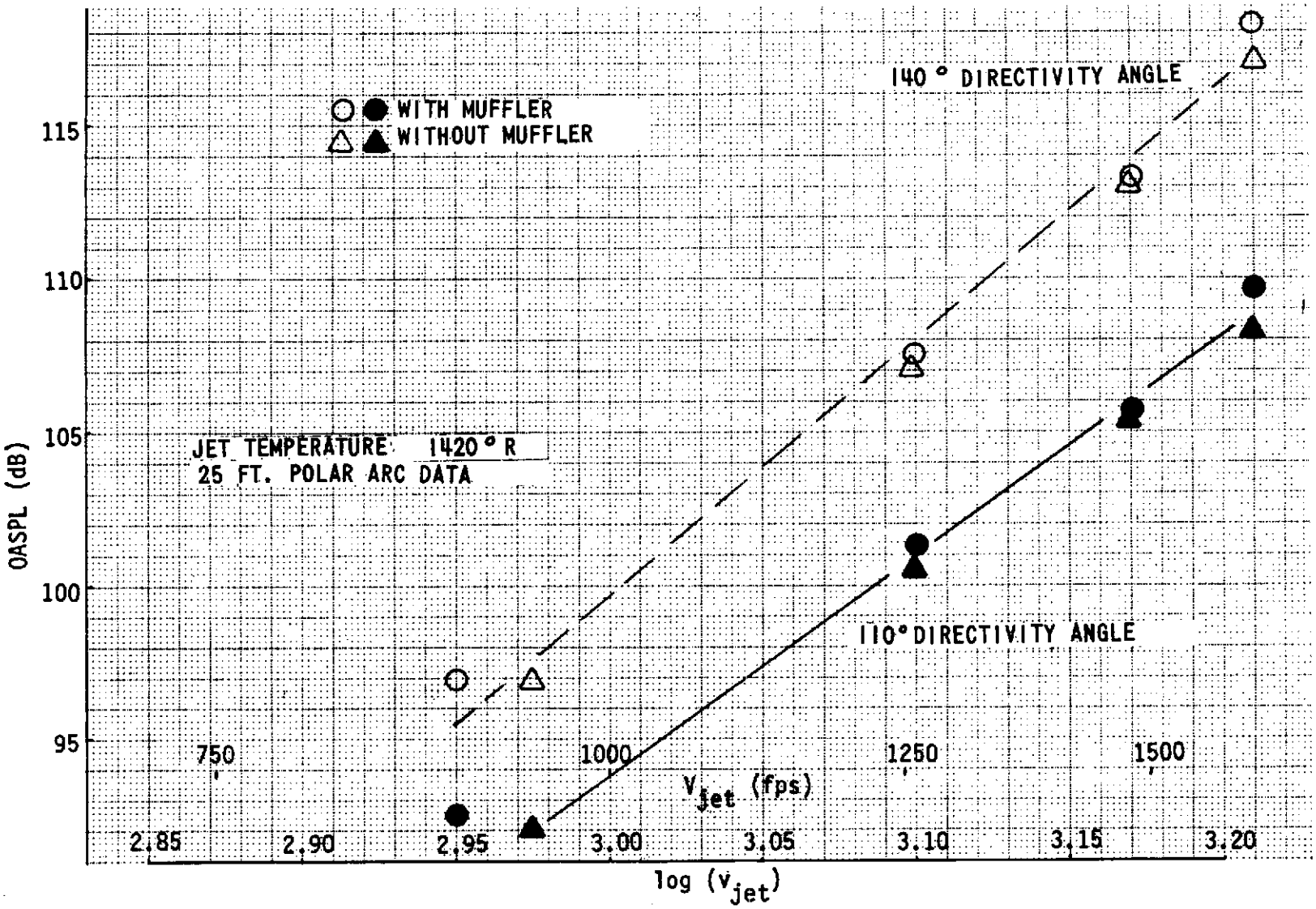

FIGURE 20. - COMPARISON OF 2" CONICAL NOZZLE THROTTLING CURVE WITH AND WITHOUT MUFFLER

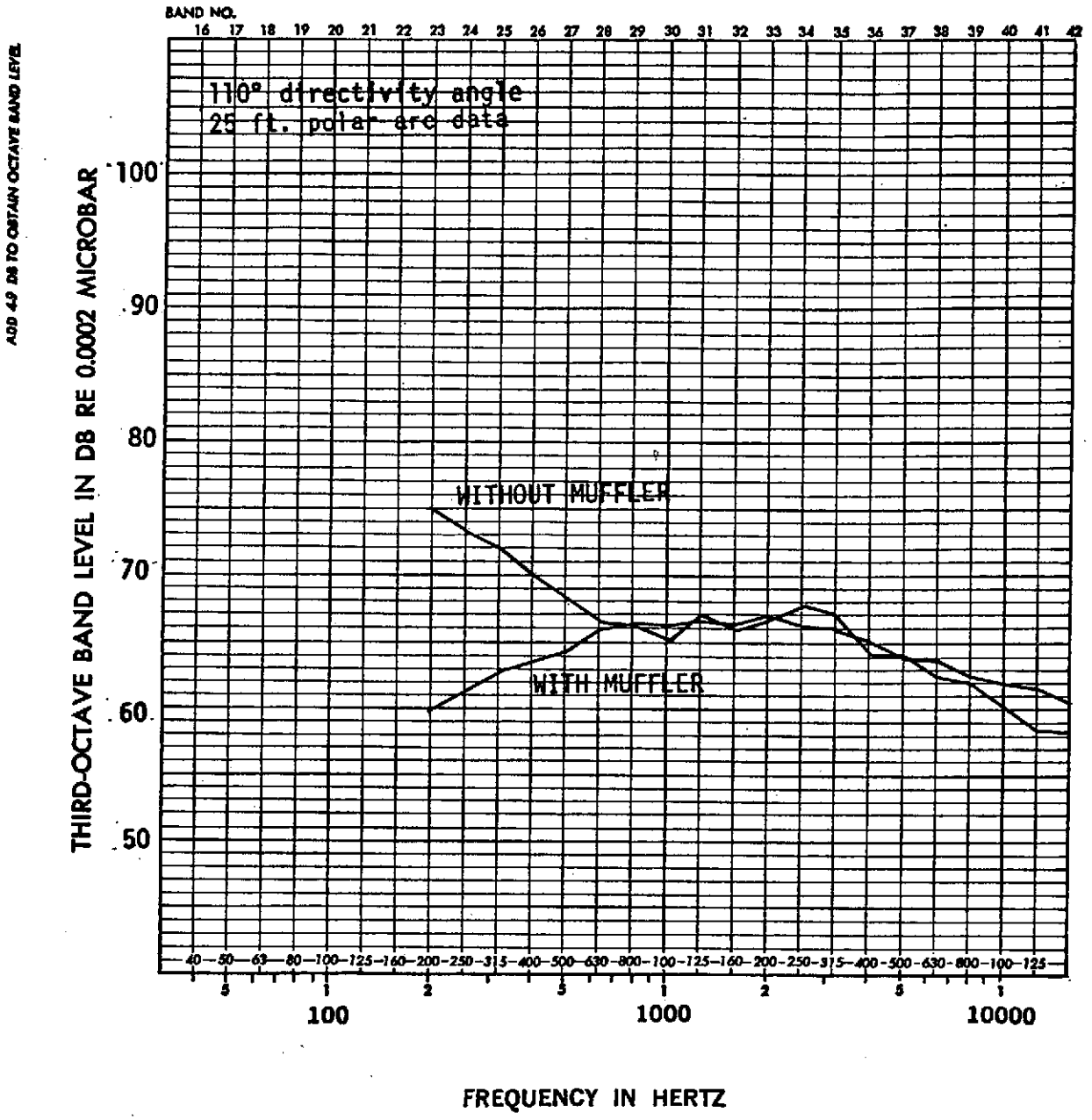

FIGURE 21. 2" CONICAL NOZZLE SPECTRA
v = 594 ft/sec
T = 1010 ^{o}R

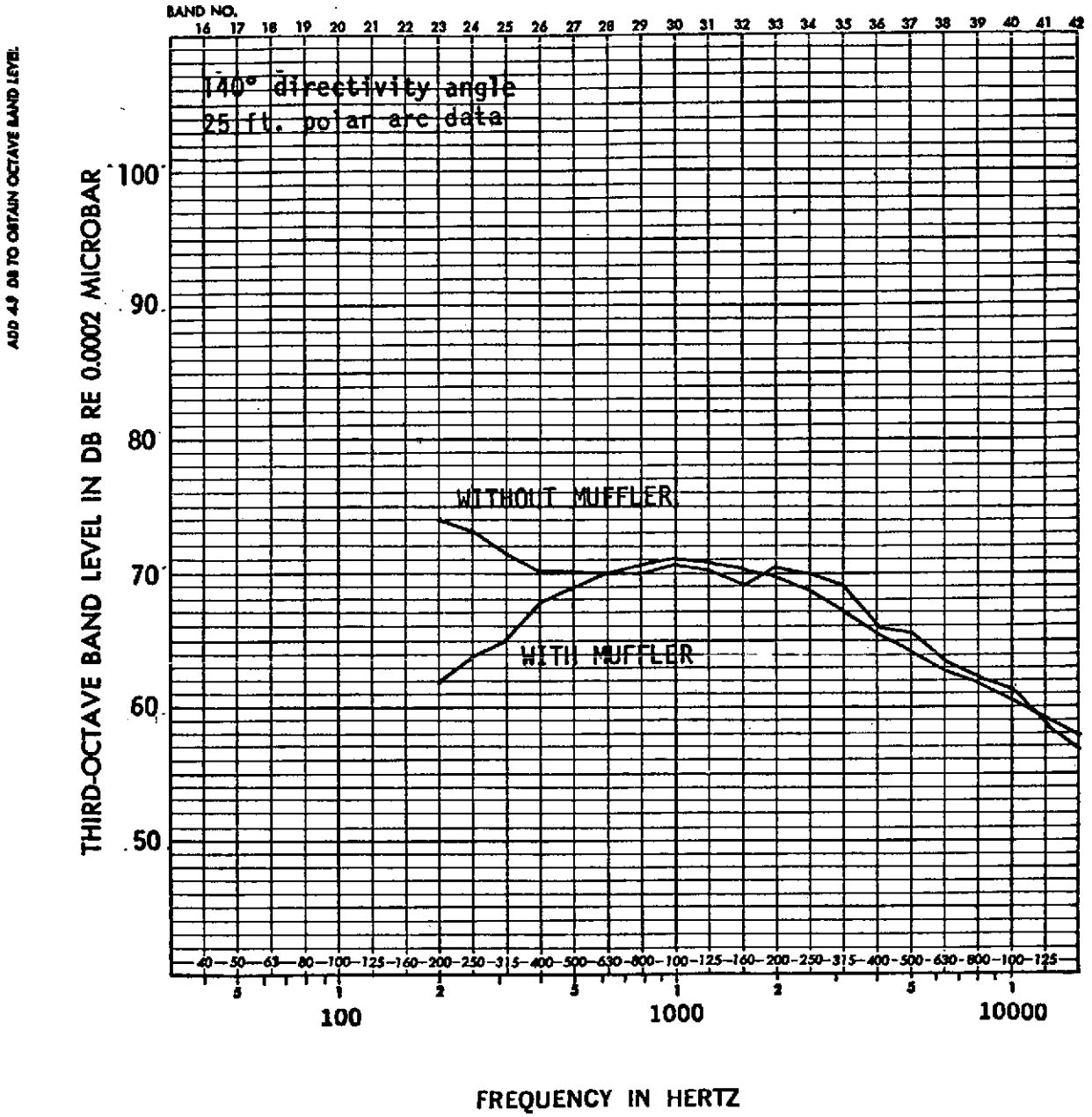

FIGURE 22. 2 " CONICAL NOZZLE SPECTRA
v = 594 ft/sec
T = 1010 °R

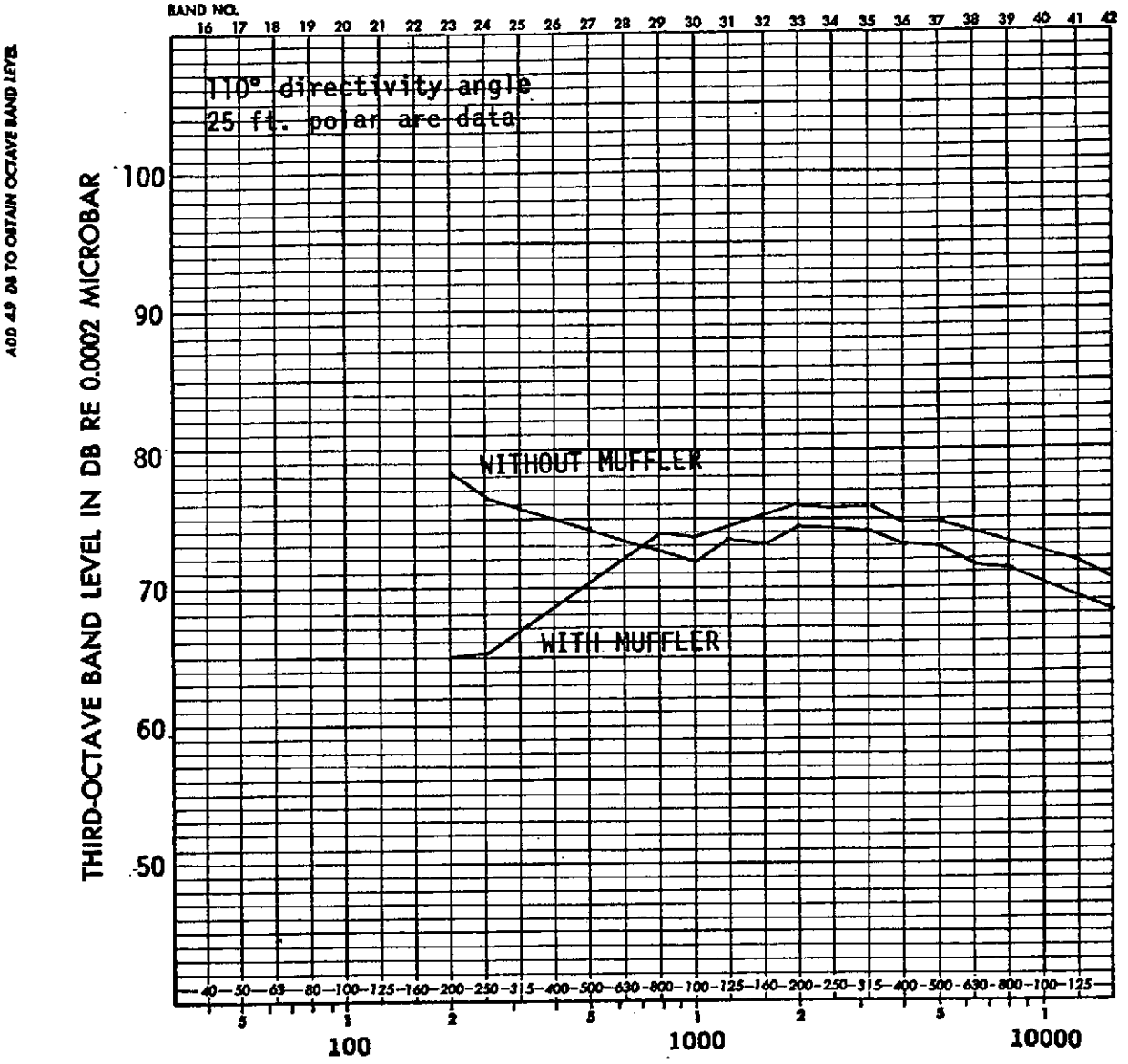

FIGURE 23. 2" CONICAL NOZZLE SPECTRA
v = 805 ft/sec
T = 1010 °R

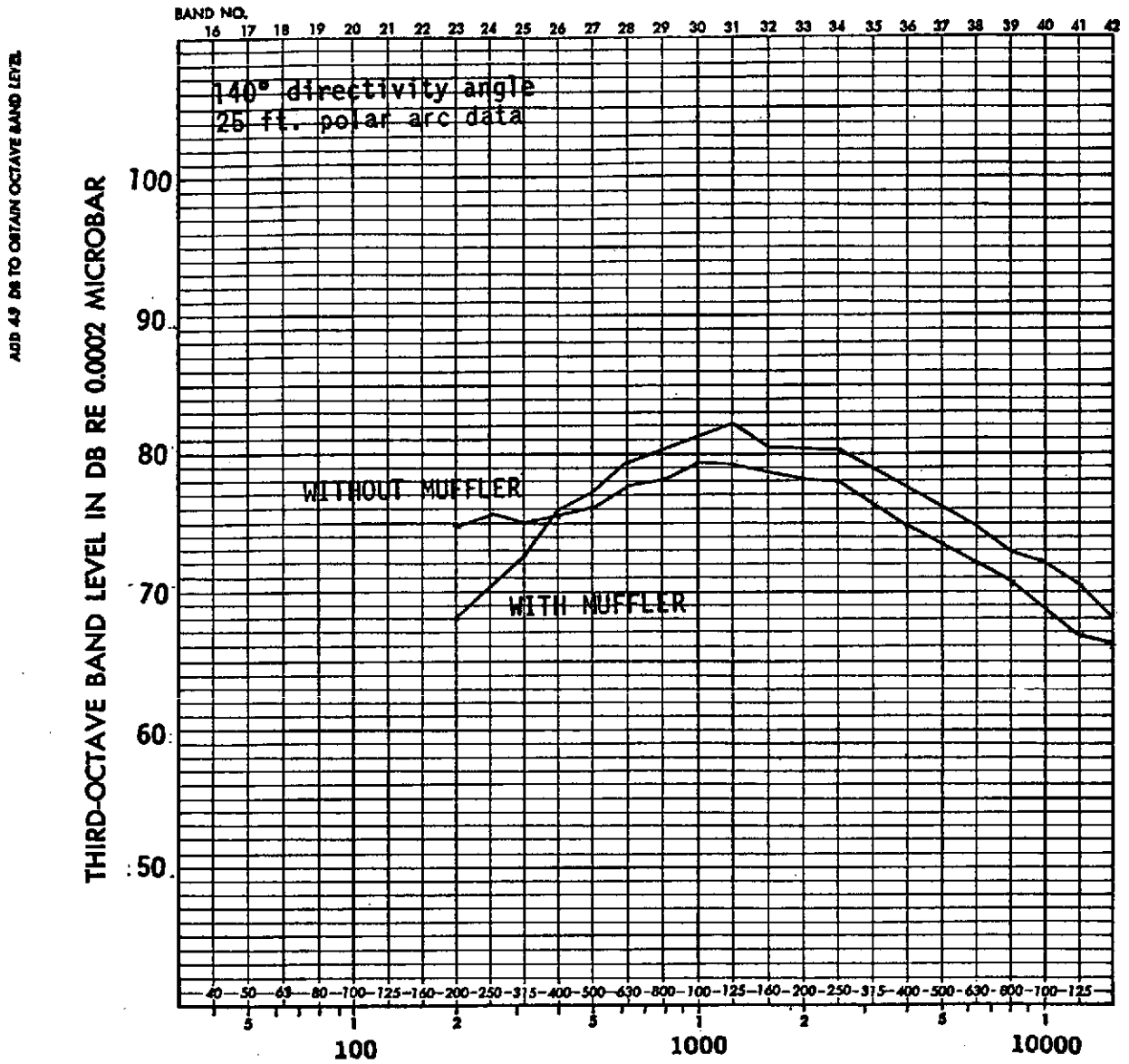

FIGURE 24. 2" CONICAL NOZZLE SPECTRA
v = 805 ft/sec
T = 1010 °R

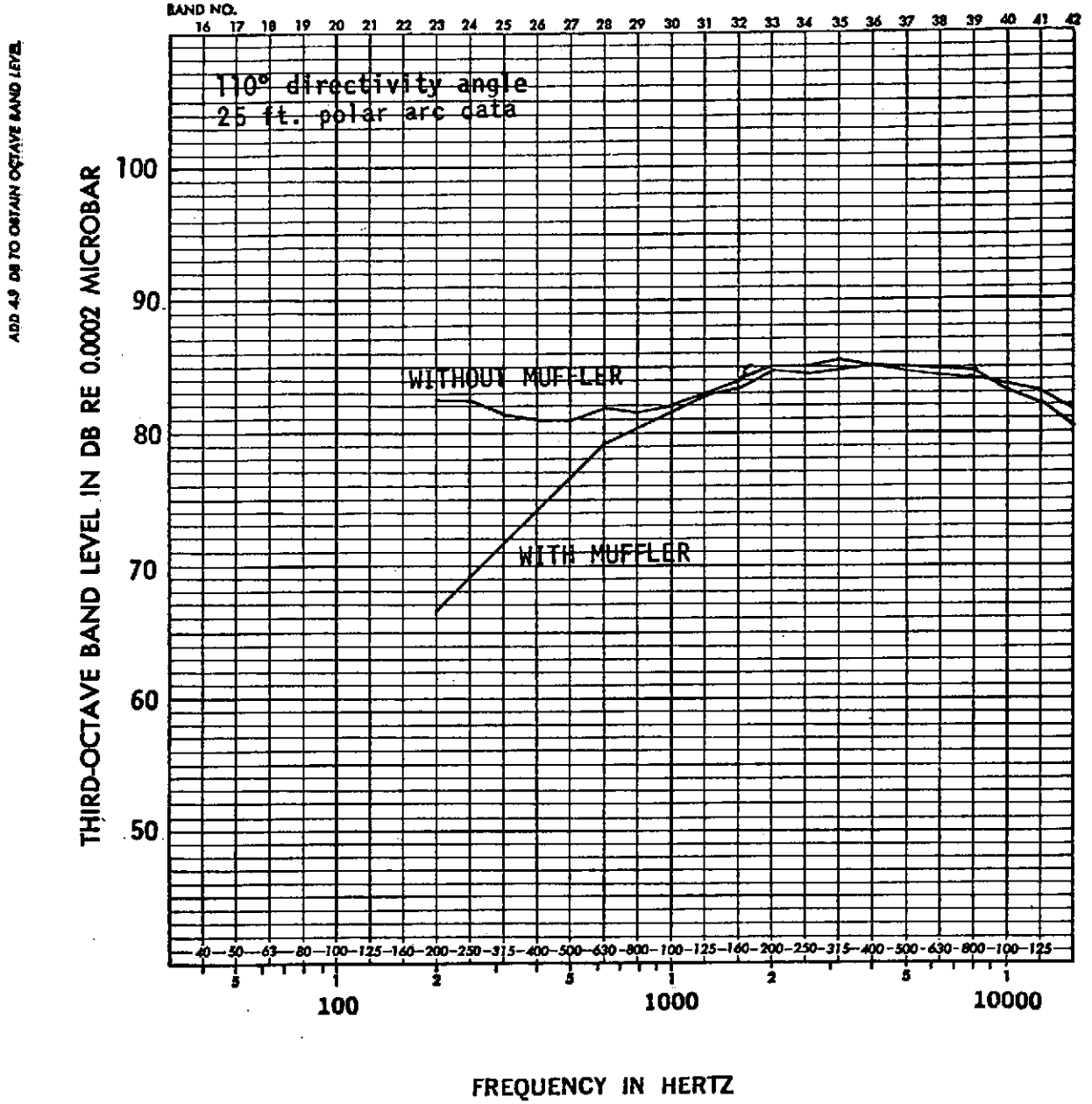

FIGURE 25. 2" CONICAL NOZZLE SPECTRA
v = 1077 ft/sec
T = 1010 °R

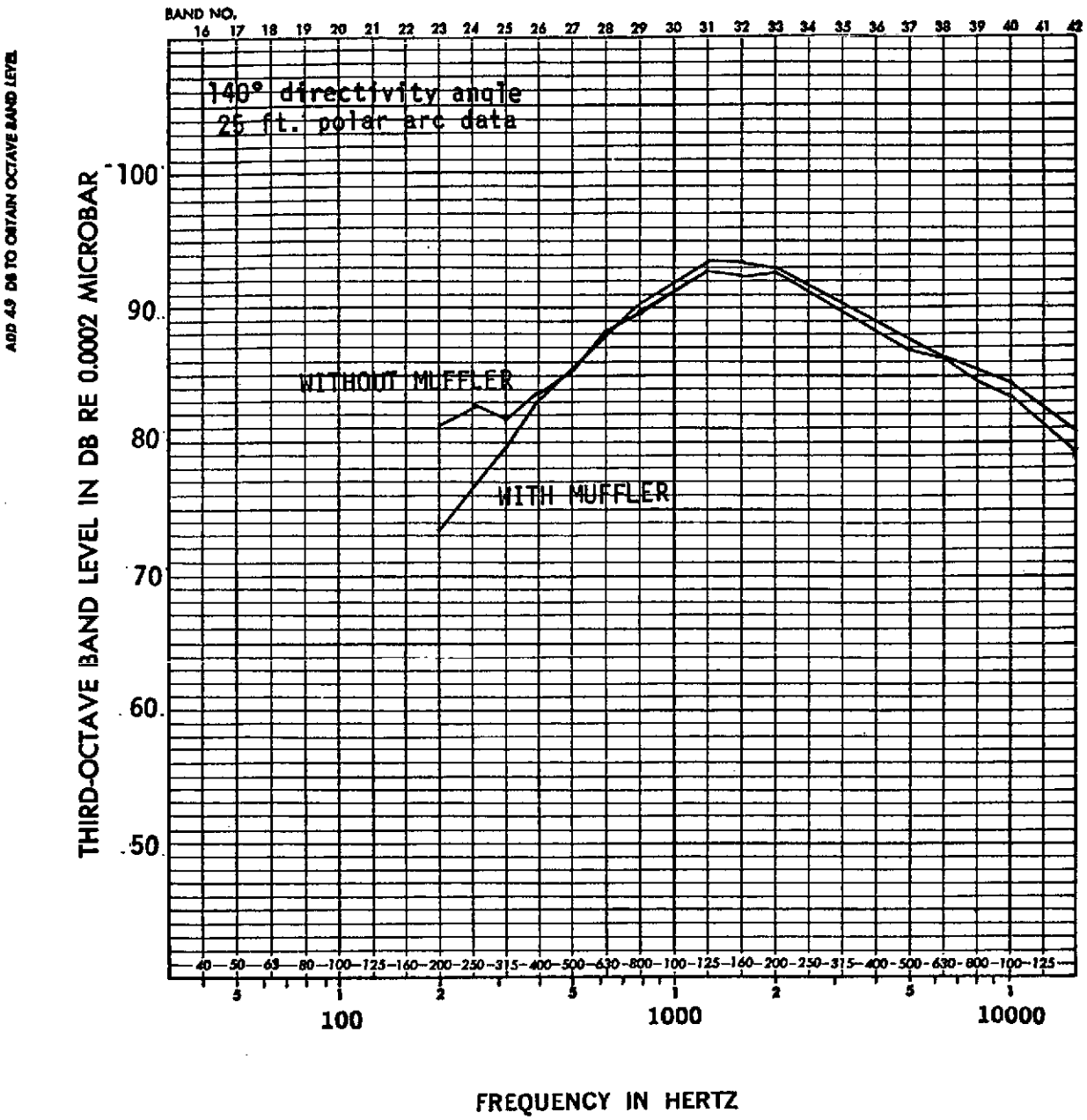

FIGURE 26. 2" CONICAL NOZZLE SPECTRA
V = 1077 ft/sec
T = 1010 °R

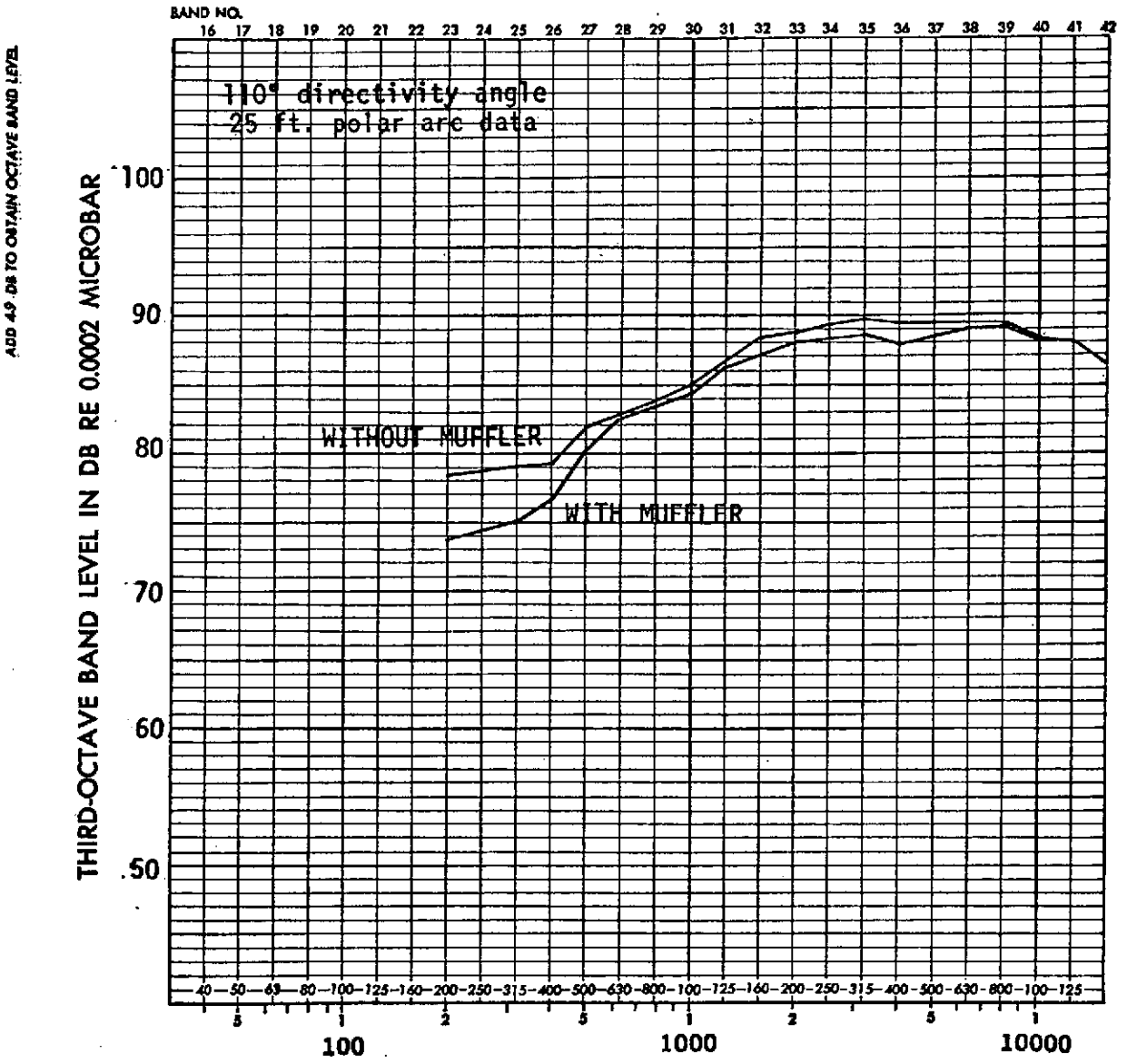

FIGURE 27. 2" CONICAL NOZZLE SPECTRA
v = 1249 ft/sec
T = 1010 °R

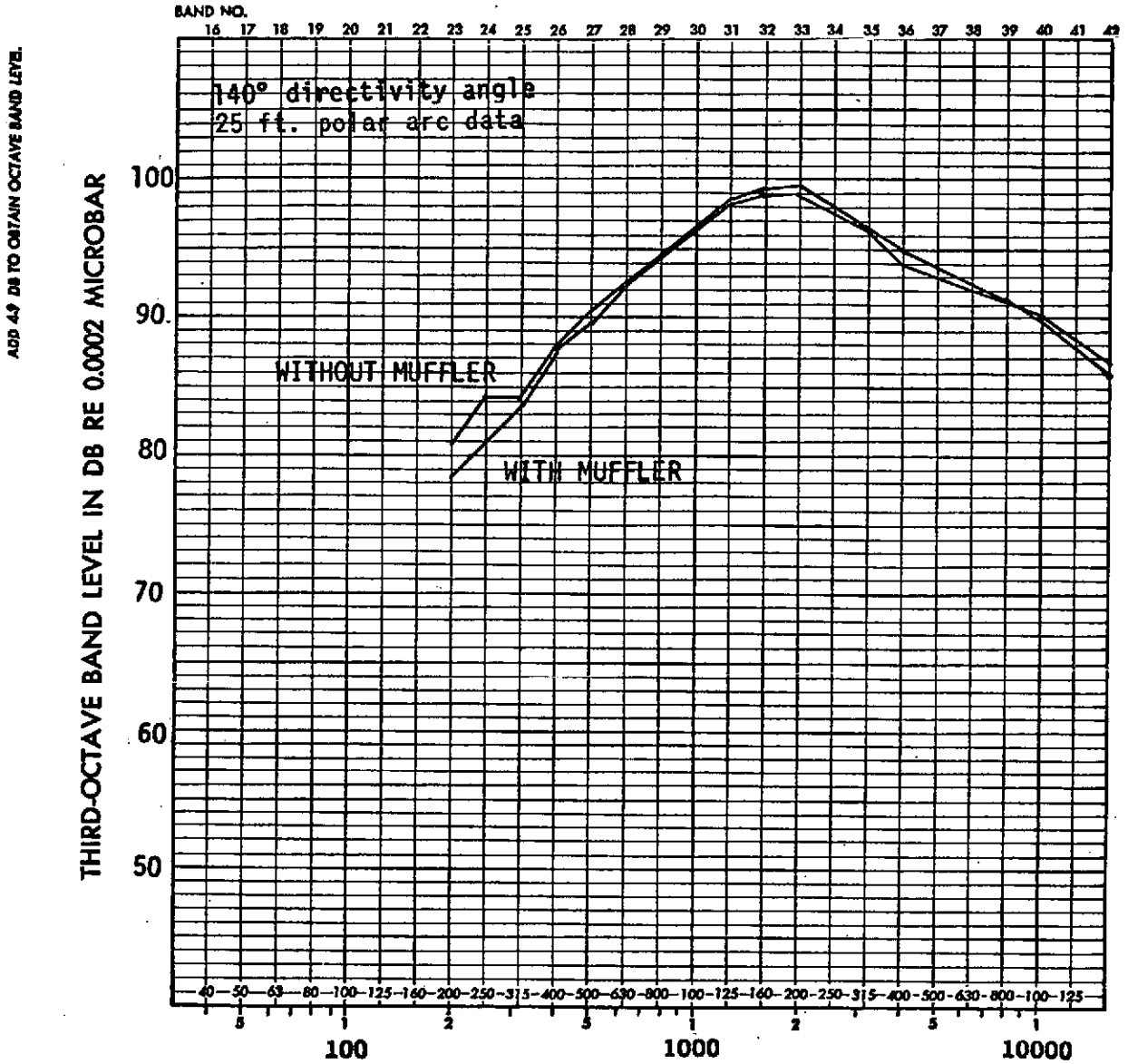

FIGURE 28. 2" CONICAL NOZZLE SPECTRA
v = 1249 ft/sec
T = 1010°R

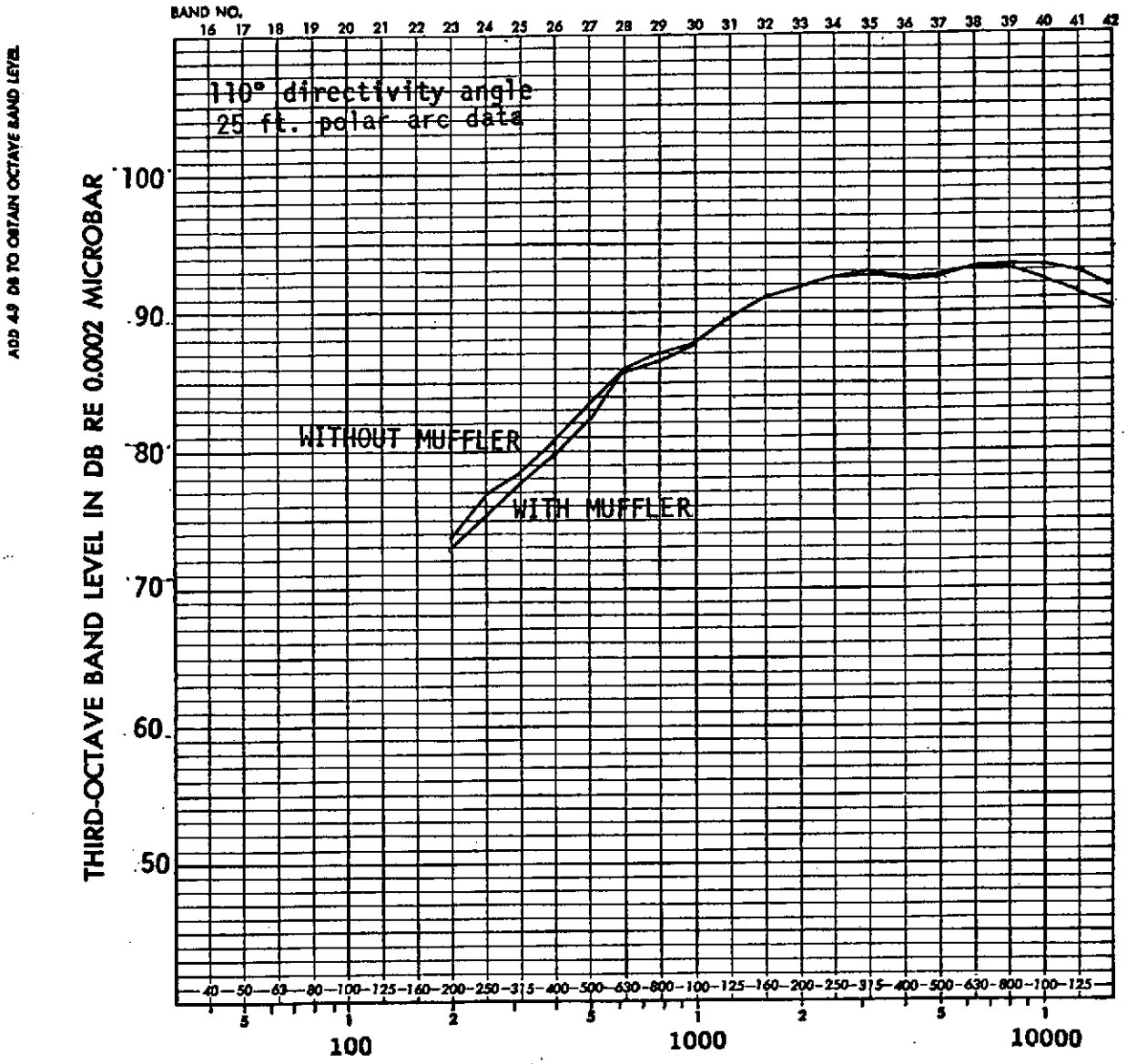

FIGURE 29. 2" CONICAL NOZZLE SPECTRA
v = 1391 ft/sec
T = 1010 °R

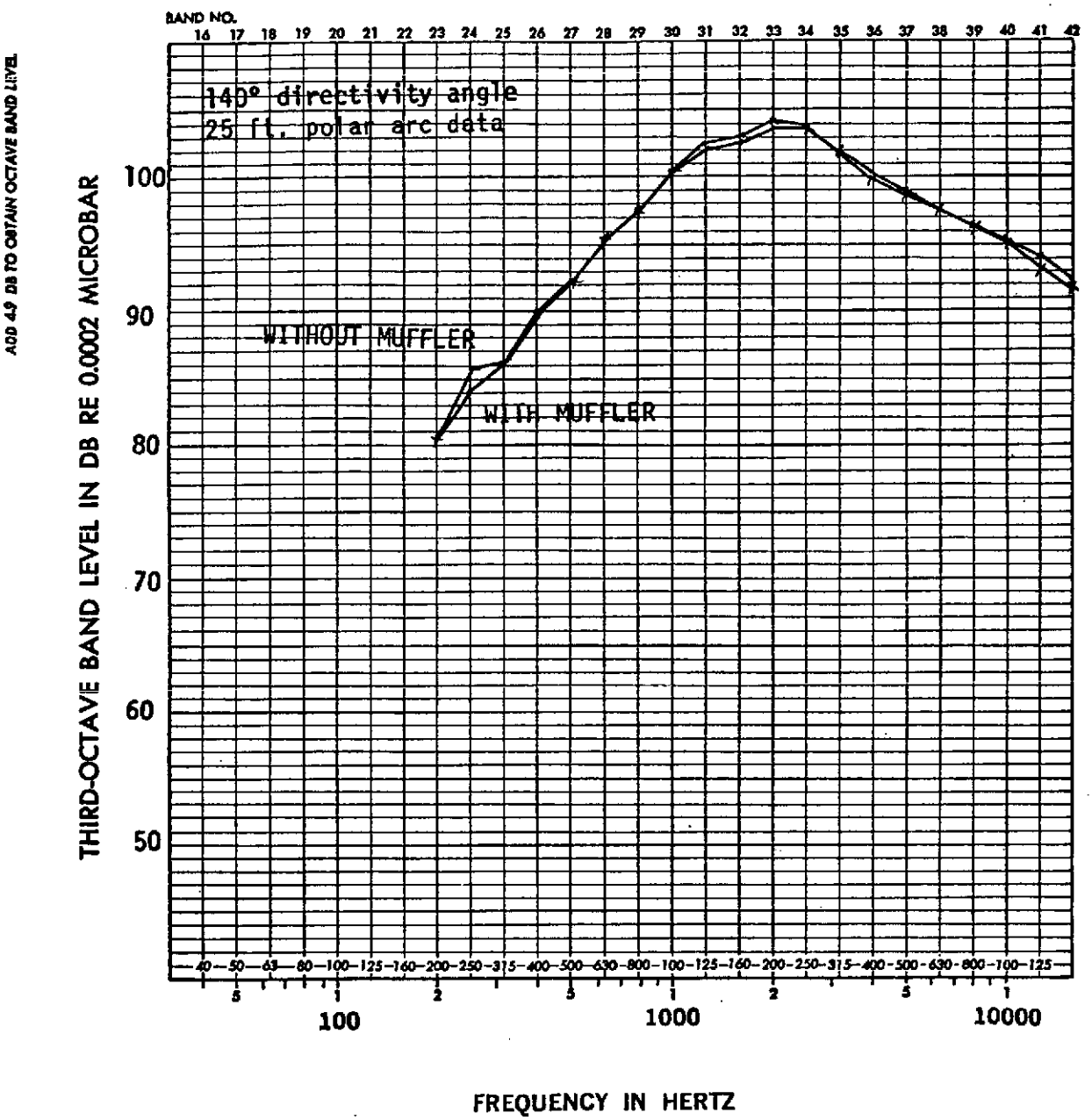

FIGURE 30 2" CONICAL NOZZLE SPECTRA
v = 1391 ft/sec
T = 1010 °R

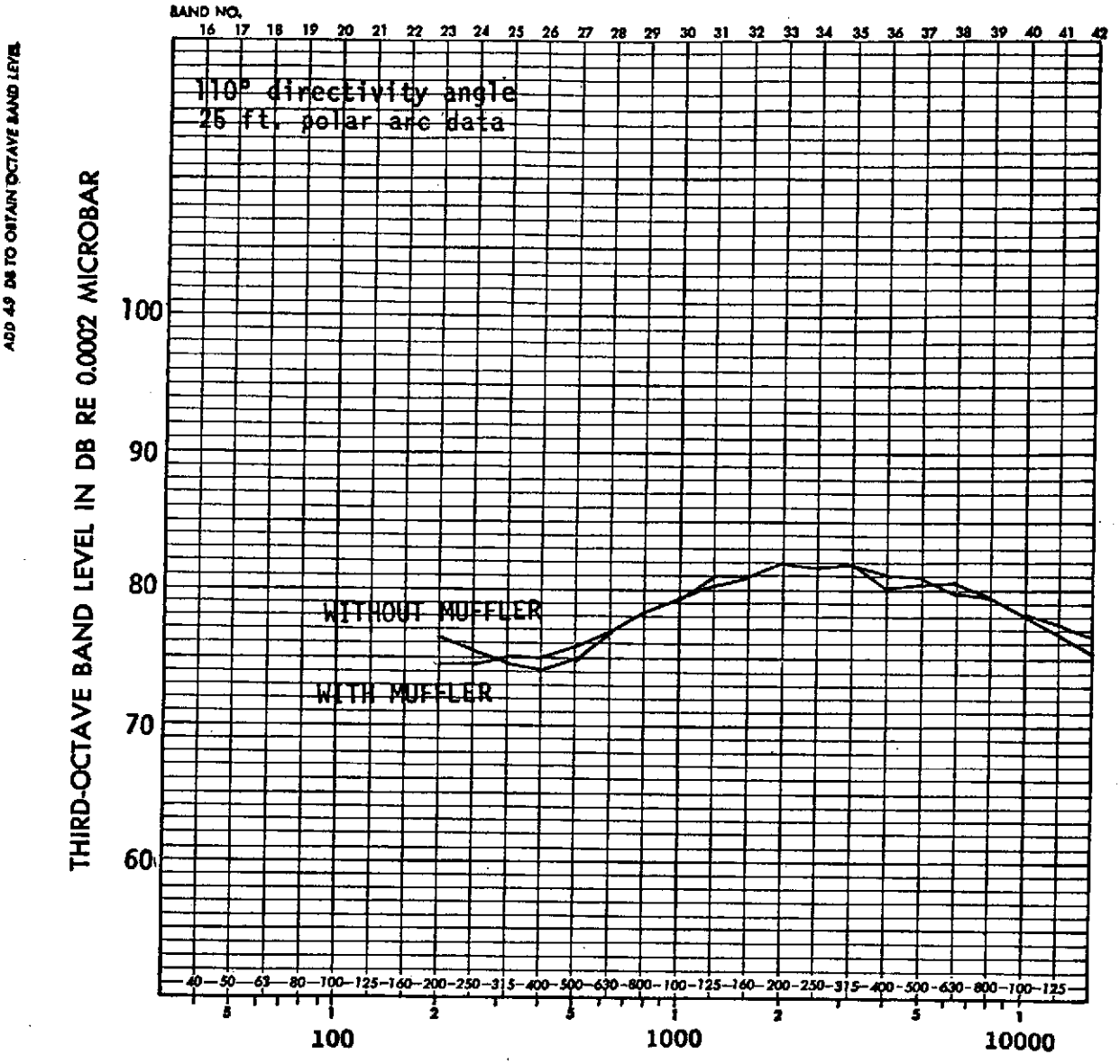

FIGURE 31. 2" CONICAL NOZZLE SPECTRA
v = 909 ft/sec
T = 1420 °R

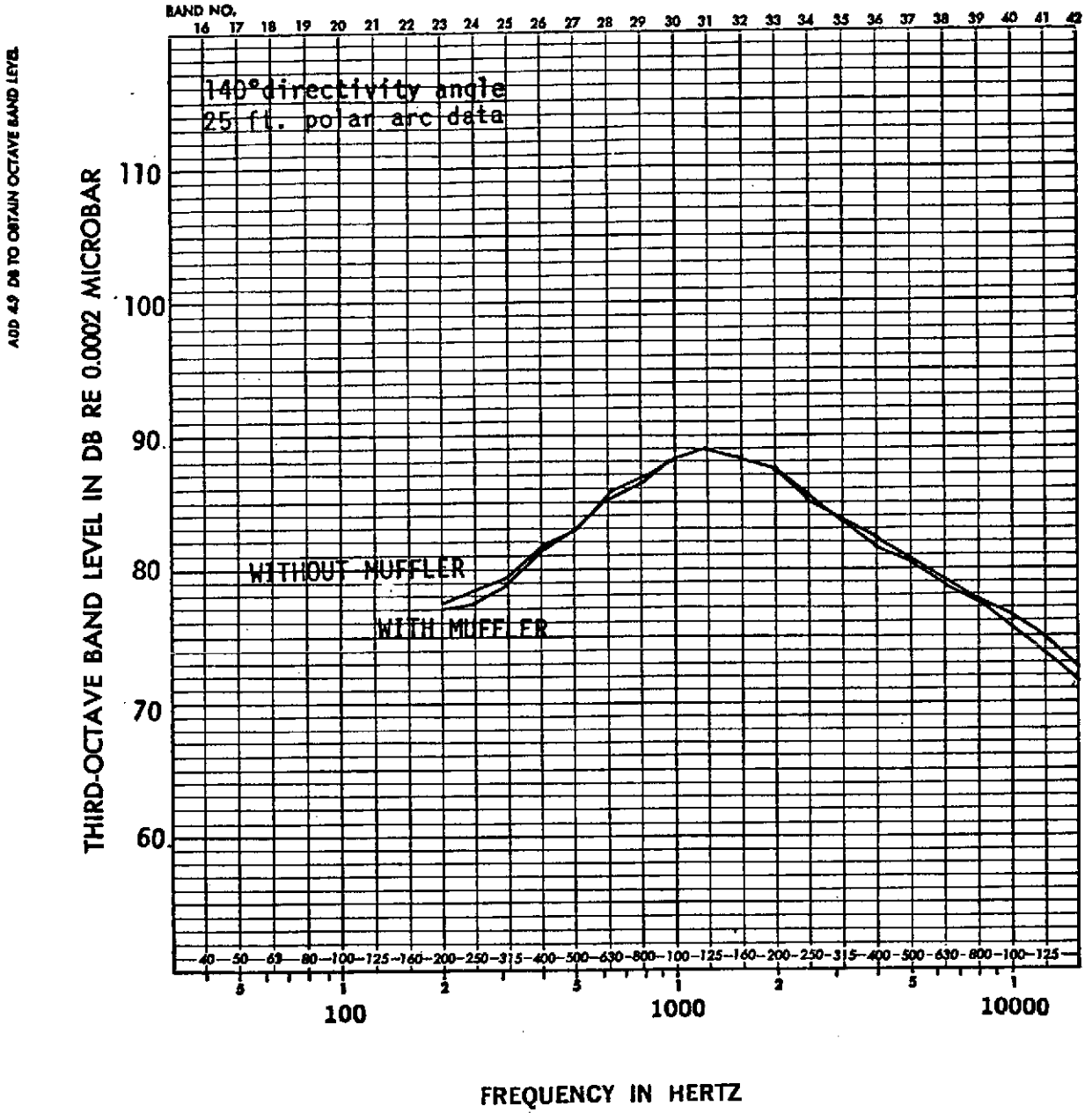

FIGURE 32. 2" CONICAL NOZZLE SPECTRA
v = 909 ft/sec
T = 1420 °R

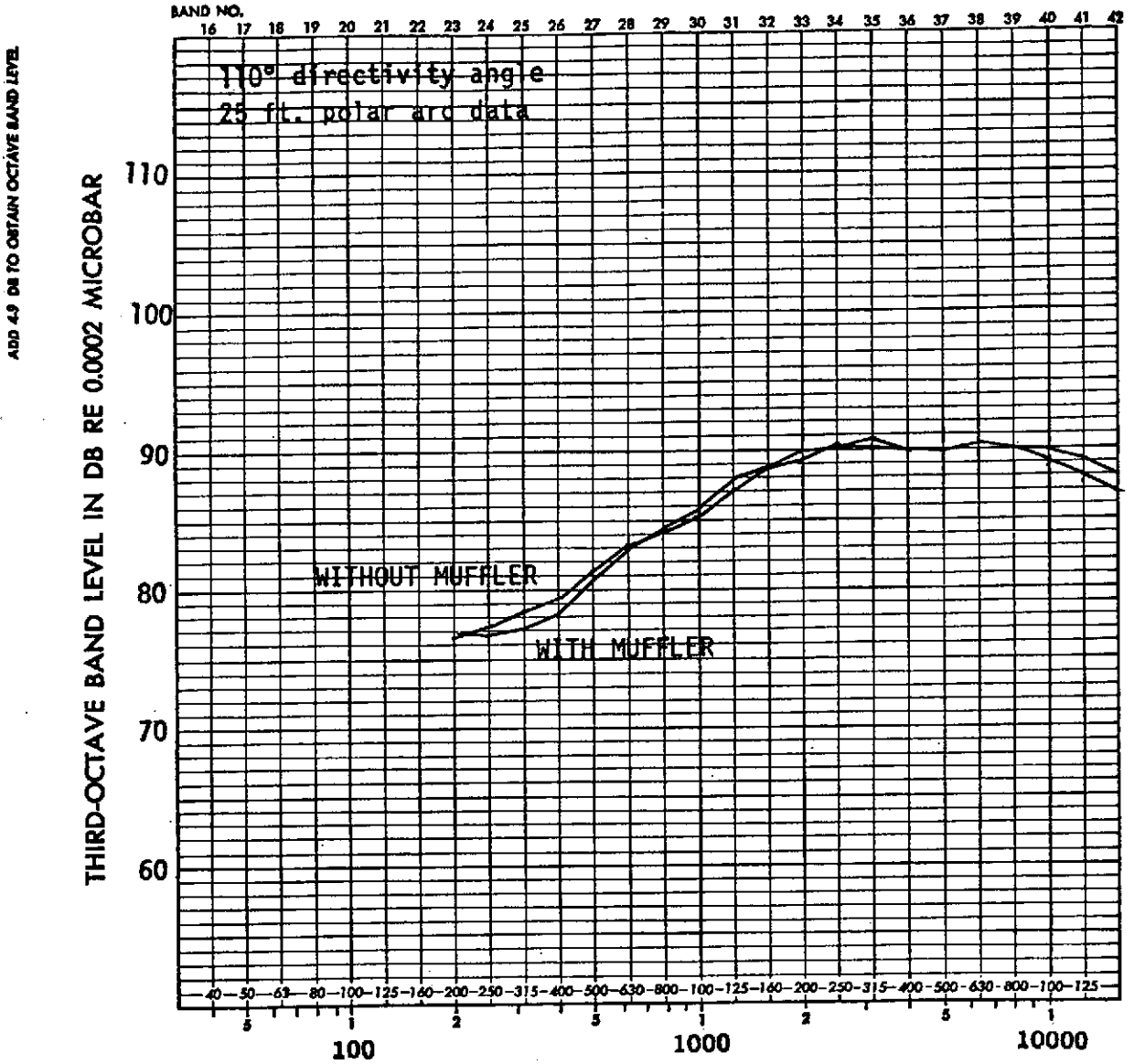

FIGURE 33. 2" CONICAL NOZZLE SPECTRA
v = 1259 ft/sec
T = 1420 °R

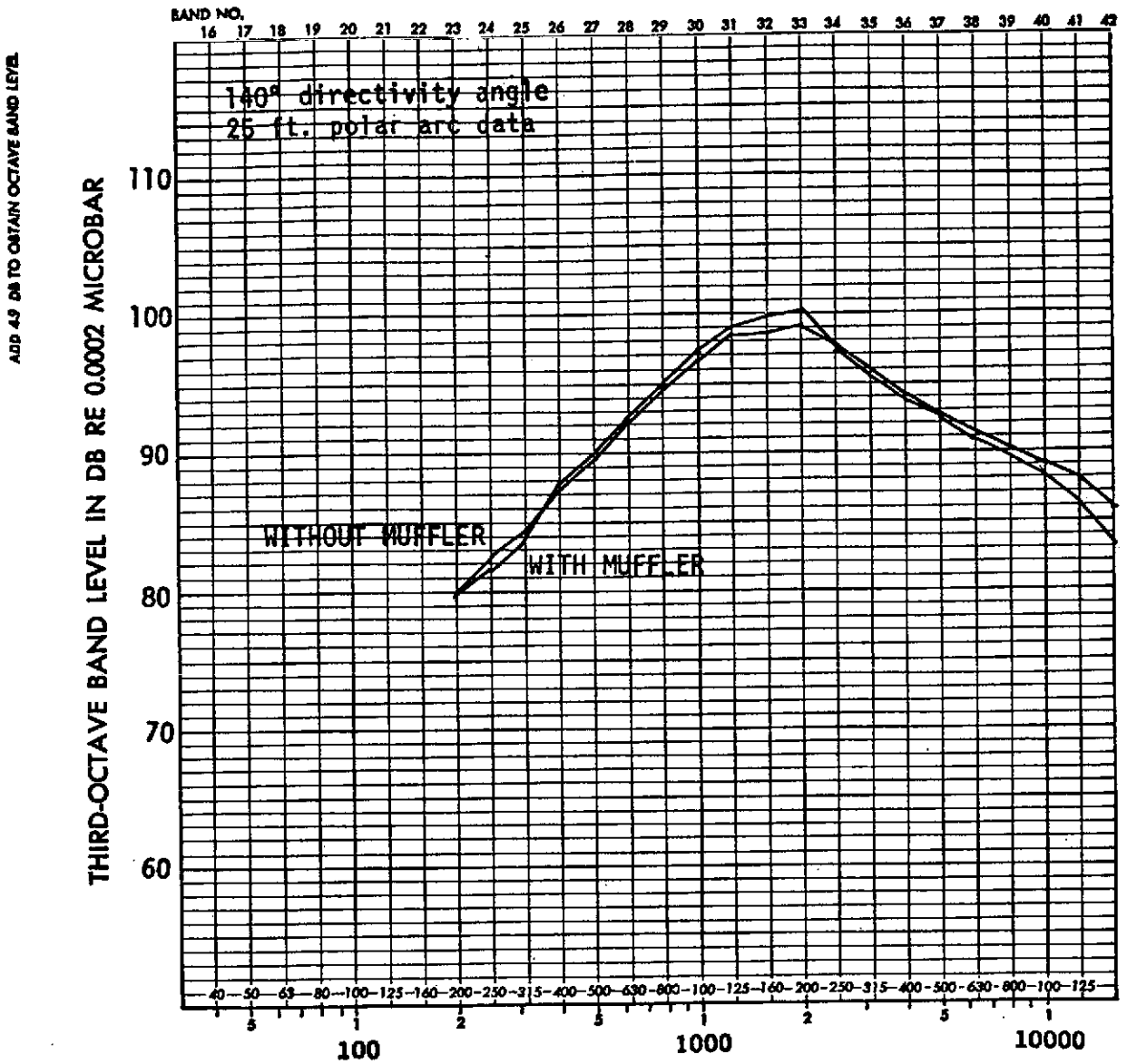

FIGURE 34. 2" CONICAL NOZZLE SPECTRA
v = 1259 ft/sec
T = 1420 °R

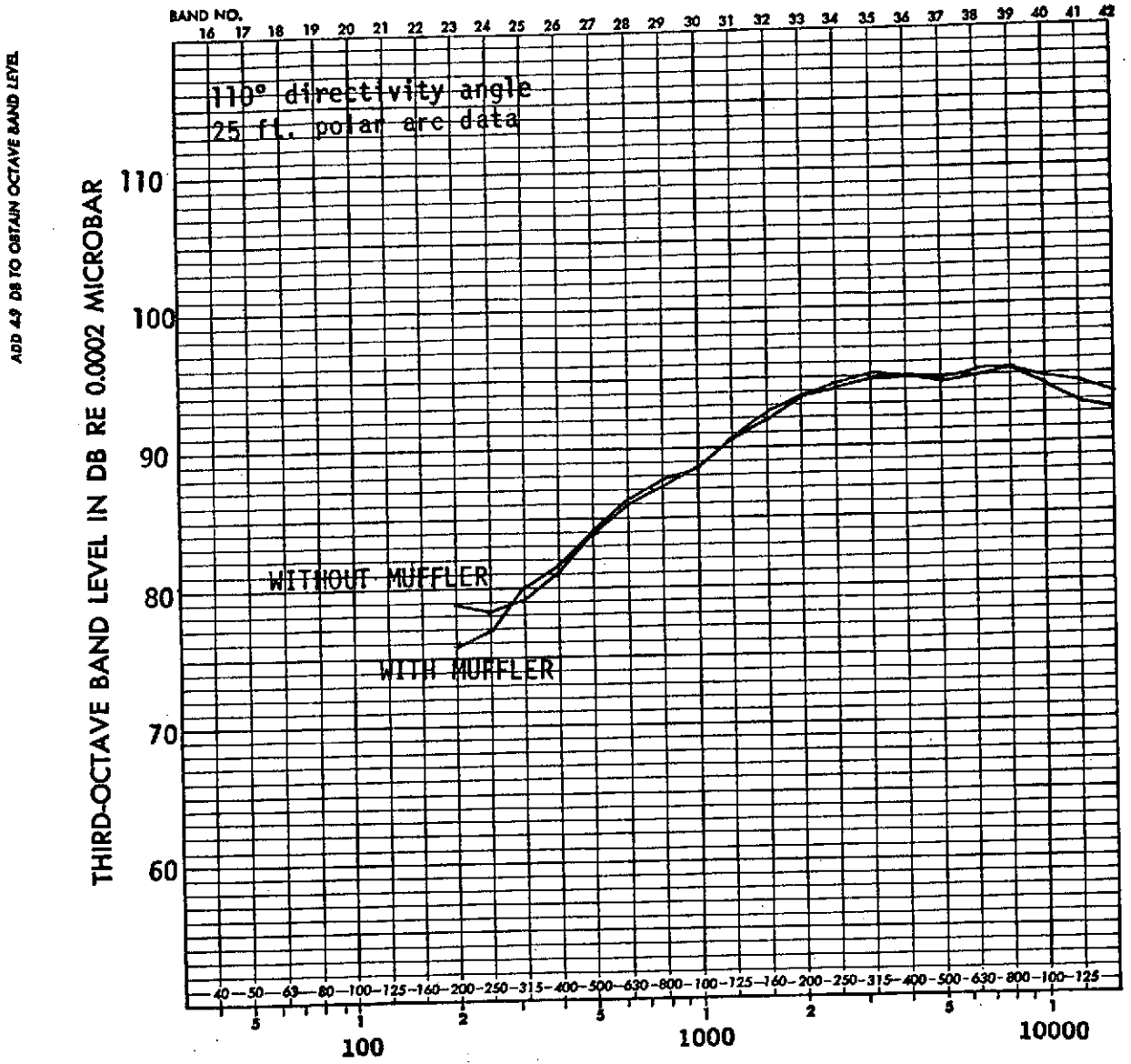

FIGURE 35. 2" CONICAL NOZZLE SPECTRA
v = 1477 ft/sec
T = 1420 °R

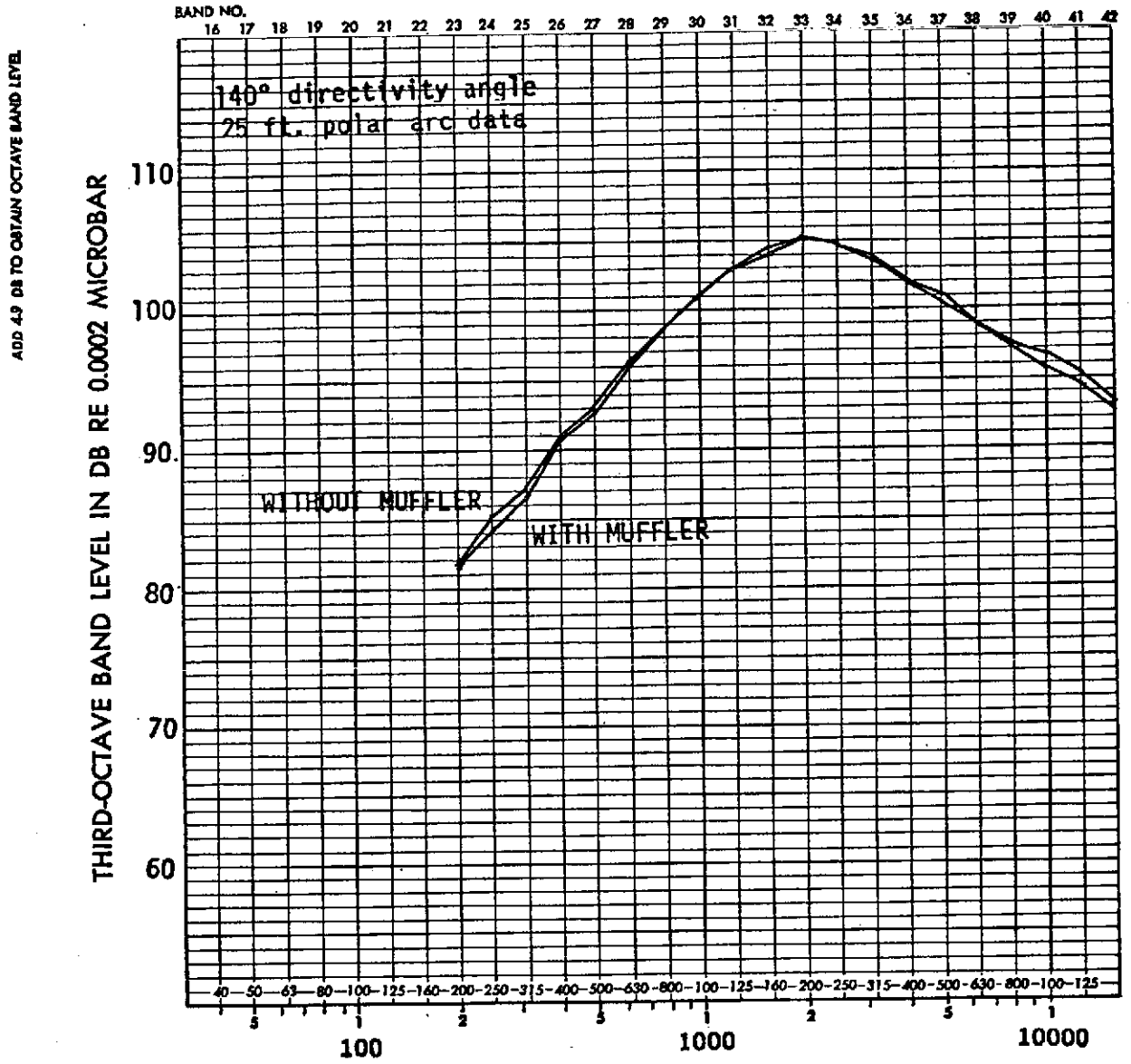

FIGURE 36. 2" CONICAL NOZZLE SPECTRA
v = 1477 ft/sec
T = 1420 °R

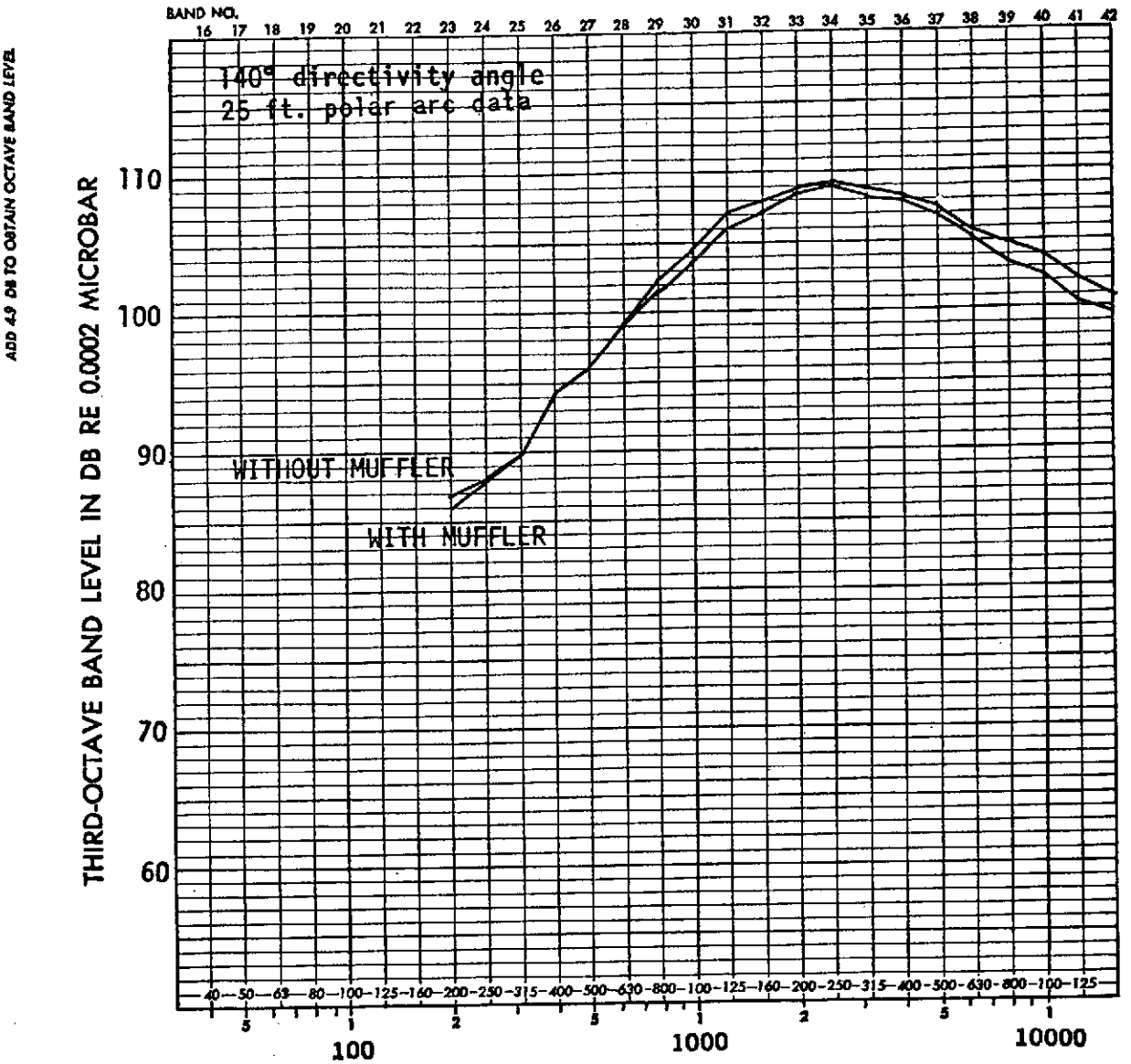

FIGURE 37. 2" CONICAL NOZZLE SPECTRA
v = 1632 ft/sec
T = 1420 °R

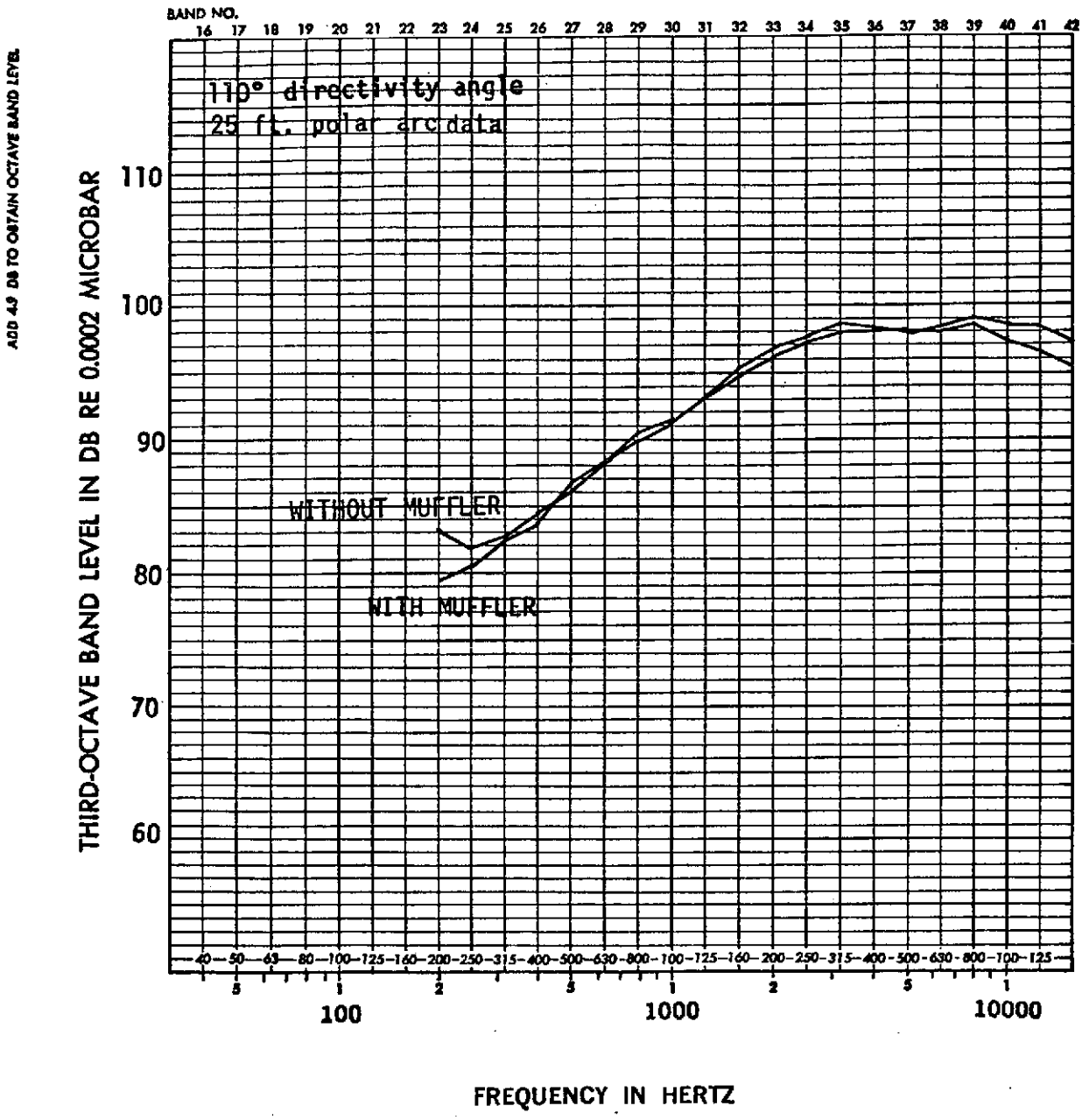

FIGURE 38. 2" CONICAL NOZZLE SPECTRA
v = 1632 ft/sec
T = 1420 °R

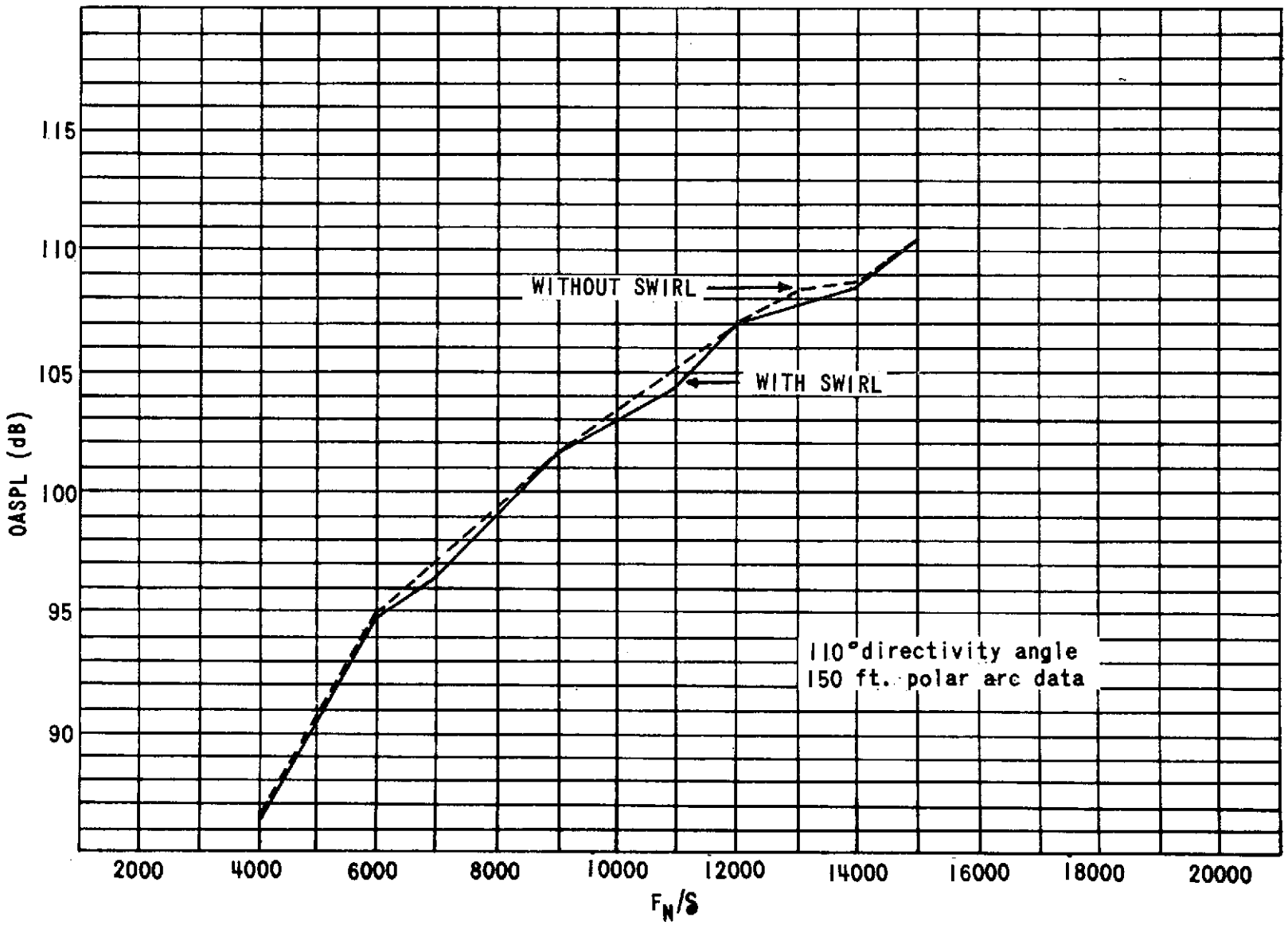

FIGURE 39. OASPL/THRUST THROTTLING CURVES FOR P&WA JT8D-109 SWIRL TEST

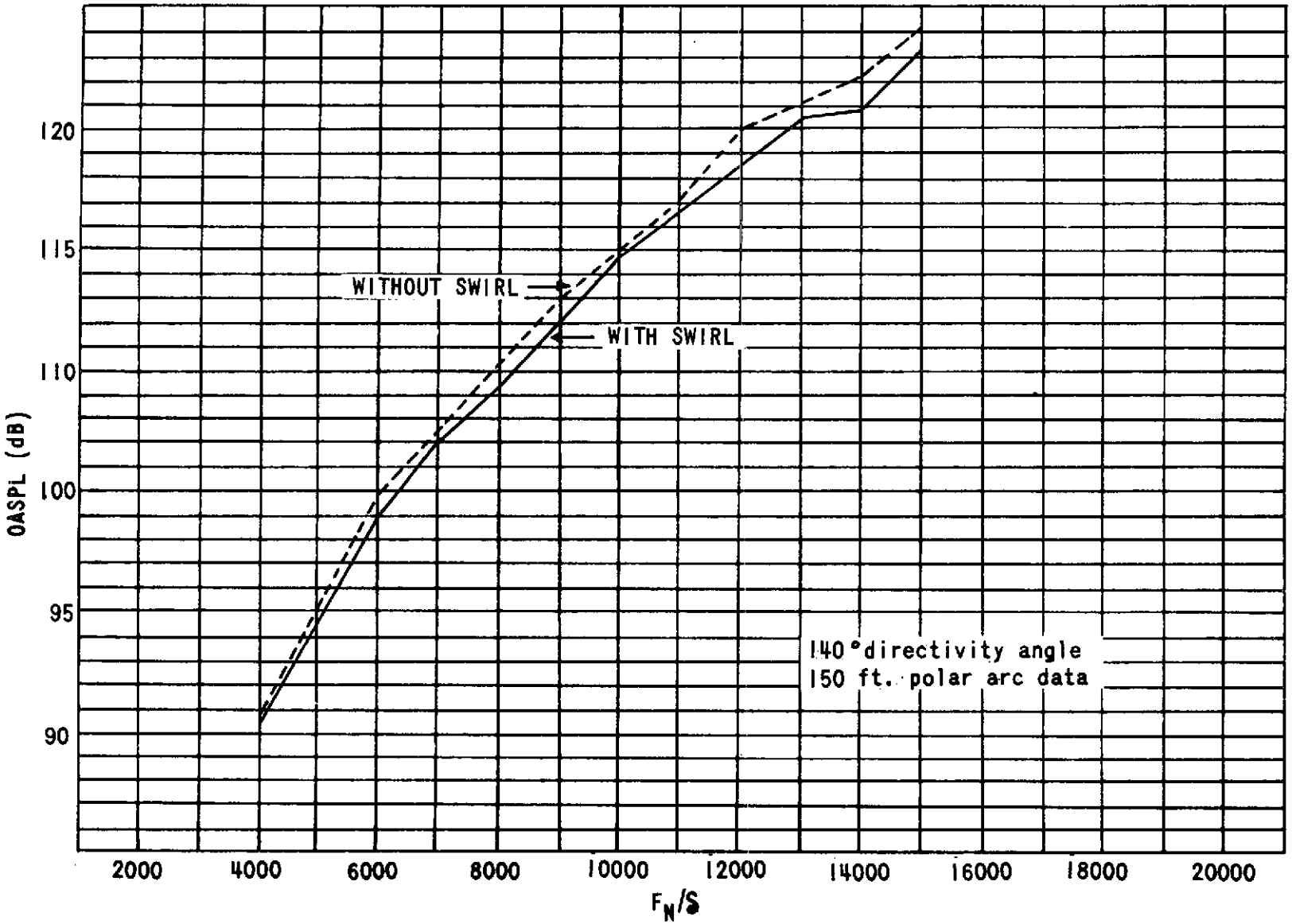

FIGURE 40. OASPL/THRUST THROTTLING CURVES FOR P&WA JT8D-109 SWIRL TEST

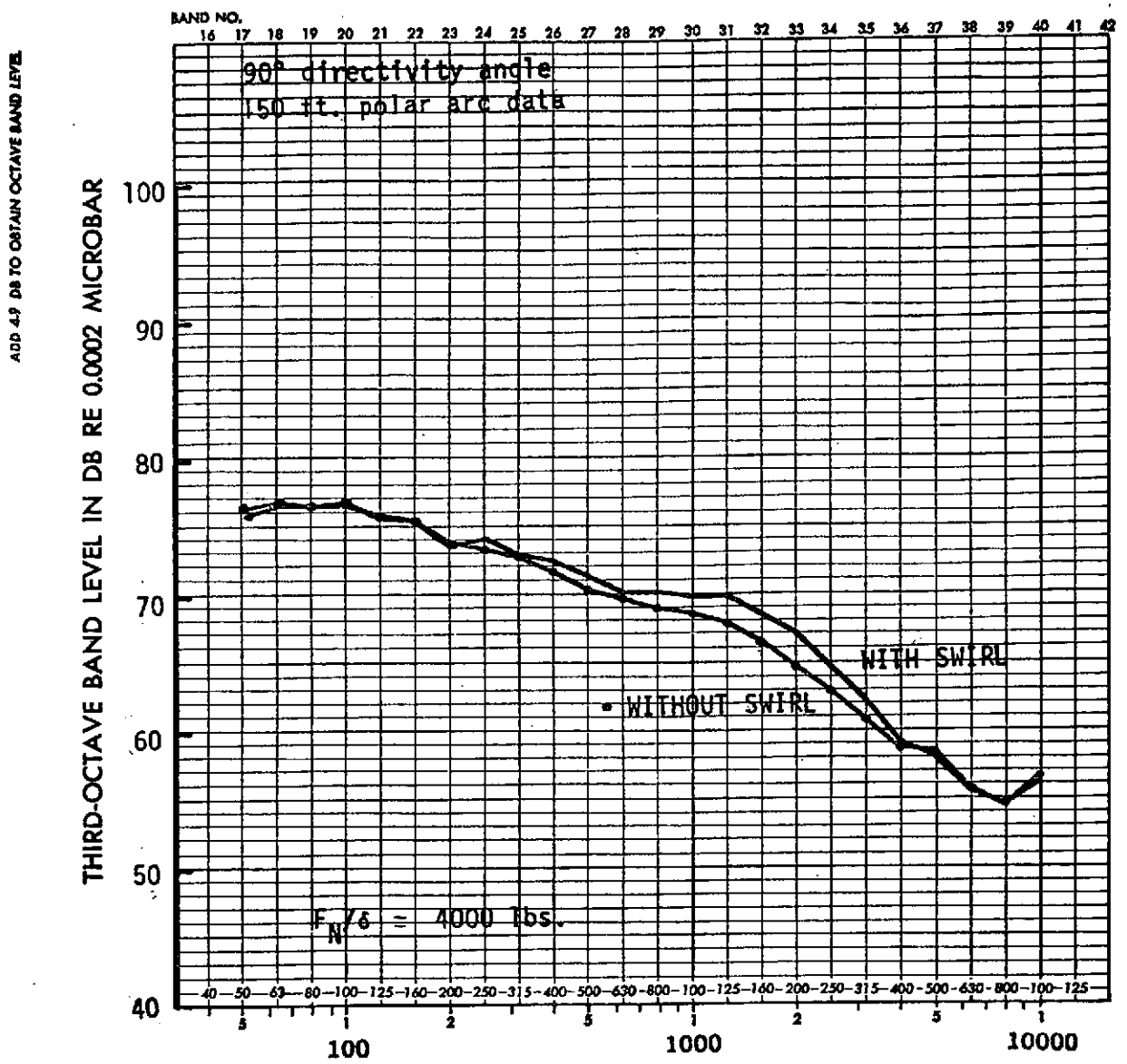

FIGURE 41. P&WA JT8D-109 NOZZLE SWIRL TEST

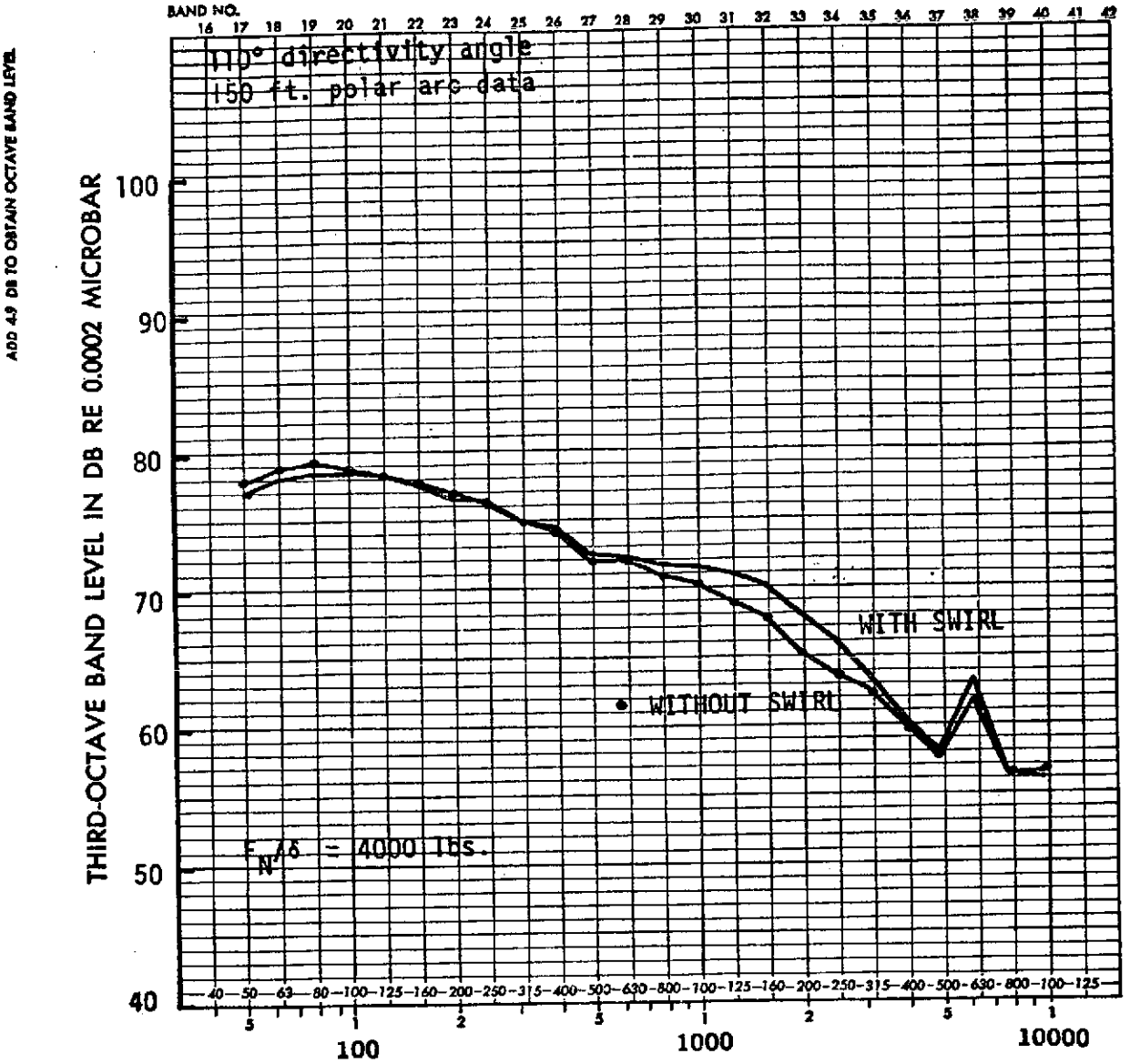

FIGURE 42. P&WA JT8D-109 NOZZLE SWIRL TEST

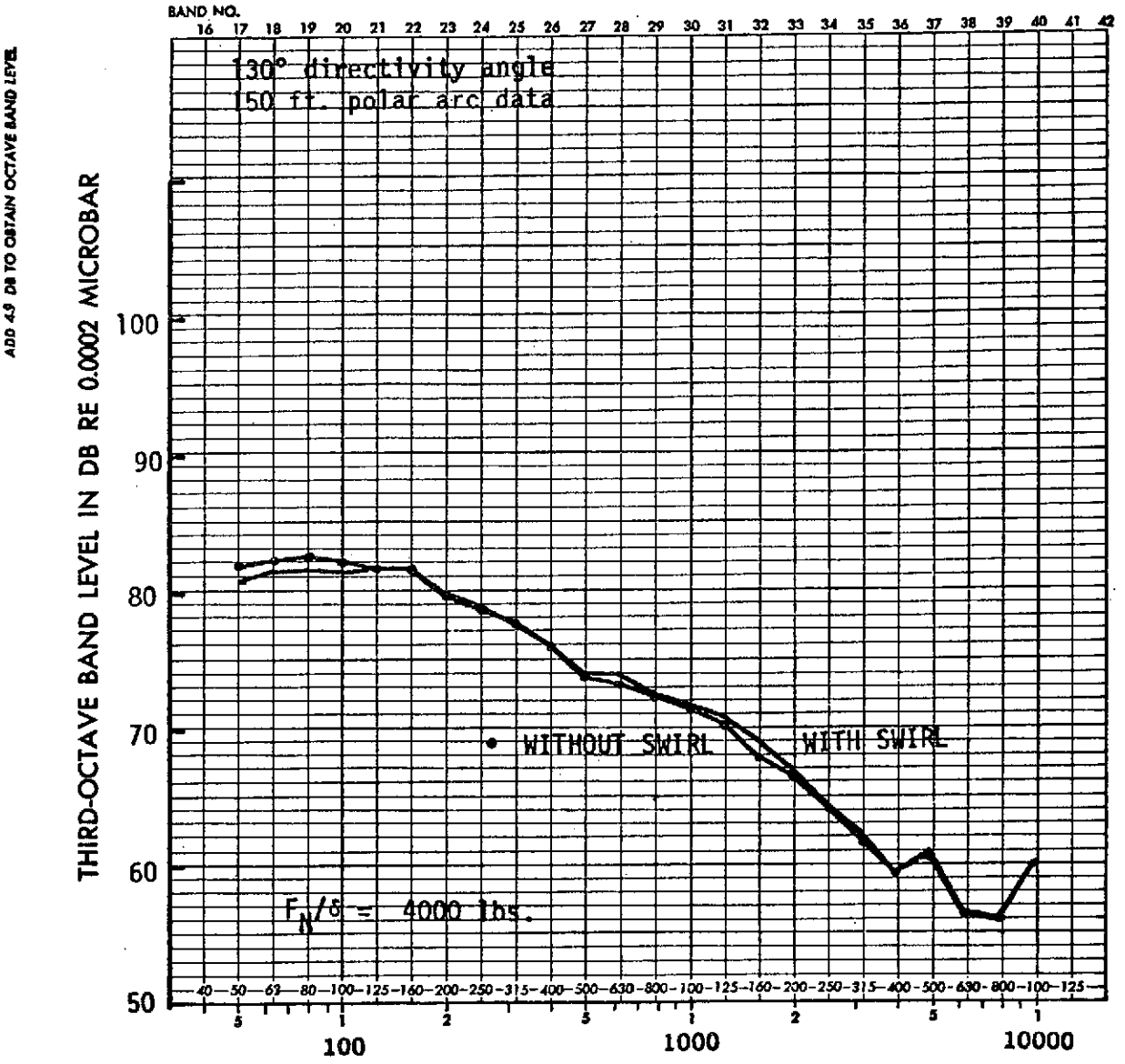

FIGURE 43. P&WA JT8D-109 NOZZLE SWIRL TEST

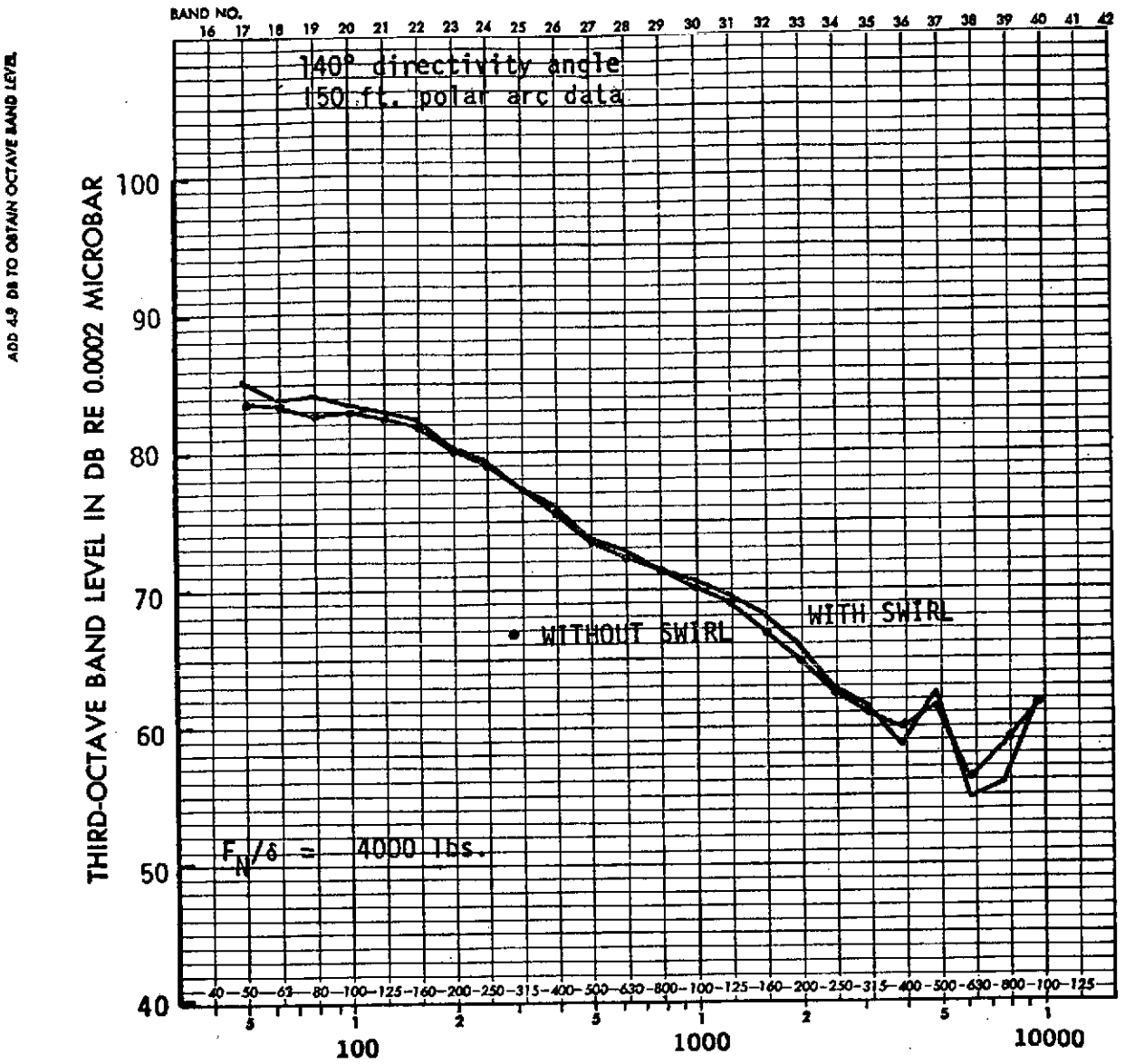

FIGURE 44. P&WA JT8D-109 NOZZLE SWIRL TEST

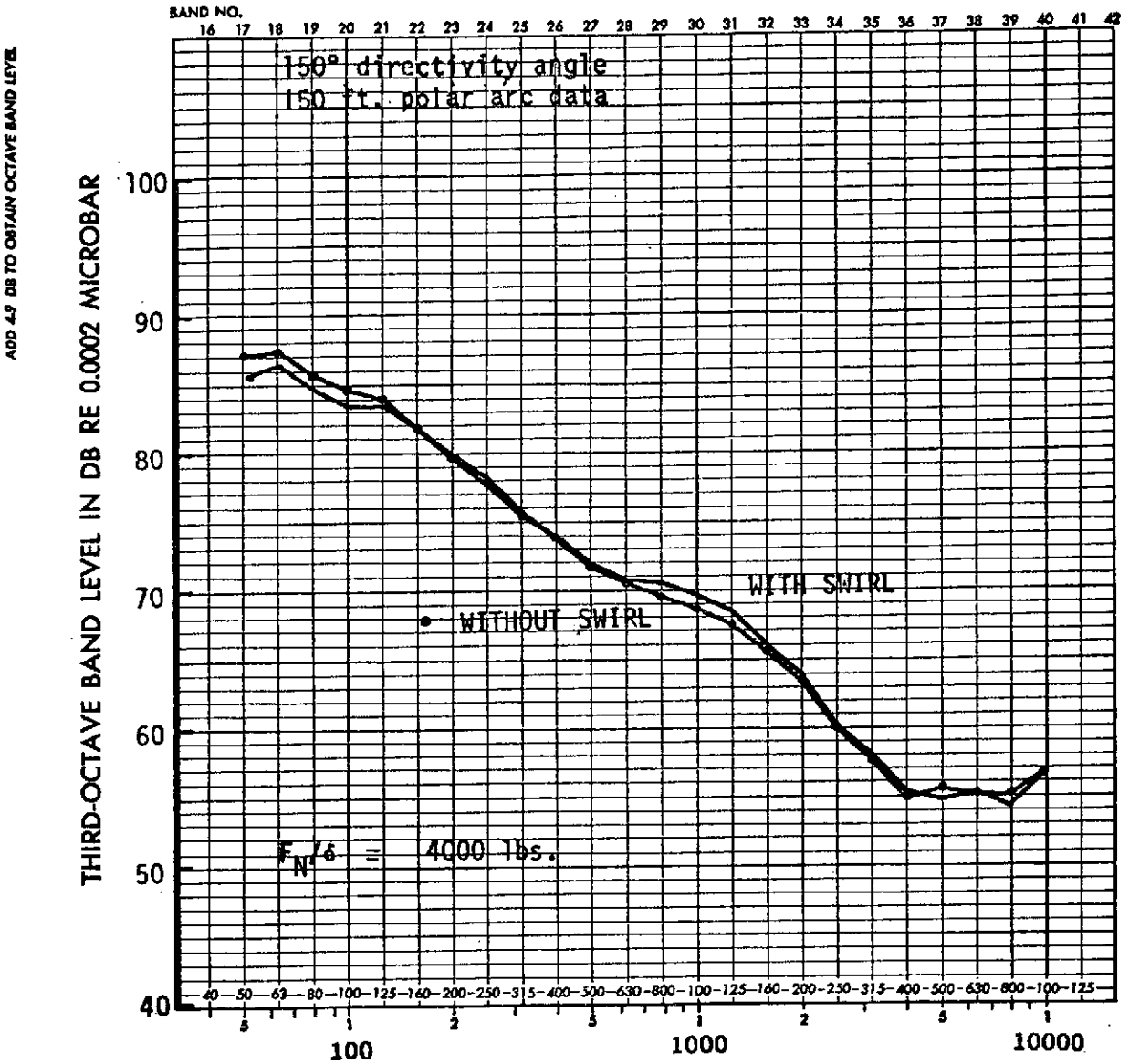

FIGURE 45. P&WA JT8D-109 NOZZLE SWIRL TEST

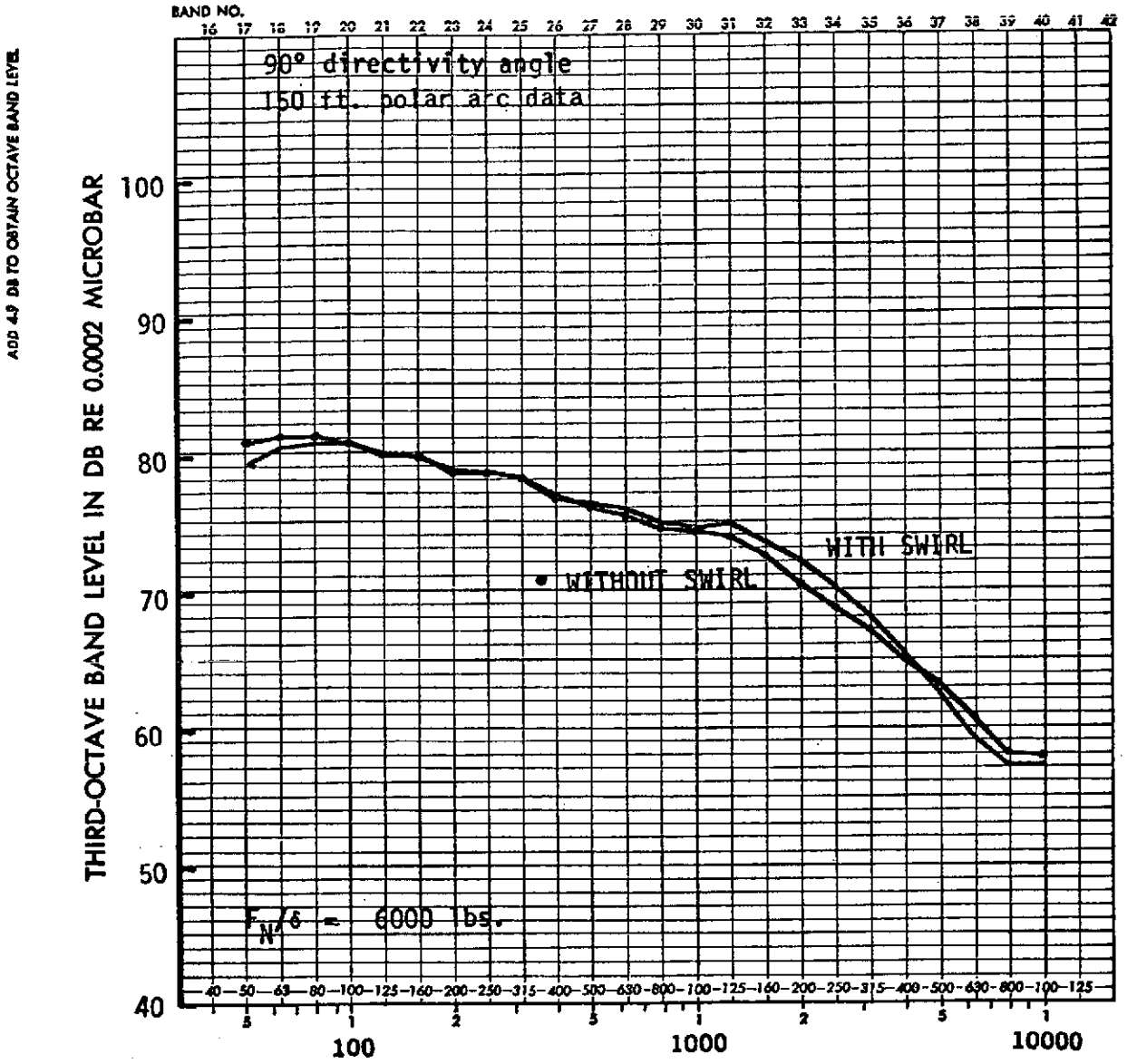

FIGURE 46. P&WA JT8D-109 NOZZLE SWIRL TEST

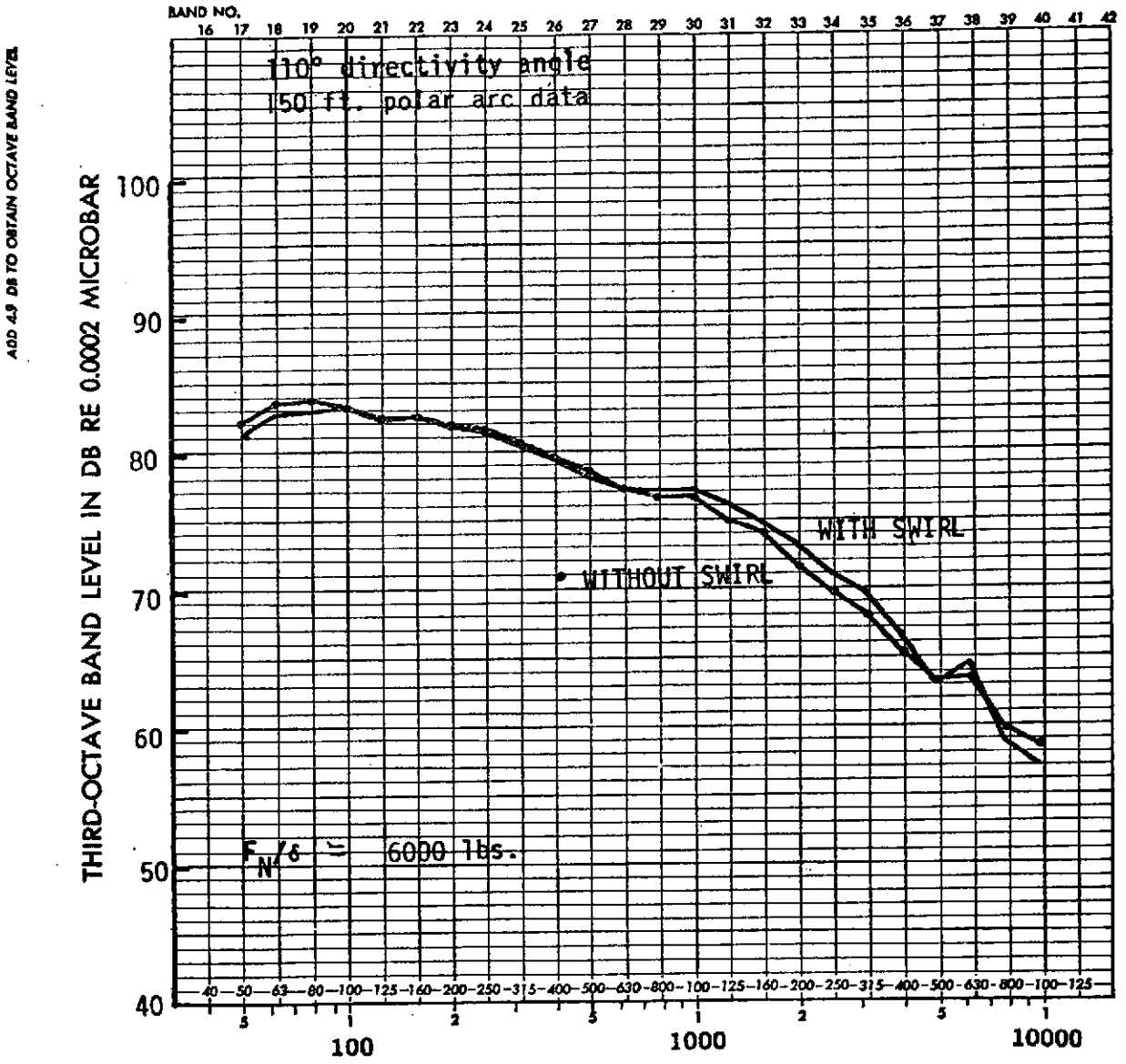

FIGURE 47. P&WA JT8D-109 NOZZLE SWIRL TEST

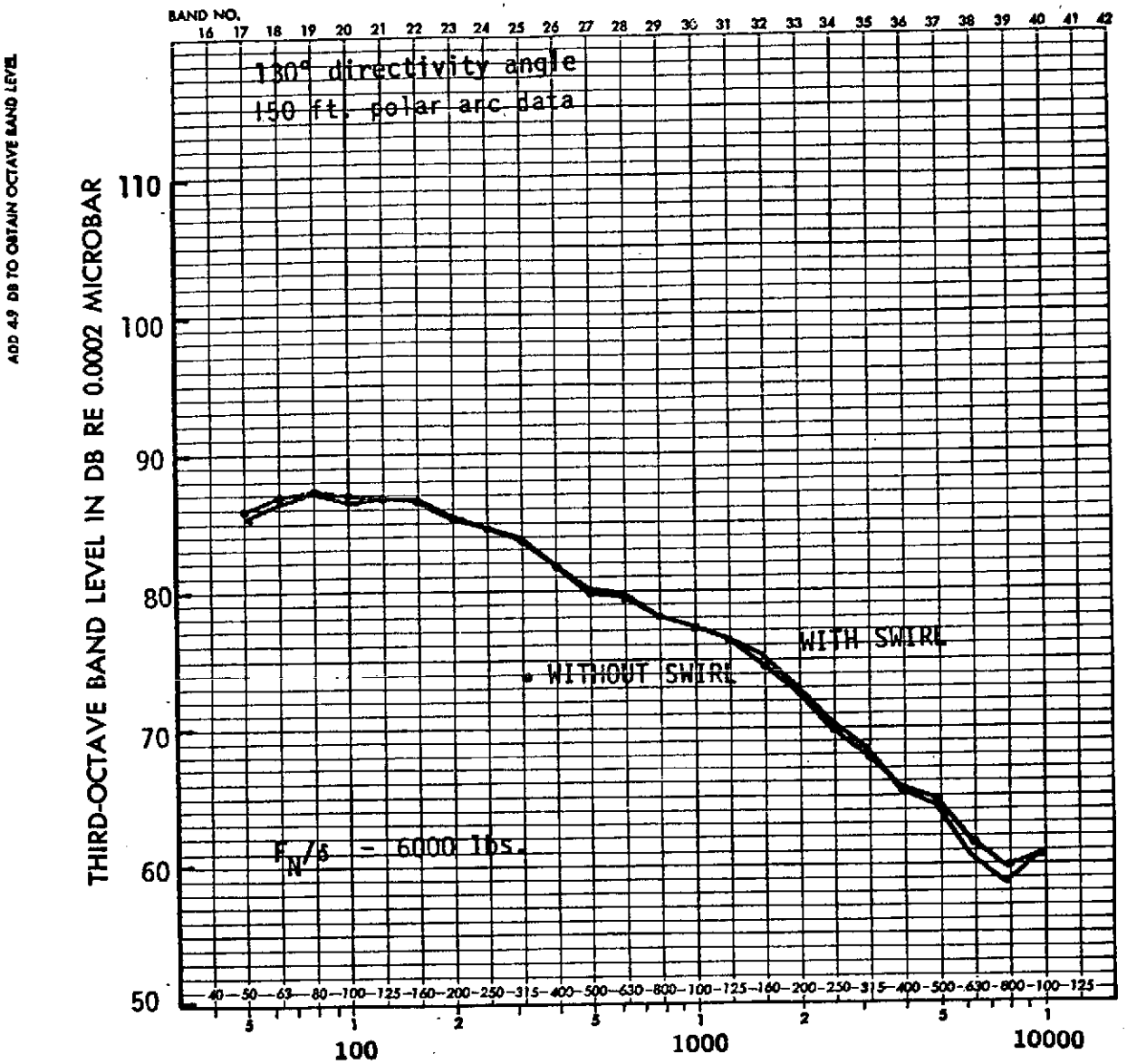

FIGURE 48. P&WA JT8D-109 NOZZLE SWIRL TEST

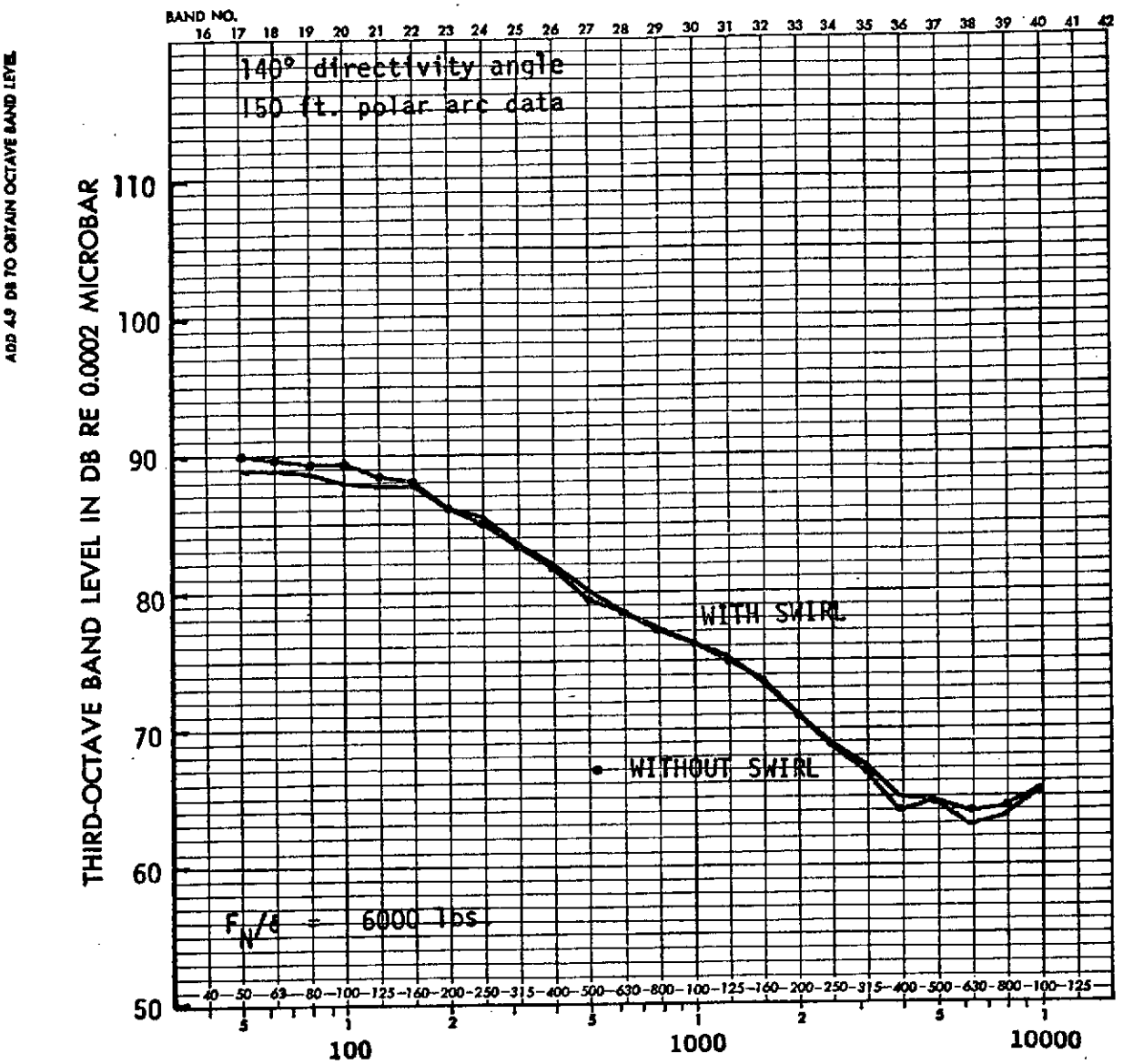

FIGURE 49. P&WA JT8D-109 NOZZLE SWIRL TEST

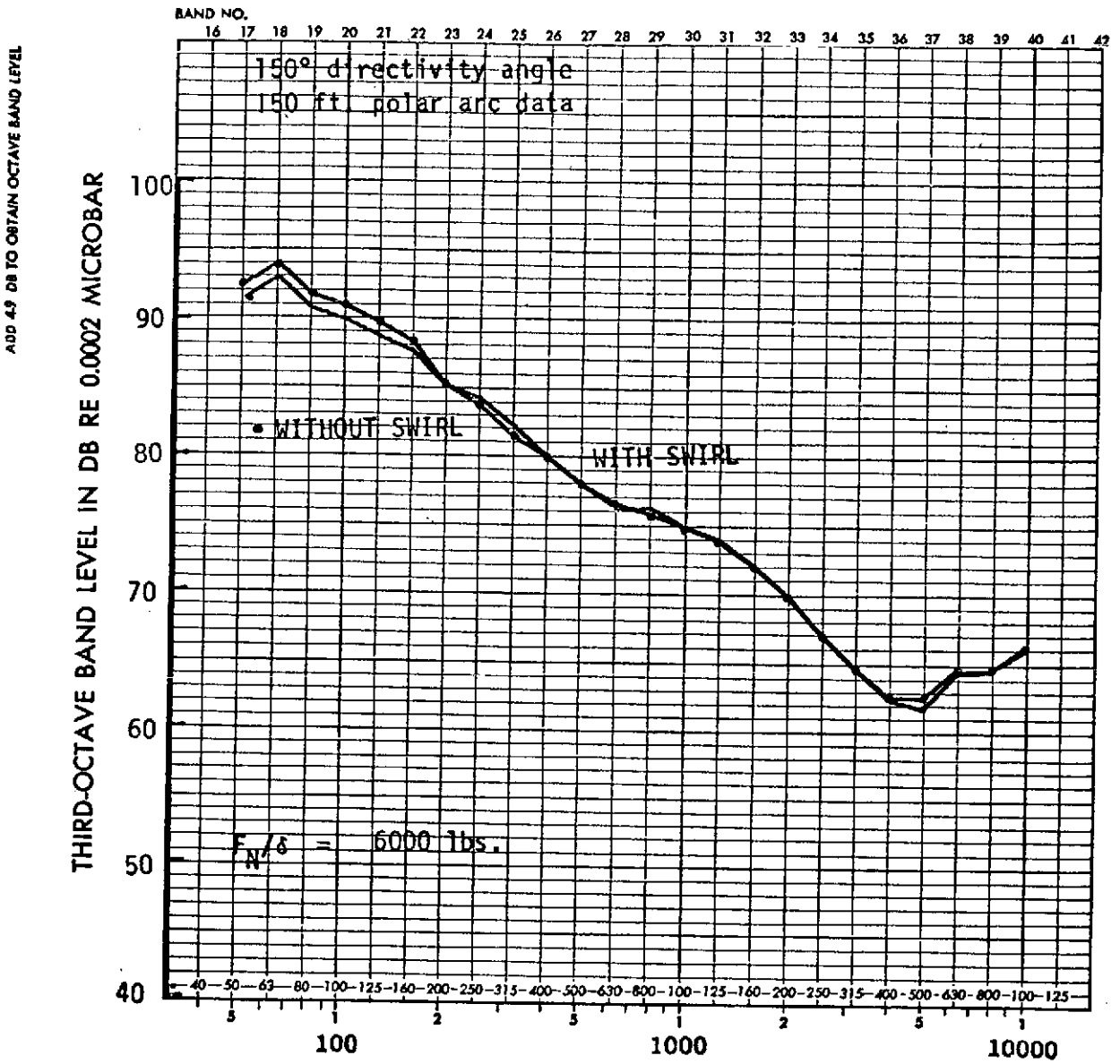

FIGURE 50. P&WA JT8D-109 NOZZLE SWIRL TEST

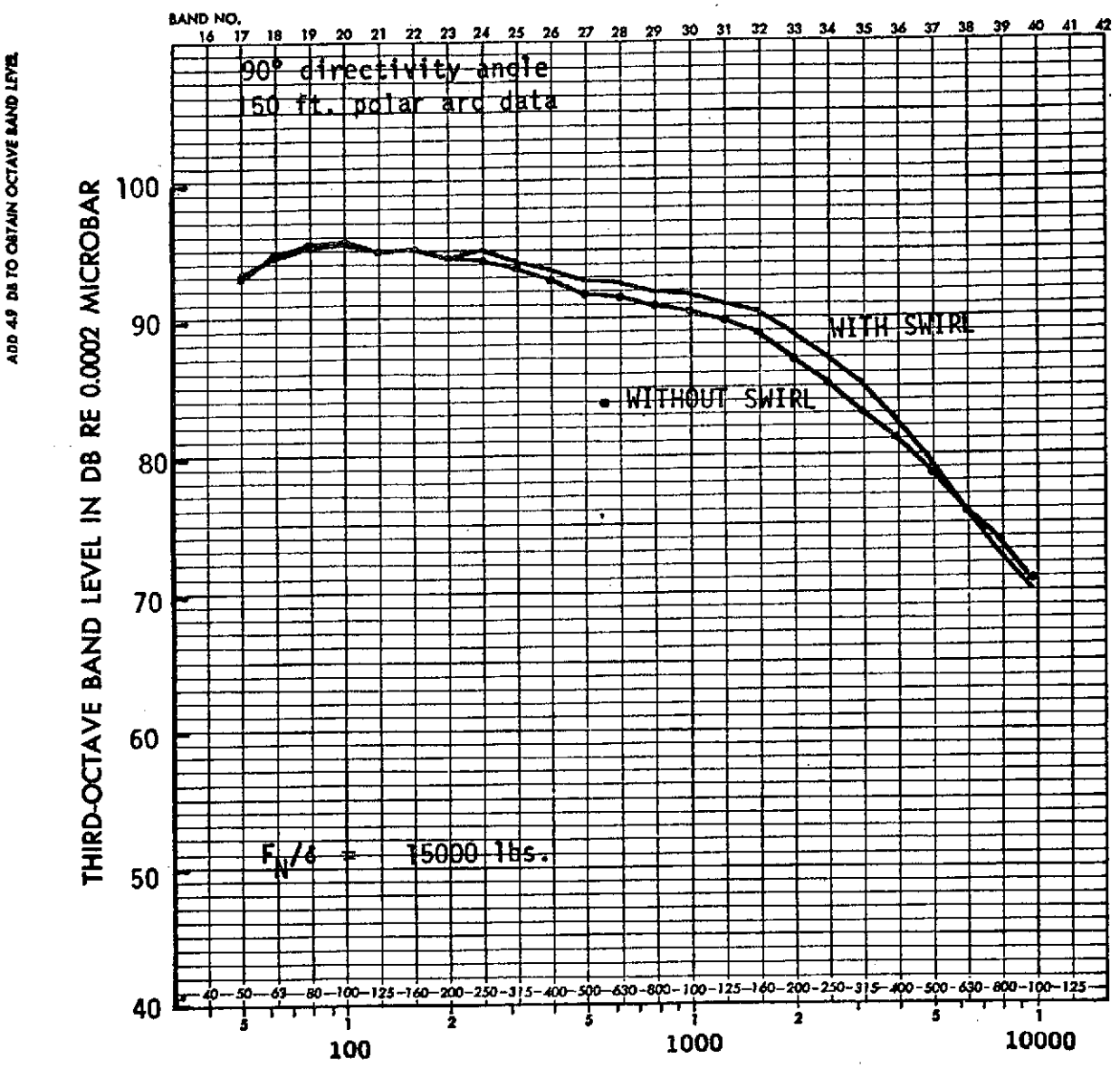

FIGURE 51. P&WA JT8D-109 NOZZLE SWIRL TEST

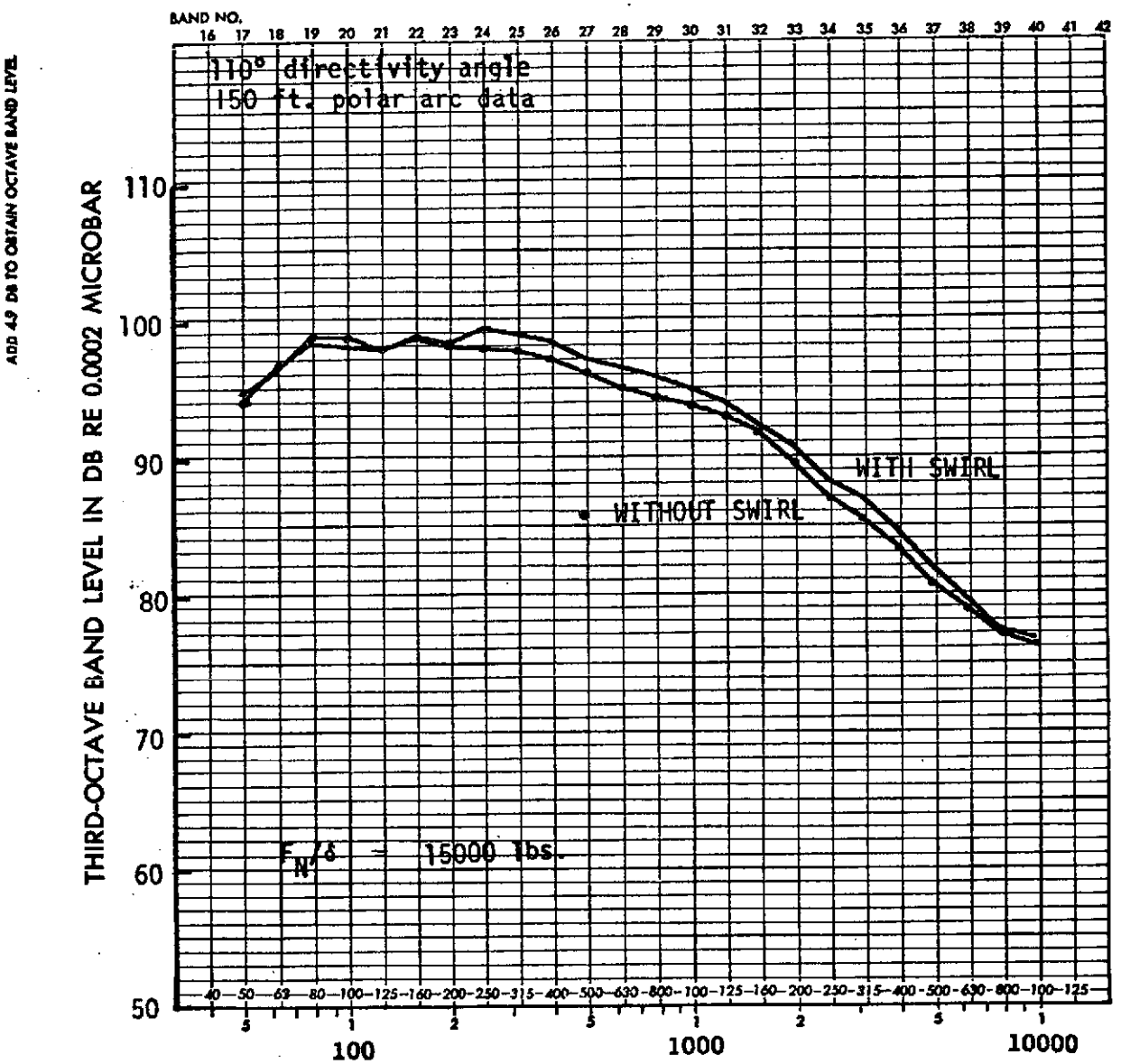

FIGURE 52. P&WA JT8D-109 NOZZLE SWIRL TEST

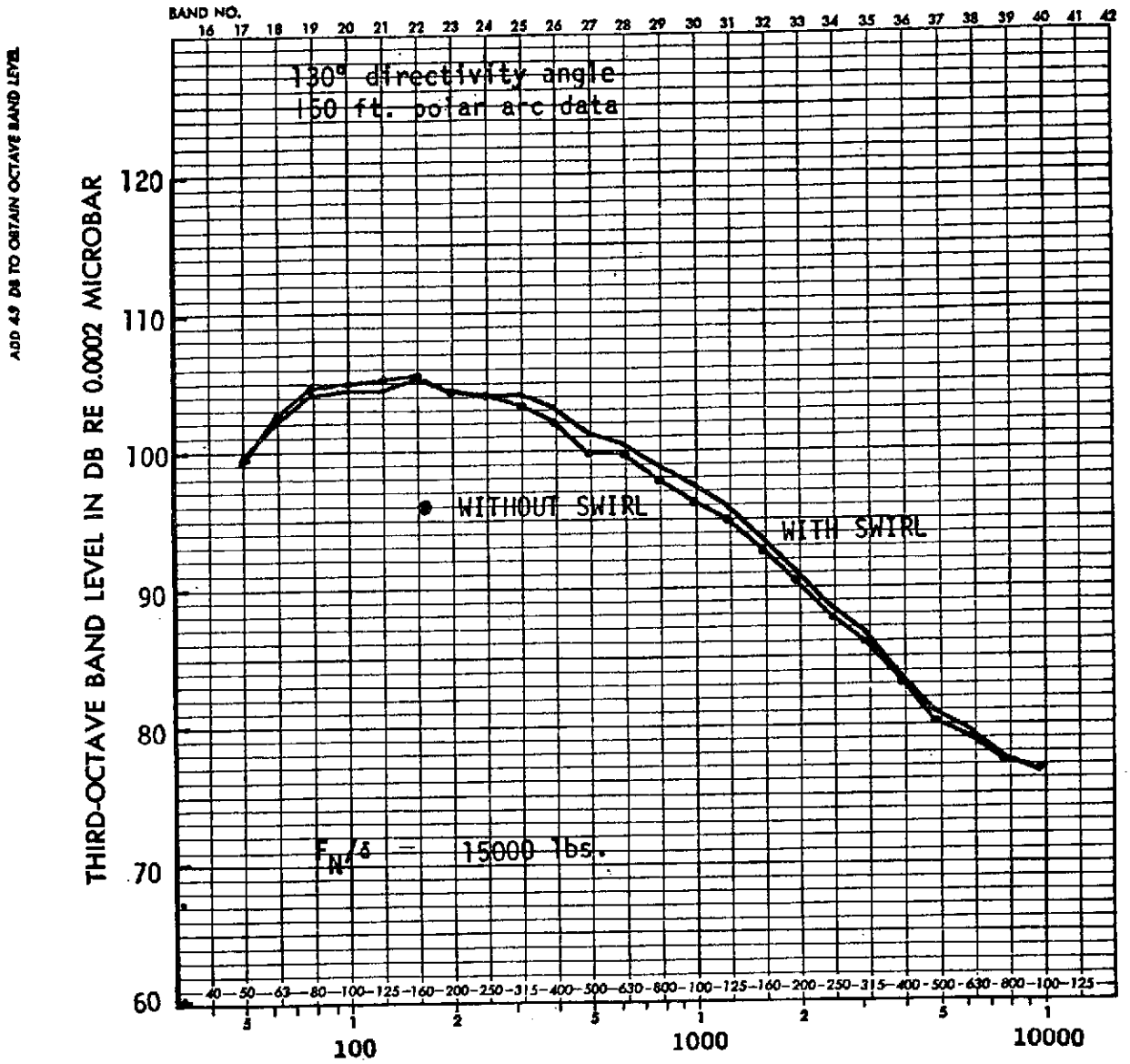

FIGURE 53. P&WA JT8D-109 NOZZLE SWIRL TEST

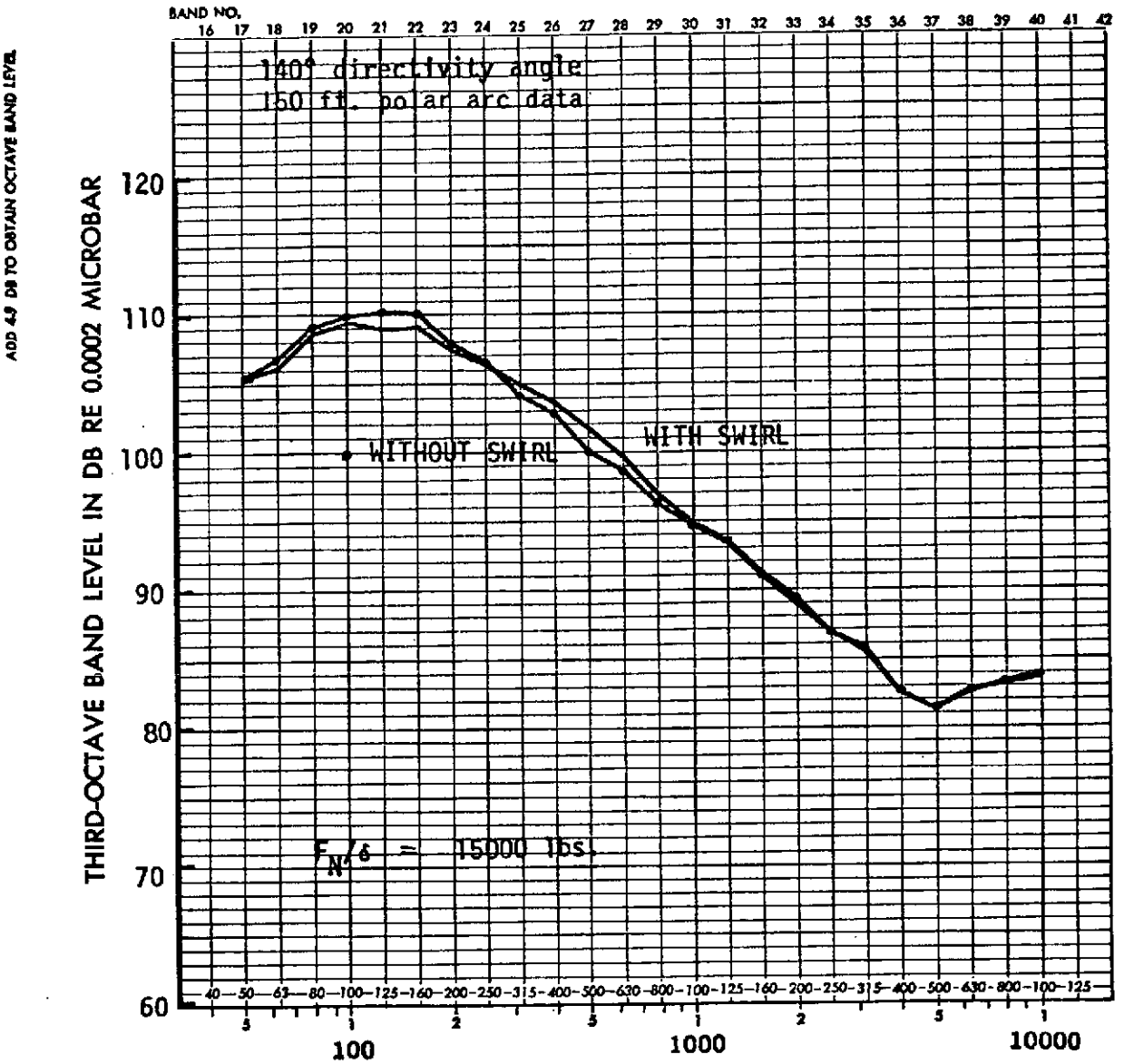

FIGURE 54. P&WA JT8D-109 NOZZLE SWIRL TEST

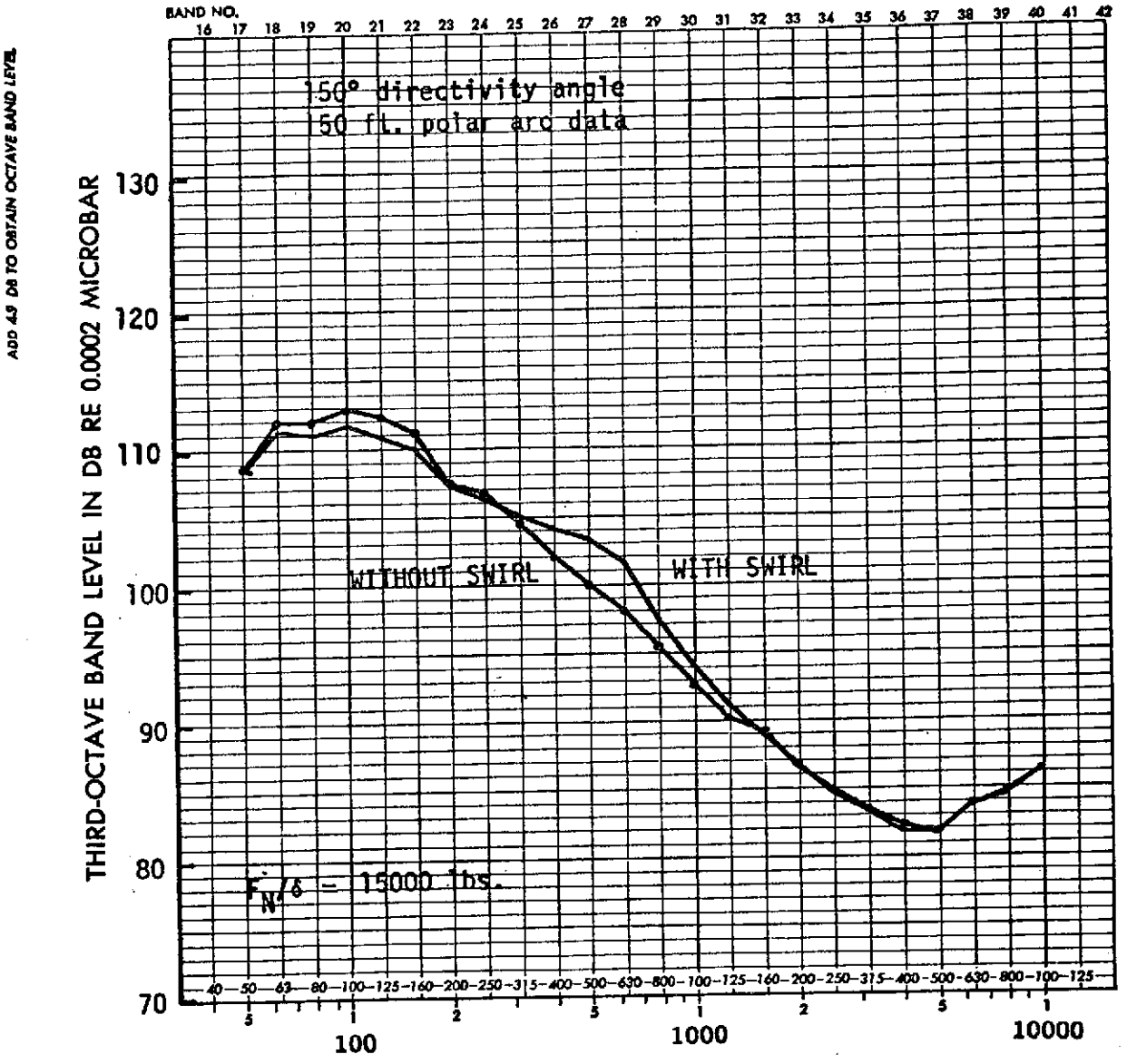

FIGURE 55. P&WA JT8D-109 NOZZLE SWIRL TEST

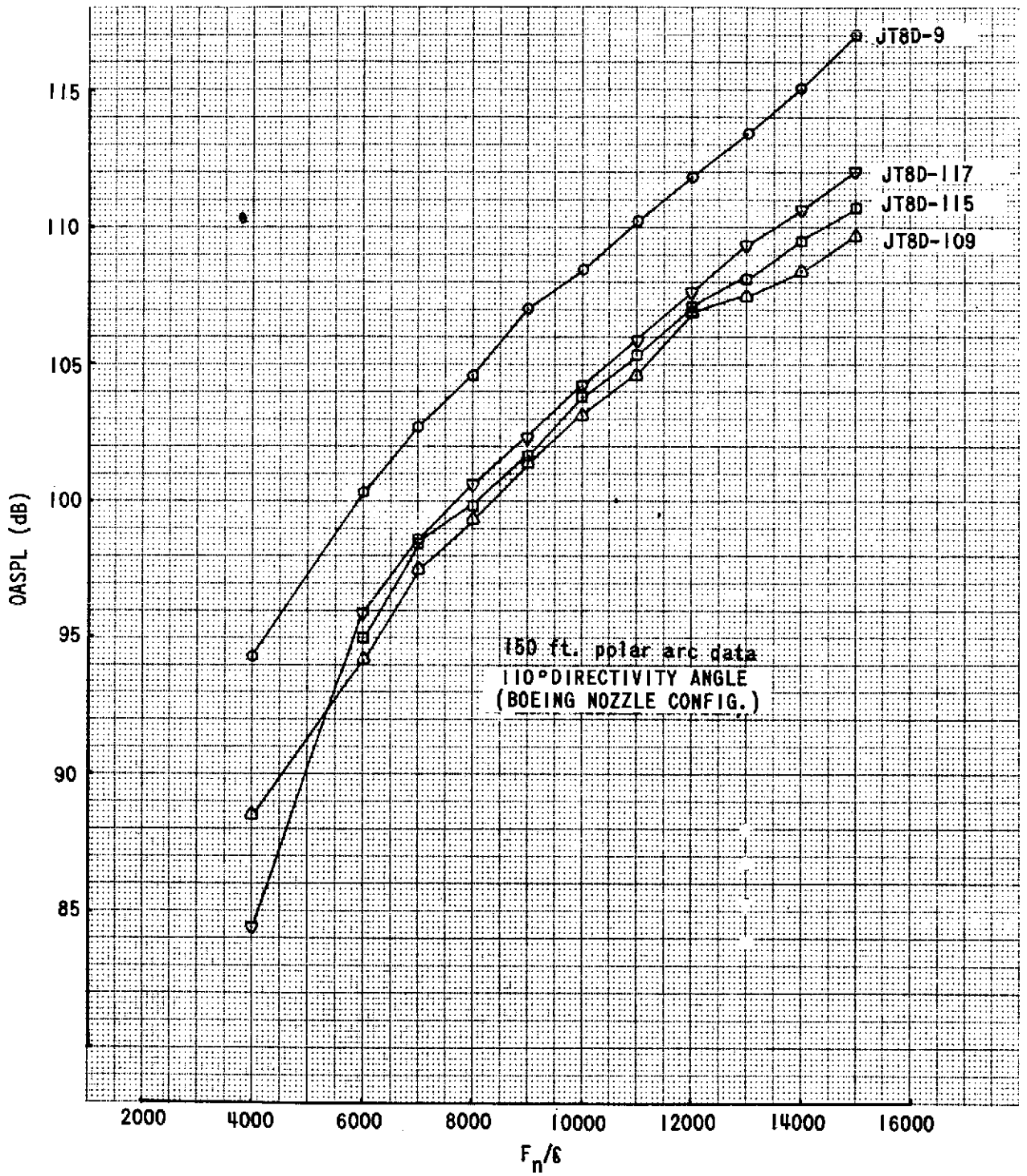

FIGURE 56. - OASPL/THRUST THROTTLING CURVES FOR JT8D-9, -109, -115, -117 NOZZLES

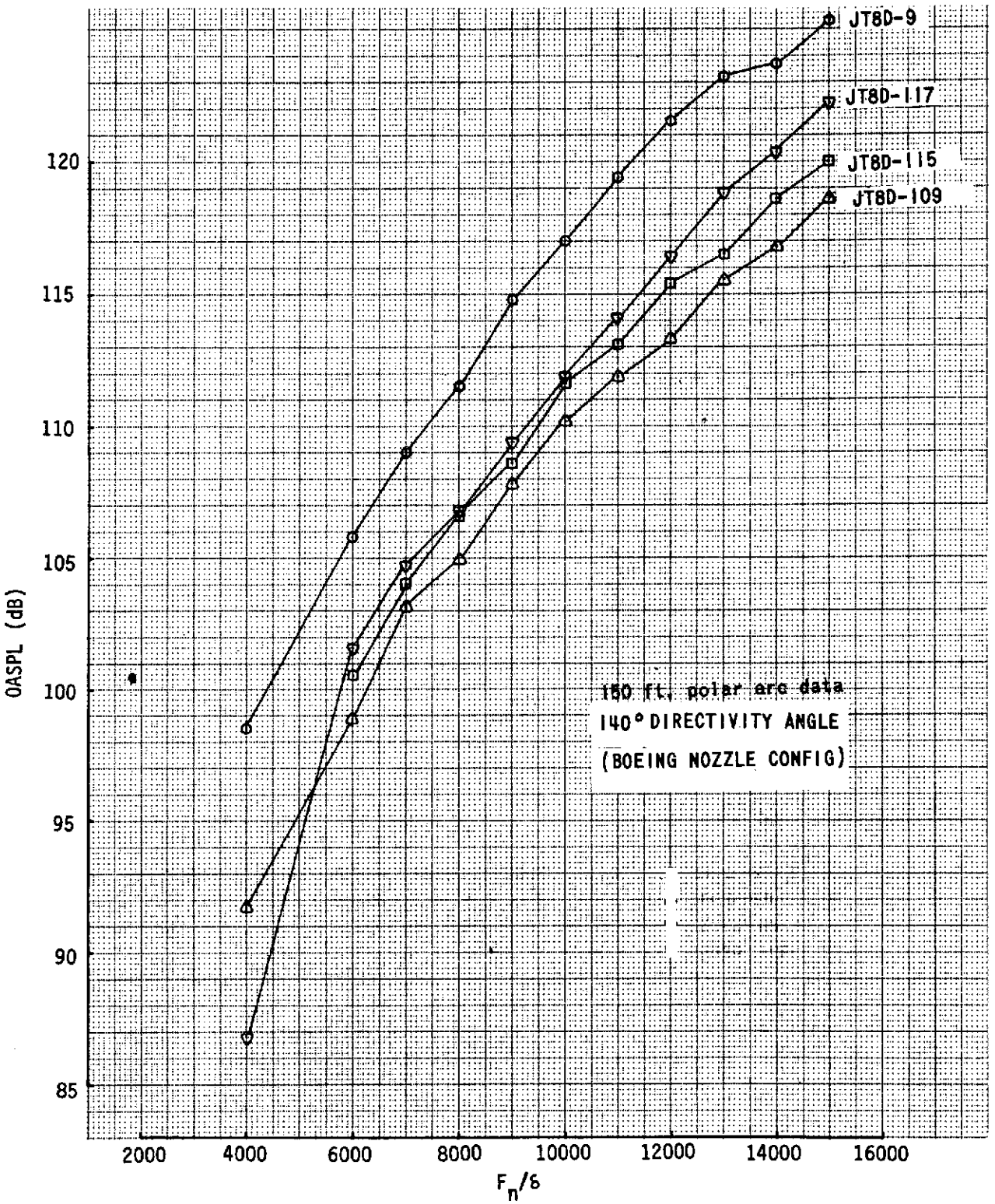

FIGURE 57. - OASPL/THRUST THROTTLING CURVE FOR JT8D-9, -109, -115, -117 NOZZLES

C 52

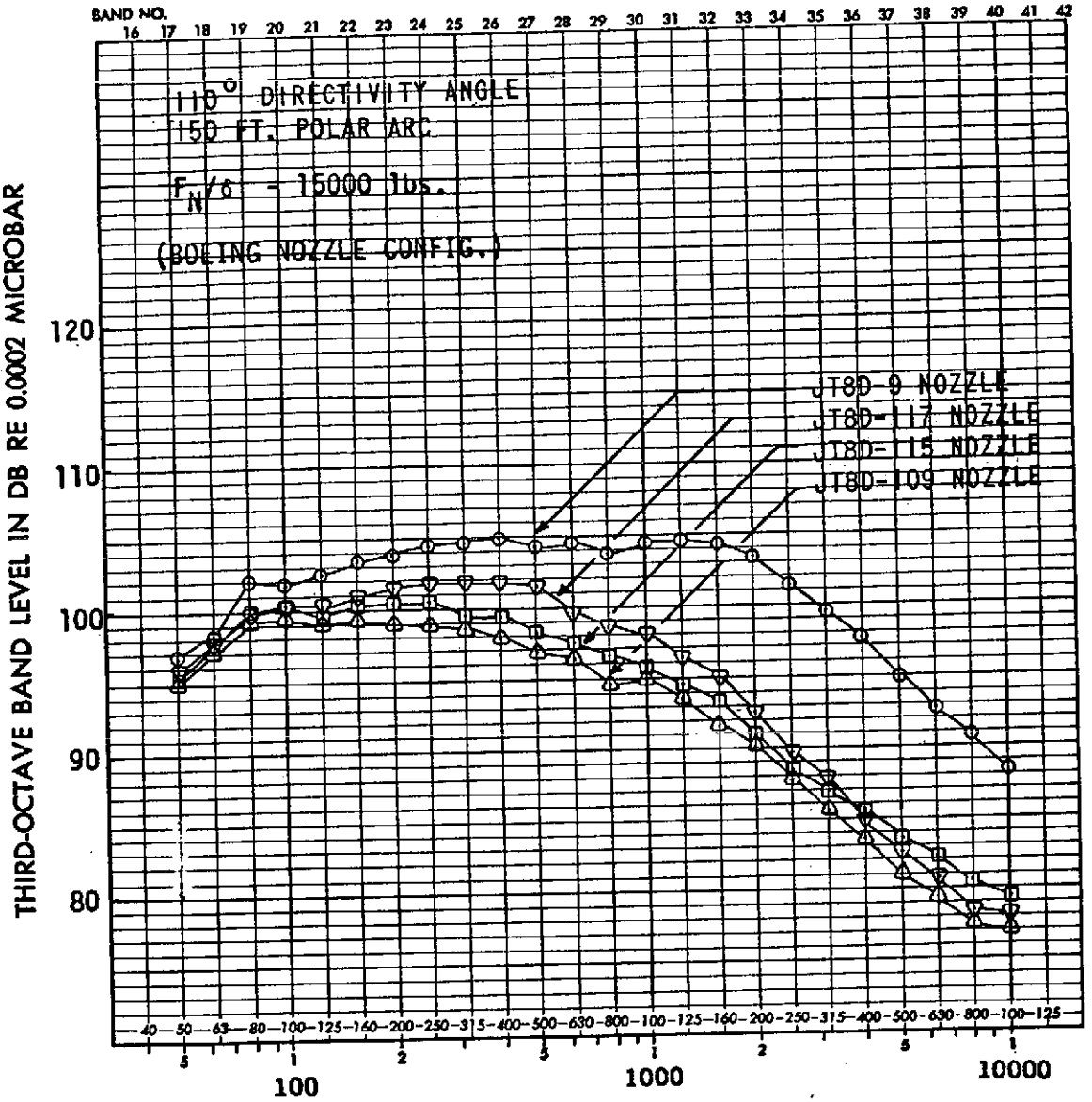

FIGURE 58. - 1/3 OCTAVE BAND SPECTRA
JT8D-9,-109,-115,-117 COMPARISON

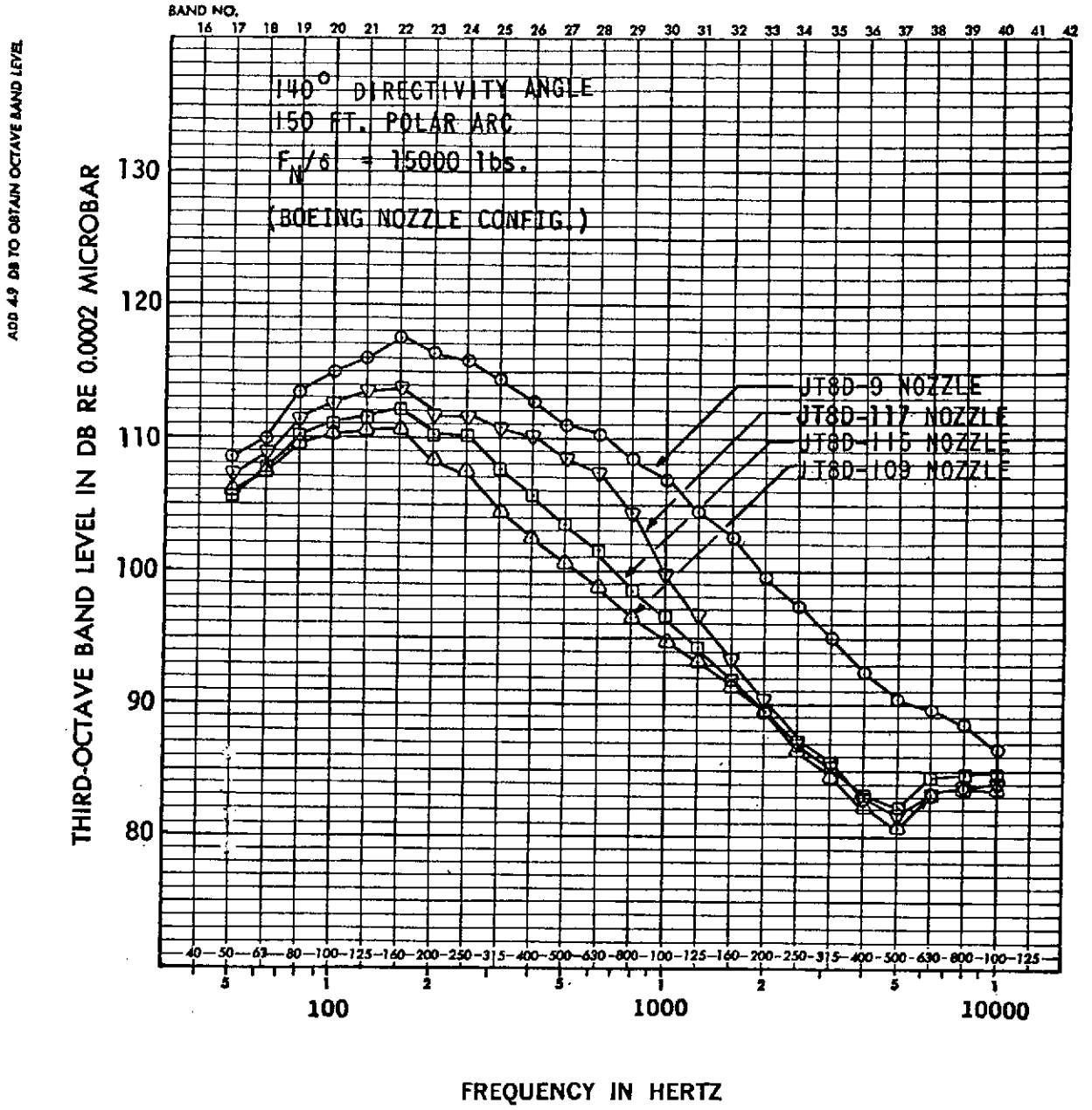

FIGURE 59. - 1/3 OCTAVE BAND SPECTRA
JT8D-9,-109,-115,-117 COMPARISON

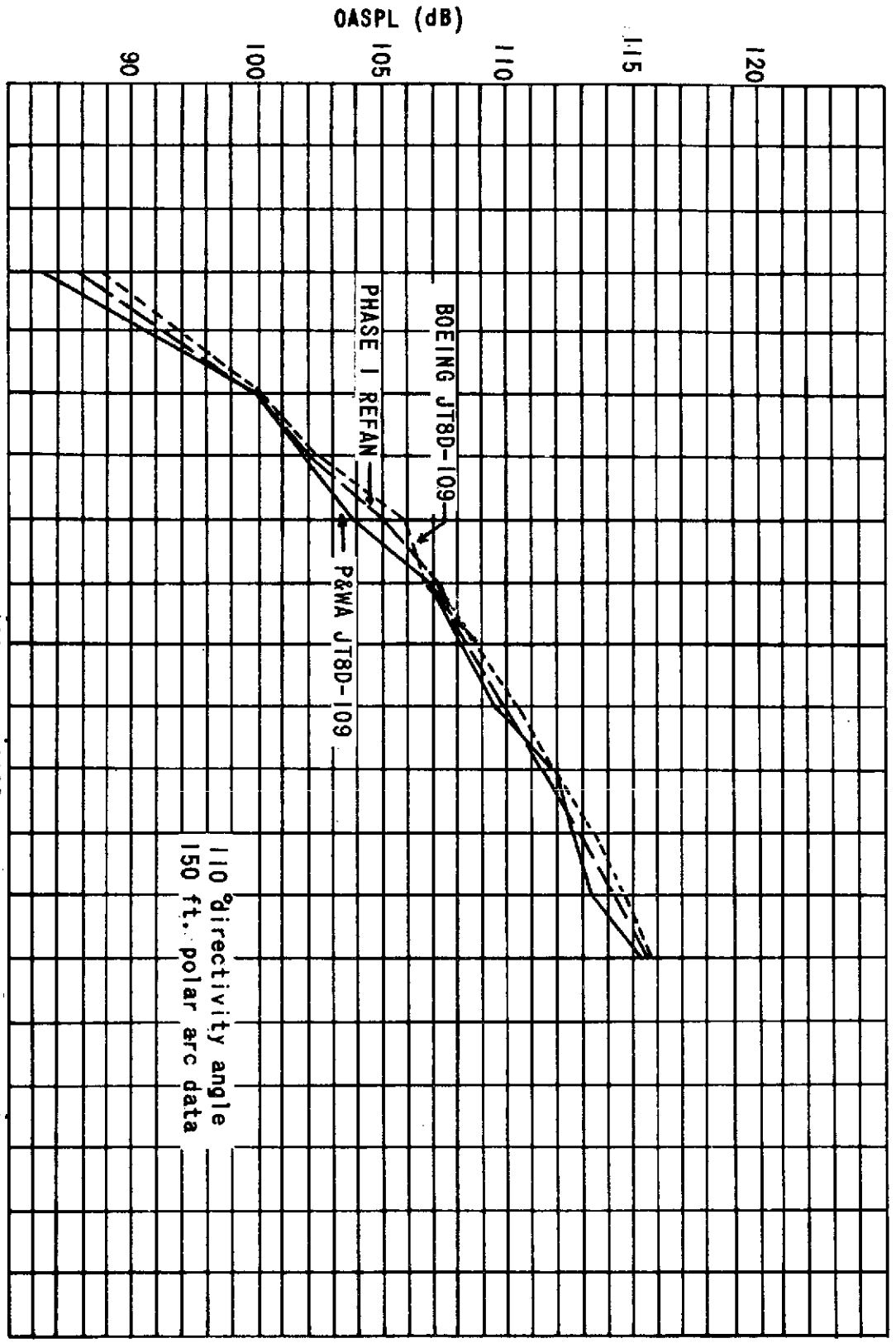

FIGURE 60. OASPL/THRUST THROTTLING CURVES FOR JT8D-109 NOZZLES

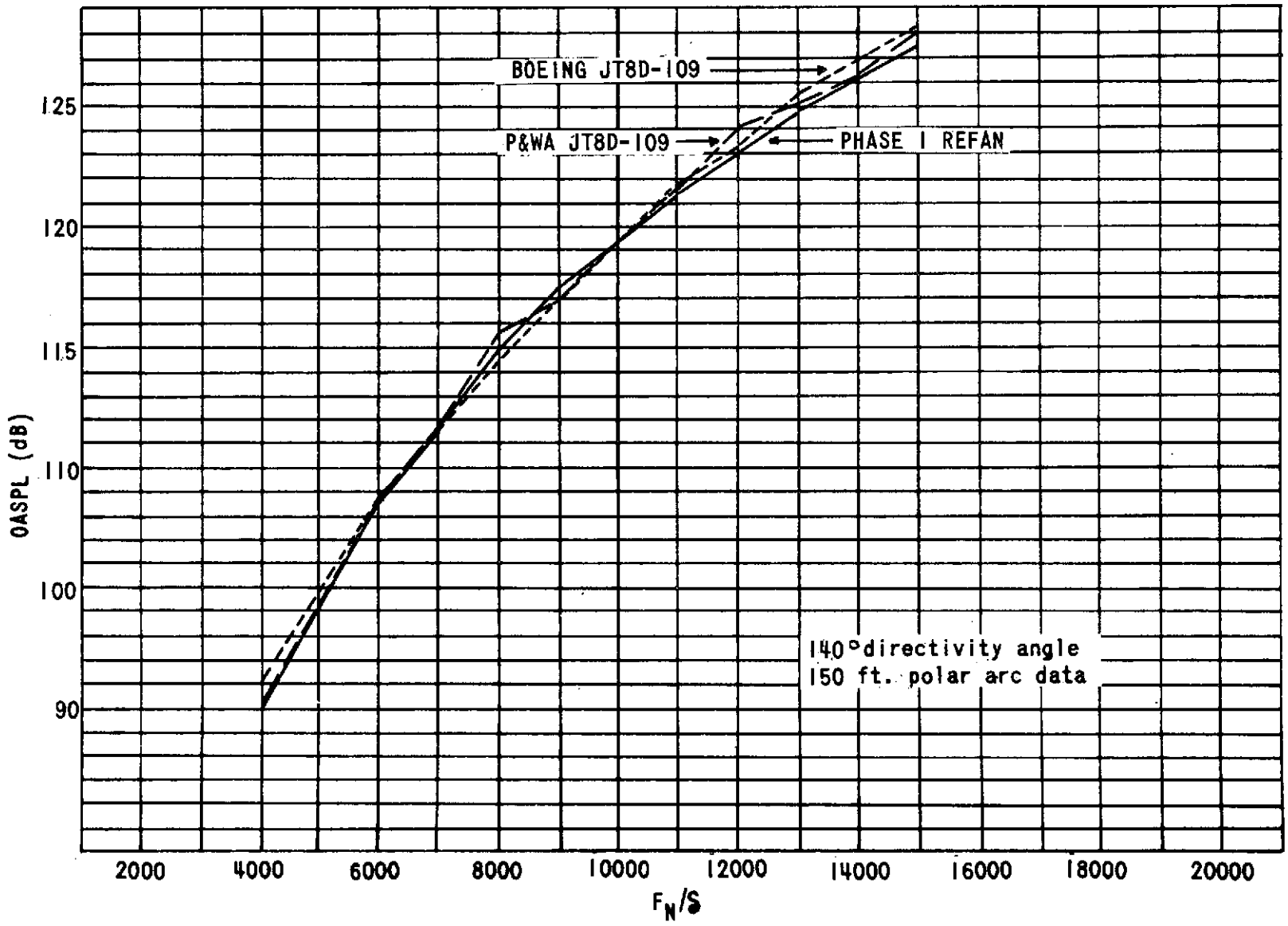

FIGURE 61. OASPL/THRUST THROTTLING CURVES FOR JT8D-109 NOZZLES

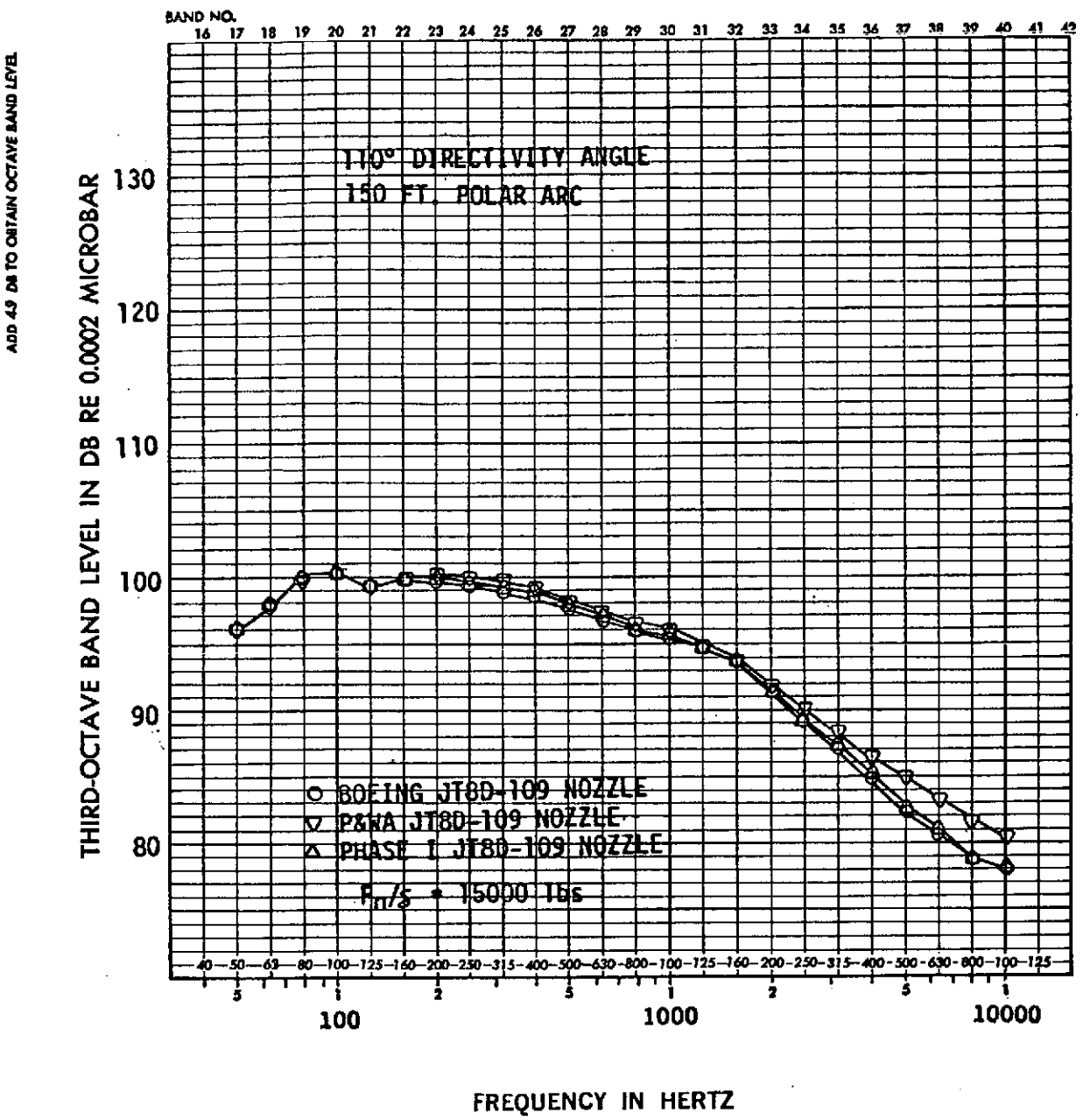

FIGURE 62. - 1/3 OCTAVE BAND SPECTRA
BOEING, P&WA, PHASE I
JT8D-109 NOZZLE COMPARISON

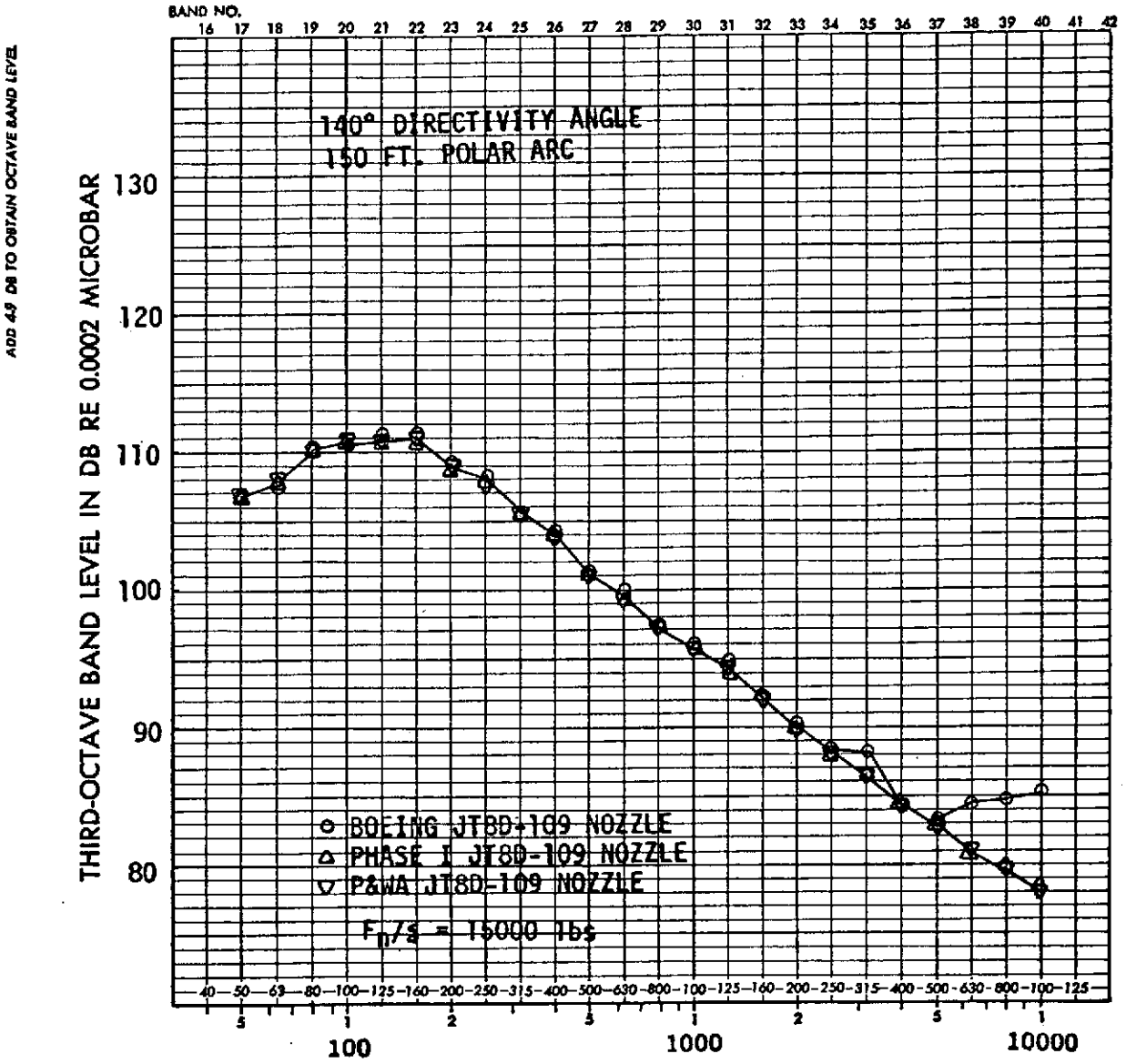

FIGURE 63. - 1/3 OCTAVE BAND SPECTRA
BOEING, P&WA, PHASE I
JT8D-109 NOZZLE COMPARISON

FIGURE 64. OASPL/THRUST THROTTLING CURVES FOR JT8D-115 NOZZLES

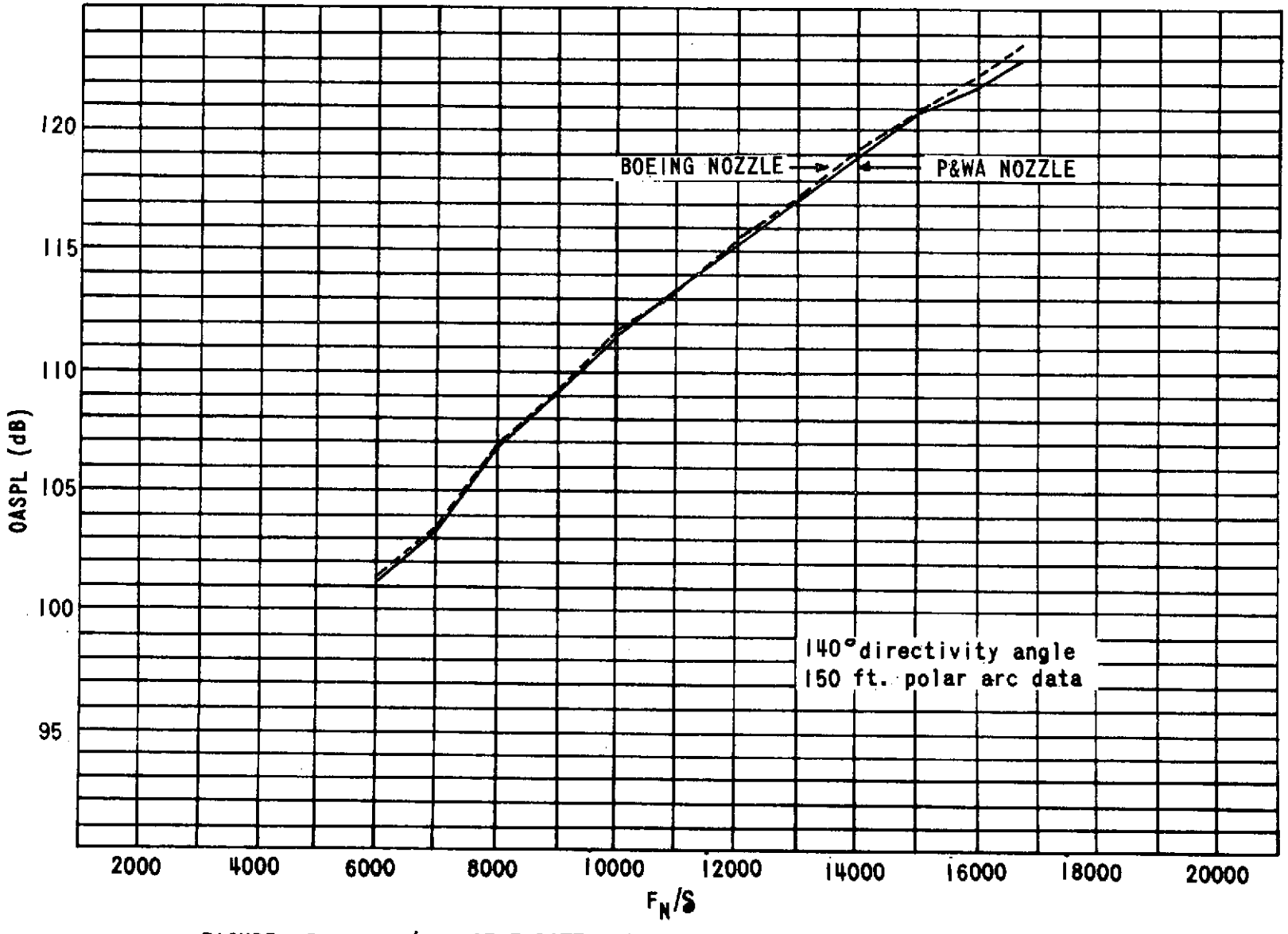

FIGURE 65. OASPL/THRUST THROTTLING CURVES FOR JT8D-115 NOZZLES

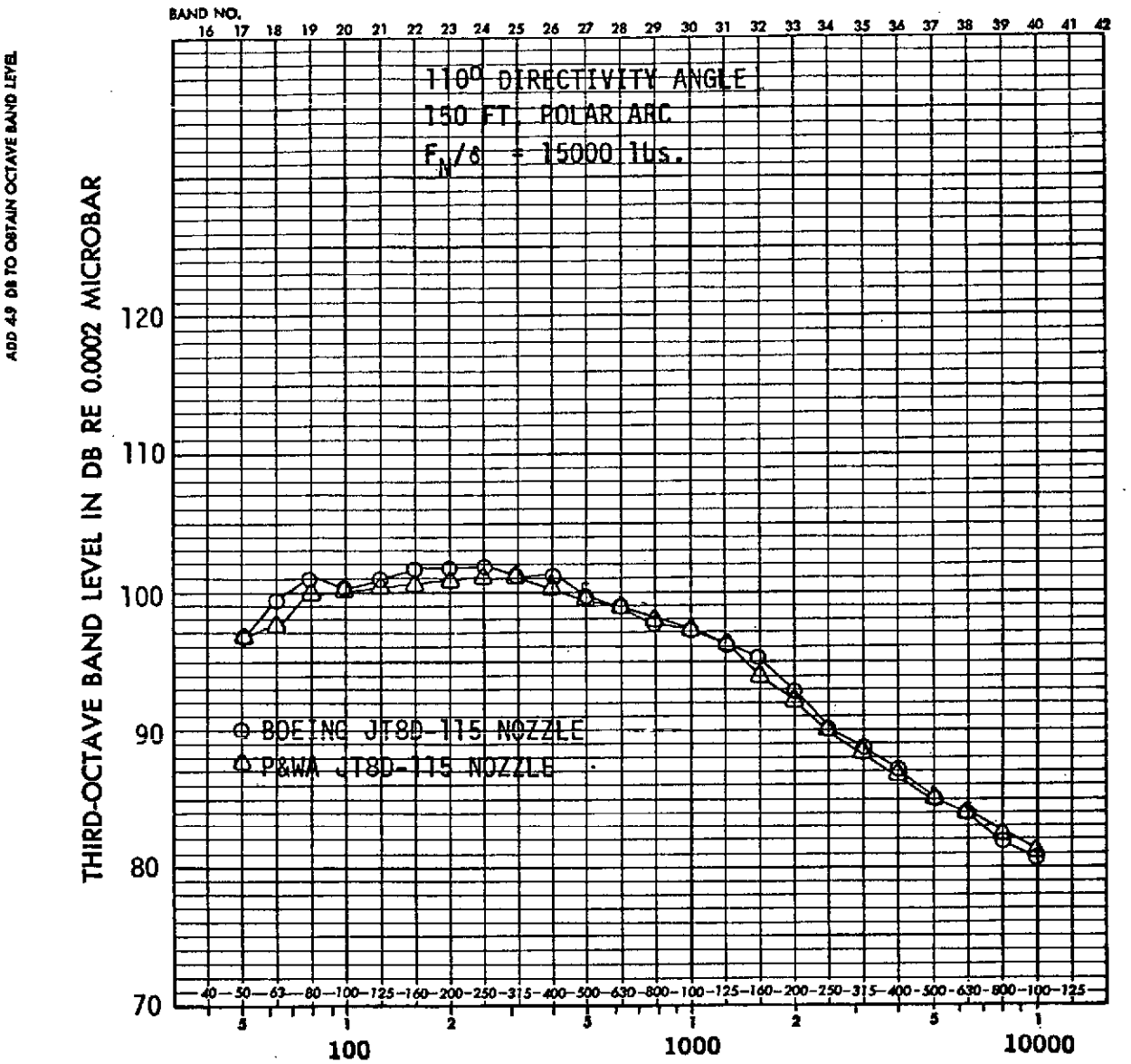

FIGURE 66. - 1/3 OCTAVE BAND SPECTRA BOEING, P&WA JT8D-115 NOZZLE COMPARISON

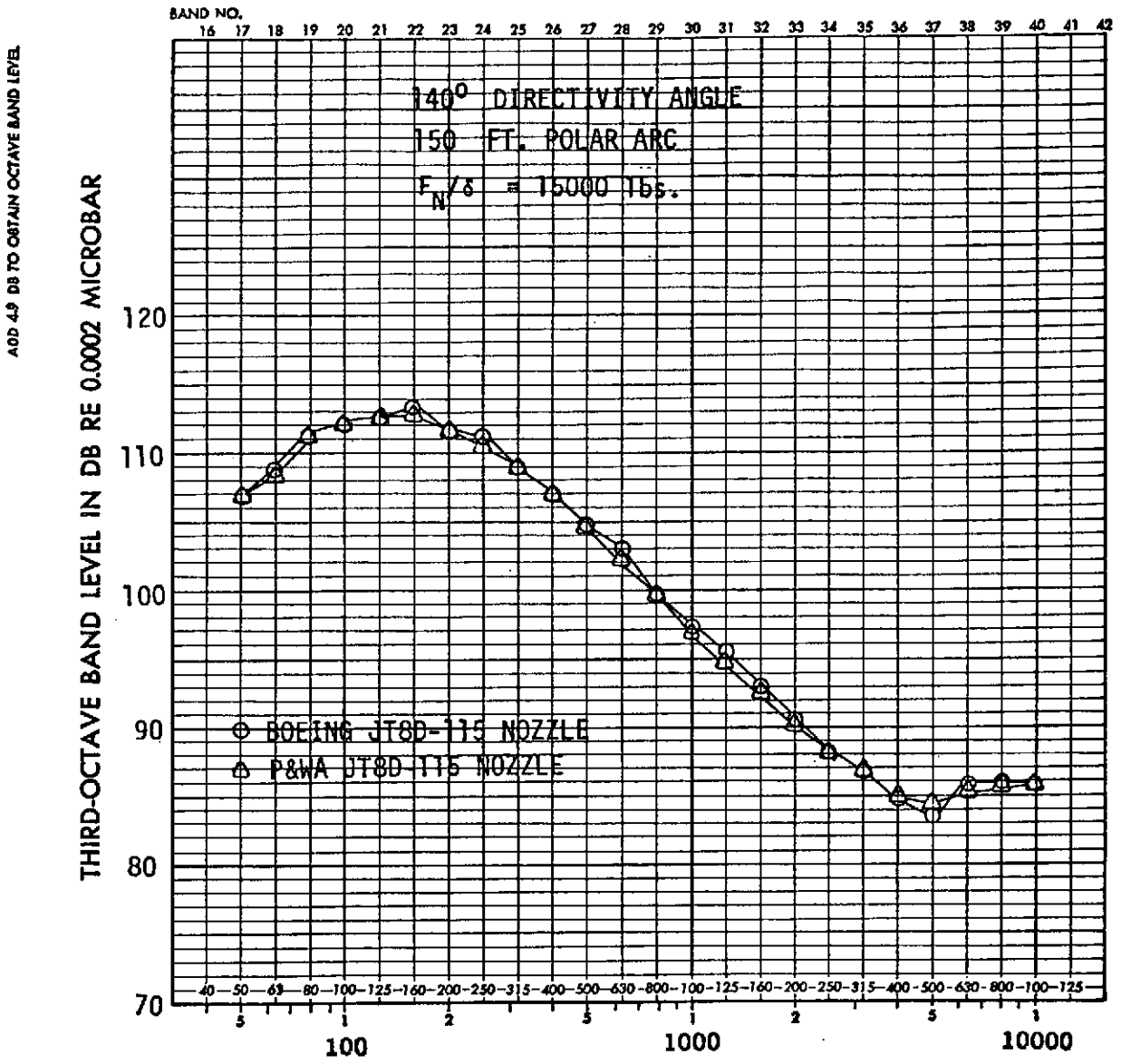

FIGURE 67. - 1/3 OCTAVE BAND SPECTRA
BOEING, P&WA JT8D-115 NOZZLE COMPARISON

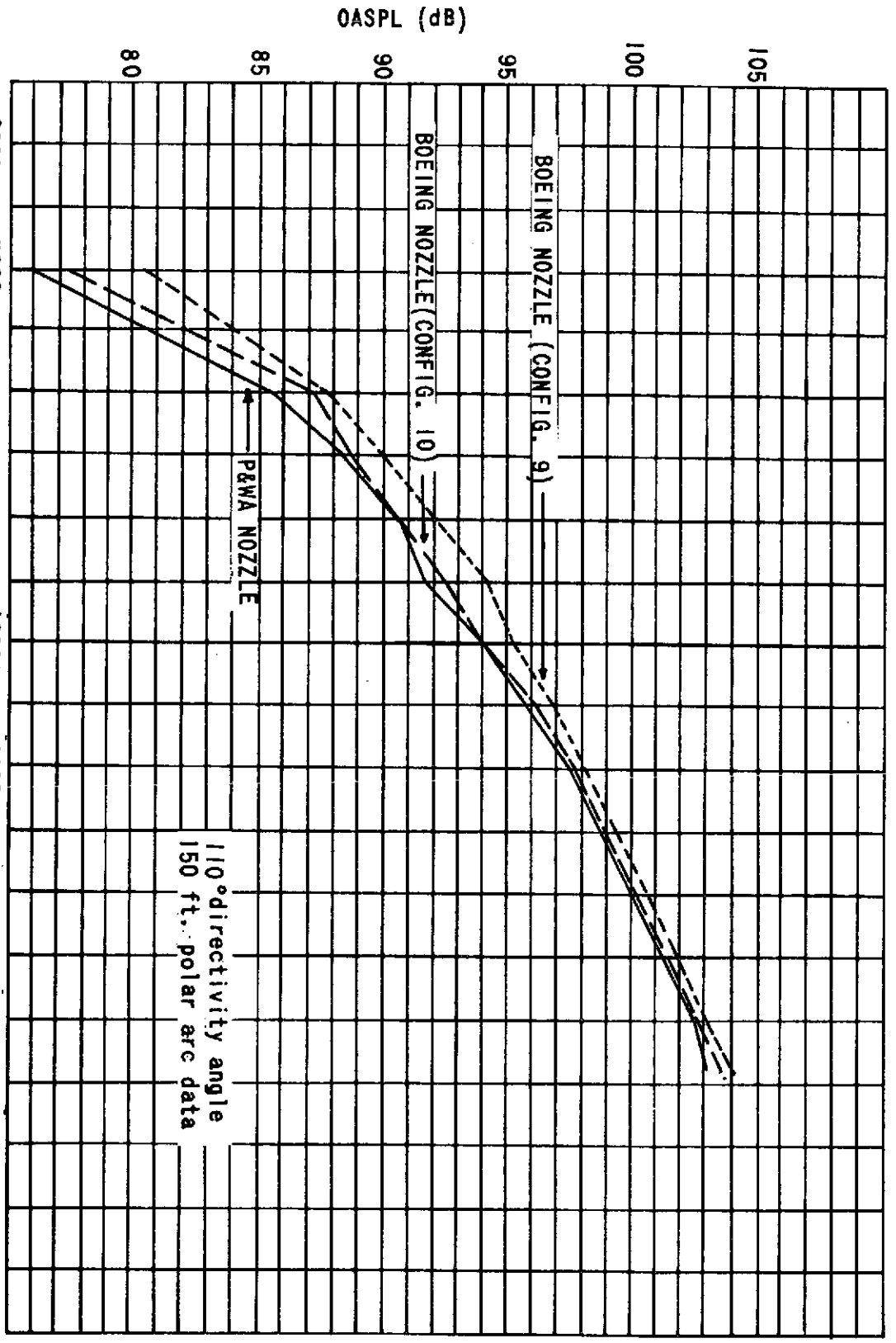

FIGURE 68. OASPL/THRUST THROTTLING CURVES FOR JT8D-117 NOZZLES

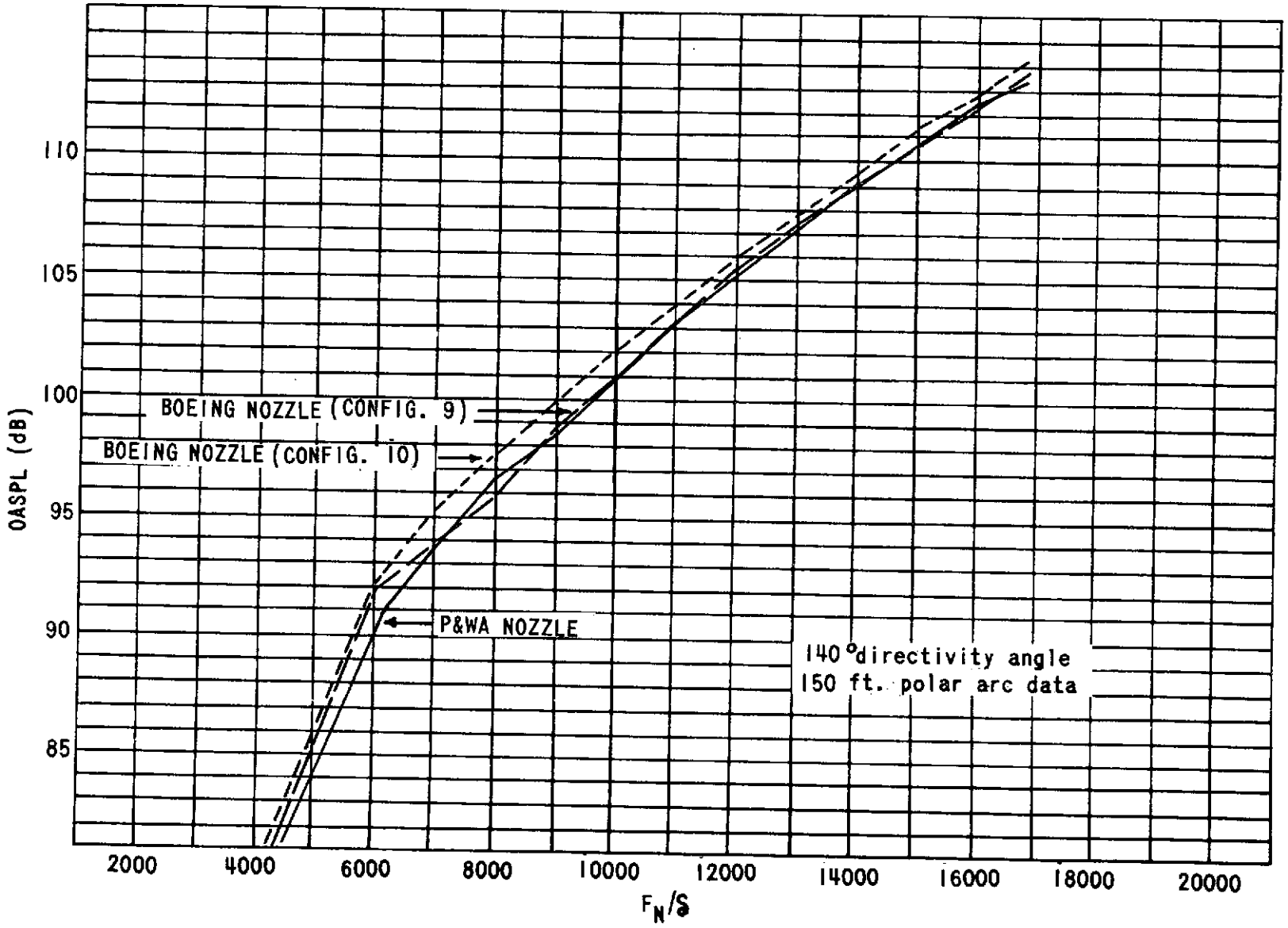

FIGURE 69. OASPL/THRUST THROTTLING CURVES FOR JT8D-117 NOZZLES

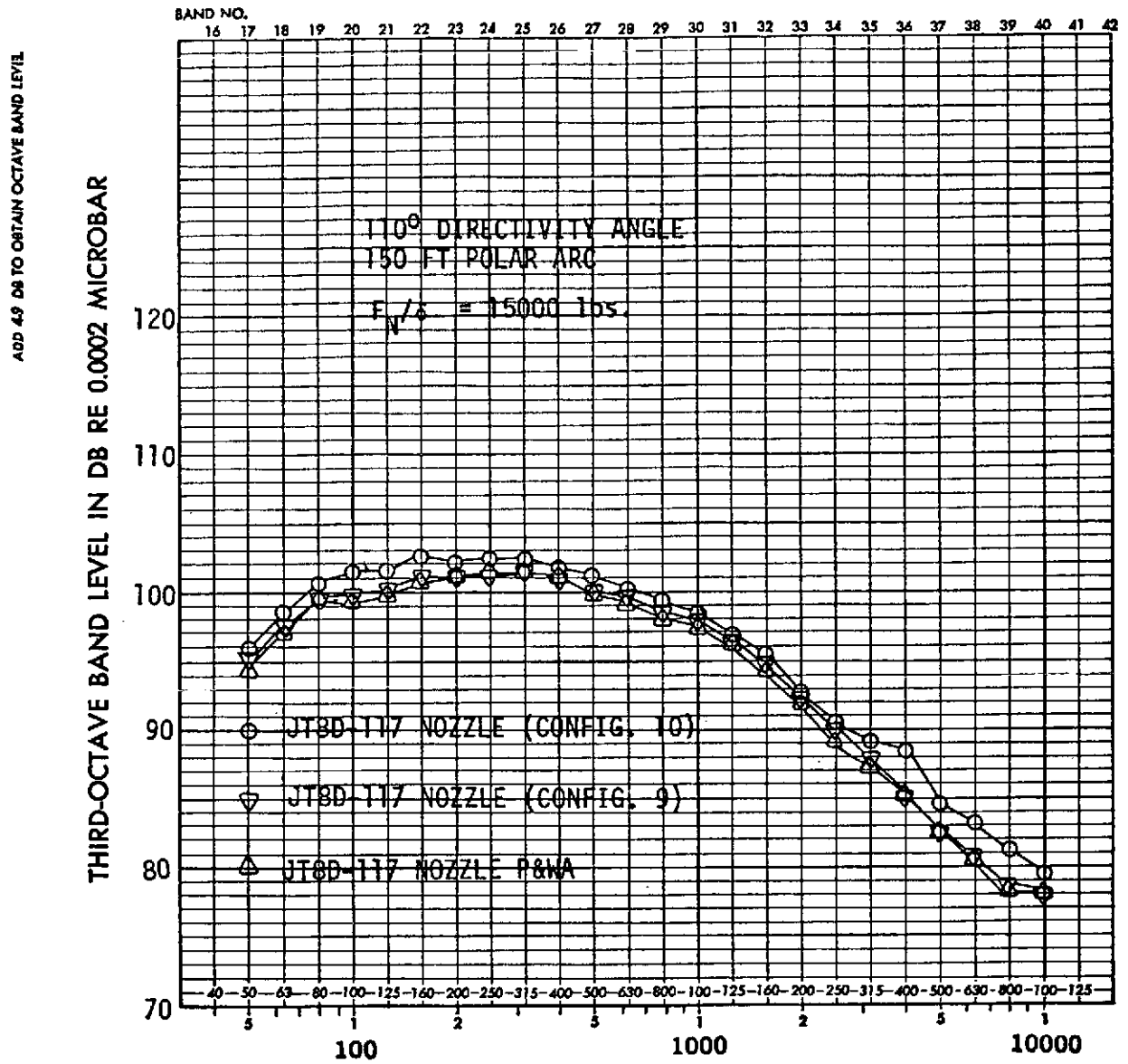

FIGURE 70. - 1/3 OCTAVE BAND SPECTRA BOEING, P&WA JT8D-117 NOZZLE COMPARISON

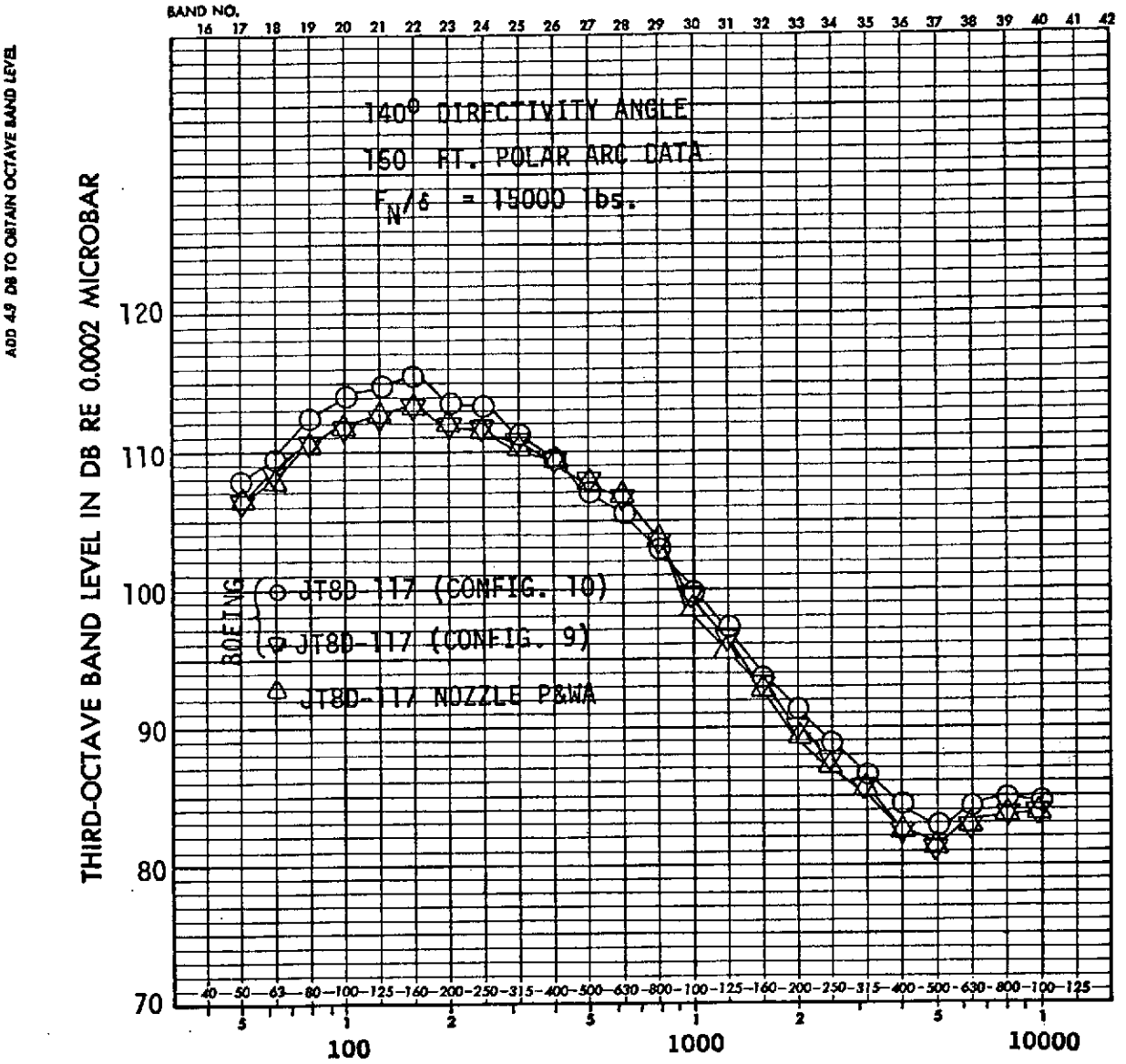

FIGURE 71. - 1/3 OCTAVE BAND SPECTRA BOEING, P&WA JT8D-117 NOZZLE COMPARISON

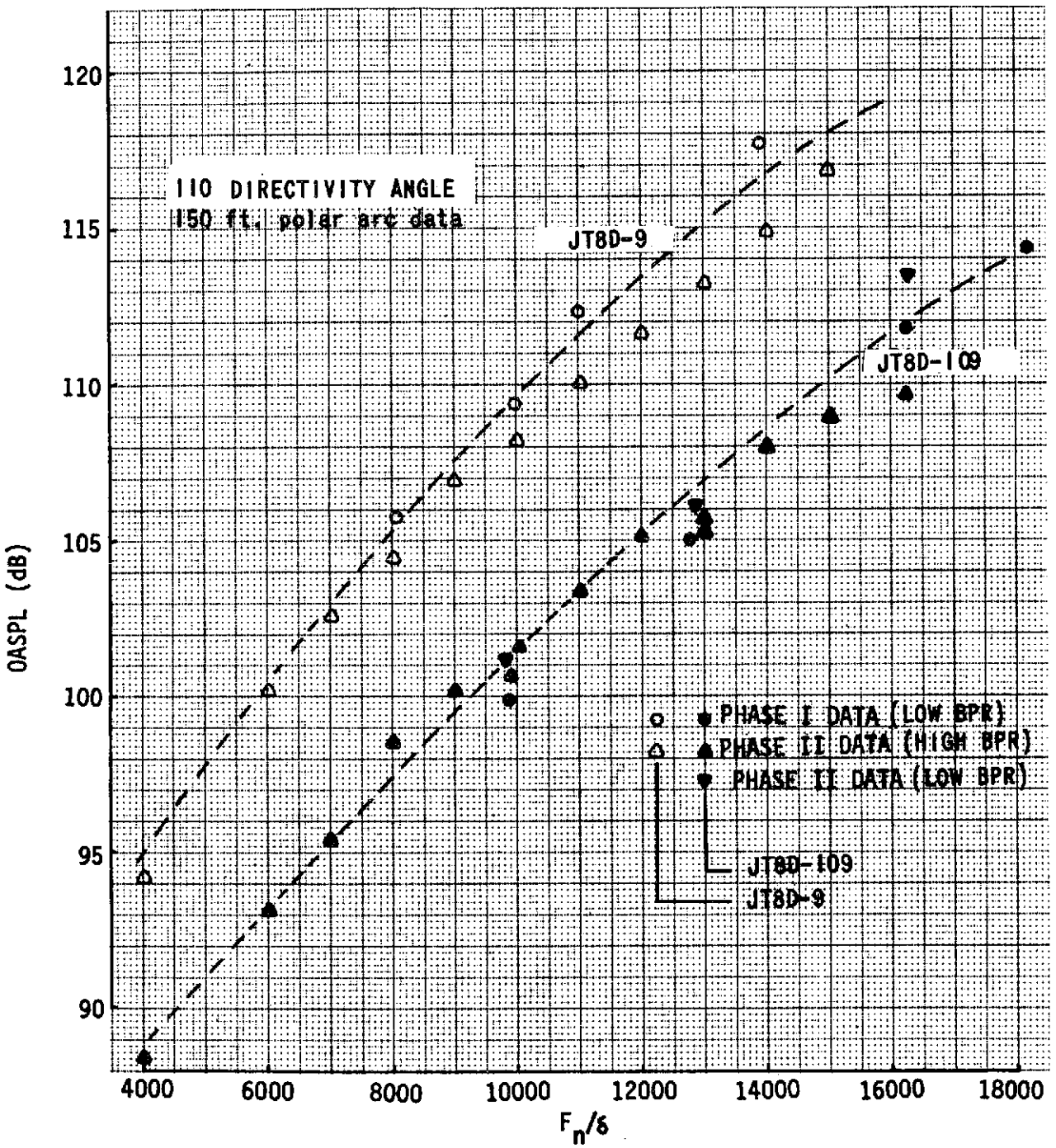

FIGURE 72. - COMPARISON OF JT8D-9 BASELINE AND JT8D-109 (PHASE I) OASPL/THRUST THROTTLING CURVES

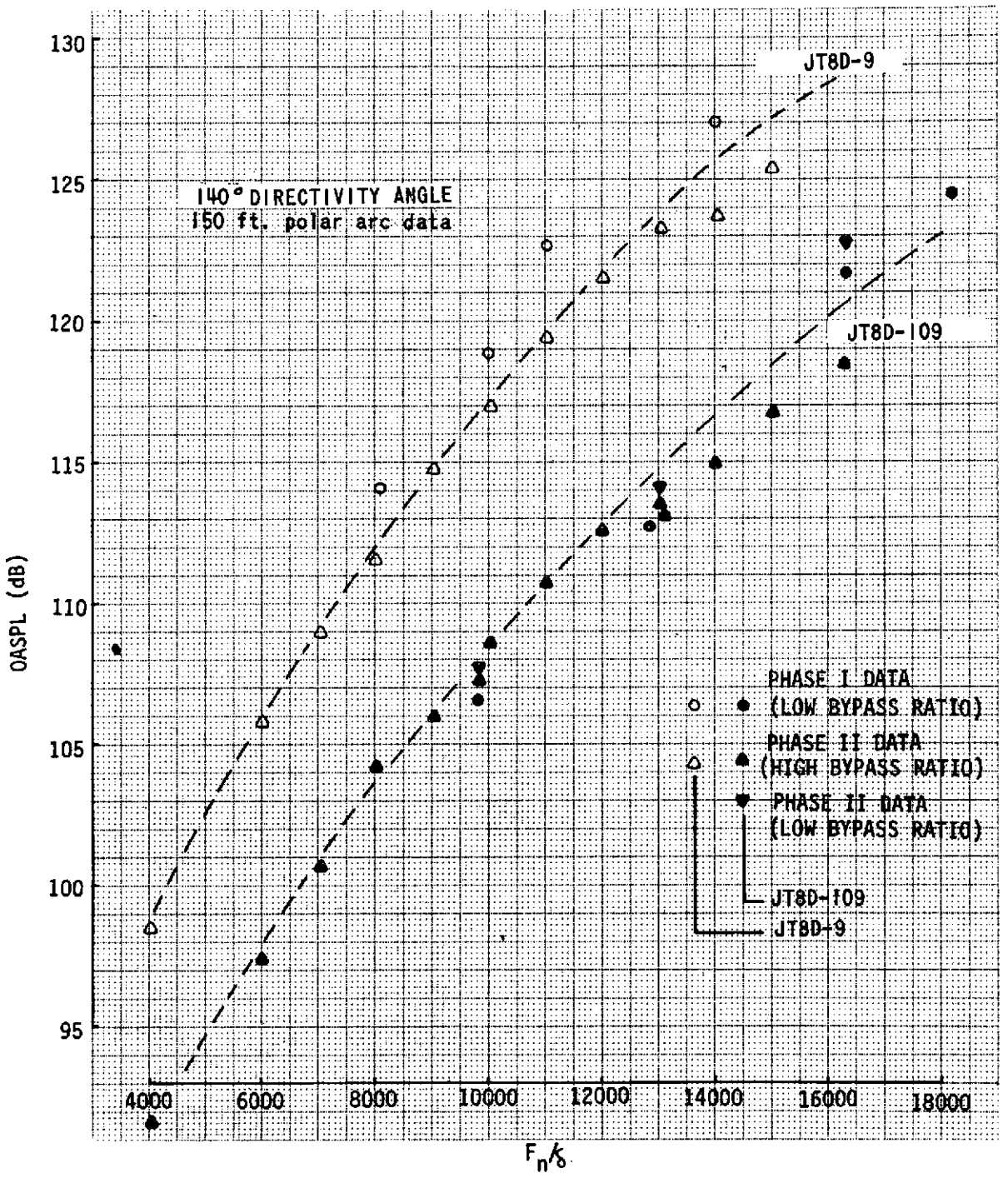

FIGURE 73. - COMPARISON OF JT8D-9 BASELINE AND JT8D-109 (PHASE I) OASPL/THRUST THROTTLING CURVES

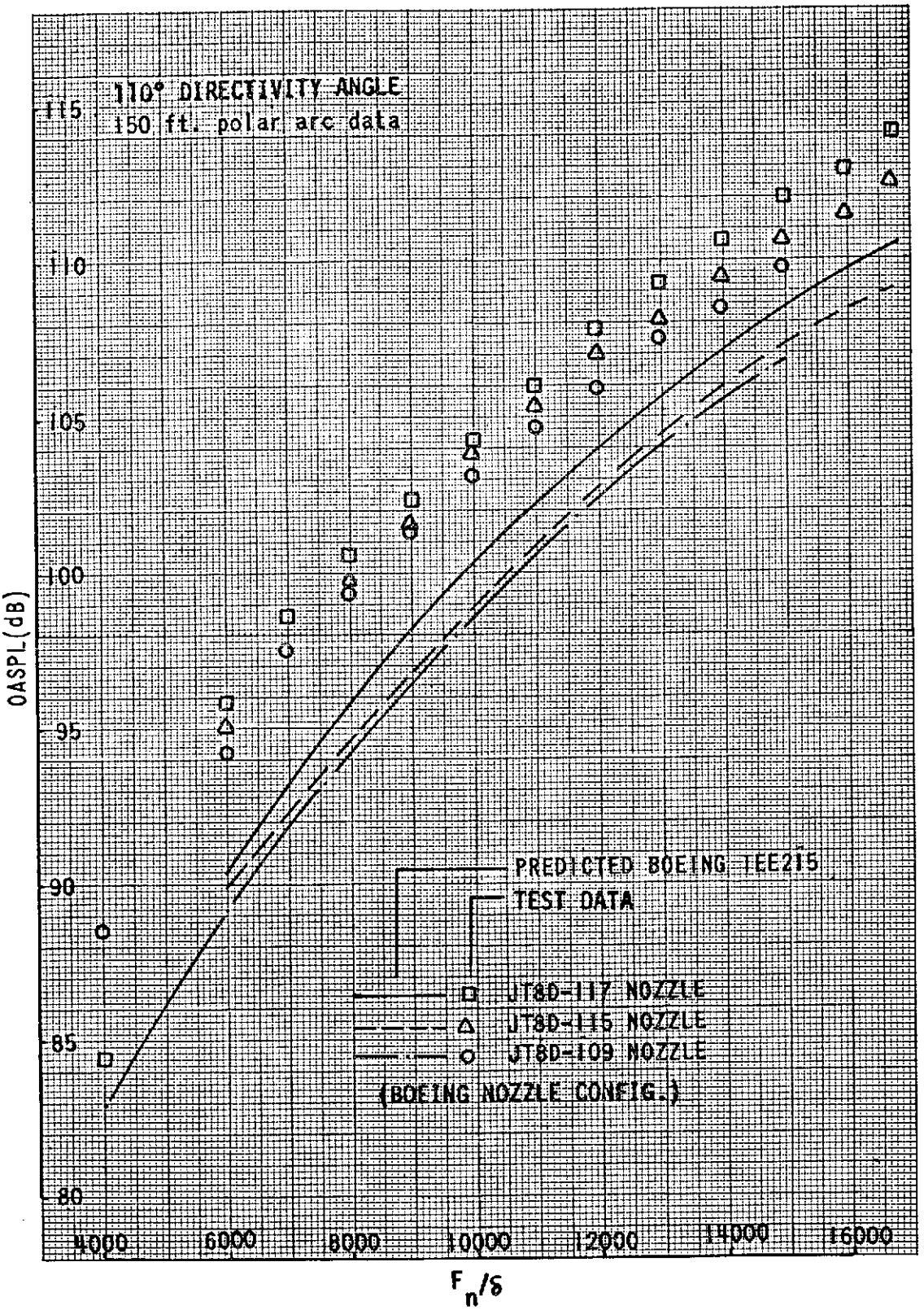

FIGURE 74. - OASPL/THRUST THROTTLING CURVES MEASURED AND PREDICTED DATA, JT8D-109,-115,-117 NOZZLES

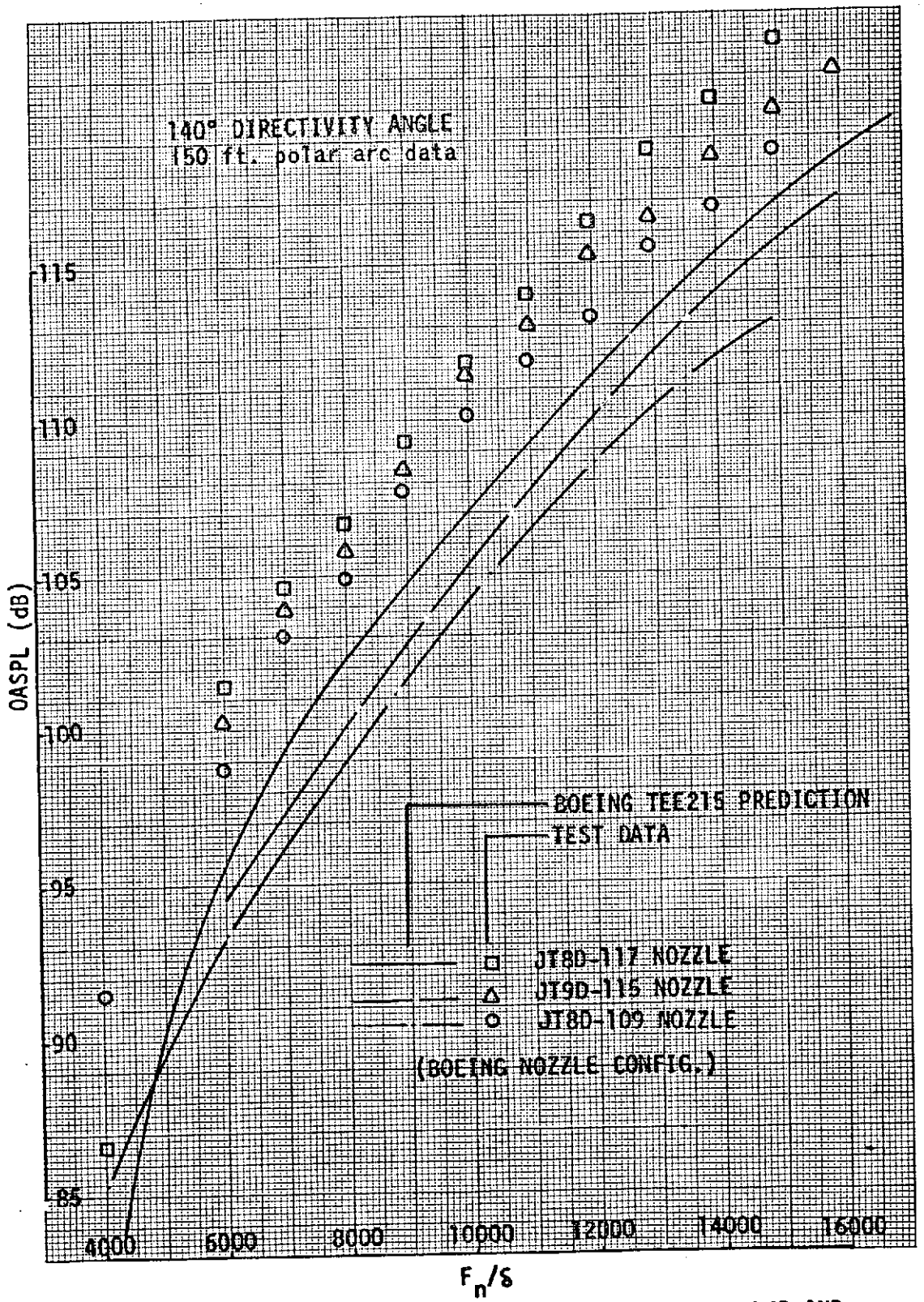

FIGURE 75. - OASPL/THRUST THROTTLING CURVES MEASURED AND PREDICTED DATA, JT8D-109,-115,-117 NOZZLES

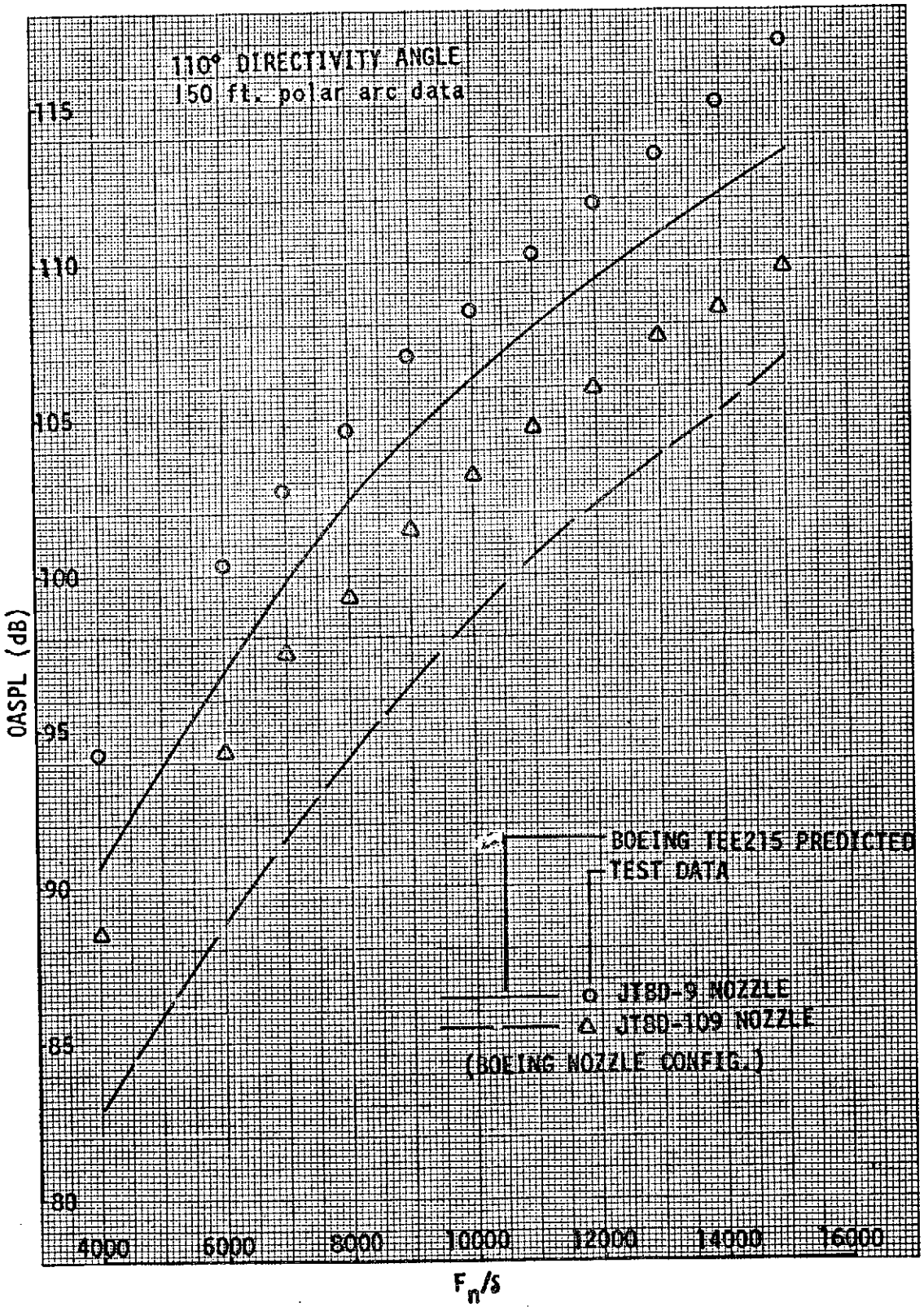

FIGURE 76. - OASPL/THRUST THROTTLING CURVES MEASURED AND PREDICTED DATA JT8D-9,-109 NOZZLES

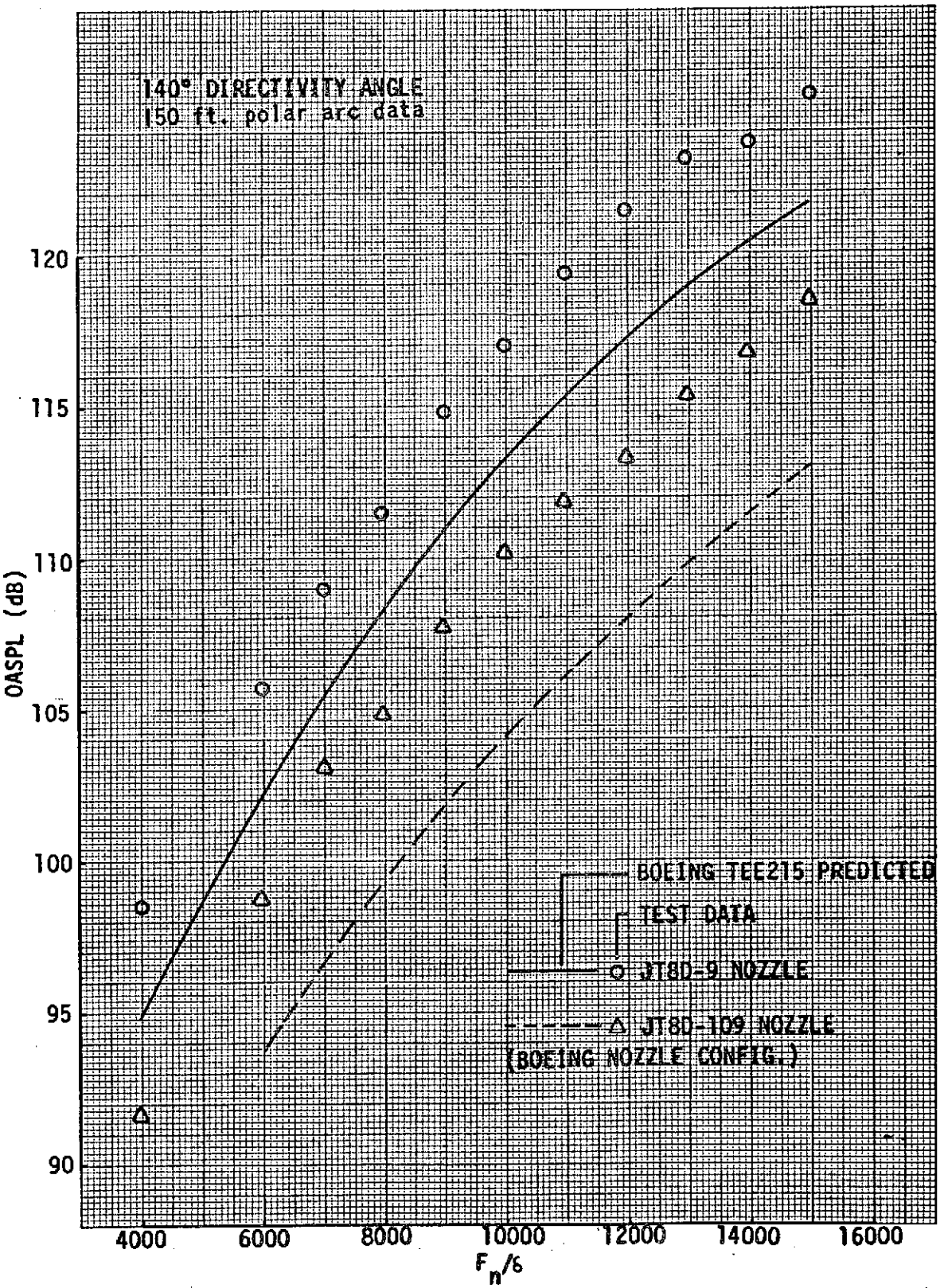

FIGURE 77. - OASPL/THRUST THROTTLING CURVES JT8D-9,-109 NOZZLES MEASURED AND PREDICTED DATA AT MODEL TEST CONDITIONS

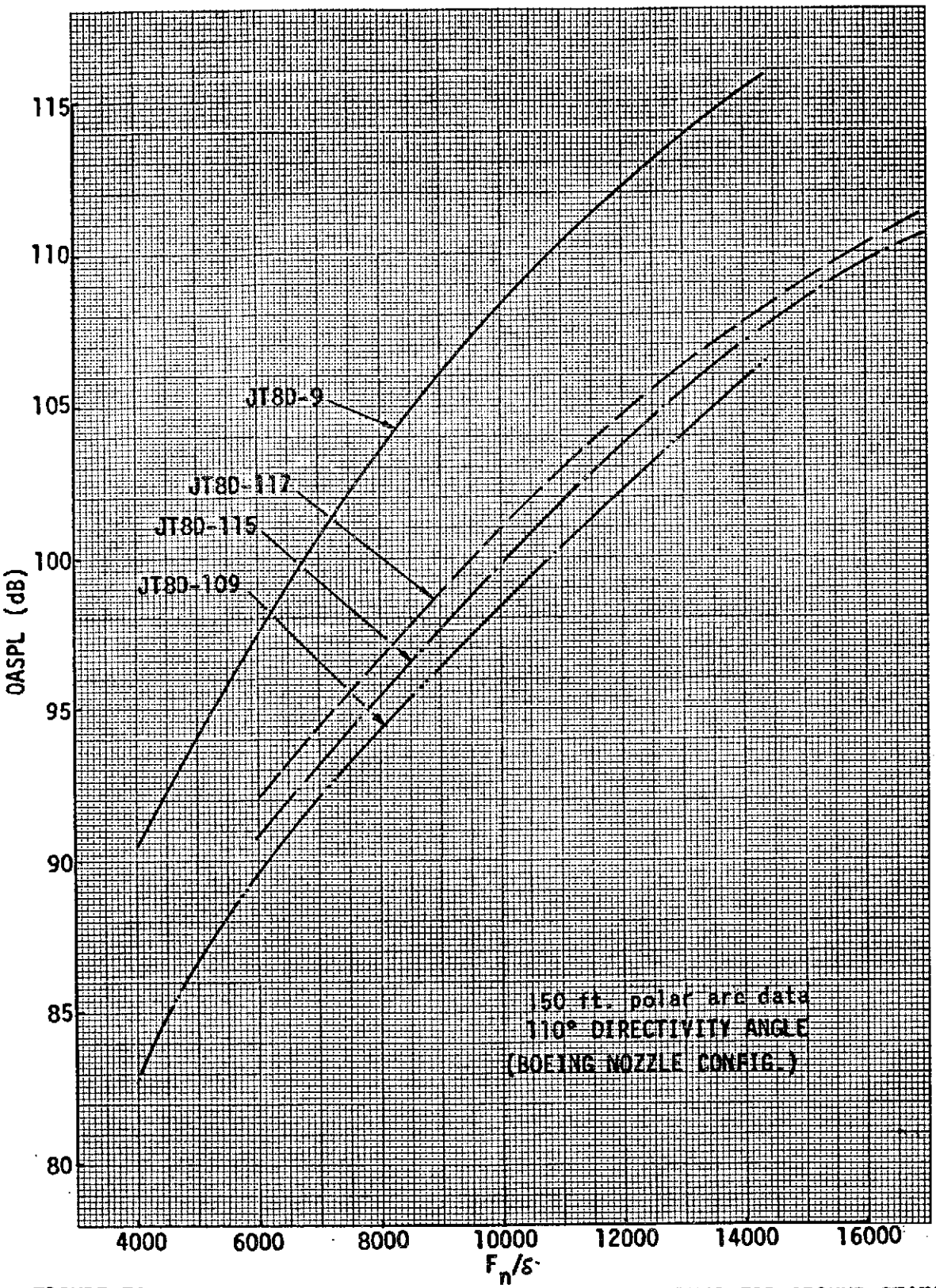

FIGURE 78. - PREDICTED OASPL/THRUST THROTTLING CURVES FOR GROUND STATIC ENGINE CONDITIONS BOEING PREDICTION PROCEDURE TEE215

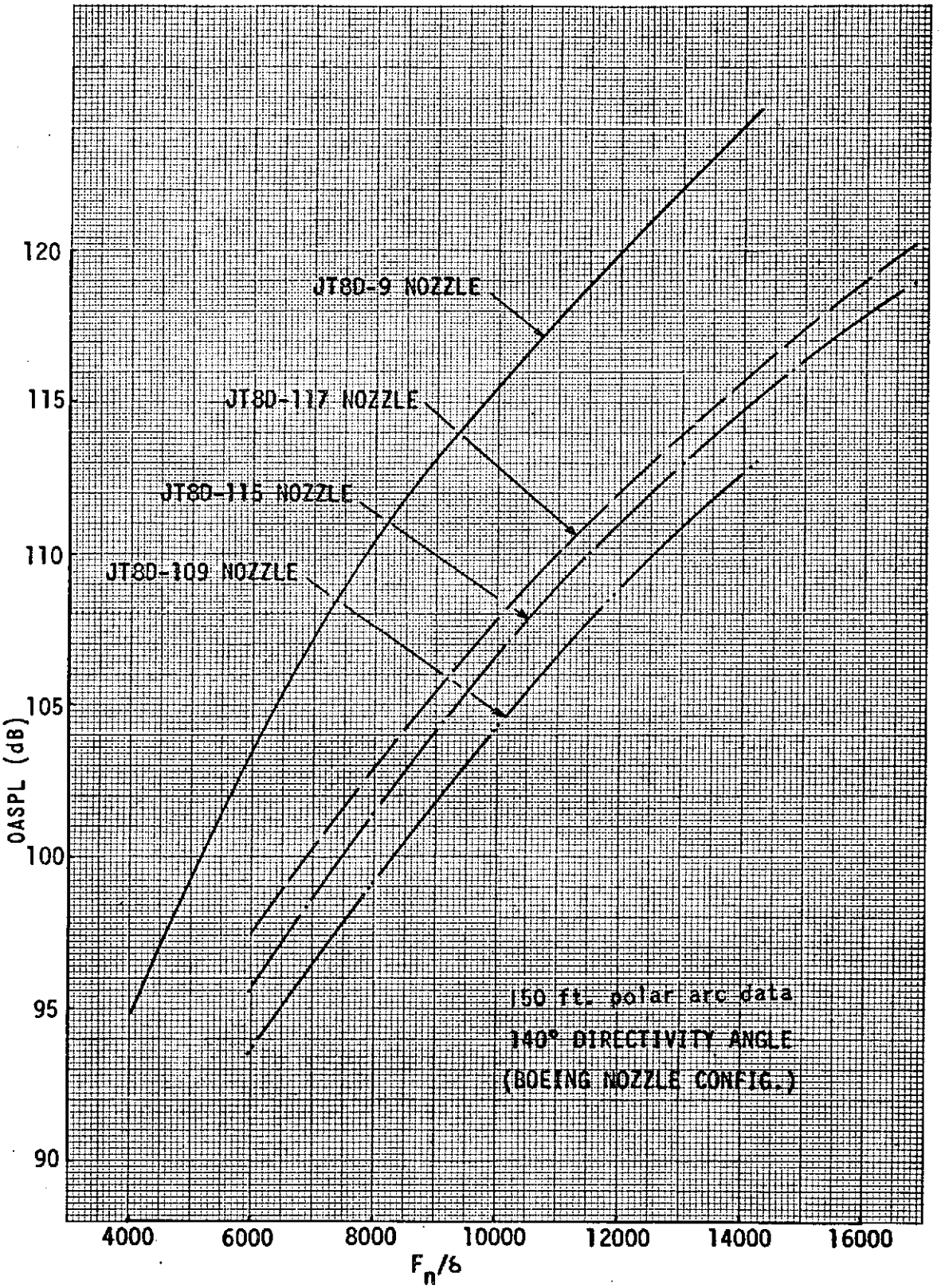

FIGURE 79. - PREDICTED OASPL/THRUST THROTTLING CURVES FOR GROUND STATIC CONDITIONS USING BOEING TEE215 PREDICTION PROCEDURE

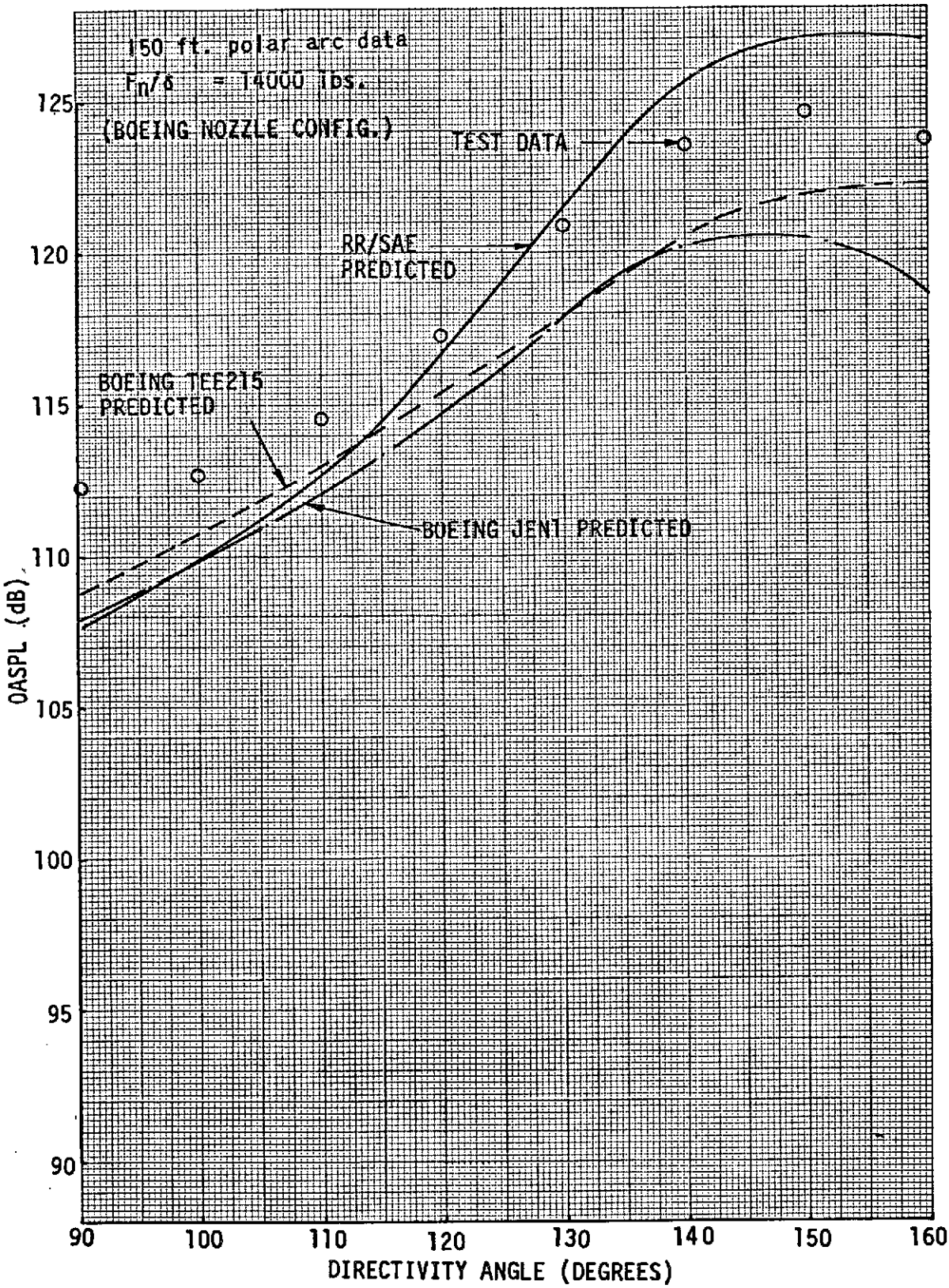

FIGURE 80. - OASPL DIRECTIVITY JT8D-9 MEASURED AND PREDICTED DATA.

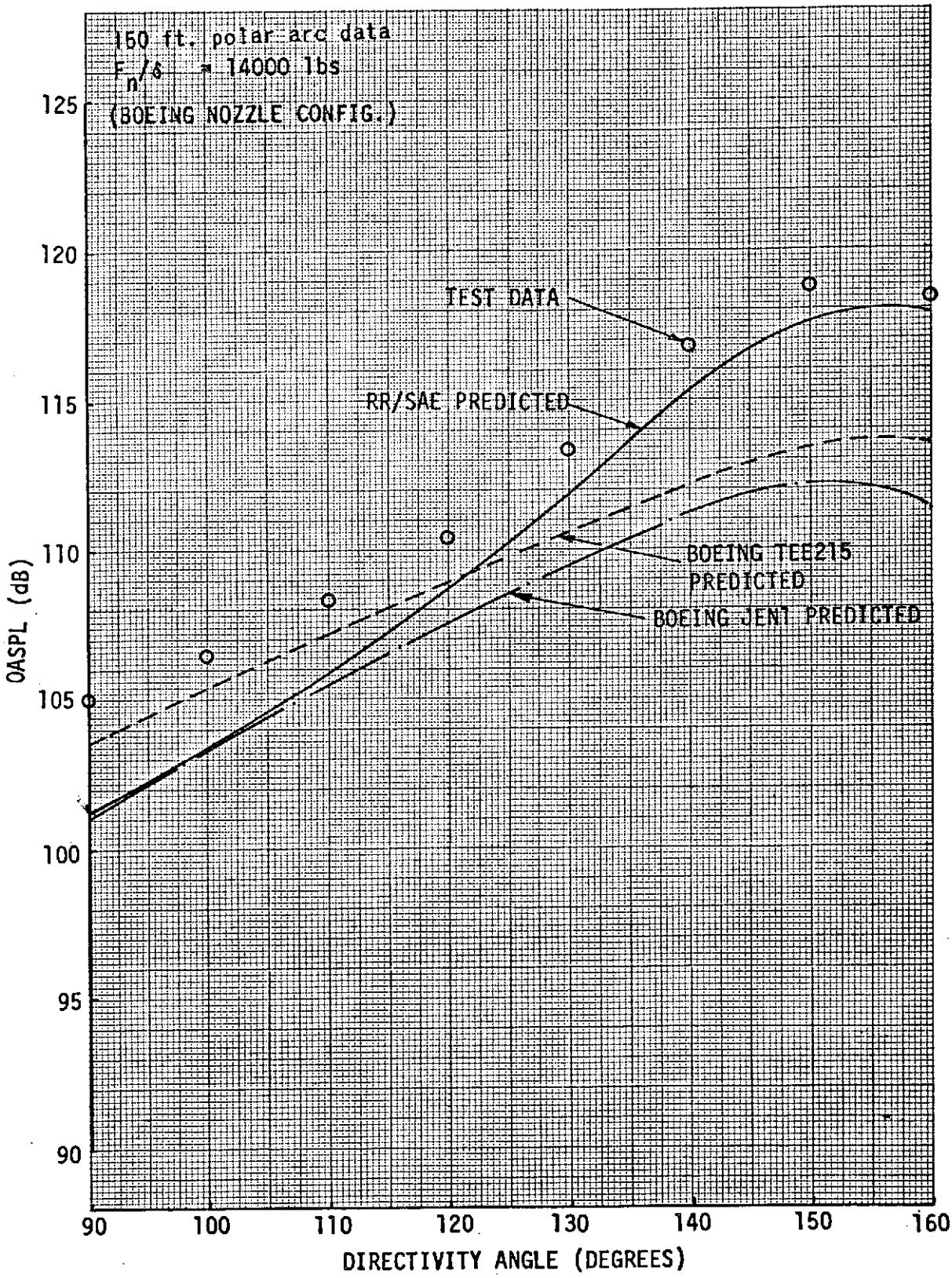

FIGURE 81. - OASPL DIRECTIVITY JT8D-109 MEASURED AND PREDICTED DATA

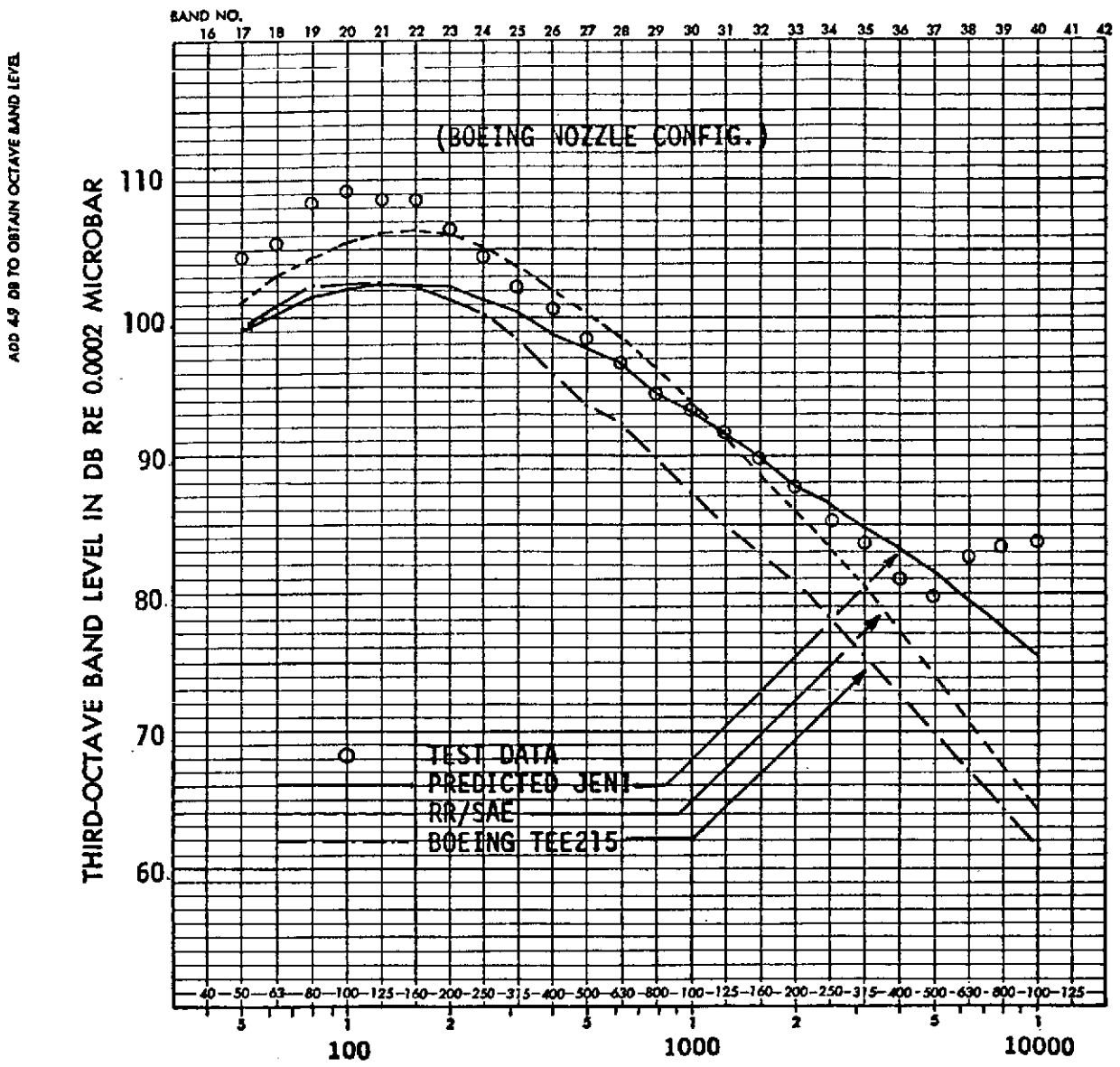

FIGURE 82. - MEASURED AND PREDICTED SPECTRA JT8D-109
MODEL TEST CONDITIONS F_N/δ = 14000 LBS.

140° DIRECTIVITY ANGLE
150 ft. polar arc data

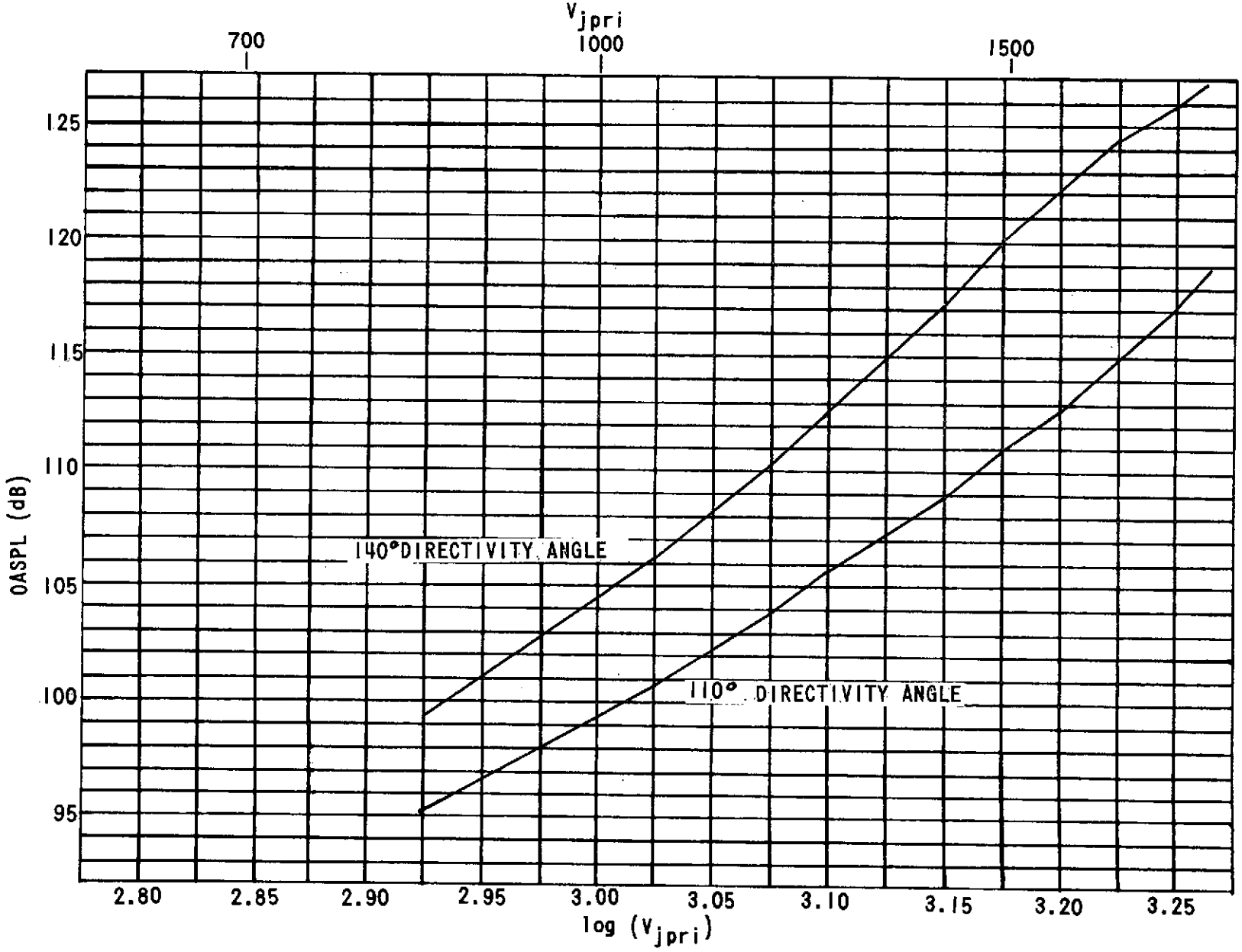

FIGURE 83. OASPL NOISE/VELOCITY THROTTLING CURVES - BASELINE JT8D-9 NOZZLE

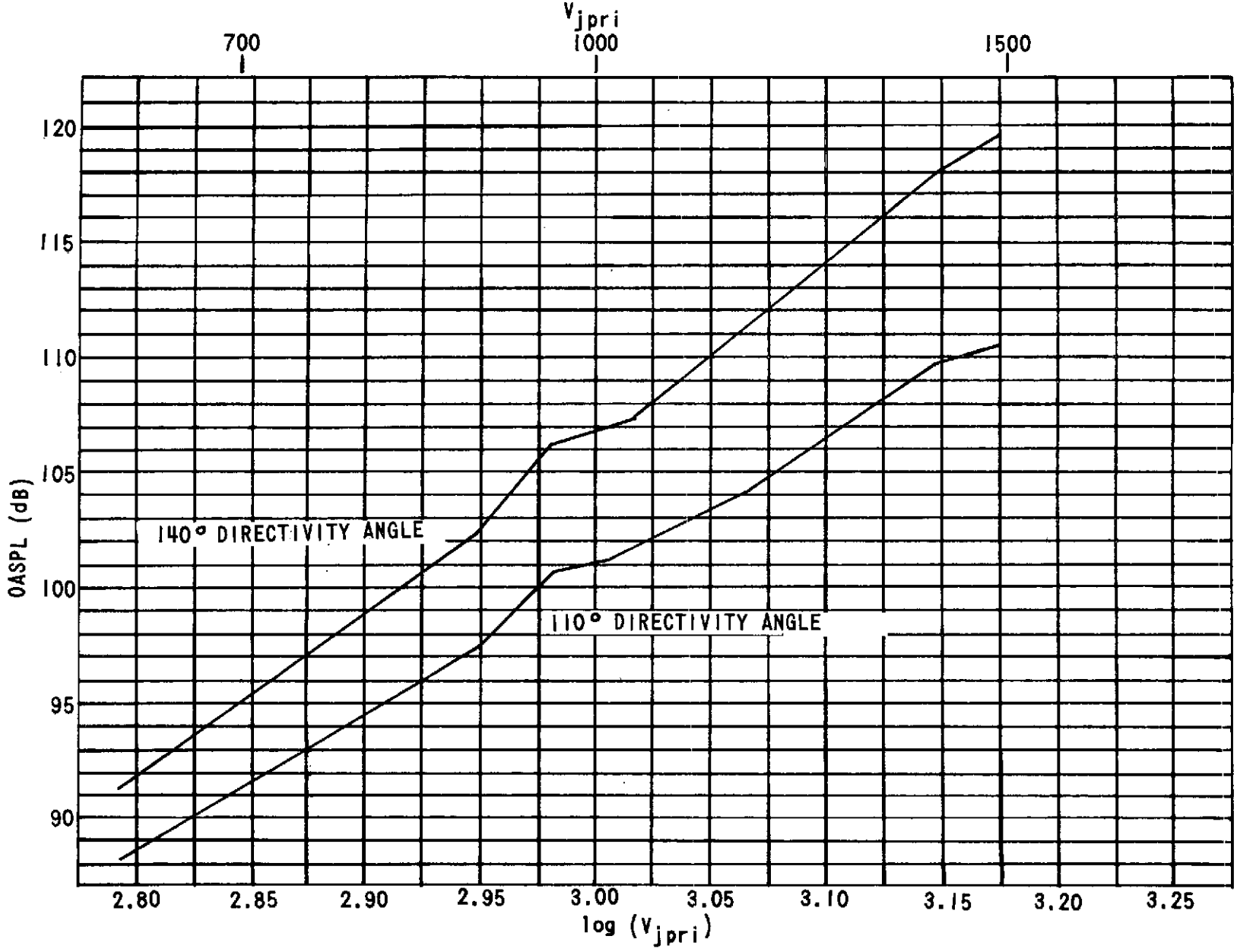

FIGURE 84. OASPL NOISE/VELOCITY THROTTLING CURVES - PHASE I REFAN NOZZLE

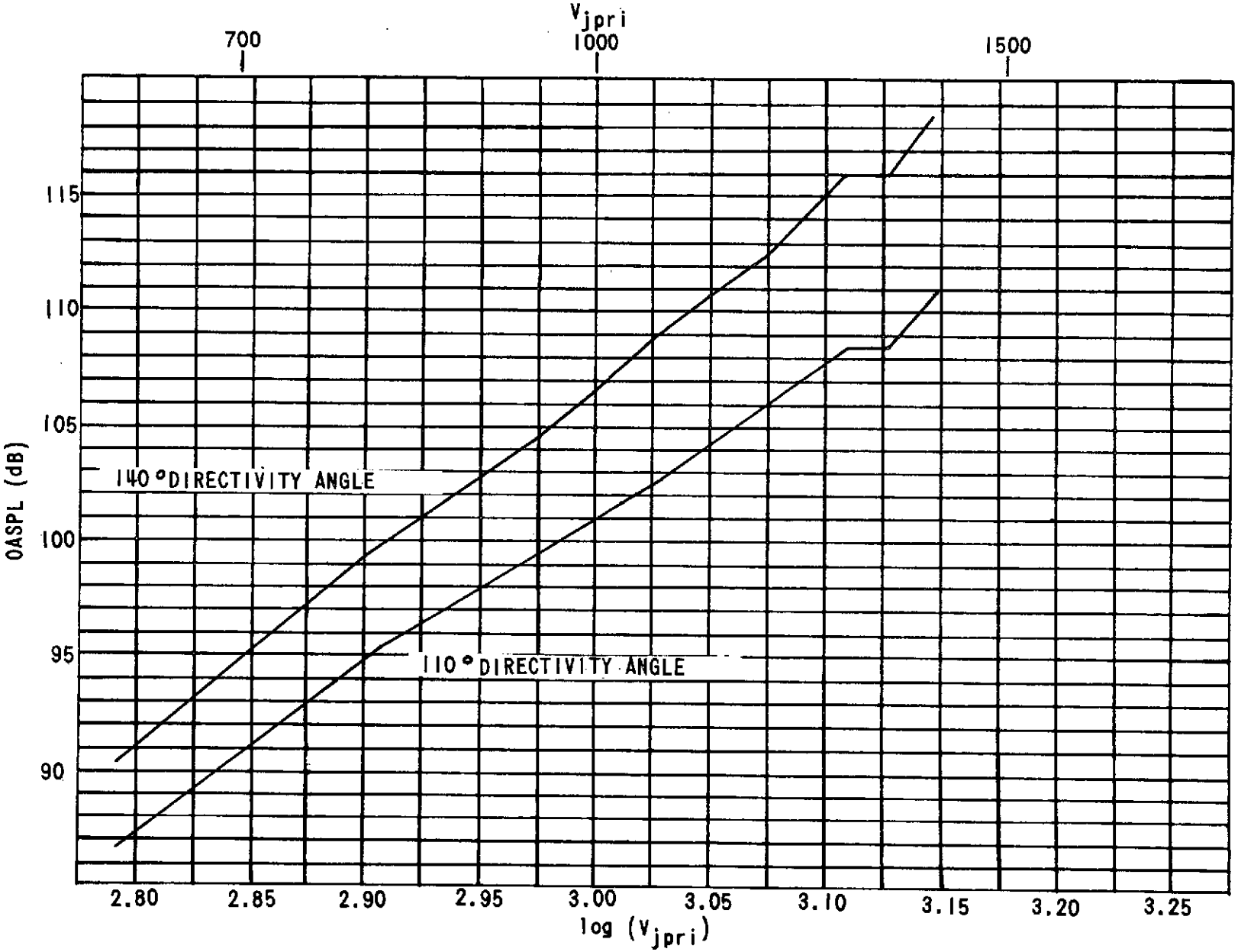

FIGURE 85. OASPL NOISE/VELOCITY THROTTLING CURVES - P&WA JT8D-109 NOZZLE WITH SWIRL

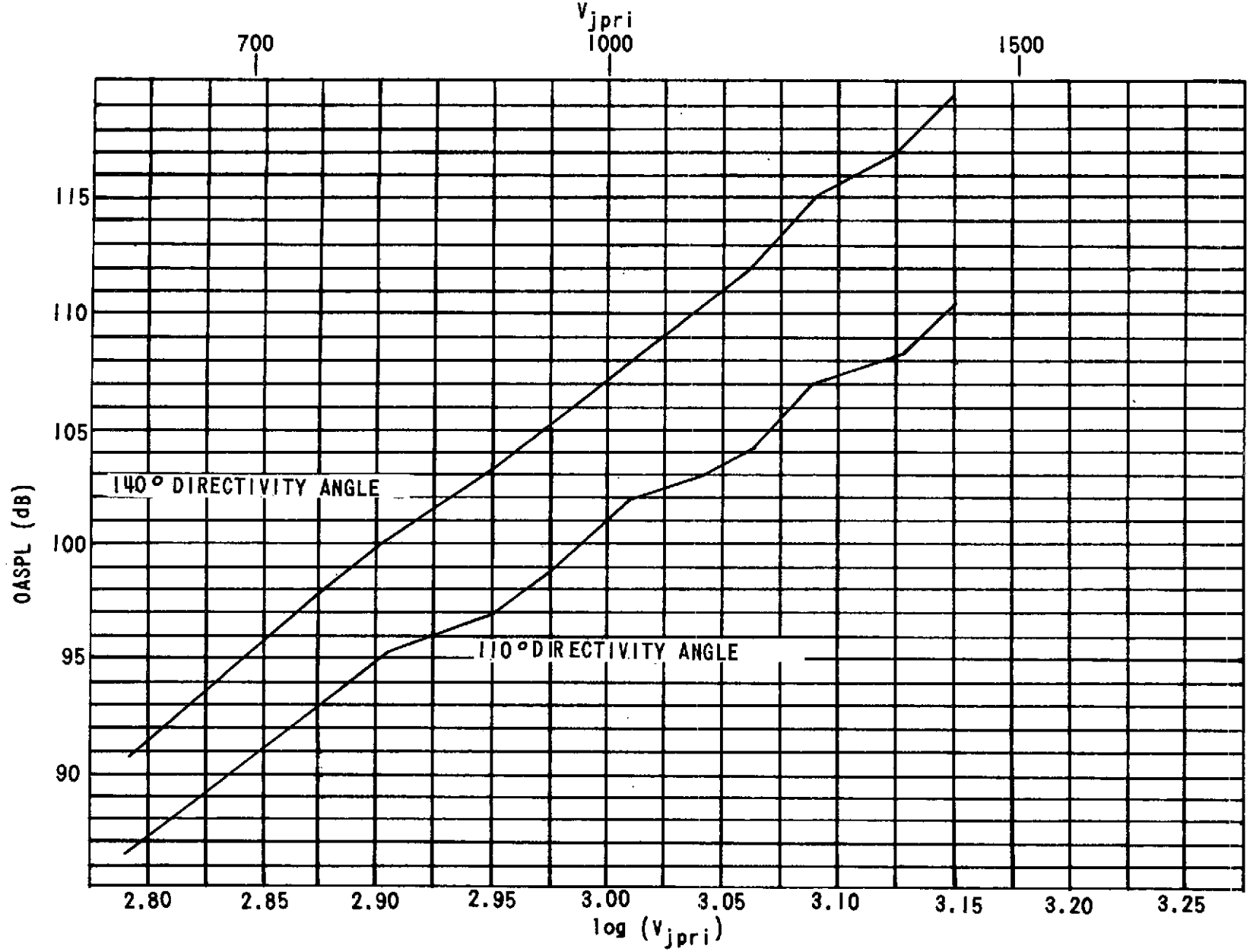

FIGURE 86. OASPL NOISE/VELOCITY THROTTLING CURVES - P&WA JT8D-109 NOZZLE

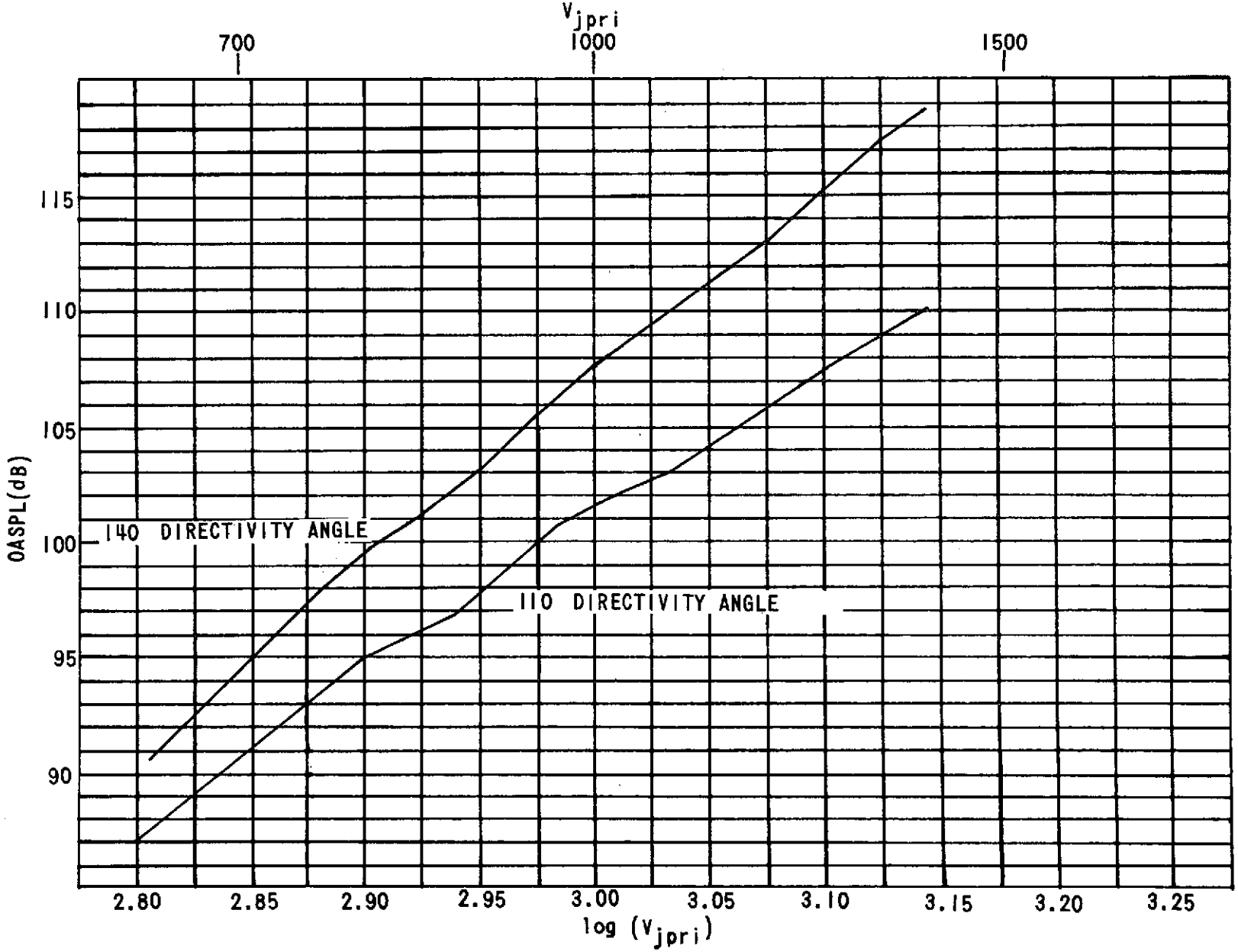

FIGURE 87. OASPL NOISE/VELOCITY THROTTLING CURVES - BOEING JT8D-109 NOZZLE

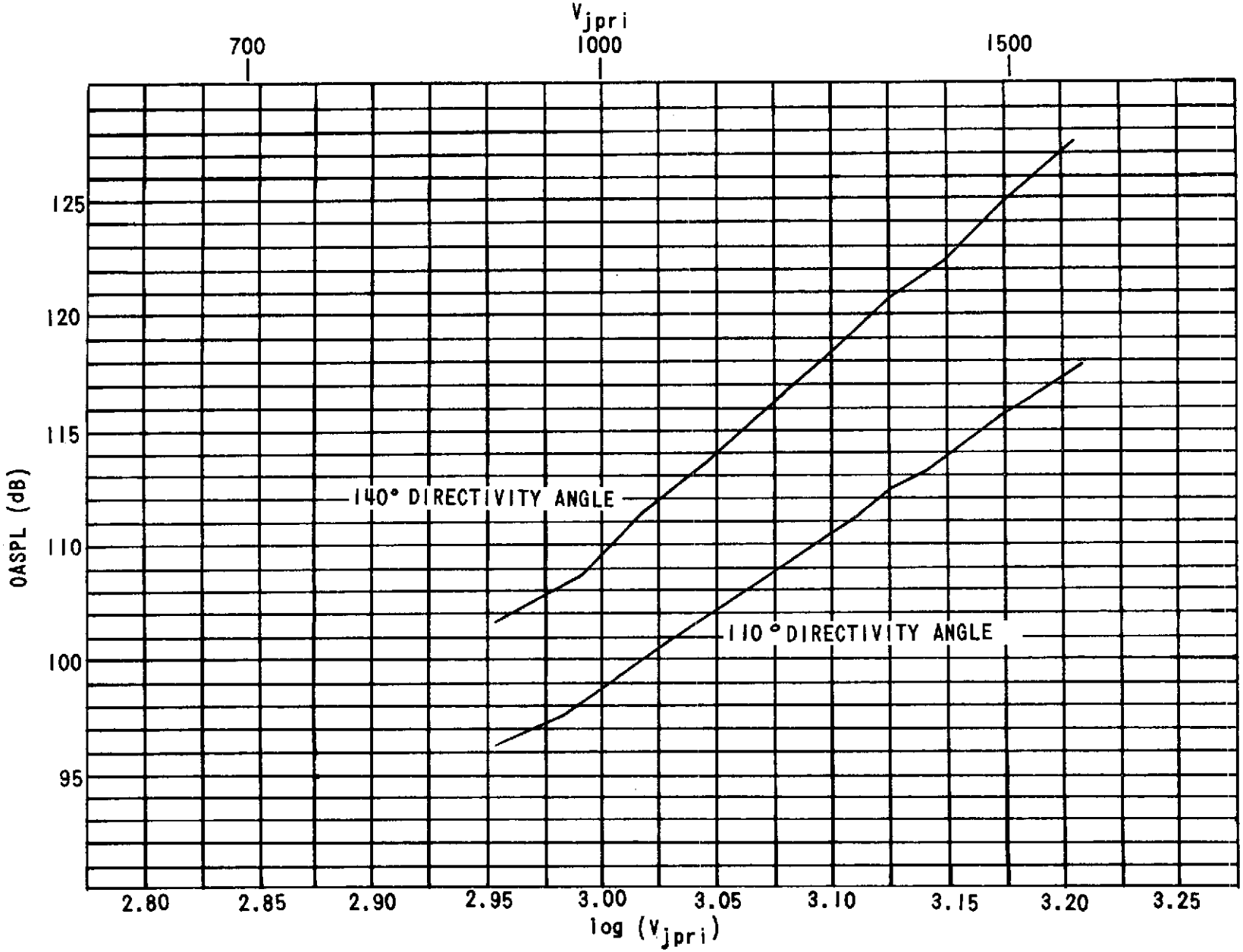

FIGURE 88. OASPL NOISE/VELOCITY THROTTLING CURVES - P&WA JT8D-115 NOZZLE

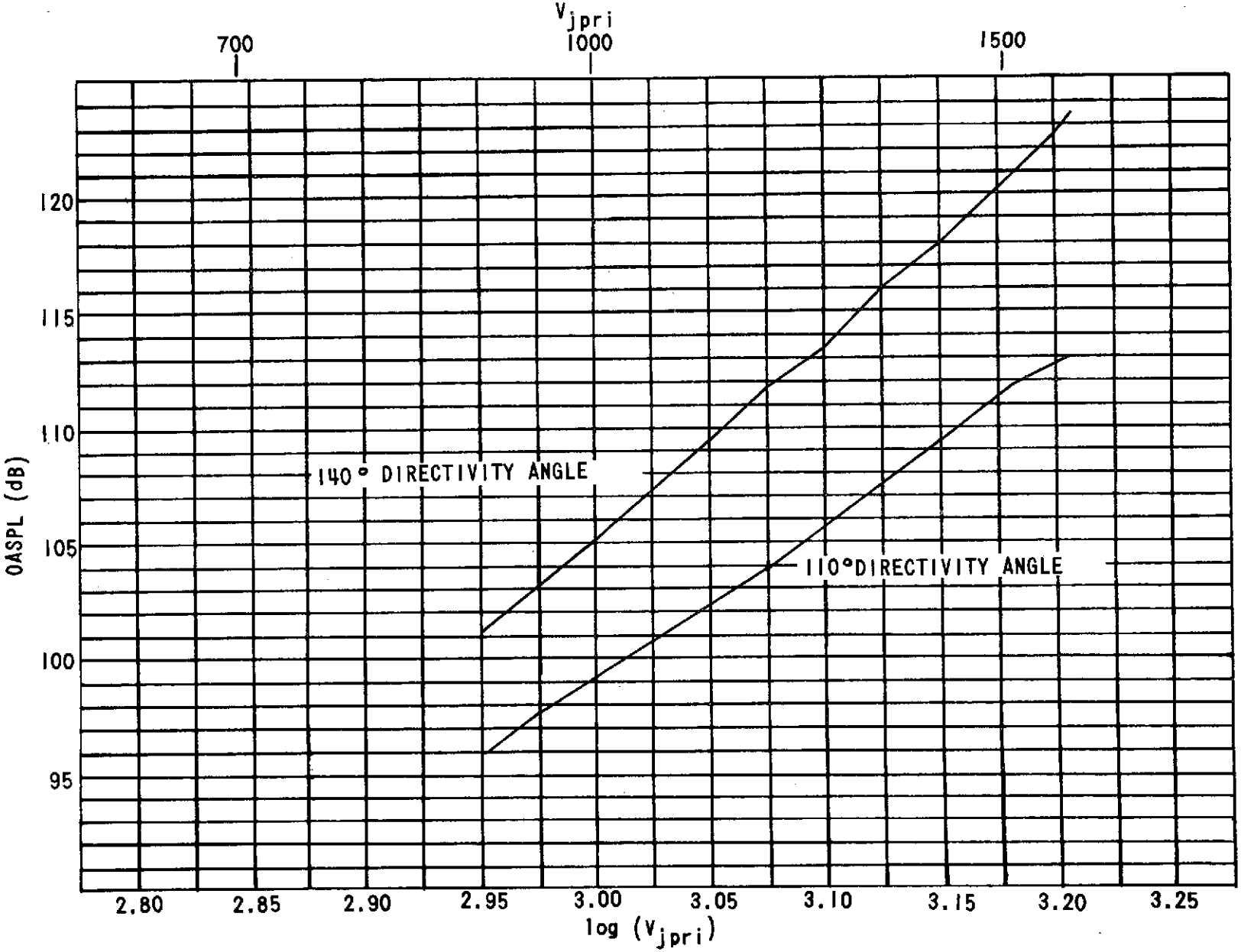

FIGURE 89. OASPL NOISE/VELOCITY THROTTLING CURVES - BOEING JT8D-115 NOZZLE

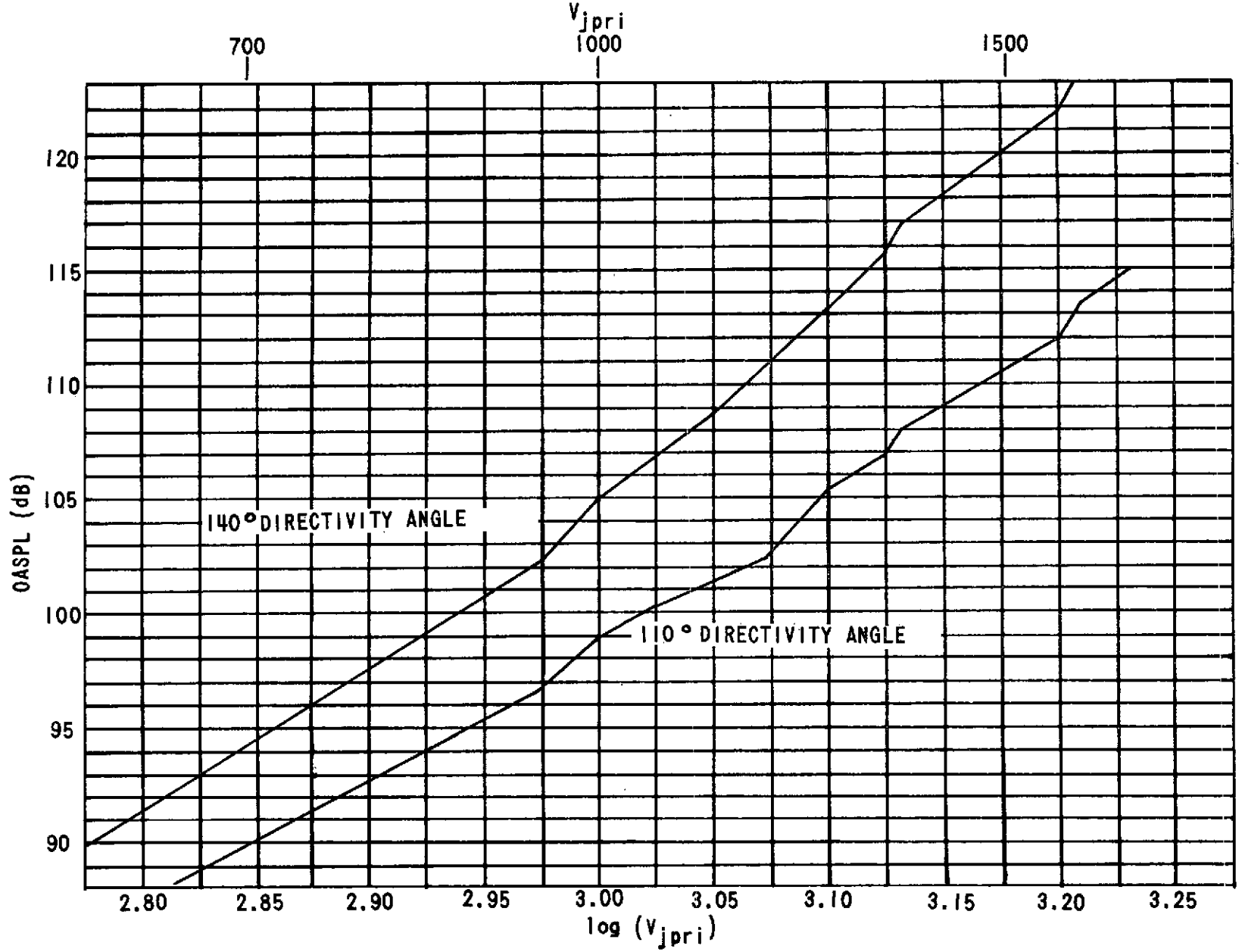

FIGURE 90. OASPL NOISE/VELOCITY THROTTLING CURVES - P&WA JT8D-117 NOZZLE

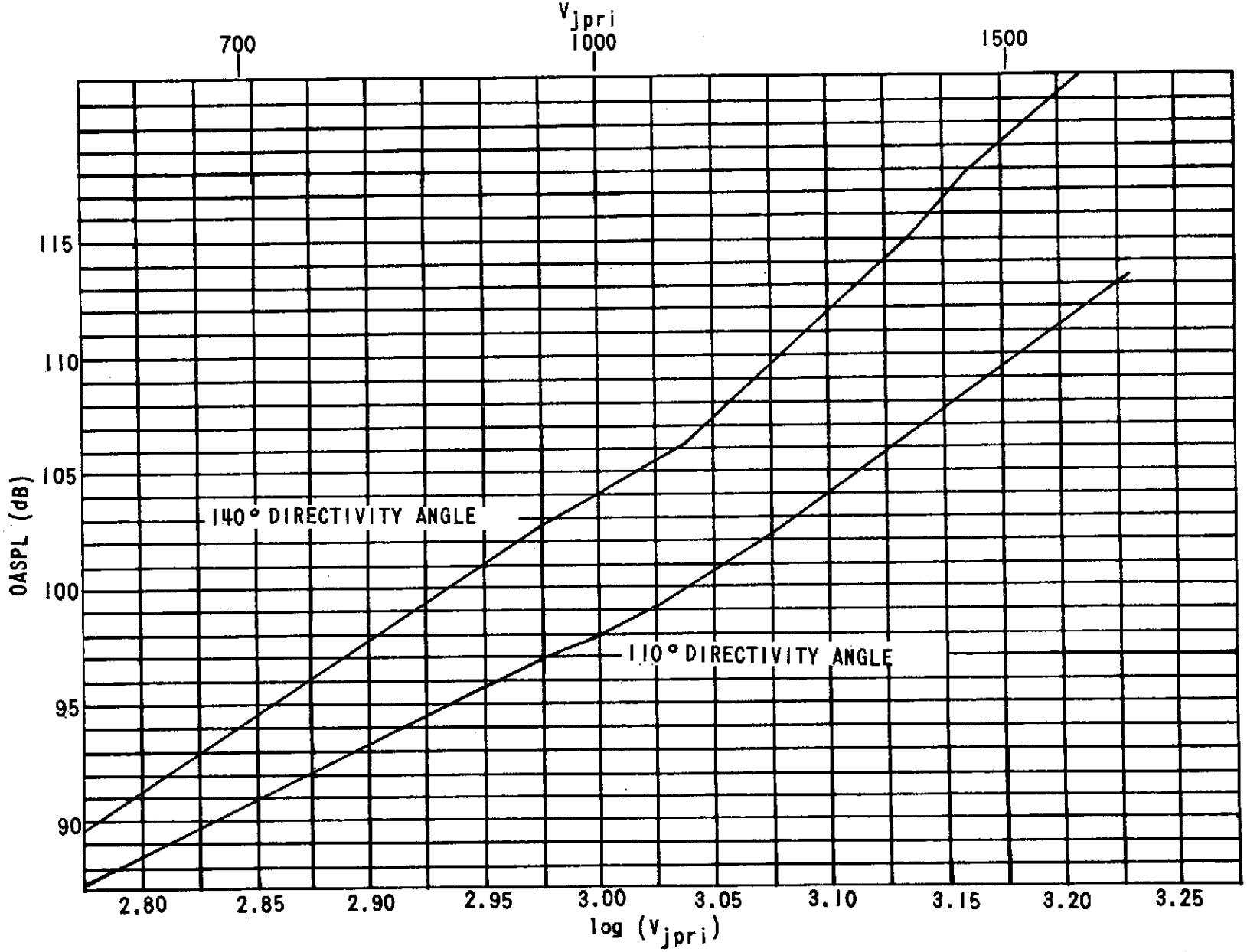

FIGURE 91. OASPL NOISE/VELOCITY THROTTLING CURVES - BOEING JT8D-117 NOZZLE (CONFIG. 9)

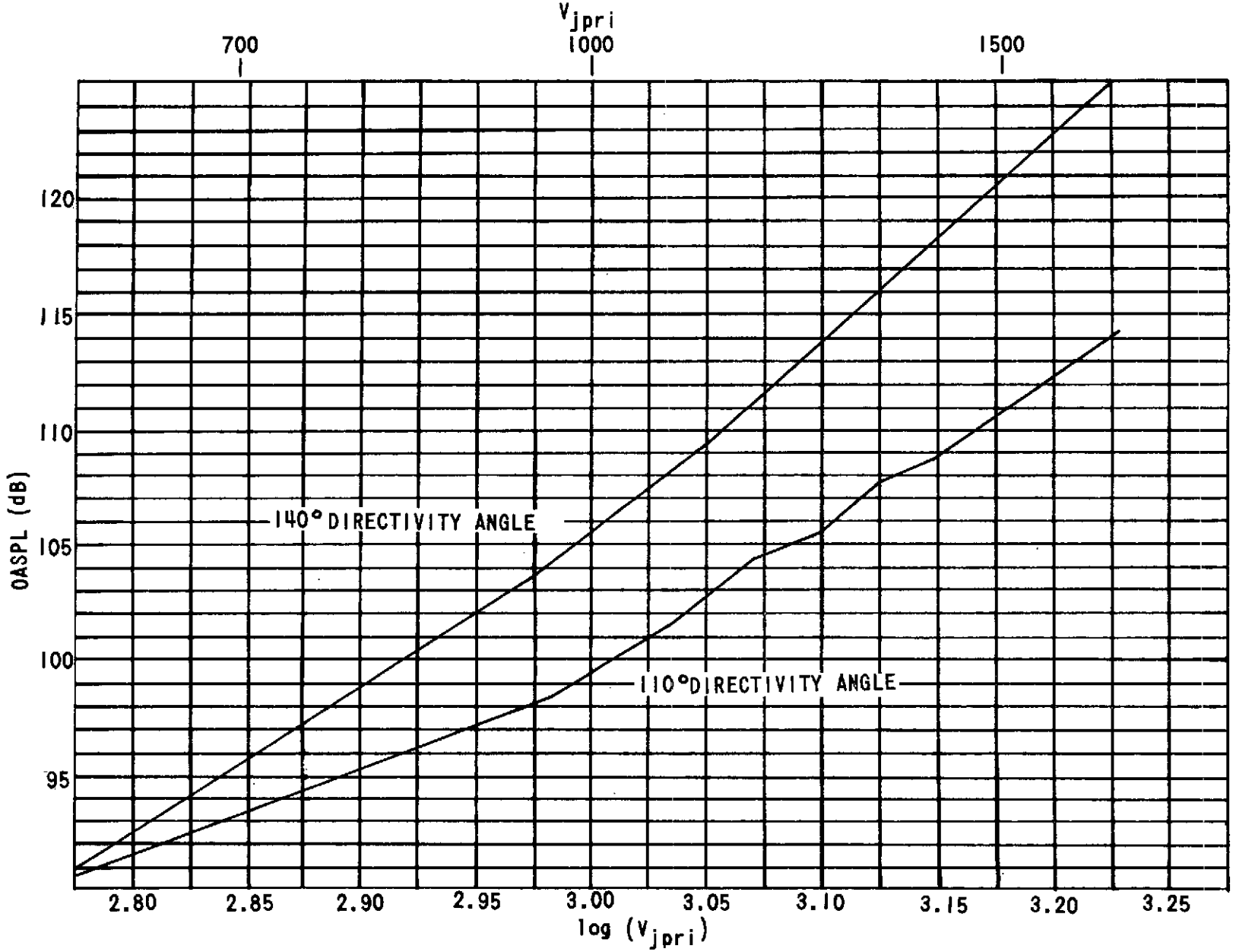

FIGURE 92. OASPL NOISE/VELOCITY THROTTLING CURVES - BOEING JT8D-117 NOZZLE (CONFIG. 10)

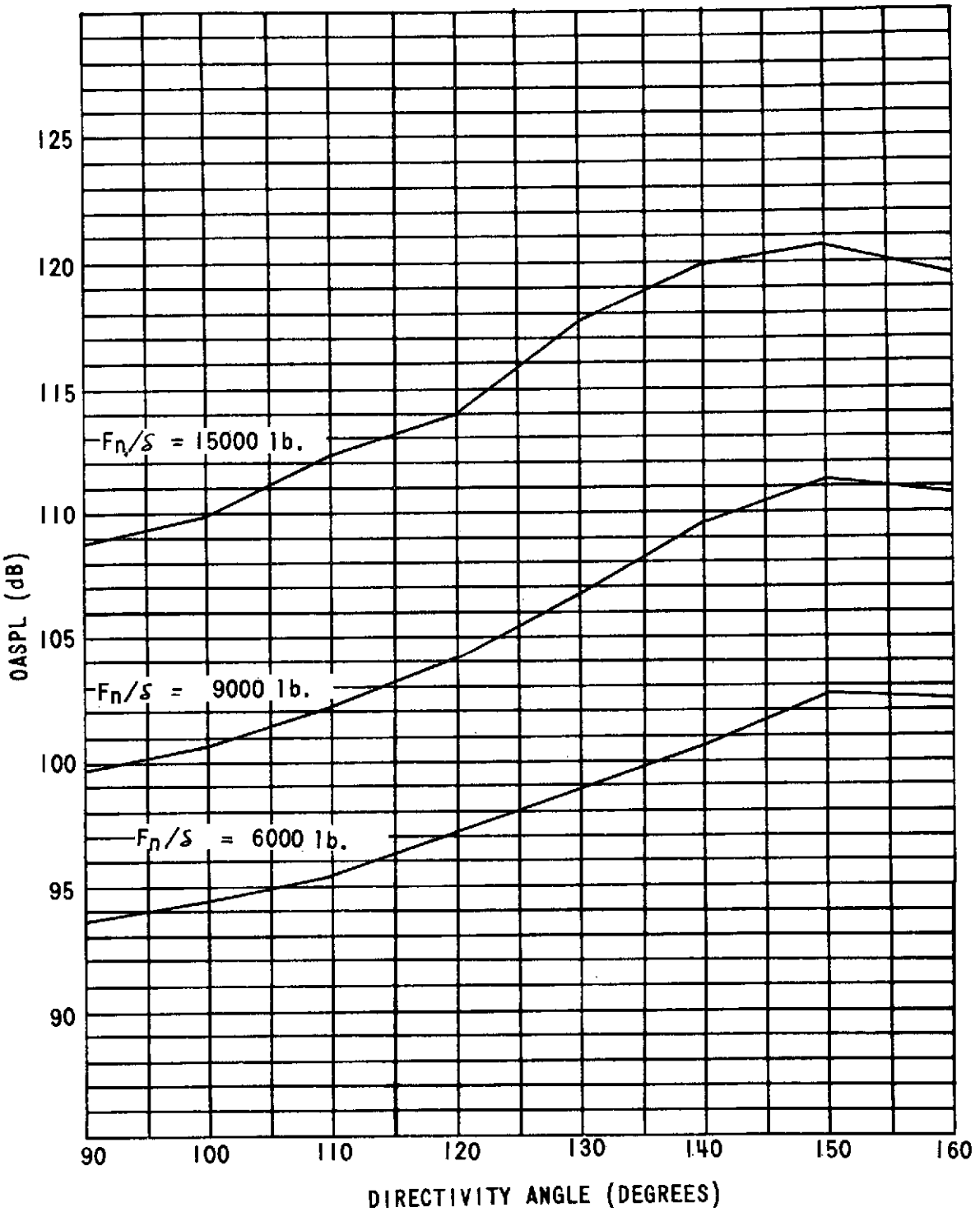

FIGURE 93. OASPL DIRECTIVITY PLOTS JT8D-9 NOZZLE

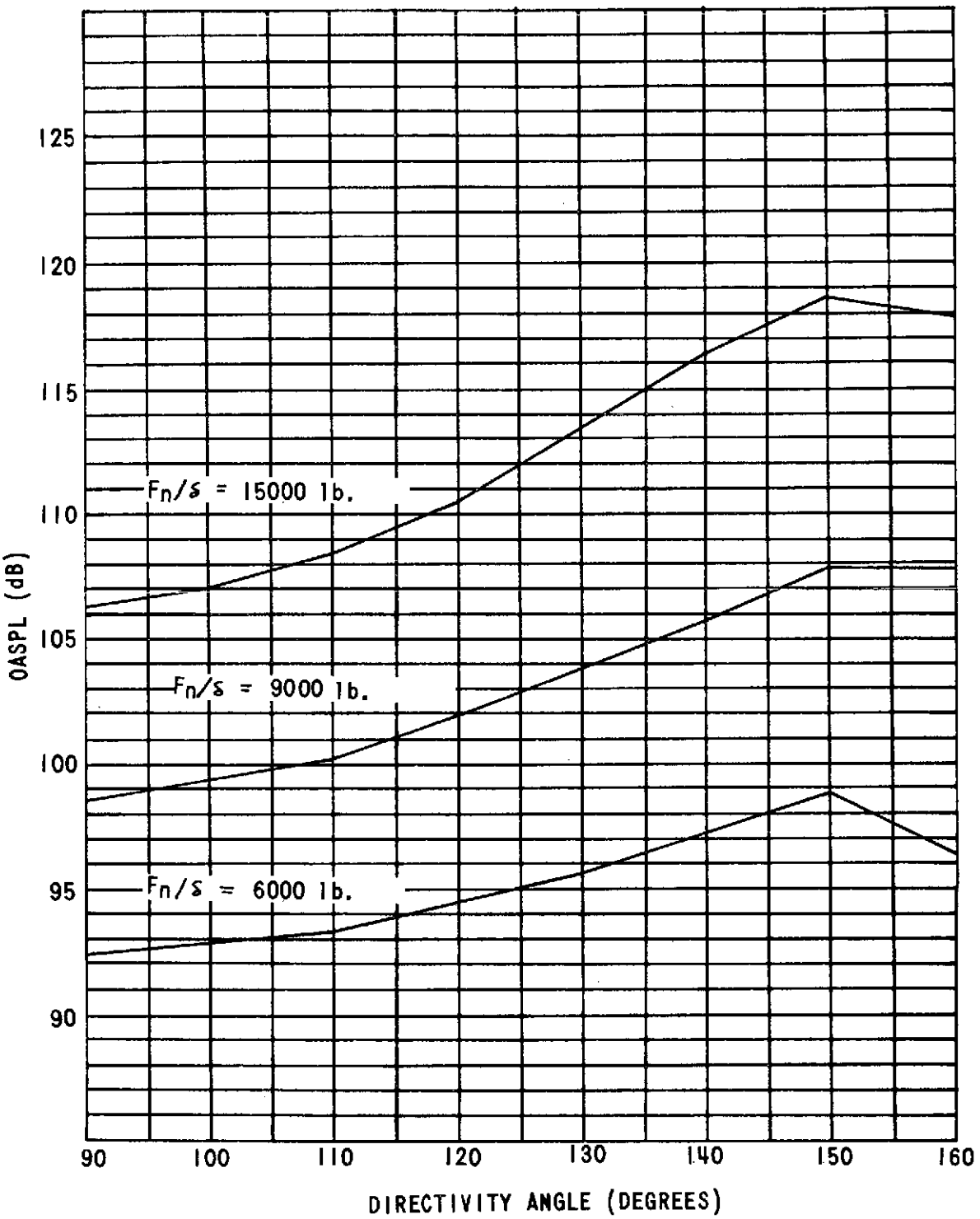

FIGURE 94. OASPL DIRECTIVITY PLOTS PHASE I REFAN NOZZLE

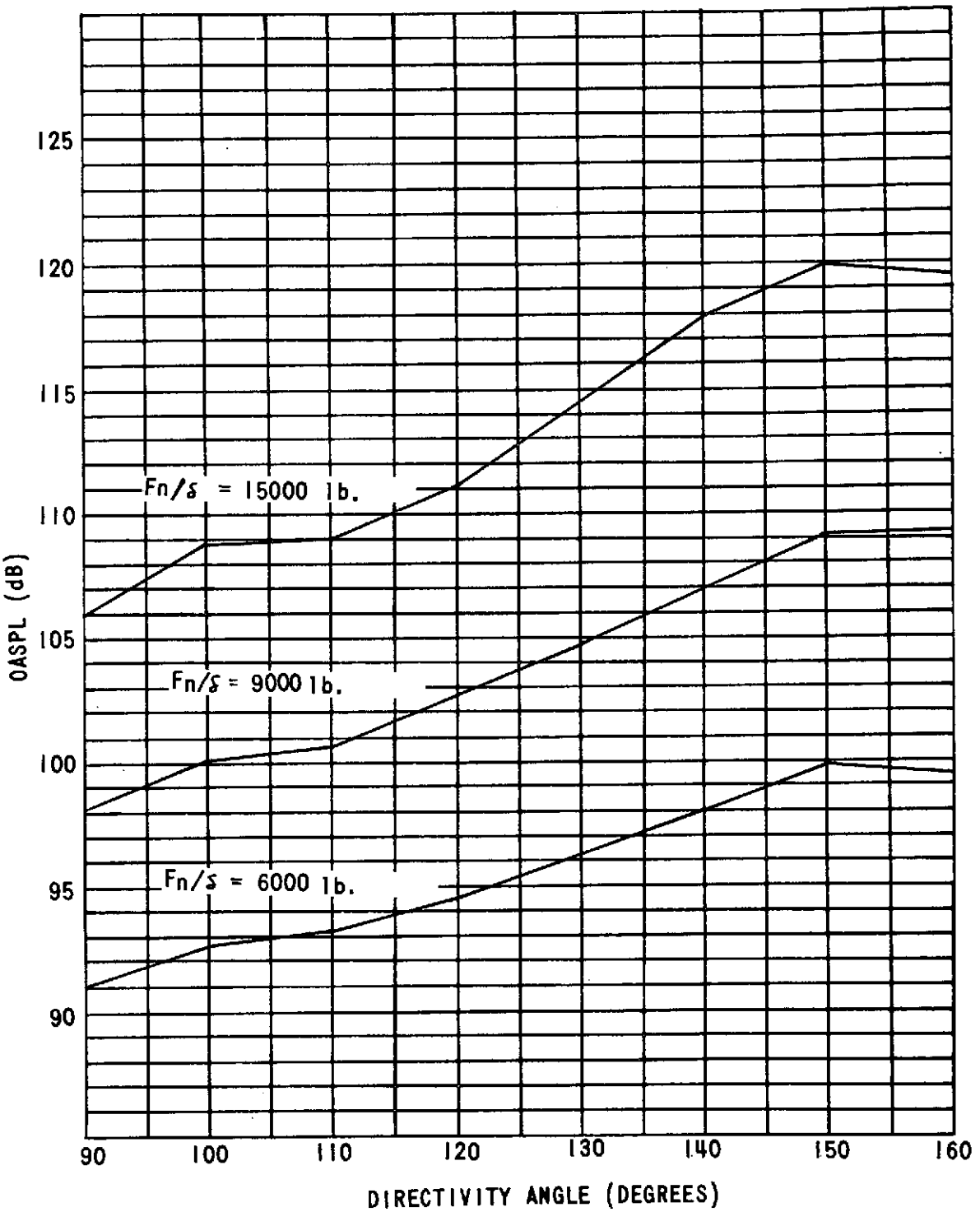

FIGURE 95. OASPL DIRECTIVITY PLOTS P&WA JT8D-109 NOZZLE

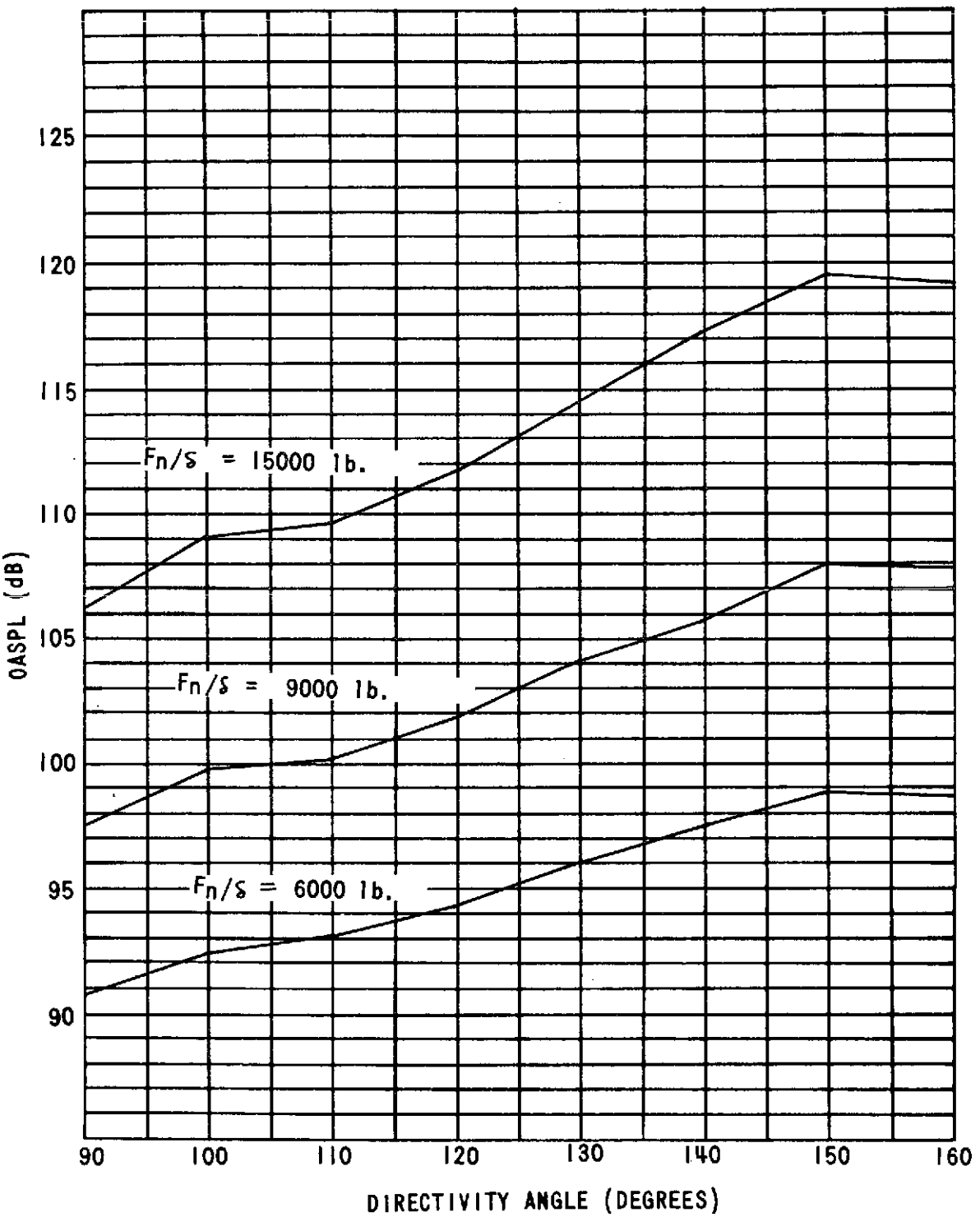

FIGURE 96. OASPL DIRECTIVITY PLOTS P&WA JT8D-109 NOZZLE (WITH SWIRL VANES)

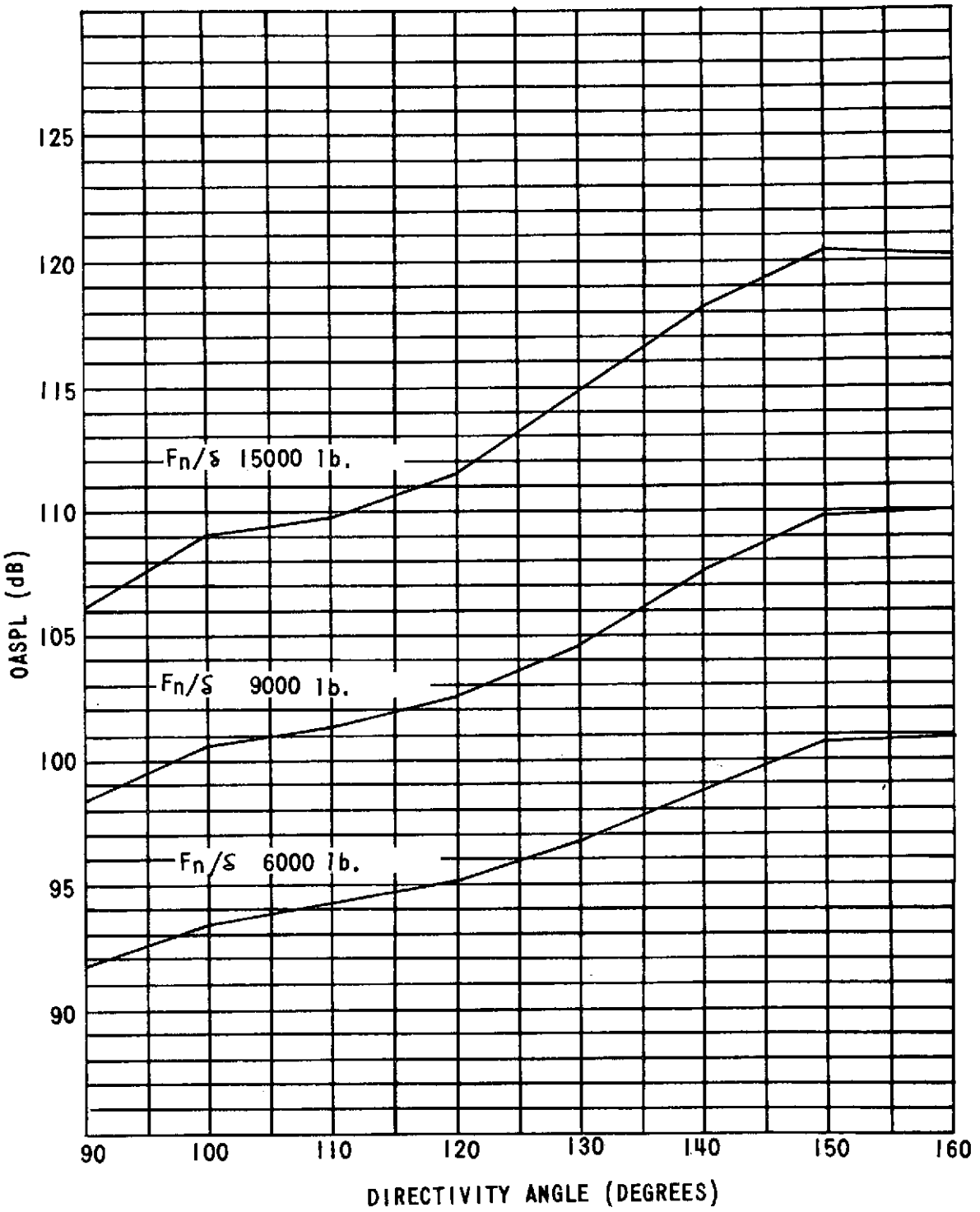

FIGURE 97. OASPL DIRECTIVITY PLOTS BOEING JT8D-109 NOZZLE

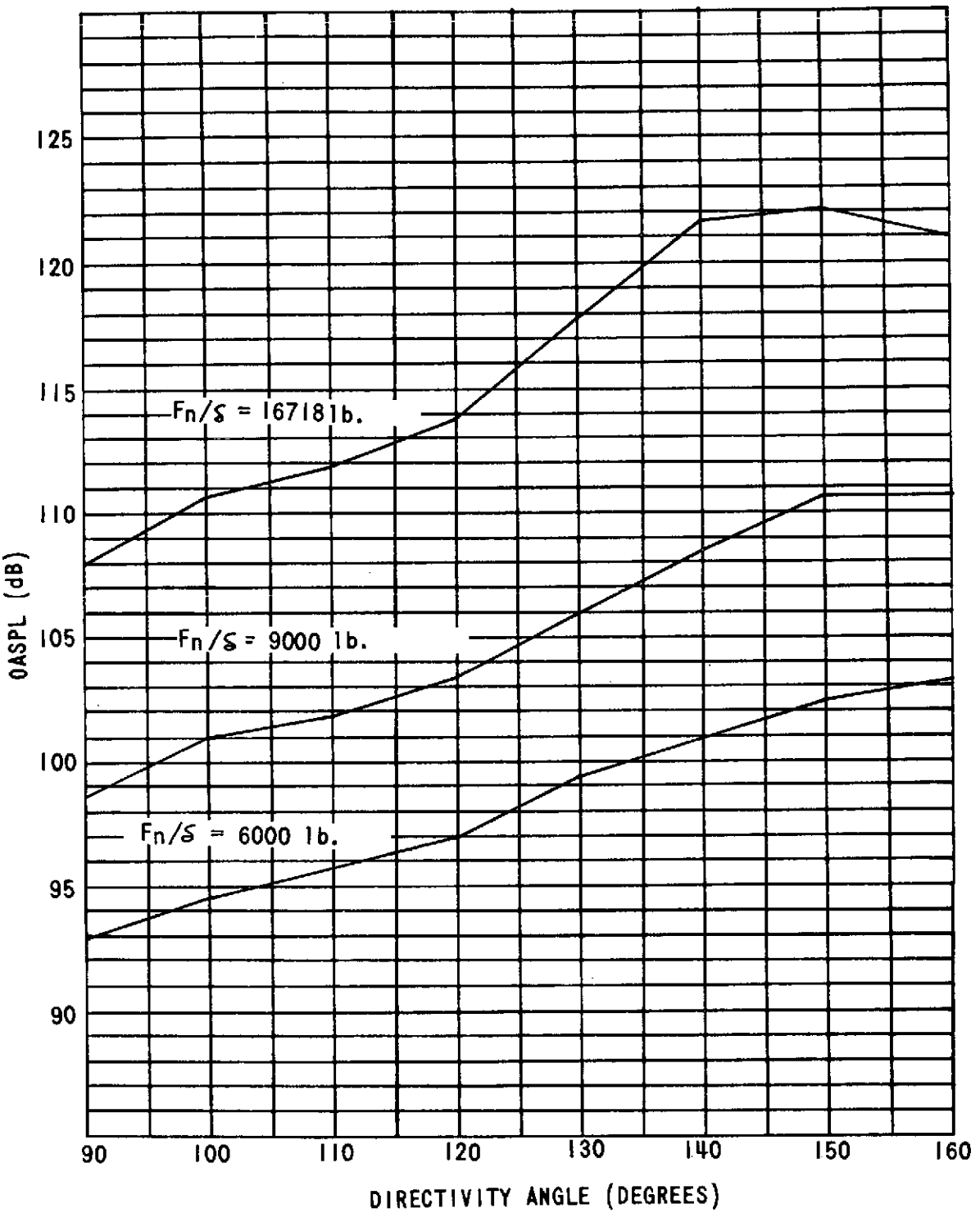

FIGURE 98. OASPL DIRECTIVITY PLOTS P&WA JT8D-115 NOZZLE

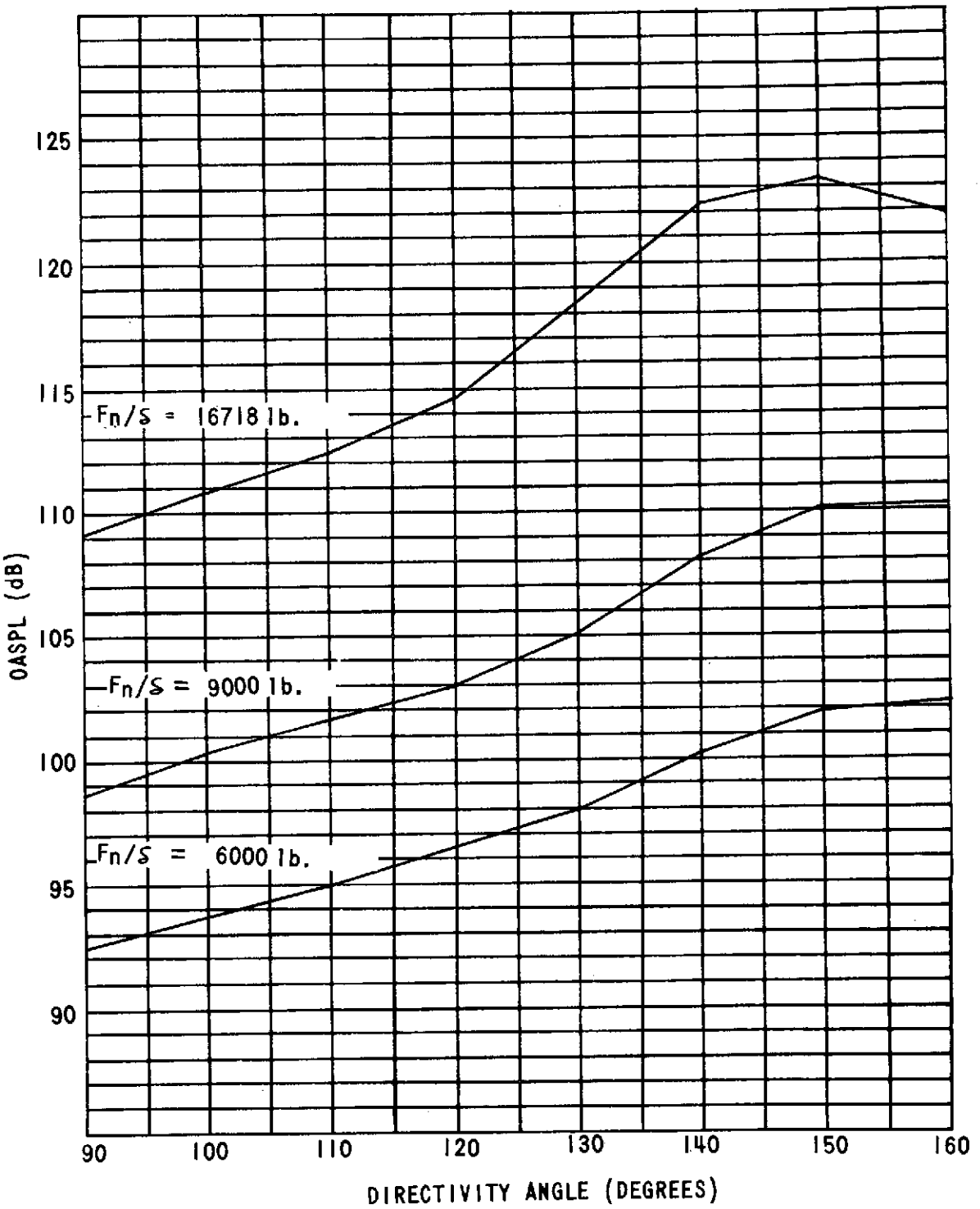

FIGURE 99. OASPL DIRECTIVITY PLOTS BOEING JT8D-115 NOZZLE

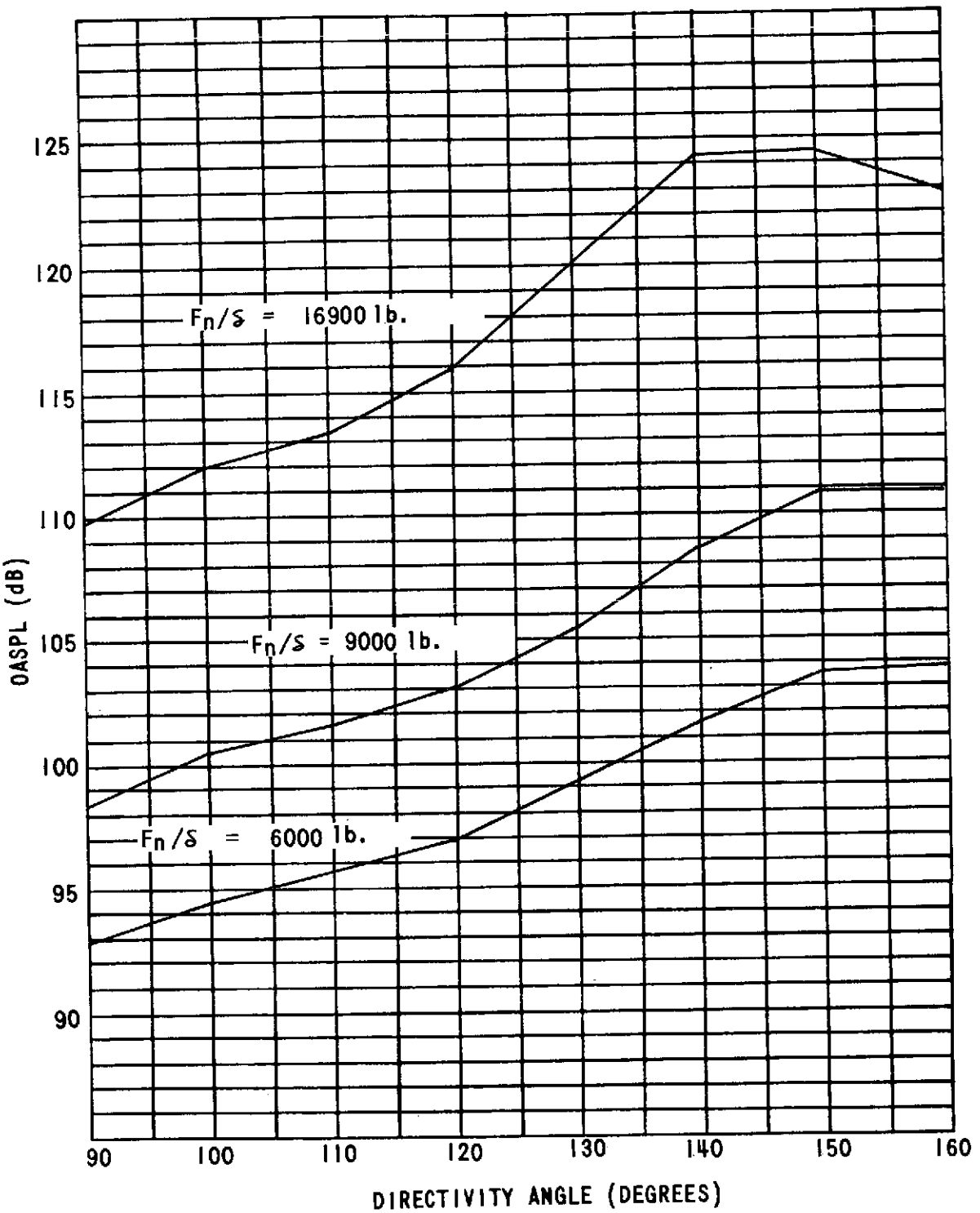

FIGURE 100. OASPL DIRECTIVITY PLOTS P&WA JT8D-117 NOZZLE

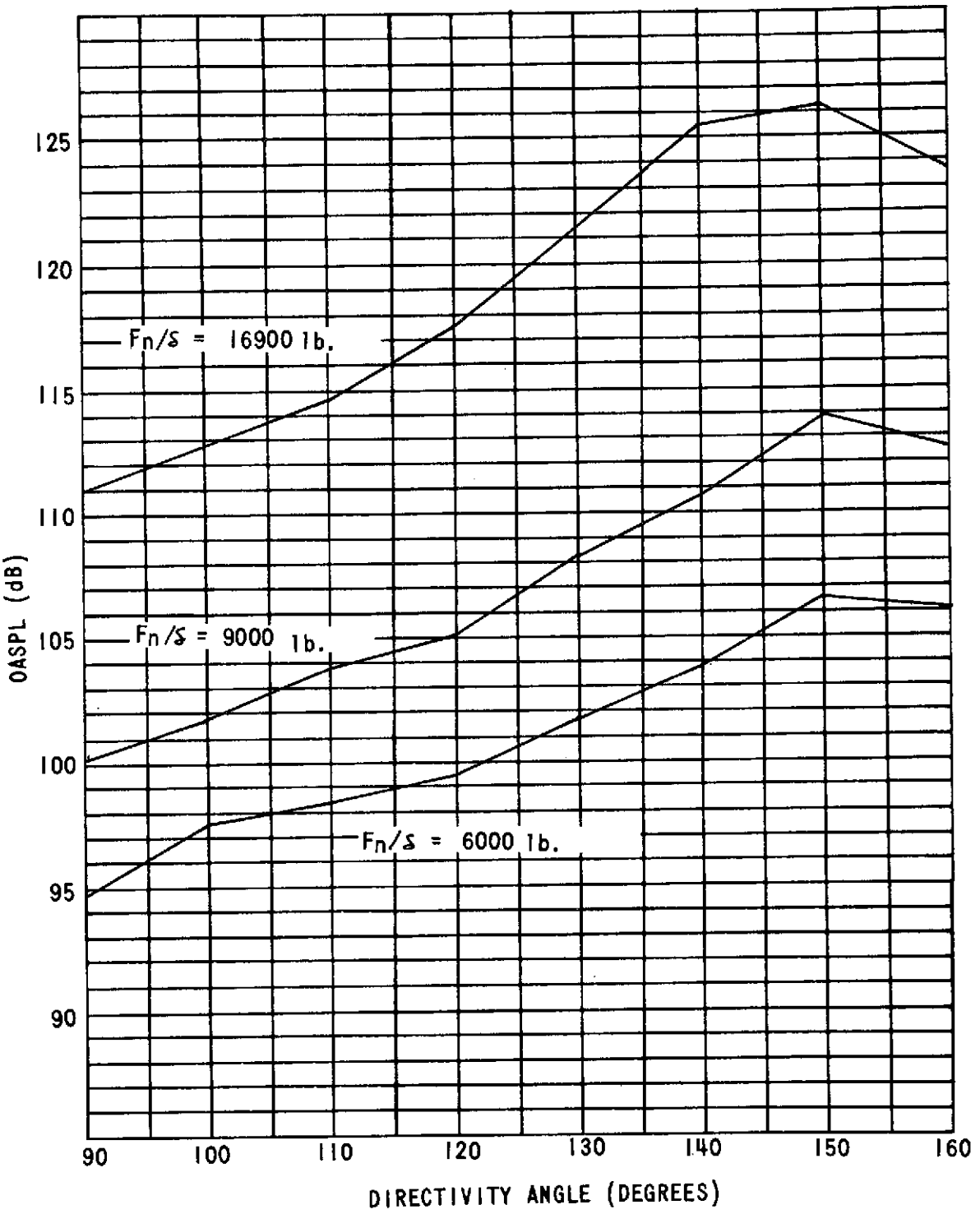

FIGURE 101. OASPL DIRECTIVITY PLOTS BOEING JT8D-117 NOZZLE (CONFIG. 10)

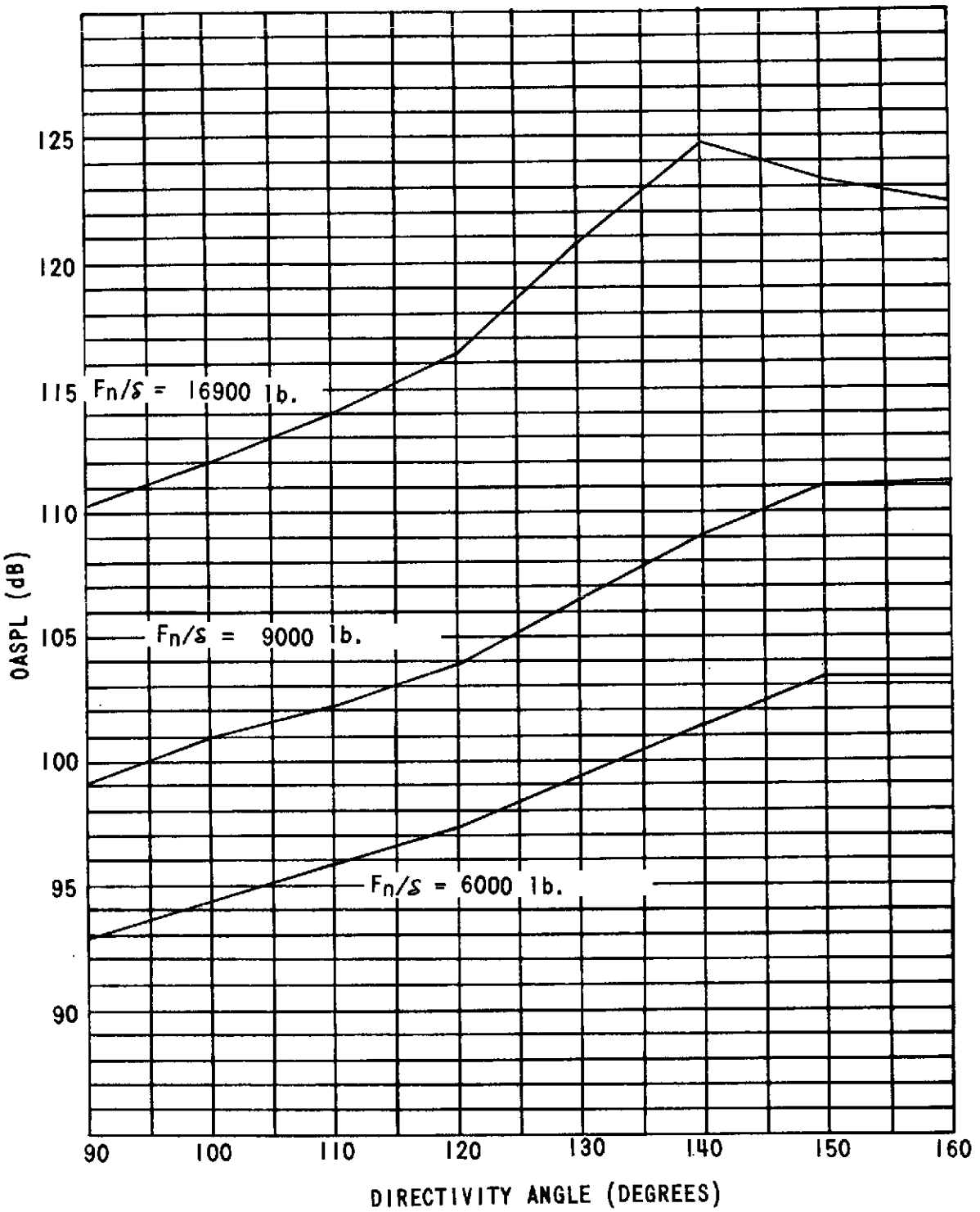

FIGURE 102. OASPL DIRECTIVITY PLOTS BOEING JT8D-117 NOZZLE (CONFIG. 9)

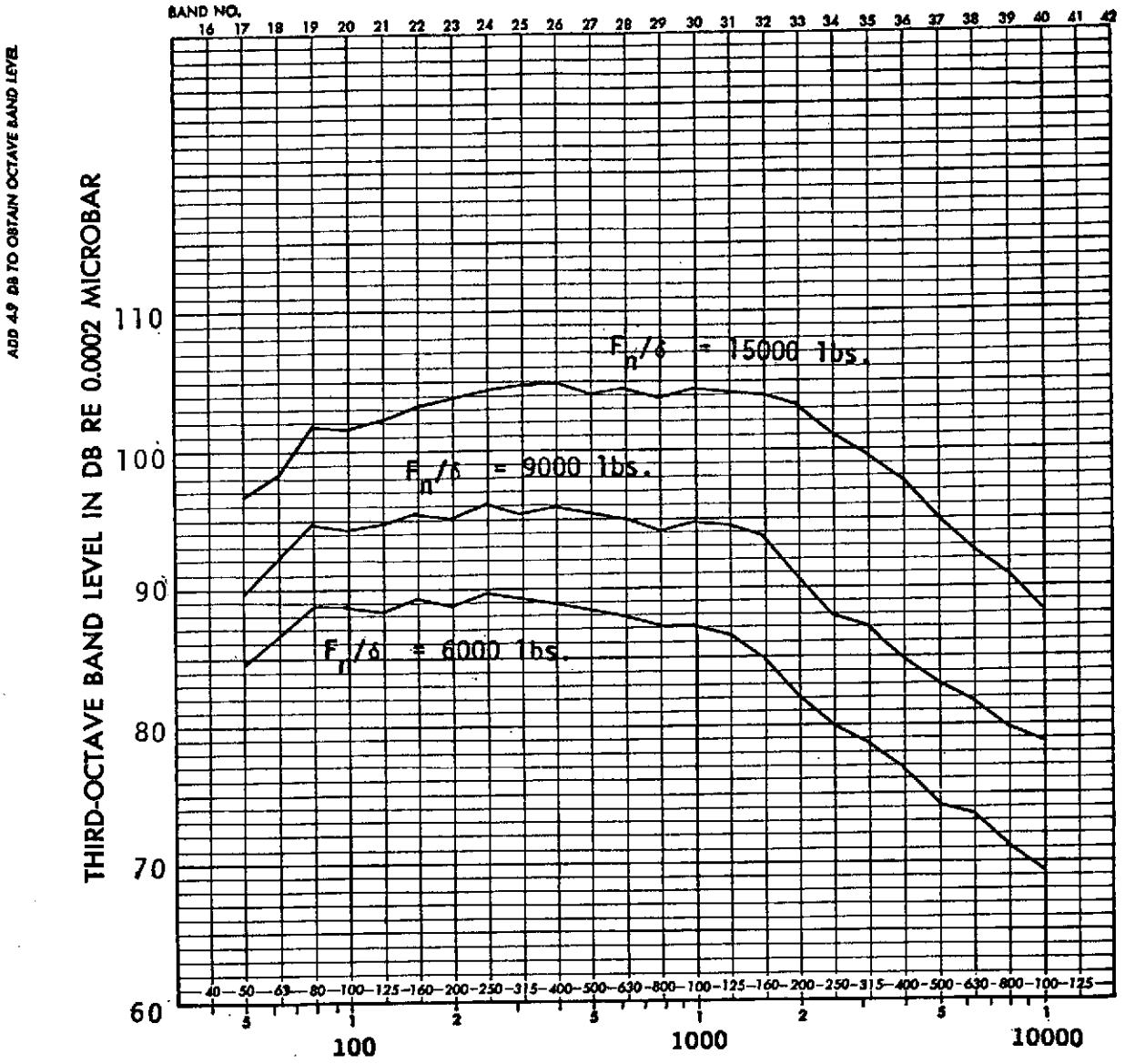

FIGURE 103. 1/3 OCTAVE BAND SPECTRA

JT8D-9 NOZZLE

110^{o} Directivity angle

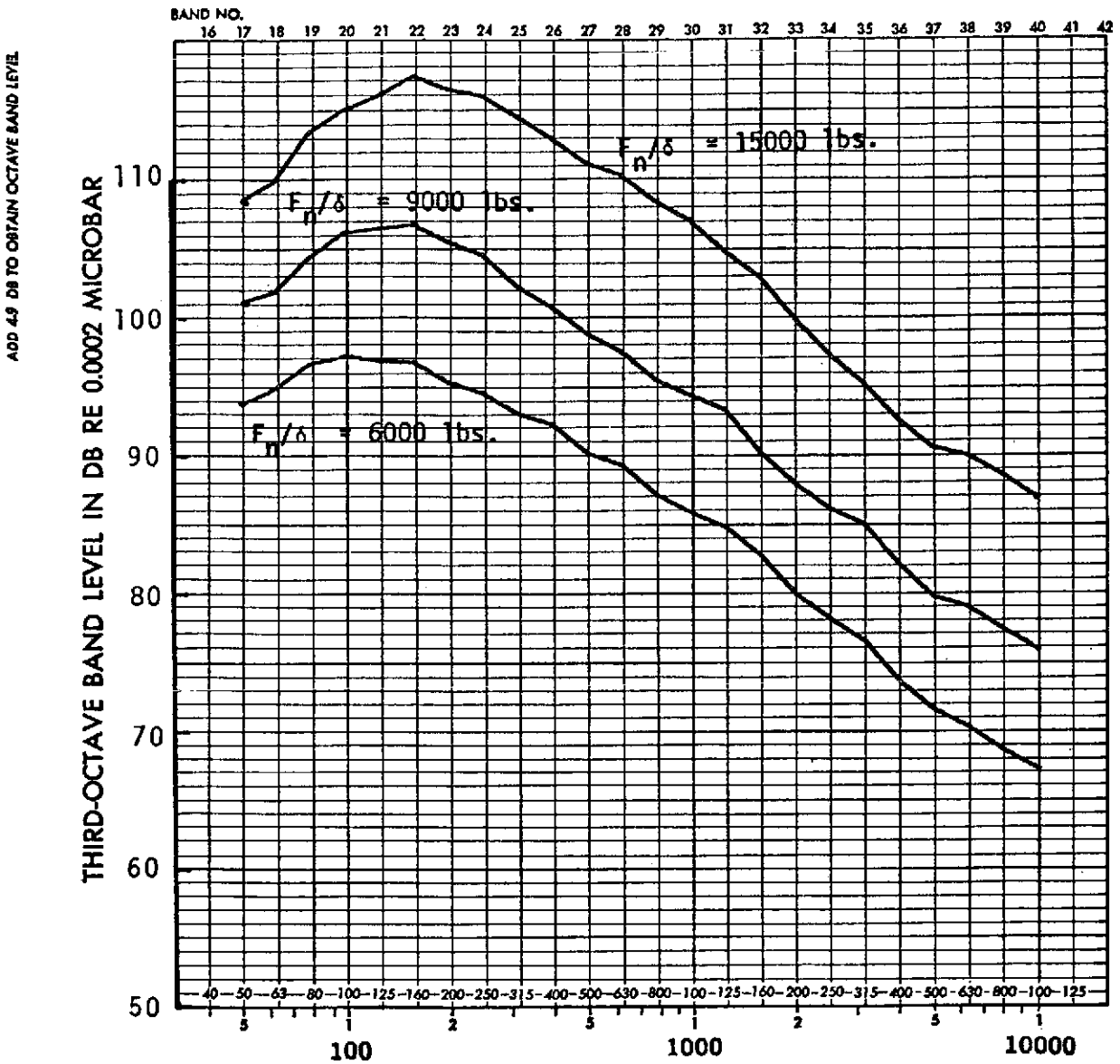

FIGURE 104. ONE-THIRD OCTAVE BAND SPECTRA
JT8D-9 NOZZLE

140^{o} Directivity angle

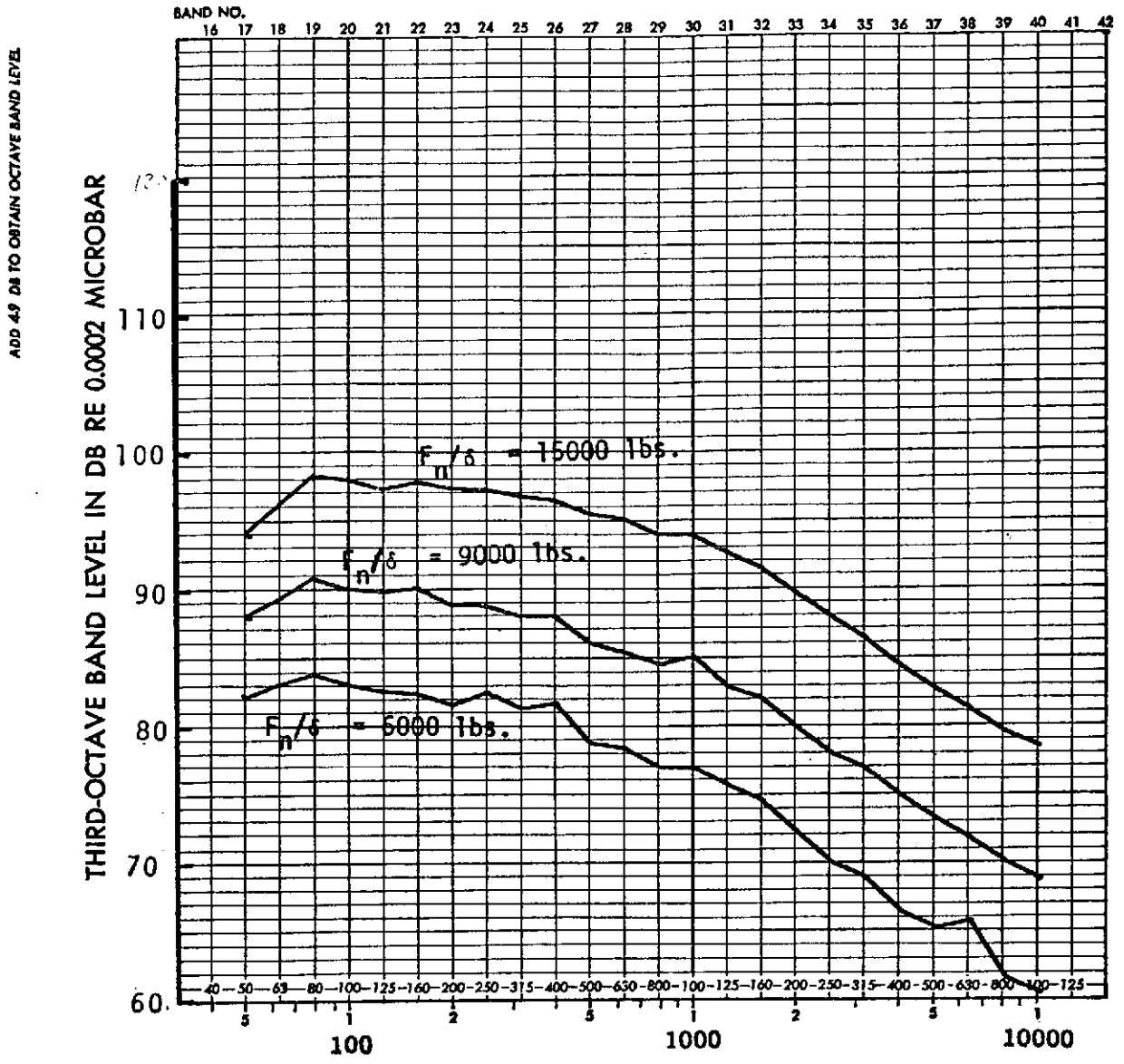

FIGURE 105. ONE-THIRD OCTAVE BAND SPECTRA
PHASE I REFAN NOZZLE
110^{o} Directivity angle

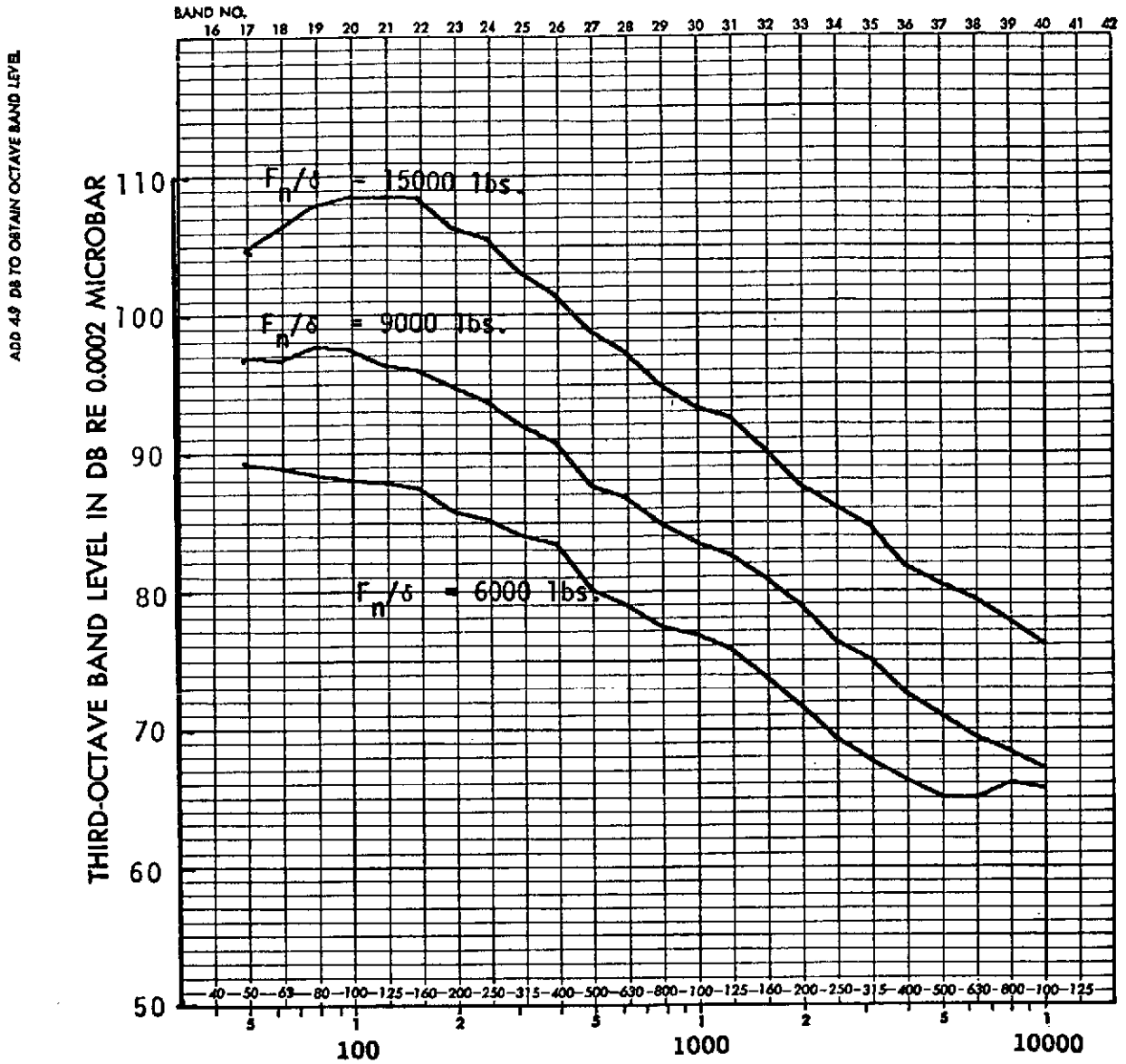

FIGURE 106. ONE-THIRD OCTAVE BAND SPECTRA
PHASE I REFAN NOZZLE

140^{o} Directivity angle

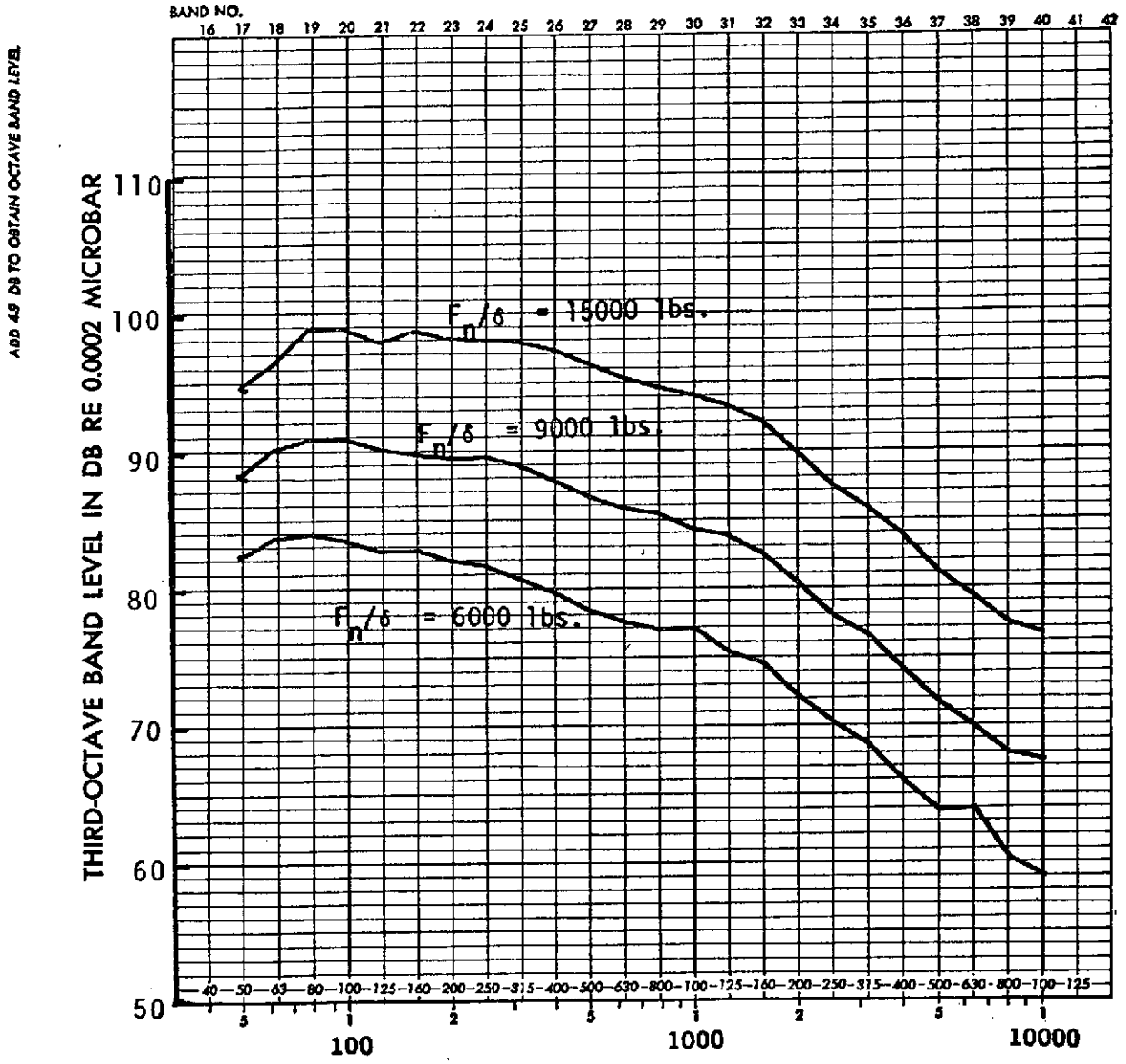

FIGURE 107. ONE-THIRD OCTAVE BAND SPECTRA
P&WA JT8D-109 NOZZLE

110^{o} Directivity angle

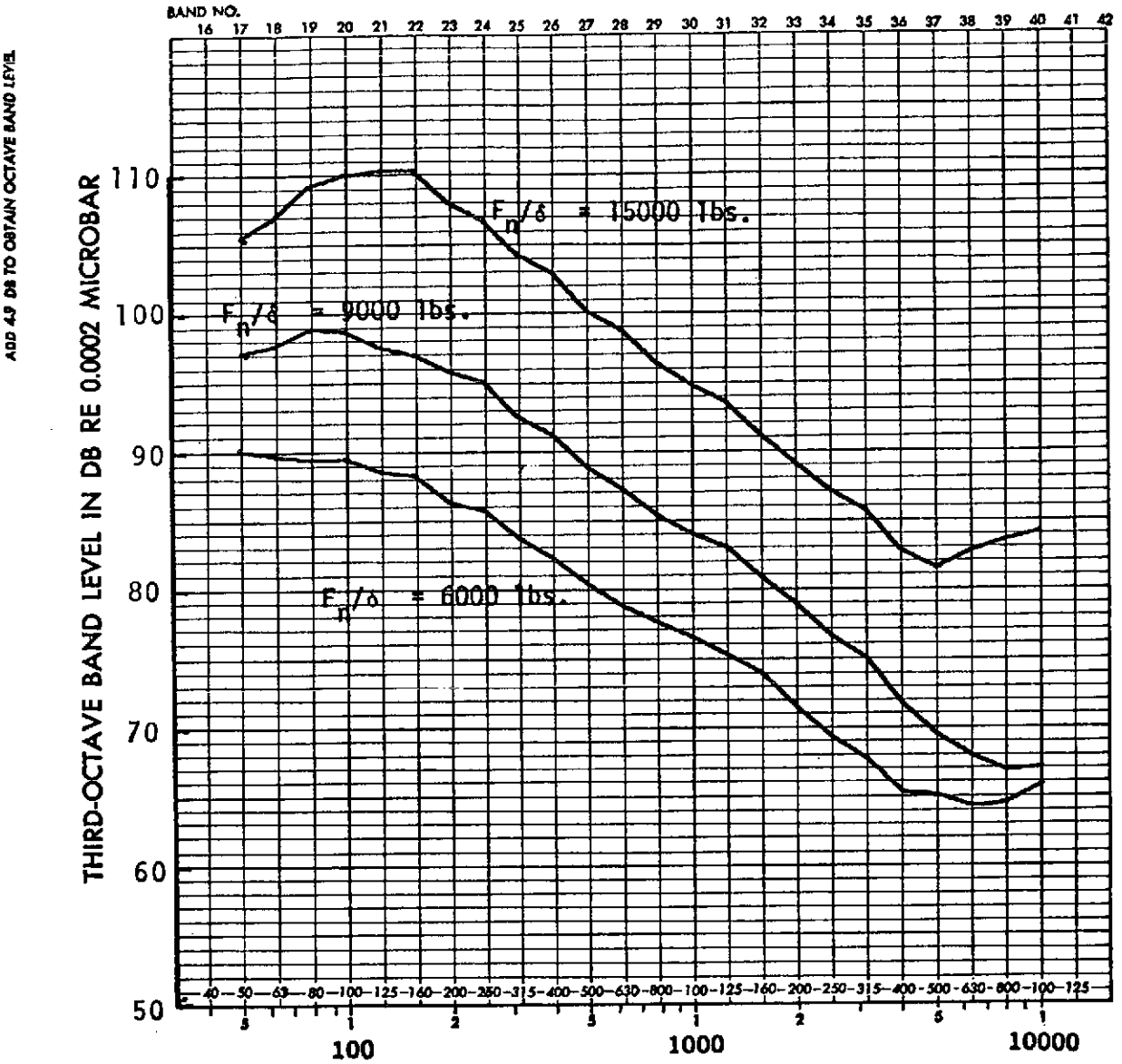

FIGURE 108. ONE-THIRD OCTAVE BAND SPECTRA
P&WA JT8D-109 NOZZLE

140^{o} Directivity angle

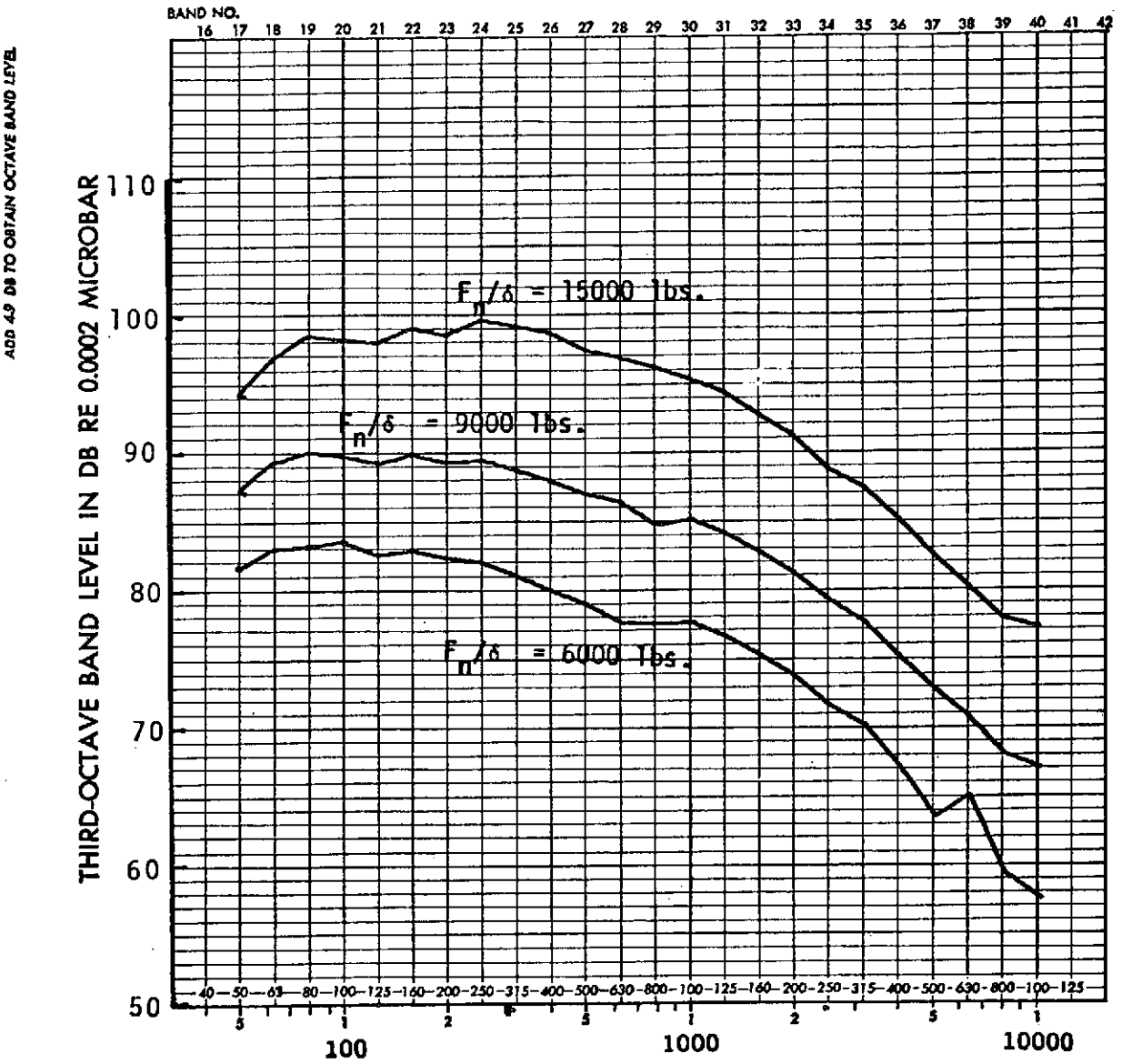

FIGURE 109. ONE-THIRD OCTAVE BAND SPECTRA
P&WA JT8D-109 NOZZLE
WITH SWIRL

110^{o} Directivity angle

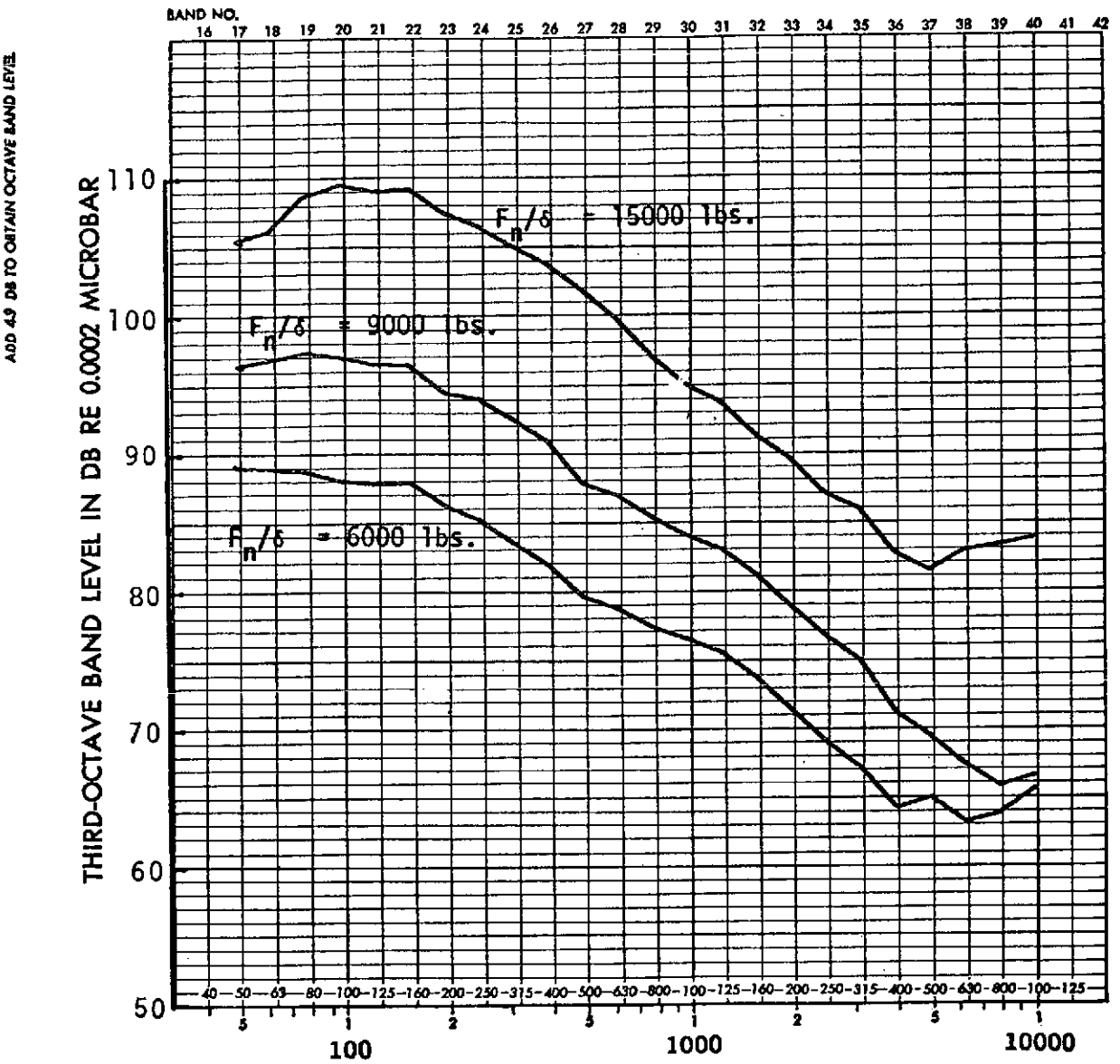

FIGURE 110. ONE-THIRD OCTAVE BAND SPECTRA

P&WA JT8D-109 NOZZLE
WITH SWIRL

140° Directivity angle

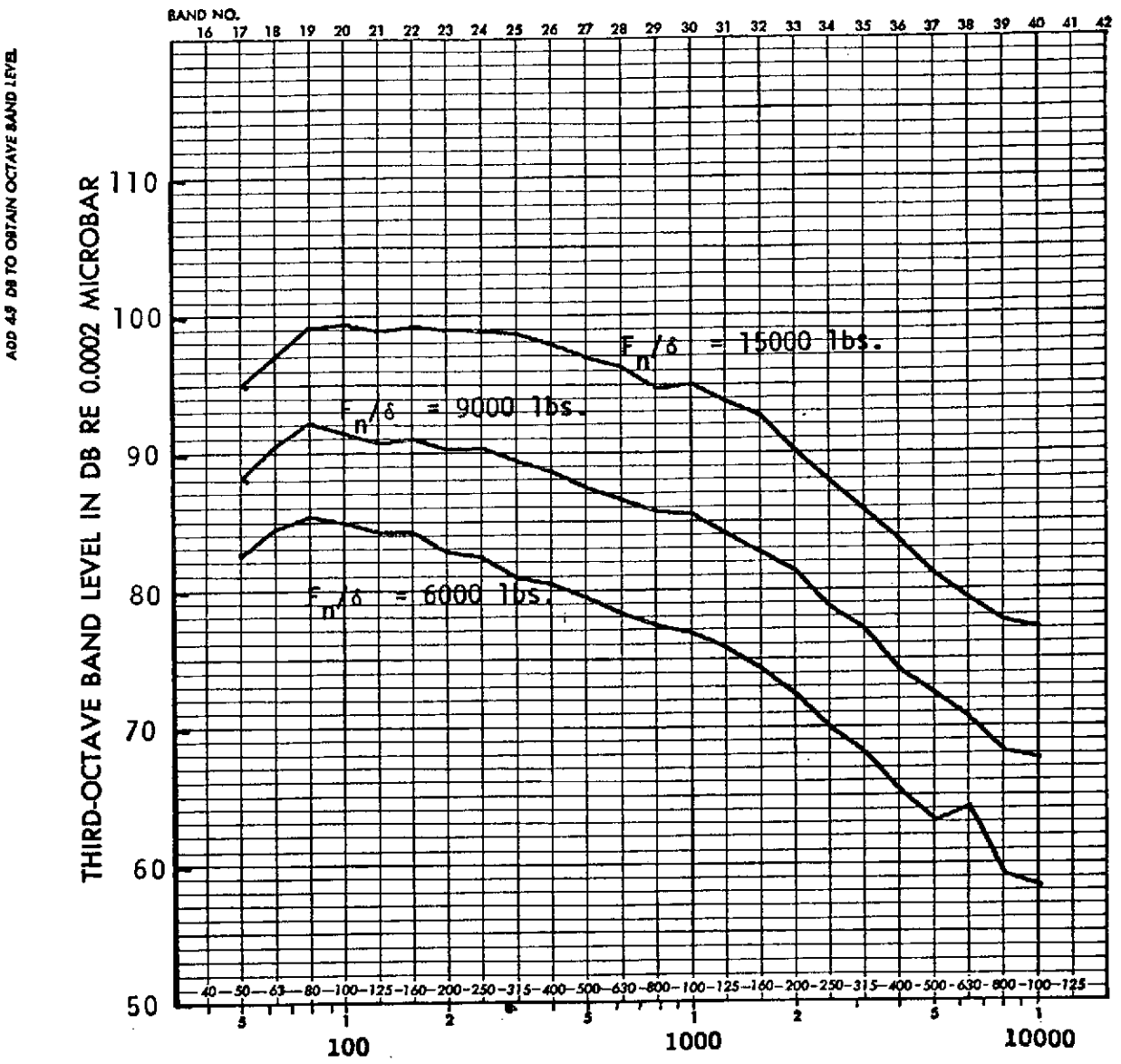

FIGURE 111. ONE-THIRD OCTAVE BAND SPECTRA
BOEING JT8D-109 NOZZLE
110^{o} Directivity angle

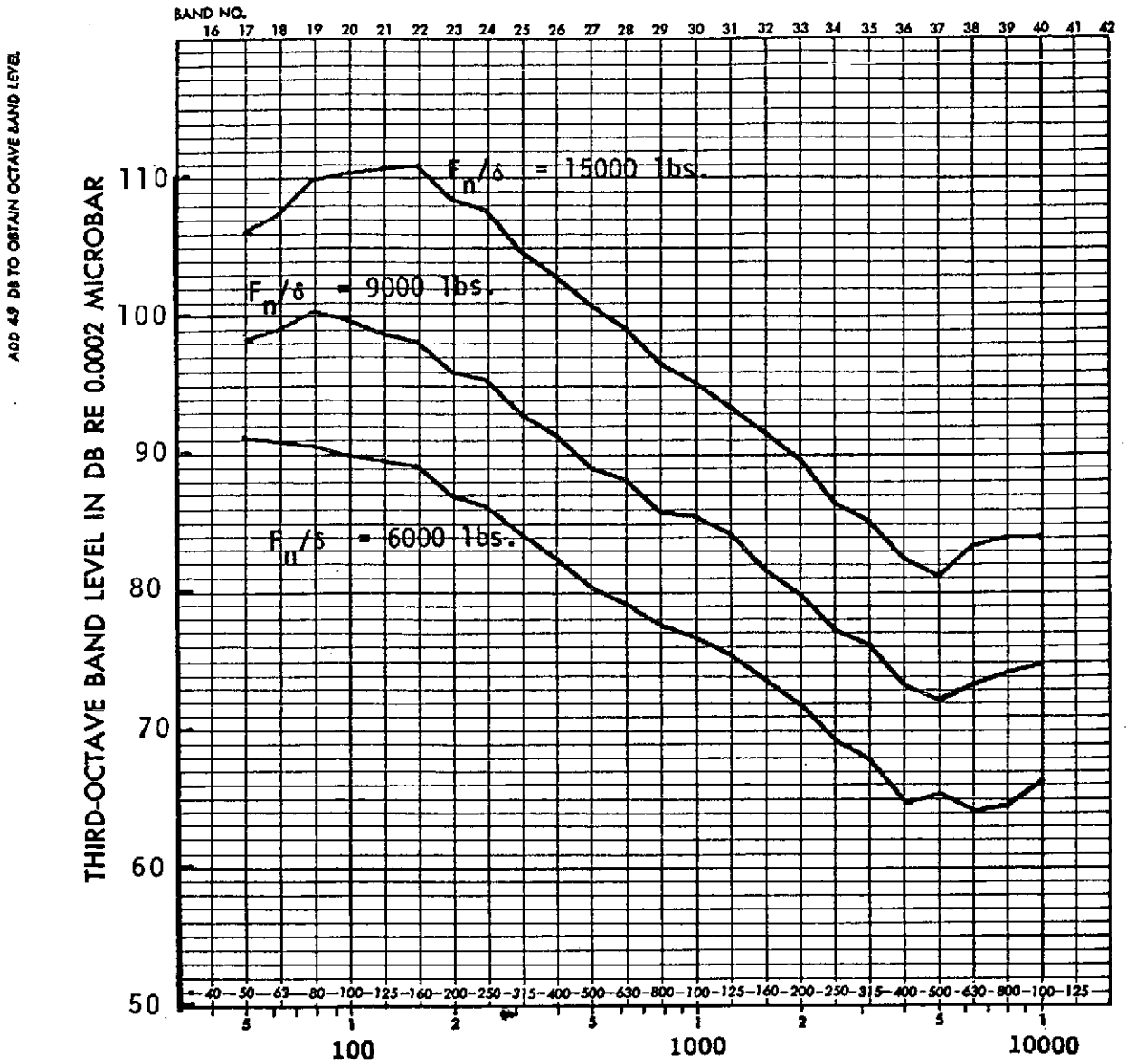

FIGURE 112. ONE-THIRD OCTAVE BAND SPECTRA
BOEING JT8D-109 NOZZLE

140^{o} Directivity angle

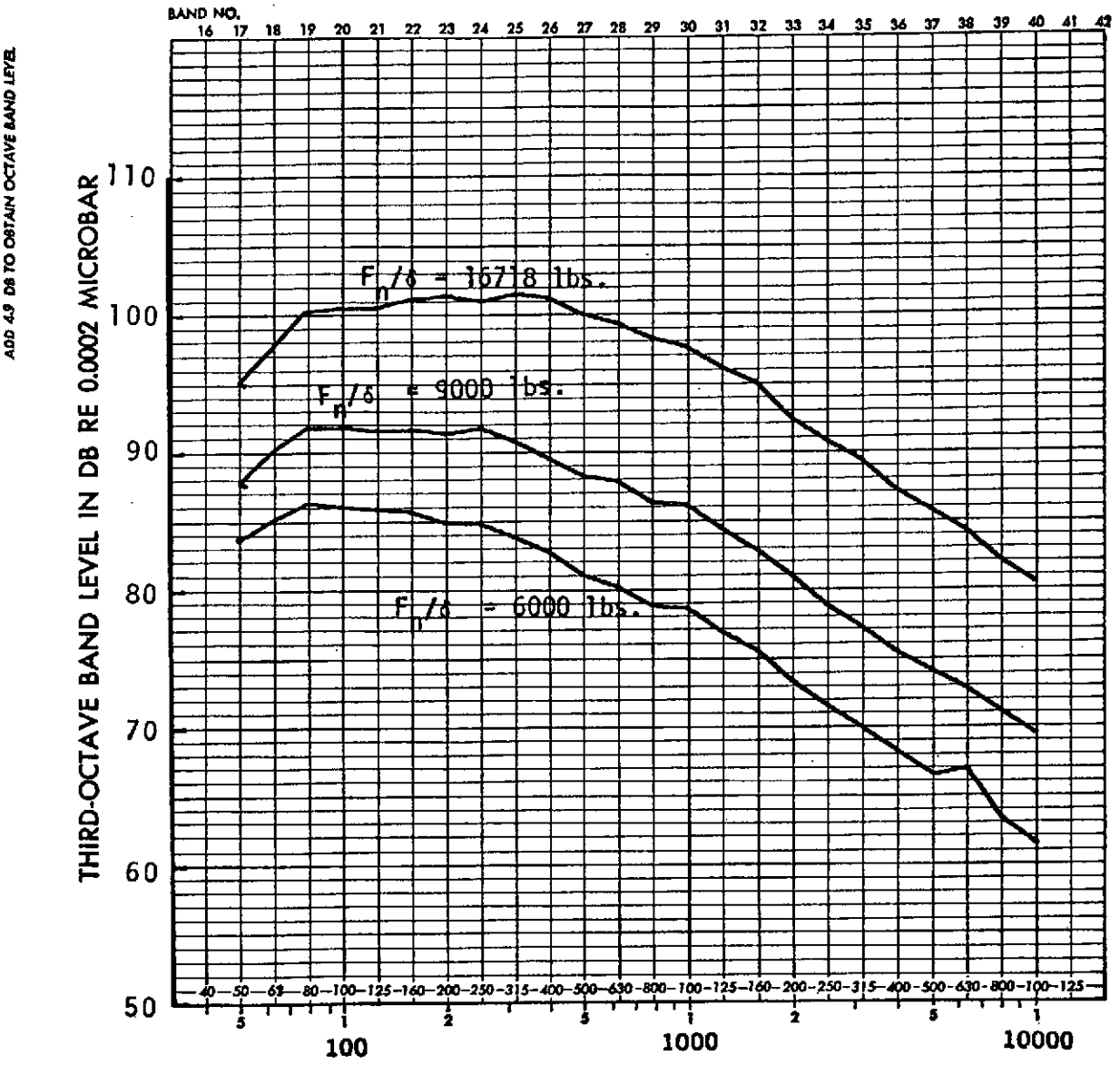

FIGURE 113. ONE-THIRD OCTAVE BAND SPECTRA
P&WA JT8D-115 NOZZLE
110^{o} Directivity angle

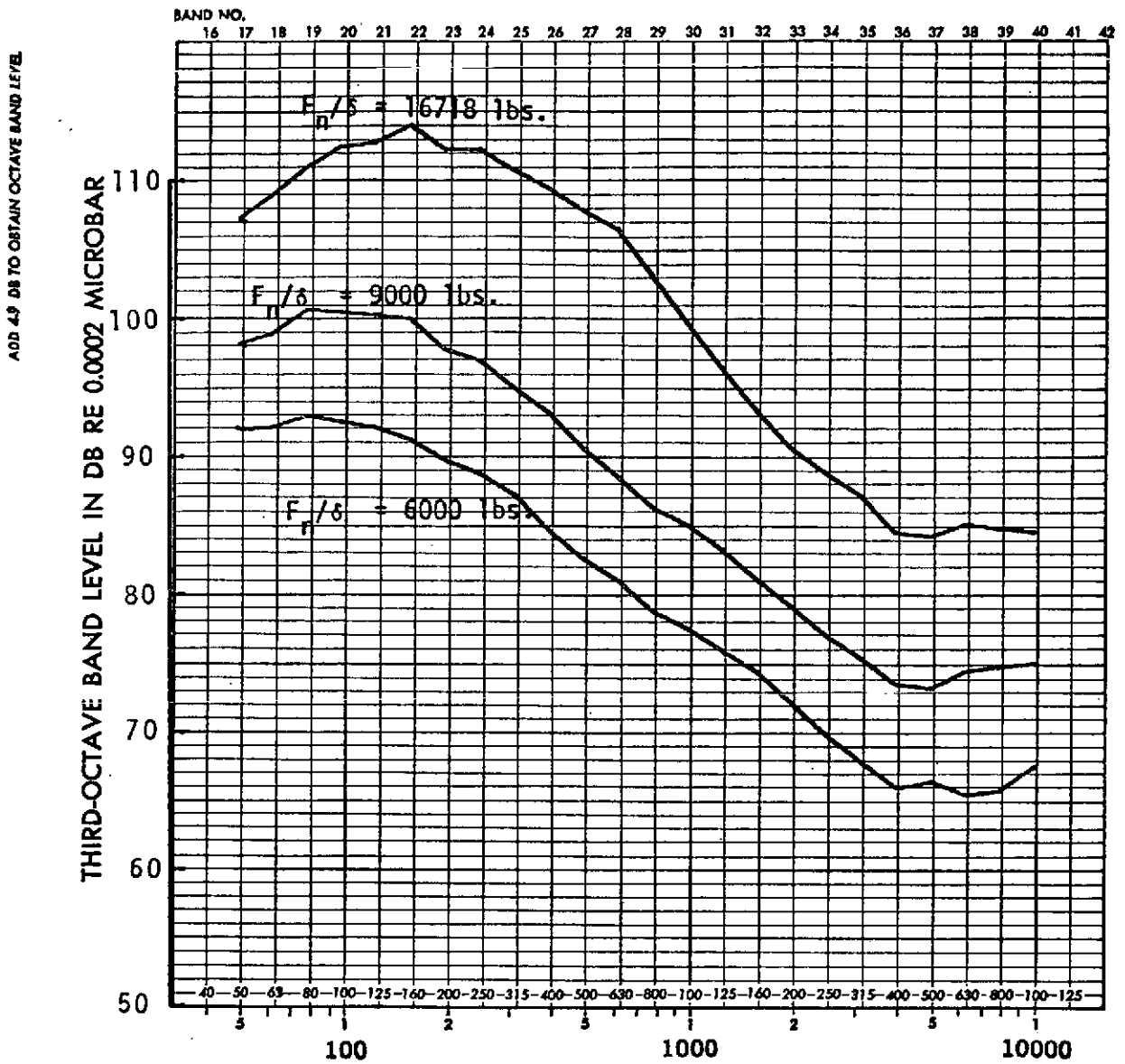

FIGURE 114. ONE-THIRD OCTAVE BAND SPECTRA

P&WA JT8D-115 NOZZLE

140° Directivity angle

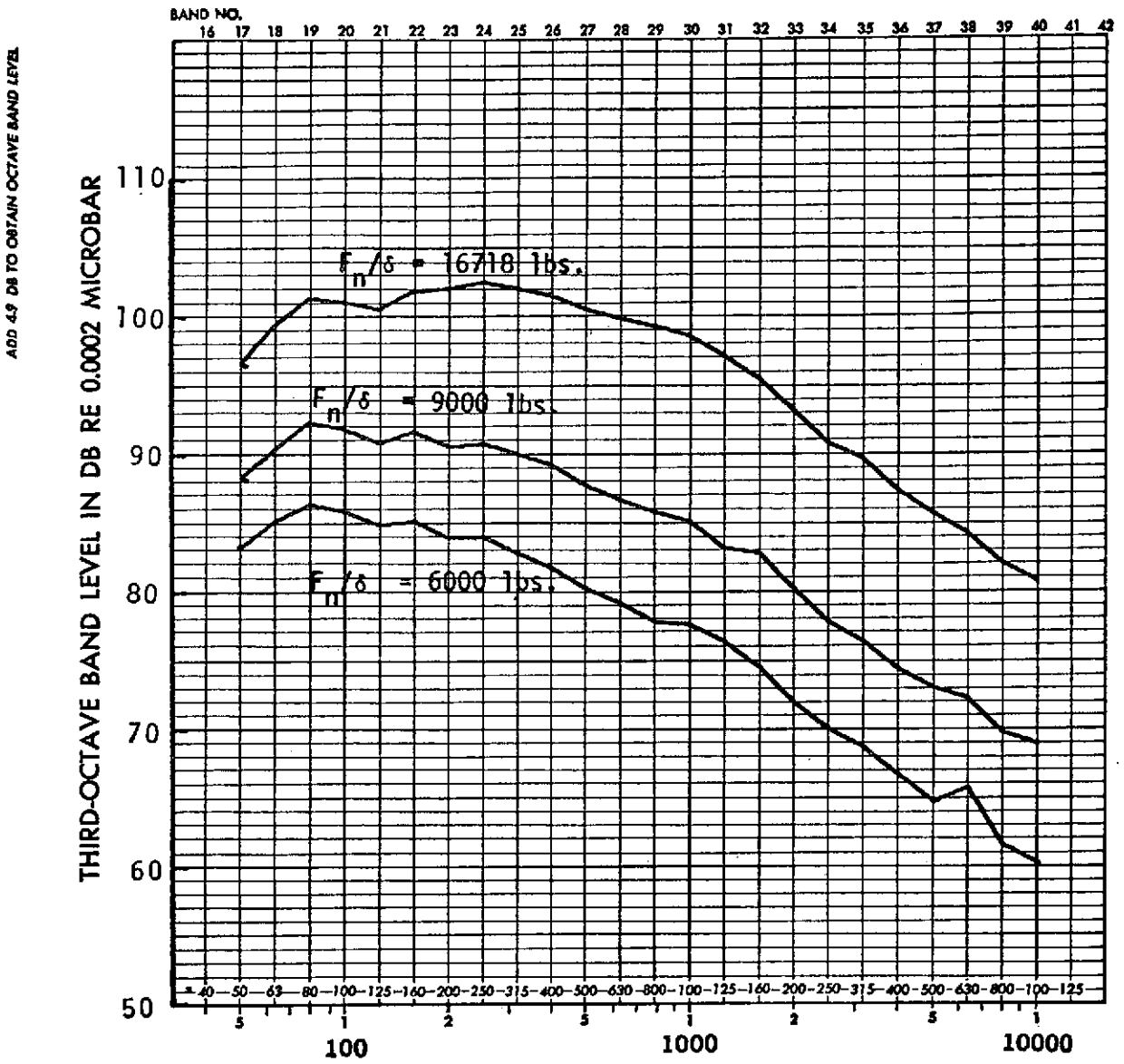

FIGURE 115. ONE-THIRD OCTAVE BAND SPECTRA

BOEING JT8D-115 NOZZLE

110° Directivity angle

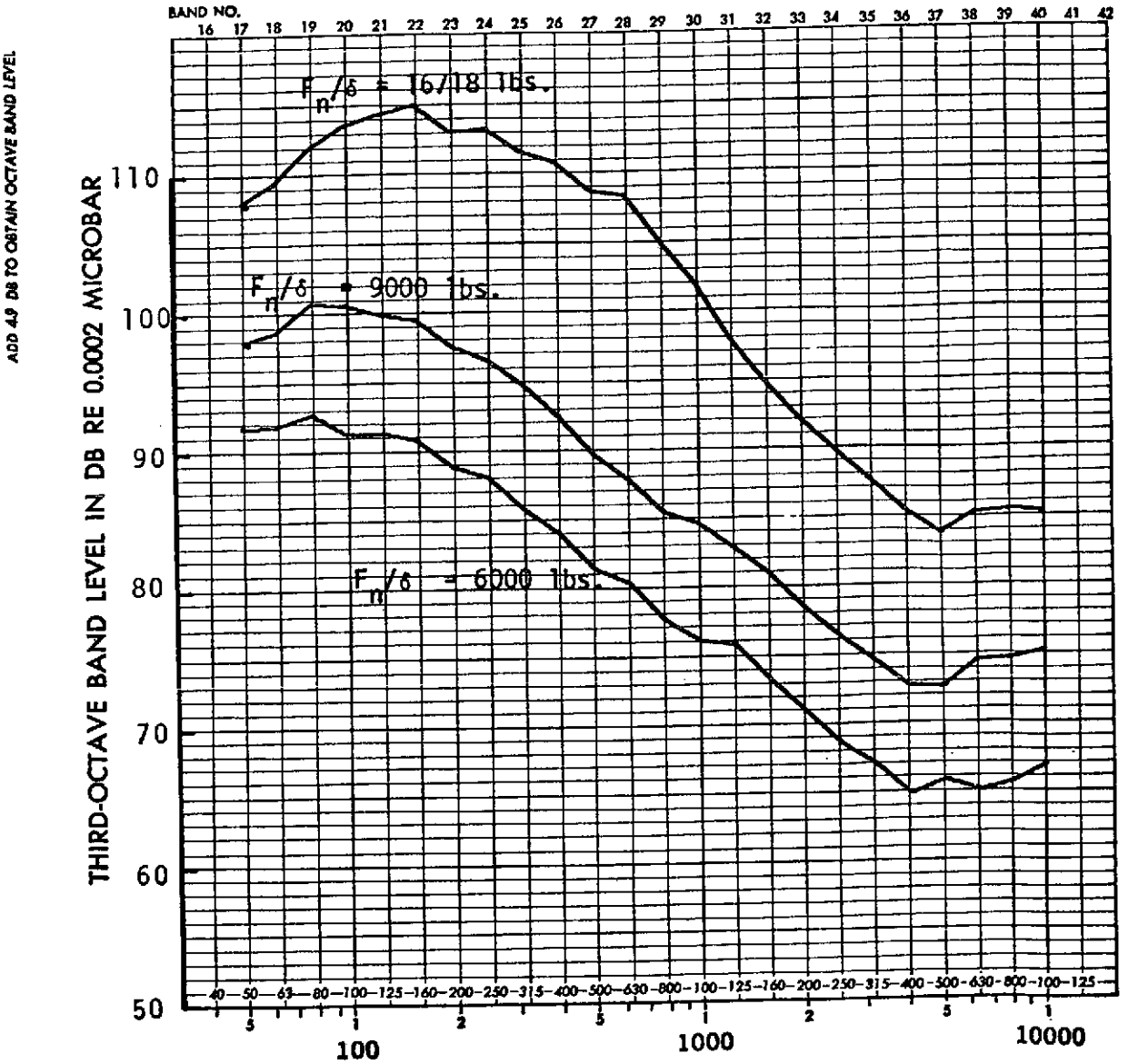

FIGURE 116. ONE-THIRD OCTAVE BAND SPECTRA

BOEING JT8D-115 NOZZLE

140° Directivity angle

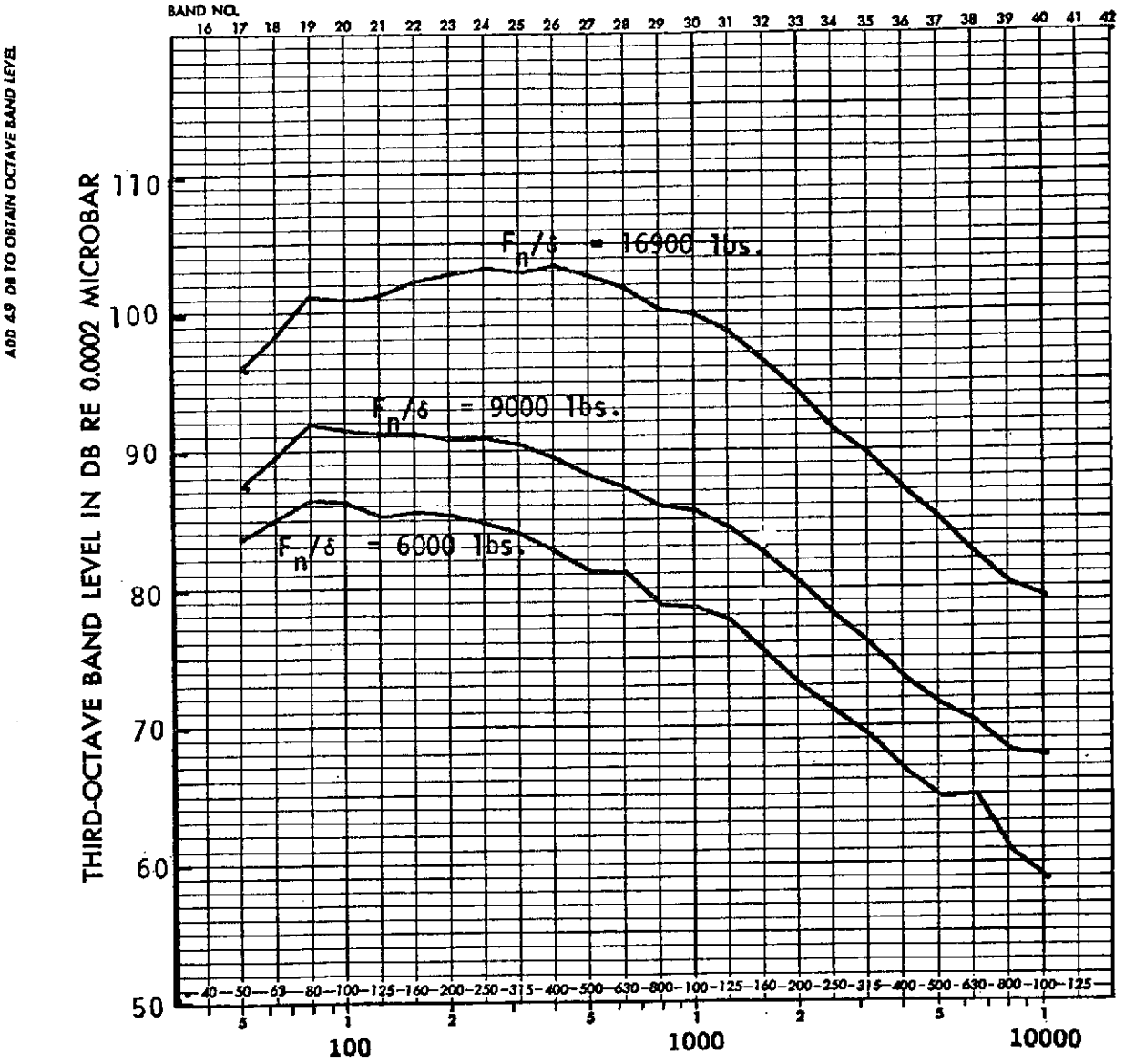

FIGURE 117. ONE-THIRD OCTAVE BAND SPECTRA

P&WA JT8D-117 NOZZLE

110^{o} Directivity angle

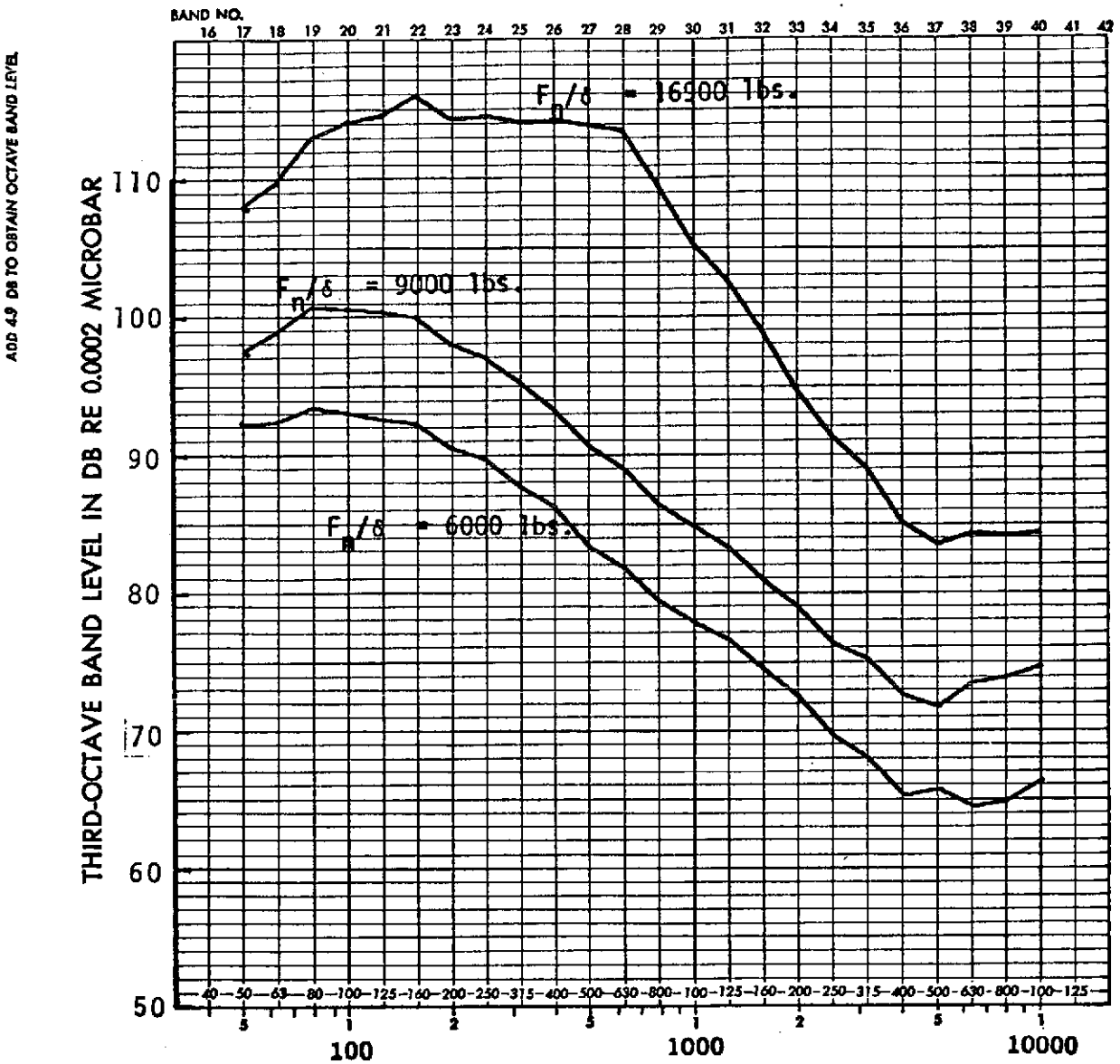

FIGURE 118. ONE-THIRD OCTAVE BAND SPECTRA
P&WA JT8D-117 NOZZLE

140^{o} Directivity angle

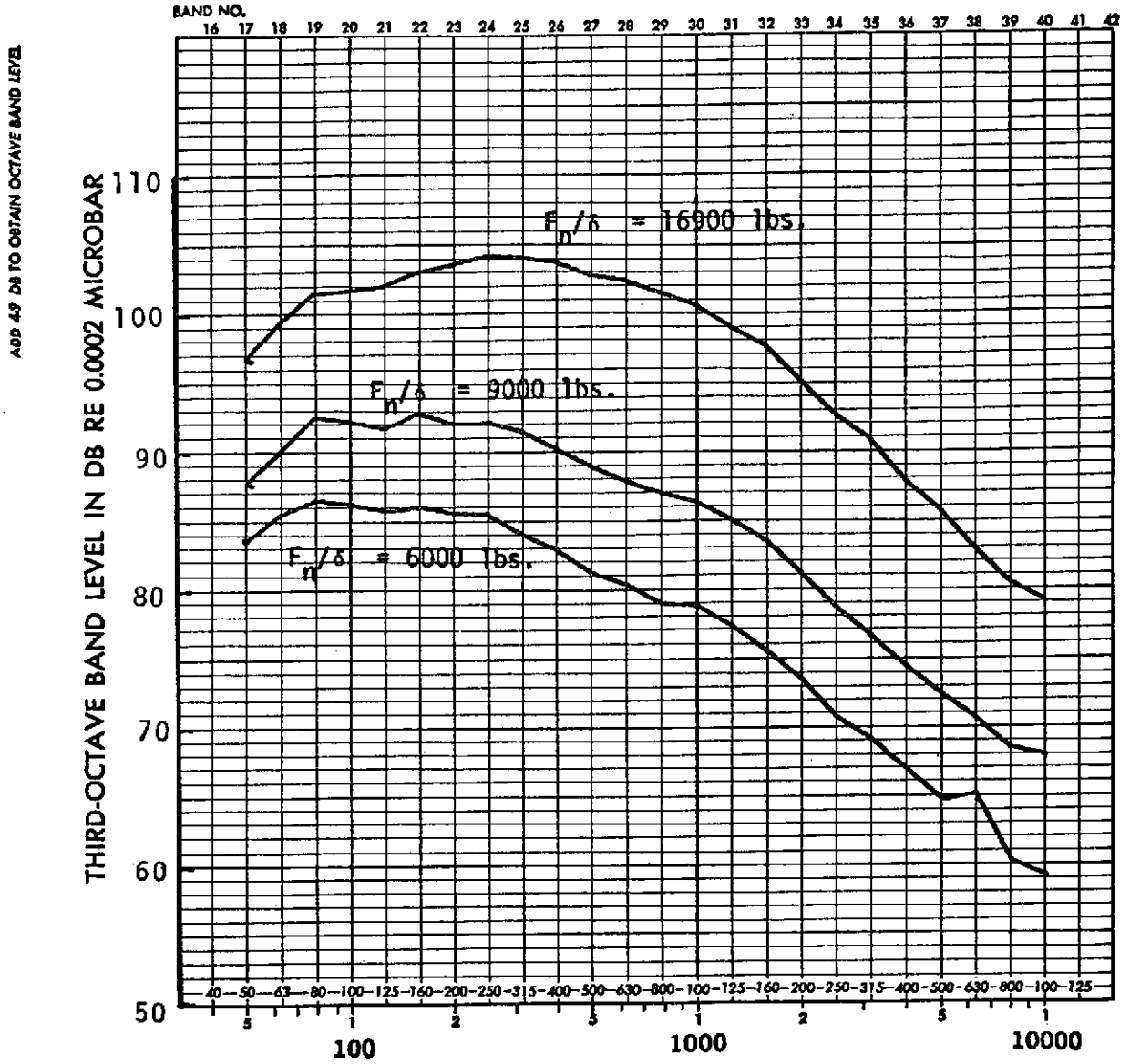

FIGURE 119. ONE-THIRD OCTAVE BAND SPECTRA
BOEING JT8D-117 NOZZLE (CONFIG. 9)
110^{o} Directivity angle

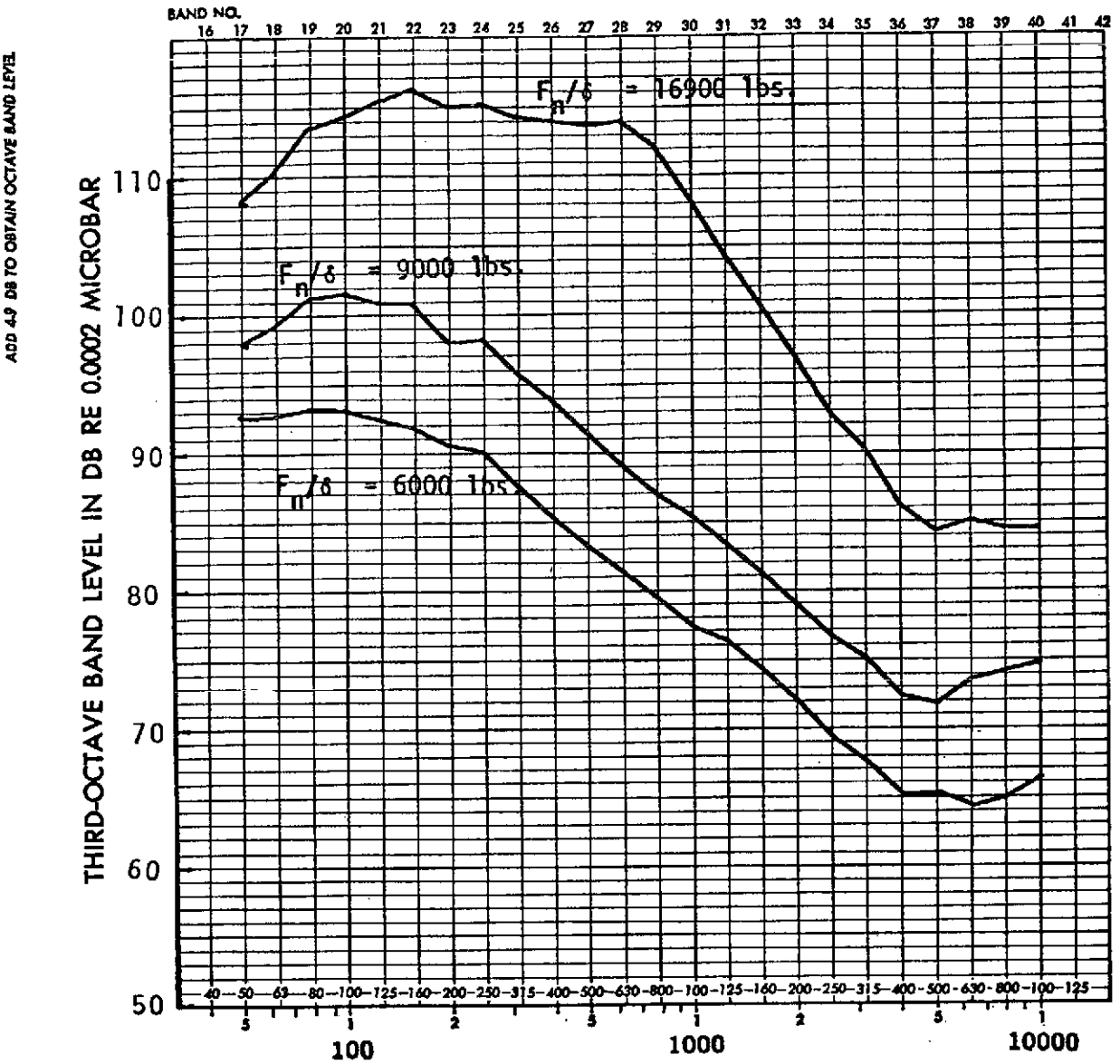

FIGURE 120. ONE-THIRD OCTAVE BAND SPECTRA
BOEING JT8D-117 NOZZLE (CONFIG. 9)
140^{o} Directivity angle

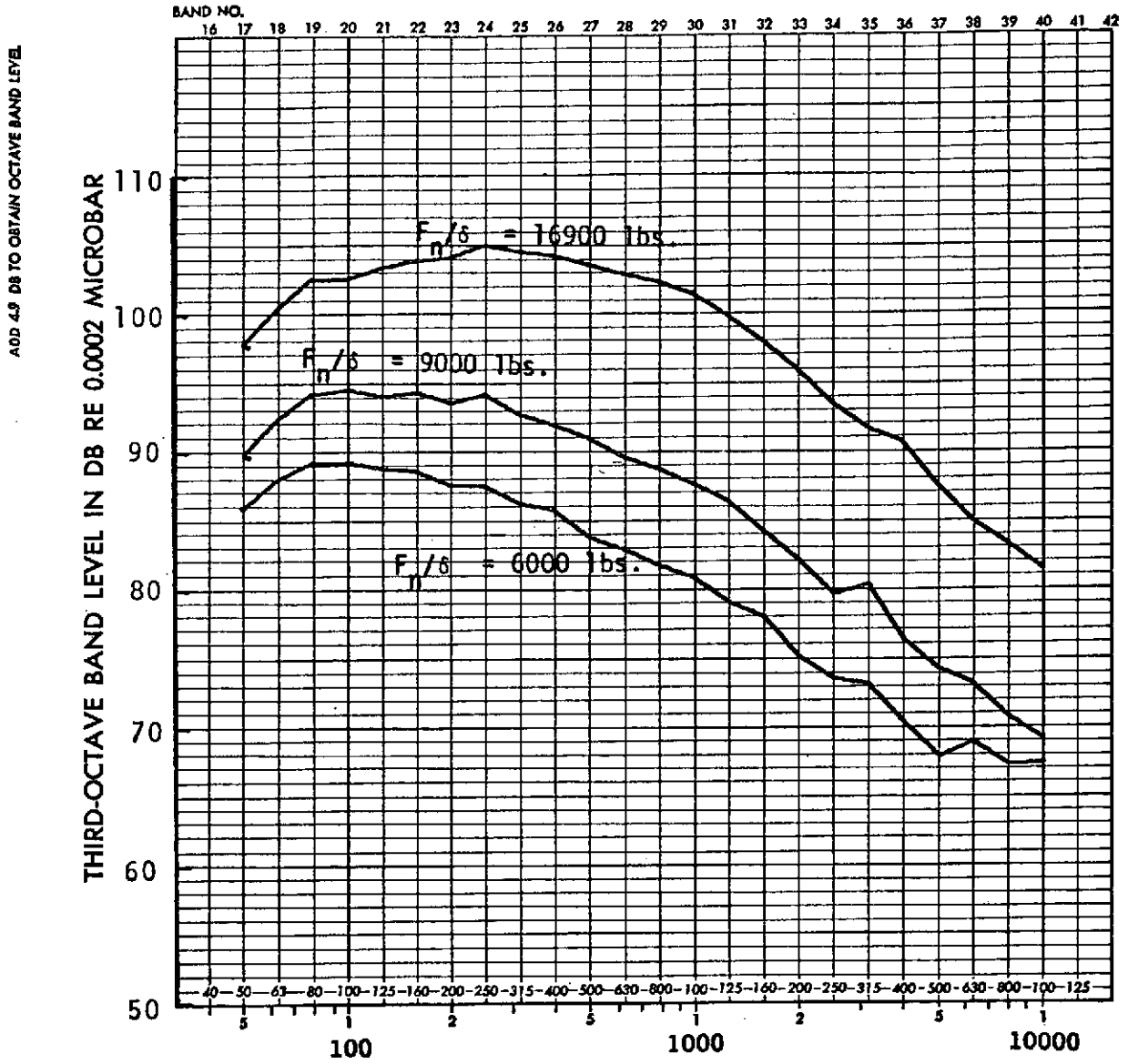

FIGURE 121. ONE-THIRD OCTAVE BAND SPECTRA
BOEING JT8D-117 NOZZLE (CONFIG. 10)

110^{o} Directivity angle

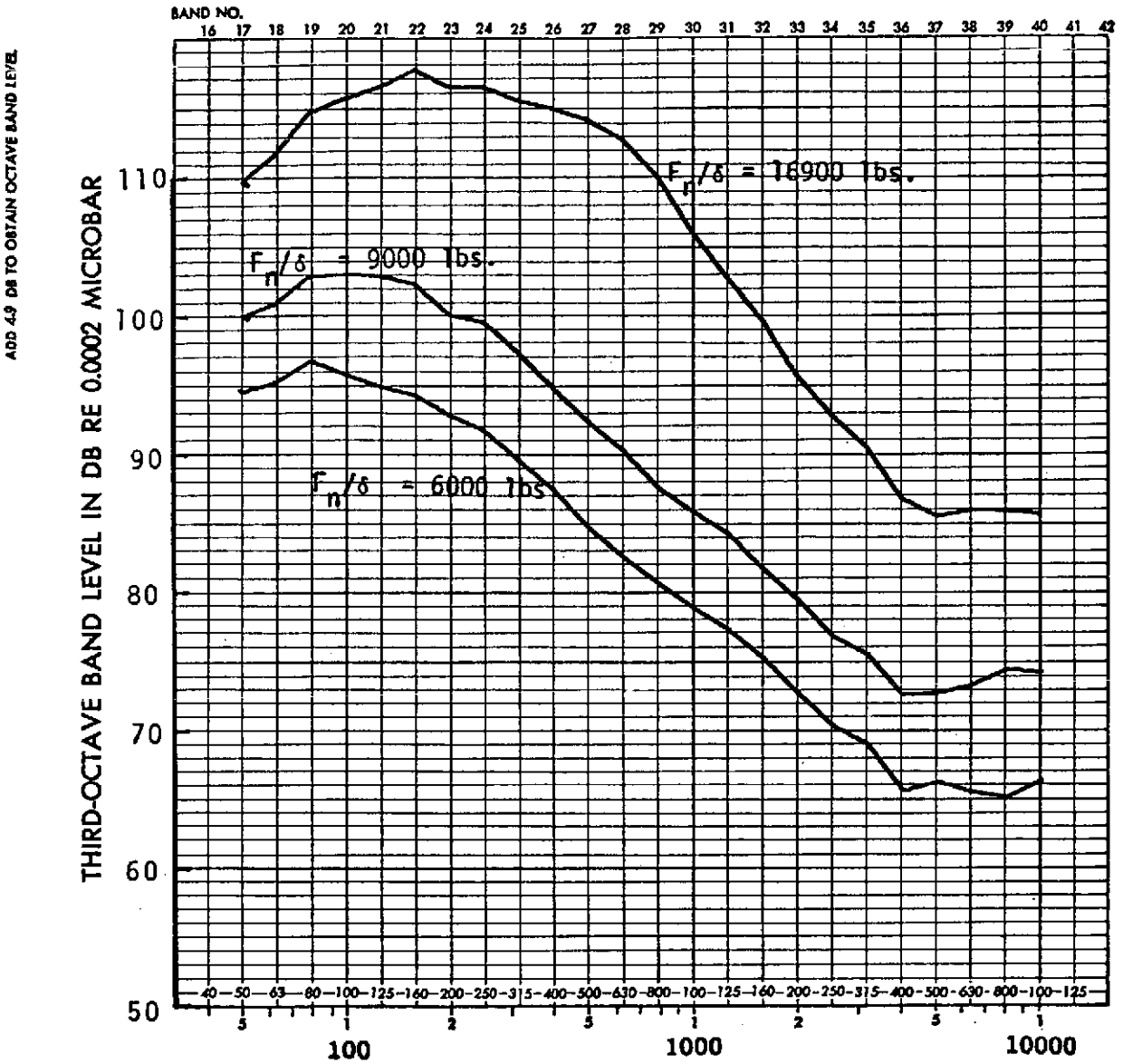

FIGURE 122. ONE-THIRD OCTAVE BAND SPECTRA

BOEING JT8D-117 NOZZLE (CONFIG. 10)

140° Directivity angle

REPORT DISTRIBUTION LIST

Addressee			No. of Copies
1. NASA Lewis Research Center 21000 Brookpark Road Cleveland, OH 44135			
Attention:	Report Control Office	MS: 5-5	1
	Library	MS: 60-3	2
	B. Lubarsky	MS: 3-3	1
	W. L. Stewart	MS: 3-5	1
	R. W. Schroeder	MS: 501-5	1
	G. K. Sievers	MS: 501-7	21
	F. O. Driscoll	MS: 500-206	1
	N. T. Musial	MS: 500-113	1
	M. A. Beheim	MS: 86-1	1
	D. N. Bowditch	MS: 86-1	1
	F. A. Wilcox	MS: 86-1	1
	D. C. Mikkelson	MS: 86-1	1
2. NASA Scientific and Technical Information Facility			
Attention:	Acquisitions Branch P. O. Box 33 College Park, MD 20740		10
3. NASA Headquarters 600 Independence Avenue, S. W. Washington, DC 20546			
Attention:	Code RJ/William H. Roudebush		6
	Code RL/Harry W. Johnson		1
	Code RO/Kenneth E. Hodge		1
4. Environmental Protection Agency Crystal Mall, Bldg. 2 1921 Jefferson Davis Highway Arlington, VA 20460			
Attention:	John Schettino	MS: AW-571	1
	William Sperry	MS: AW-571	1
5. Federal Aviation Administration 800 Independence Avenue, S. W. Washington, DC 20591			
Attention:	Robert J. Koenig (Code ARD-551)		1
	James F. Woodall (Code ARD-500)		1
6. Office of Environmental Quality 800 Independence Avenue, S. W. Washington, DC 20591			
Attention:	John O. Powers (Code AEQ-2)		1
	Richard P. Skully (Code AEQ-1)		1

Addressee			No. of Copies
7.	Department of Transportation 400 7th Street, S. W. Washington, DC 20590		
	Attention: Charles R. Foster		1
	Bernard Maggin (Code TST-51)		1
8.	NASA Langley Research Center Hampton, VA 23365		
	Attention: Harry T. Norton, Jr.	MS: 249A	1
	Thomas F. Bonner, Jr.	MS: 257	1
9.	NASA Ames Research Center Moffett Field, CA 94035		
	Attention: Stuart Treon	MS: 227-5	1
	Jim Monford	MS: 227-5	1
10.	NASA Flight Research Center P.O. Box 273 Eswards, CA 93523		
	Attention: Donald Bellman	Room 2106	1
11.	United Air Lines SFO EG San Francisco International Airport San Francisco, CA 94128		
	Attention: L. C. Ellis		1
	R. A. Gustafson		1
12.	American Airlines 633 Third Avenue New York, NY 10017		
	Attention: G. P. Sallee		1
13.	McDonnell Douglas Corporation 3855 Lakewood Boulevard Long Beach, CA 90846		
	Attention: W. A. Alden		1
	J. N. Thomas		1
	J. E. Donelson		2
14.	Pratt & Whitney Aircraft 400 Main Street East Hartford, CT 06108		
	Attention: G. M. McRae		2
15.	Rohr Corporation P. O. Box 878 Chula Vista, CA 92012		
	Attention: Steve Beggs		1

Addressee	No. of Copies
16. General Electric Company Aircraft Engine Group - E198 Cincinnati, OH 45215 Attention: John T. Kutney	1